Mariana Esteves da Silva Valente

At the Embryo's Heart:
Looking For Cardiac Repair/Regeneration Potential

Tese de candidatura ao grau de
Doutor em Ciências Biomédicas submetida ao
Instituto de Ciências Biomédicas Abel Salazar da Universidade do Porto

Orientadora – Doutora Perpétua da Conceição Pinto-do-Ó
Categoria – [1]Investigadora Auxiliar | [2]Professora Afiliada
Afiliação – [1]I[3]S | INEB | [2]ICBAS, Universidade do Porto, Portugal

Coorientadora – Doutora Ana Mafalda Simões de Bivar Cumano
Categoria – *DR1* Inserm, Directeur de Recherche IP e Chef d'unité
Afiliação – Institut Pasteur | INSERM, Paris, França

Coorientador – Doutor Professor Eduardo Jorge Sousa da Rocha
Categoria – Professor Catedrático
Afiliação – ICBAS, Universidade do Porto, Portugal

The work presented in this *Thesis* was developed at:

I^{3}S - Instituto de Investigação e Inovação em Saúde &
INEB – Instituto Nacional de Engenharia Biomédica,
Universidade do Porto, Porto, Portugal
Microenvironments for NewTherapies group | Stem-cell microenvironments in repair/regeneration Team
Rua de Campo Alegre, 823
4150-180 Porto, Portugal
www.i3s.up.pt | www.ineb.up.pt

Institut Pasteur
Unité de Lymphopoïèse, Département d'Immunologie, Paris, France
25, Rue du Dr. Roux
75724 Paris Cedex, France
www.pasteur.fr

The work presented in this *Thesis* was funded by:

Fundação para a Ciência e Tecnologia (FCT) and Fundo Social Europeu:

PhD fellowship: SFRH/BD/74218/2010.

Project grants: PTDC/SAU-OSM-68473/2006 | PTDC/SAU-ORG/118297/2010 | PEst-C/SAU/LA0002/2011 | PEst-C/SAU/LA0002/2013.

Fundo Europeu de Desenvolvimento Regional (FEDER) | Programa Operacional Factores de Competitividade – COMPETE | Quadro de Referência Estratégico Nacional (QREN) | American Portuguese Biomedical Research Fund (APBRF) | Programa Operacional Regional do Norte (ON.2-O Novo Norte) [NORTE-07-0124-FEDER-000005-Project on Biomedical Engineering for Regenerative Therapies and Cancer].

Institut Pasteur | INSERM U668 | Université Paris Diderot, Sorbonne Paris Cité, Cellule Pasteur | ANR | REVIVE Future Investment Program

“If you can't explain it simply, you don't understand it well enough."

– Albert Einstein (1879 - 1955) at Gare du Nord in Paris

(by Ronald W. Clark, 1971, *Einstein: The Life and Times*)

ACKNOWLEDGMENTS

Desde o primeiro momento em que decidi embarcar neste percurso académico, eu sabia que este seria um caminho extremamente desafiante e exigente. No entanto, apenas quando lá cheguei é que me apercebei que realmente não é fácil, e mesmo que nós digam que é natural, é sempre difícil de o viver. Quando eu olho para trás tudo na minha vida está diferente: tive uma grande perda e alguns momentos realmente difíceis, mas acho que apesar de tudo o balanço final é positivo para mim e para quem me rodeia. E isso é muito bom!

Esta viagem permitiu-me enriquecer a vários níveis: conhecer pessoas fabulosas, que passei a admirar; a experienciar uma vida nova num país diferente do meu (e ainda "levar" para lá o meu apêndice), que passei a adorar; e inesperadamente relembrei/reaprendi o essencial do meu francês, o que deu para sobreviver. Depois desta viagem nada mais será como dantes! Mas não posso deixar de relembrar que para eu ter consigo completar esta odisseia várias, muitas, pessoas me ajudaram e as quais eu estarei imensamente grata.

Em primeiro lugar quero agradecer do fundo do coração à minha orientadora, Perpétua Pinto-do-Ó, por ter acreditado em mim desde o início e me ter dado a oportunidade para vivenciar este desafio. Penso que tudo o projeto que "magicou" foi perfeito em todos as suas vertentes: espaço, local e intervenientes. Obrigada por me ter "mandado" para Paris, eu adorei a experiência. Também gostei, como já tive a oportunidade de lhe dizer, de a ter por perto em Paris.

Obrigada por me ter apoiado SEMPRE durante todos estes anos de trabalho, principalmente quando o problema era fora do âmbito do trabalho. Muito obrigada pela paciência e todo o trabalho duro nesta fase final. Muito muito obrigada por tudo!

A segunda palavra vai para a Ana (Cumano). Muito obrigada por me teres aceite no teu laboratório e teres embarcado com tanto entusiasmo nesta aventura no mundo do desenvolvimento cardíaco. Esta aventura, realmente, não teria sido a mesma sem a tua participação. Aprendi muito contigo e guardo muitas das tuas palavras não só para o meu trabalho, mas também para o dia-a-dia: Keep it simple! Don't complicate your life! Too complicate! Bad luck! This is going to be very funny! Let see what do we get! These guys do not exist!
Ah, e obrigada por me teres incentivado a acabar a tese o mais rapidamente possível.

Ao Professor Eduardo Rocha que para além de Diretor do Programa Doutoral em Ciências Biomédicas, que estou a frequentar, aceitou ser coorientador/tutor da minha tese de doutoramento, permitindo e facilitando a ligação com a Universidade. À Ana Paula Pereira, um muito obrigada pela sua ajuda em todo este processo. E ainda um especial agradecimento à comissão de acompanhamento da minha tese por toda a discussão e feedback: à Doutora Margarida Lima e à Doutora Raquel Andrade.

Um profundo e sincero agradecimento à minha equipa que será para sempre a minha, a HEART TEAM! Sem vocês realmente isto não seria possível, OBRIGADA por tudo (pelas vossas mãos, cabeças, corações, TUDO). Tatiana, começo por ti. Obrigada por tudo isto, obrigada por criares pequenos objectivos que me ajudam a atingir o fim. A tua calma (quando não tens fome, nem sono) faz-me bem. Obrigada! Diana, tu estas a acompanhar o meu percurso desde o início e muitas das pequenas conquistas desta tese foram conseguidas trabalhando lado a lado contigo. Obrigada por tentares sempre extrair o melhor para o meu, o nosso trabalho! Ana F., minha companheira

que agora já se bandeou para o outro lado ;). Também sobrou para ti. Muito obrigada por todo o apoio e ajuda. Nunca esquecerei os nosso momentos no laboratório quando éramos pequeninas! Desejo-te muito boa sorte para esta nova fase. Vais ser feliz, tenho a certeza. E aos mais pequeninos que, nos últimos tempos têm sido poupados a este furacão, mas muitos deles também o viveram: Ana S., muito obrigada pelo enorme entusiasmo e carinho que tens SEMPRE para me dar. Desejo-te muita força e muito boa sorte nos states, tu também vais conseguir! Ah, e não te esqueças de "alimentar" a artista que está dentro de ti. Vasco e Tiago, muito obrigada por me ajudarem sempre que estou aflita! Vocês estão sempre lá no momento certo! Desejo muito boa sorte aos dois para a nova fase. Aos restantes, Francisca (muito boa sorte! E ainda nos cruzamos em Paris! :)), Sílvia, Luís, Marcel, um beijinho e obrigada por ajudarem a manter o bom ambiente, que tão bem caracteriza a equipa.

Agradeço ao INEB e sua direção (antiga e presente), ao Professor Mário Barbosa e ao Professor Fernando Jorge. E ainda um agradecimento muito especial à Ana Paula Filipe por estar sempre disponível para nos ajudar em tudo o que precisamos.

Ao meus colegas do INEB (antigos e presentes), ALT, António, Bianca, Carla, Catarinas, Cátia, Cristinas, Danielas, Eliana, Filipa, Francisca, Inês, Isabel, Juliana, Lili, Marias, Meriem, Odila, Paula, Raquel, Ritas, Sara, Sidónio, Susanas. Obrigada pelas palavras sempre incentivadoras. Adoro toda a união que existe no INEB. Um beijinho especial a Estrela que me tem acompanhado nesta jornada desde o início e me disponibiliza sempre um abraço e um sorriso especiais cada vez que chego ao laboratório. Para além dos colegas, algumas pessoas responsáveis pelo bom desempenho dos serviços, tão importantes no nosso dia-a-dia no INEB, facilitando e proporcionando o desenvolvimento do meu trabalho: à Catarina Leitão (Advanced Flow Cytometry Unit at IBM | INEB); à Sofia Lamas e Isabel Duarte (Animal Facility at IBMC | INEB); à Daniela Azevedo, Dulce Carqueijó, Eliana Vale, Gabriela Afonso, Manuela Brás, Raquel Coelho, Ricardo Silva, Virgínia Fonseca, e ainda à Dona Rosa.

To Marie-Christine, thank you very much for your kindness and help with all problems, especially with the French spoken ones. To my (former and present) colleagues at Pasteur: Claire, thank you very much by welcome me since the very first day at Pasteur, your help in the lab all the time, and your nice and calming words ;)! Sylvestre, the chinese and magic hands, thank you very much your help in the lab and with the bioinformatic analysis!!! Odile, always worried with our safety and well-being. Thank you very much for your help with the embryos (I learned I lot with you). To Sandrine, Rachel, Thibaut, Alex, Delfine, Ana Catarina, Marie-Pierre for the good moments and discussions. To Paulo VIEIRA, António BANDEIRA, António FREITAS, Pablo PEREIRA for the rich and helpful discussions (we will continue them), and also for the beers at the end of the day, the ones that I participated. To Sophie NOVAULT and Sandrine SCHMUTZ at the Flow Cytometry Platform for all help and to Koji Futamura and Cédric AIT-MANSOUR during the implementation of the Sony SP6800. To Didier MONTARRAS and Sigolène MEILHAC for the useful discussions about heart development. To Gerard EBERL and Lucie PEDUTO thank you very much for all the borrowed antibodies and the good discussions. To Vincent ROUILLY, thank you for your stimulating words. I'm expecting the great time life after the PhD. To Paola MINOPRIO and Alain COSSON, thank you very much to receive me and open me the world of the parasites. And Alain, thank you for working hard to improve my French! To my PhD tutor at Pasteur, Jerome GROS, thank you very much for the motivating discussions and invaluable advices. I'll keep them.

To all my friends in Paris: Tozé, tu vens no grupo francês. Muito obrigada por me teres recebido nos teus 23m^2. Silvia M and Filippo, thank you very much for the good moments (me and Joao are waiting for you in Portugal)!. Patrick, Carla and Antonello, Silvia L and Igor, Mariana, Francesca, Barbara, Giulia, Ailng, Andrea, Carine, Eleonora, Emi, Hanane, Cristina, Sasha, Selena, Sophie, Inês and Rosa.

I know that not all of you belong to it, but I have to say: I'm really in love with the Italian mafia. To Rute, for the very very nice lunchtime that we have spent together. And finally, to Fernando, thank you very much to make me feel at home in the 5éme.

Aos meus amigos de sempre que me fazem quebrar as regras e descontrair muito, mesmo nos momentos difíceis: aos recém casados :) Mafalda e Albano, Soraia e Peter, Joana, Guilherme e Eduarda, Gonçalo, Tomané, Tó Luís e Carina, Matilde e Francisco, Carina, João, Major (João David), Bootsh (Rafael), Luís e Raquel,… Um especial muito obrigada à Patrícia, por me ligar sempre nos momentos certos, não percebo :) !!

À minha família obrigada por serem o meu porto seguro e por me fazerem sentir que está tudo bem cada vez que entro em casa. À minha mãe que acredita em mim acima de tudo, e que me mostrou com naturalidade que os problemas são para ser resolvidos e que há muita vida para ser vivida. Pai, a perseverança foste tu que me a deste, mas eu vou usá-la noutro contexto. David (e Catarina) obrigada pelos momentos de descontração em família aos fim-de-semana. Adoro-vos!

João, obrigada por me obrigares a viver e descontrair, mesma nas fases mais difícil. Apesar de muitas vezes começar contrariada foram sempre esses momentos que me ajudaram a manter o equilíbrio e ser feliz, como eu sou.

Por tudo isto, quando eu olho para trás, sinto que realmente eu consegui aproveitar muito da minha vida durante este percurso e isso é muito bom de sentir.

Dedico esta tese a todos vocês que fazem parte da minha vida, e desculpem o meu mau feitio!

LIST OF PAPERS

The work presented in this *Thesis* collects the following scientific articles published and manuscripts under preparation for submission in international peer-reviewed journals:

Valente, M., Nascimento, D.S., Cumano, A., and Pinto-do-Ó, P. Sca-1+ Cardiac Progenitor Cells and Heart-Making: A Critical Synopsis. ***Stem Cells and Development***, 2014, 23(19):2263-2273, DOI: 10.1089/scd.2014.0197. [*Thesis Chapter I* | *Appendix I*]

Valente, M.*, Resende, TP.*, Nascimento, D.S., Cumano, A.[§], and Pinto-do-Ó, P.[§]. Surface Markers Identifying Different Cardiac Populations Reveal Two Distinct Subsets of Cardiomyocytes in the Mouse Fetal Heart. ***Manuscript***. *co-first authors and [§]co-senior authors. [*Thesis Chapter III*]

Nascimento, D.S.*, **Valente, M.***, Esteves, T., Guedes, J.G., Freire, A., Pina, M.F., Quelhas, P. and Pinto-do-Ó, P. *MIQuant* – Semi-automation of Infarct Size Assessment in Models of Cardiac Ischemic Injury. ***PLoS ONE***, 2011, 6(9): e25045. DOI: 10.1371/journal.pone.0025045. *equal contribution. [*Thesis Chapter IV*]

Valente, M., Araújo, A., Esteves, T., Laundos, T.L., Freire, A.G., Quelhas, P., Pinto-do-Ó P.* and Nascimento, D.S.*. Optimized Heart Sampling and Systematic Evaluation of Cardiac Therapies in Mouse Models of Ischemic Injury: Assessment of Cardiac Remodeling and Semi-Automated Quantification of Myocardial Infarct Size. ***Current Protocols in Mouse Biology***. 2015, 5(4). *equal contribution. [*Thesis*

Chapter IV | *Appendix II*]

Valente, M., Resende, TP., Nascimento, D.S., Laundos, T.L., Cosson A., Minoprio P., Cumano, A., and Pinto-do-Ó, P. Differential Re-Activation of Specific Embryonic Cellular Phenotypes in the Adult Mouse Heart Subjected to Ischemia and Infection Injuries. ***Short-Report***. [*Thesis Chapter V*]

Published or accepted articles are reproduced with permission from Copyright © 2014, Mary Ann Liebert, Inc. (Chapter I and Appendix I) and Copyright © 1999-2015 John Wiley & Sons, Inc. (Chapter IV Paper II). © 2011 Nascimento et al. (Chapter IV Paper I) is an open-access article distributed under the terms of the Creative Commons Attribution License, which permits unrestricted use, distribution, and reproduction in any medium, provided the original author and source are credited.

ABSTRACT

The adult mammalian heart is well known by its inability to restore lost cardiomyocytes (CMs), which are instead replaced by fibrotic scar tissue following injury. However, in recent years, detection, although at limited levels, of CMs turnover during adulthood has revolutionized the field. The cellular origin of the renewed adult CMs is not yet clarified and debate persists as to whether they may result from differentiation of putative cardiac progenitor cells (CPCs) or from pre-existing CMs.

In this *Doctoral Thesis* original work is presented and discussed in the context of central unresolved questions in the cardiovascular field. To this end, current understanding of heart-resident $Lin^{-}Sca\text{-}1^{+}$ CPCs has been critically reviewed in light of what is known for cellular compartments with similar phenotypes in other organs. This appraisal of the literature highlighted a lack of in-depth studies directed to the identification of the cardiac cell signatures (phenotypes) during heart morphogenesis.

In order to achieve this knowledge, we have defined a strategy novel in heart research by assembling a multi-parametric phenotypic screening with single cell multiplex transcriptional analysis. Our approach allowed the discrimination of the major cell types throughout fetal heart development. We defined surface phenotypes that enabled tracing epicardial cells and different subsets of fibroblasts from the myocardium and the valves. Notably, we identified surface signatures differentially expressed in two subsets of CMs that relate to different stages of maturation. The mature CM subset expresses Caveolin-3, is detected from E13.5 onwards and is maintained in the adult myocardium. On the other hand, the immature compartment expressing CD24, CD146

and CD166, but negative for Caveolin-3, proliferates extensively at mid-gestation decreasing in frequency during development to be undetected in postnatal life.

Following the observation that adult cardiac cells change their phenotype after birth, we have decided to analyze the cellular phenotypes in the adult myocardium after injury. The aim was to determine whether in the repair response to injury (myocardial infarction (MI) and Chagas' disease) a "fetal program" would be re-activated/ replicated in the heart. In this context, the relevance of the cardiac ischemia experimental model established was fully validated by examining whether functional cardiac impairment (assessed by transthoracic echocardiography) correlated with the extension of the collagen deposition (infarct size). Furthermore, in order to decrease reported discrepancies between laboratories on the methodology of heart sampling and during the calculation of ischemic tissue, we have developed both semi-automated software to accurately and faster assess the MI extension and a detailed protocol for the heart sampling and cellular analysis (*i.e.* quantification of neovascularization and detection of transplanted cells engraftment).

Finally, we have investigated the surface protein profiles (cell phenotypes) in the adult myocardium after cardiac injury (induced MI and Chaga's disease). Our proof-of-principle study revealed that surface signatures specific of the fetal cardiac populations were re-expressed in both experimental models in use, and thus proved the significance of the identification of cell components of the developing heart to better understand adult pathology.

Overall, work in the *Doctoral Thesis* herein contributed with i) new surface signatures to discriminate the main embryonic mouse cardiac cells and their progenitors, as well as potential hierarchical relationships (single cell transcriptional profile); ii) new methodology, *i.e. MIQuant* software, for the standardized evaluation of the MI-experimental injury and thus allowing exact comparisons between laboratories; and finally, iii) new insights about the reactivation of the "fetal program" in diseased heart settings

RESUMO

O coração adulto de mamífero tem capacidade limitada para re-estabelecer o elevado número de cardiomiócitos perdido após lesão, sendo que estes são substituídos por tecido cicatricial. No entanto, ao longo dos últimos anos, diferentes estudos reportaram renovação de cardiomiócitos adultos, apesar de limitada e insuficiente. Este facto veio revolucionar esta área de investigação, abrindo o debate sobre qual será a fonte para esta renovação: progenitores cardíacos adultos ou cardiomiócitos já presentes no miocárdio.

Nesta *Tese de Doutoramento* será apresentado e discutido trabalho original que abrange questões não resolvidas na área. Desta forma, começámos pela revisão crítica da literatura sobre o conhecimento existente acerca das células cardíacas Lin^- $Sca\text{-}1^+$ cells e outras populações com fenótipo semelhante noutros órgãos. Esta revisão da literatura levou-nos a considerar a necessidade de um estudo detalhado sobre o desenvolvimento do coração e populações que participam na sua formação, com o objectivo de identificar marcadores de superfície específicos de cada tipo celular.

De forma a colmatar esta falha no conhecimento, propusemos uma nova abordagem para analisar o coração, combinando o estudo fenótipico e multi-paramétrico com a verificação do perfil de transcritos. A nossa estratégia permitiu a discriminação das principais populações que constituem o coração ao longo do desenvolvimento. Para além da definição de diferente populações de fibroblastos e células epicardiais, identificámos duas populações de cardiomiócitos que apresentam uma assinatura

molecular específica do seu estadio de desenvolvimento. Os cardiomiócitos maduros expressam Caveolin-3, enquanto a fracção celular imatura expressa CD24, CD166 e CD146, prolifera durante o desenvolvimento embrionário e diminui ao longo da maturação do coração.

Após verificação de que as células cardíacas adultas não mantêm o fenótipo identificado na vida fetal, decidimos analisar as proteínas de superfície após lesão do miocárdio (enfarte do miocárdio e doença de Chagas). A relevância do modelo experimental de isquémia foi validada através da relação directa entre as alterações morfológicas (extensão de enfarte) e funcionais. Para além disso, procedemos à standardização da avaliação histológica da lesão por enfarte do miocárdio, de forma a permitir a comparação de resultados entre laboratórios. Nesse sentido, desenvolvemos um software semiautomático que facilita a medição objectiva da deposição de colagénio e estabelecemos um protocolo para a amostragem representativa do coração, quantificação de neovascularização e detecção de células humanas em tecido de murganho.

Por último, verificámos a expressão proteica membranar nas células cardíacas adultas após lesão. Nesta análise, verificámos a re-expressão de proteínas de superfície em ambos os modelos de lesão cardíaca, mostrando a importância no conhecimento do desenvolvimento cardíaco para melhor compreender a patologia no miocárdio adulto.

Resumidamente, esta tese de *Doutoramento* contribui para: i) caracterização de novas assinaturas de superfície que permitem discriminar diferentes populações cardíacas embrionárias; ii) desenvolvimento de novas metodologias para a standardização da avaliação histológica no contexto de enfarte do miocárdio; iii) identificação de mecanismos de re-activaçao do programa fetal em situação de lesão cardíaca.

LIST OF CONTENTS

LIST OF NON-STANDARD ABBREVIATIONS

A	Atria (*Chapter I & III*) Area (*Chapter IV*)
ALCAM	Activated Leukocyte Cell Adhesion Molecule
AV	Auriculo-Ventricular
AVC	Auriculo-Ventricular Canal
AVJ	Auriculo-Ventricular Junction
AVN	Auriculo-Ventricular Node
BSA	Bovine Serum Albumin
CADUCEUS	CArdiosphere-Derived aUtologous Stem CElls to Reverse ventricULar dySfunction
Cav3	Caveolin-3
CCC	Chronic Chagasic Cardiomyopathy
cCFU	Cardiac Colony-Forming Units
CI	Confidence Interval
CM	Cardiomyocyte
cNCC	cardiac Neural Crest Cell
CPC	Cardiac Progenitor Cell
CS	Cardiosphere
Ddr2	Discoidin domain receptor tyrosine kinase 2
d.p.i.	Days post-infection
E	Embryonic Day
EC	Endothelial Cell

ECM	Extracellular Matrix
EF	Ejection Fraction
EndoC	Endocardial Cell
EPDC	EPicardial-Derived Cell
EpiC	Epicardial Cell
ES	Embryonic System
FBS	Fetal Bovine Serum
FHF	First Heart Field
FS	Fractional Shortening
HE	Hematoxylin-Eosin
HF	Heart Failure
HIER	Heat-Induced Epitope Retrieval
HSA	Heat-Stable Antigen
HSC	Hematopoietic Stem Cell
ICAM-1	InterCellular Adhesion Molecule 1
iFB	interstitial FiBroblast
ip	intraperitoneal
KCl	Potassium Chloride
LAD	Left Anterior Descending
Lin	Lineage
LV	Left Ventricle
LVIDd	Left Ventricle Internal Dimension at diastole
LVIDs	Left Ventricle Internal Dimension at systole
MCAM	Melanoma Cell Adhesion Molecule
MCR	MATLAB™ Component Runtime
MI	Myocardial Infarction
MIQuant	Myocardial Infarction Quantification

ML	Midline Length
MMP	Metalloproteinase
MT	Masson's Trichrome
Neg	Negative
OFT	OutFlow Tract
P	Postnatal Day
PA	Primitive Atrium
PBS	Phosphate-Buffered Saline
PCA	Principal Component Analysis
PDGFr	Platelet-Derived Growth Factor receptor
PEO	ProEpicardial Organ
pH3	Phosphorylated histone H3
PIER	Proteolytic-Induced Epitope Retrieval
PV	Primitive Ventricle
r	Correlation Coefficient
ROI	Region Of Interest
RV	Right Ventricle
SAN	Sino-atrial Node
SCIPIO	Cardiac Stem Cell Infusion in Patients with Ischemic CardiOmyopathy
S.E.M.	Standard Error of the Mean
SHF	Second Heart Field
SIRP□	SIgnal-Regulatory Protein Alpha
SMC	Smooth Muscle Cell
SP	Side Population
Tβ4	Thymosin β4
T. cruzi	*Trypanosome cruzi*
Tnnt	cardiac Troponin

V	Ventricle
VCAM-1	Vascular Cell Adhesion Molecule 1
VIC	Valvular Interstitial Cell
5-aza	5-azacytidine

CHAPTER I

GENERAL INTRODUCTION

GENERAL INTRODUCTION

Adult Mouse Heart*

All living animals are dependent on an uninterrupted and long-term heart function that start early in embryogenesis and lasts throughout adulthood. Therefore, it is predictable that congenital and acquired heart disorders can have devastating effects and that heart diseases are the leading cause of death worldwide (Mozaffarian et al., 2015).

Despite the limited, nonetheless acknowledged, capacity to adapt to novel functional demands, such as the physiological growth after intense exercise (Frenzel et al., 1988) or pregnancy (Gonzalez et al., 2007), by reversible and beneficial hypertrophy (Heineke and Molkentin, 2006; Vikstrom et al., 1998), the adult mammalian heart is unable to regenerate after an injury (Zak, 1974). Distinct insults can result in heart disease, which is frequently characterized by impaired cardiomyocyte (CM) function, CMs loss, and formation of fibrotic scar tissue, decreased pump function, arrhythmias and eventual death (Hill and Olson, 2008).

This section of the General Introduction Chapter is part of the review article, from which the full version is available in the Appendix I.

Composition of the Adult Myocardium

Cell types composing the functional heart include atrial (A) and ventricular (V) CMs, smooth muscle (SMCs) and endothelial (ECs) cells, fibroblasts (FBs), valvular interstitial cells (VICs), conductive cells, and endocardial (EndoCs) and epicardial cells (EpiCs) that constitute, respectively, the inner and outer layers of the myocardium (Banerjee et al., 2006; Nag, 1980) (Figure 1). Under physiological conditions, cellular elements interact in order to maintain the electrical, chemical and biomechanical properties of the organ, as well as the three-dimensional heart structure (Nag, 1980). Briefly, the myocardium is defined by CMs organized in sheets termed *laminae*, which are surrounded by a collagen-rich extracellular matrix (ECM) and dispersed FBs. ECs and SMCs are confined to the coronary vasculature and the great vessels (inflow and outflow); ECs are also constituents of the endocardium (Borg and Caulfield, 1981; Nag, 1980). From all the heart cellular components, CMs and FBs constitute the most frequent cell types. The CM/cardiac FBs ratio composing the adult cardiac histological structure varies among mammalian species, and is estimated to be 2:1 in the murine heart (Banerjee et al., 2006). The rigorous balance between the number of CMs and cardiac FBs is tightly regulated in all animal species, since increased amount of cardiac FBs impinges on myocardial stiffness and contractility (Weber and Brilla, 1991).

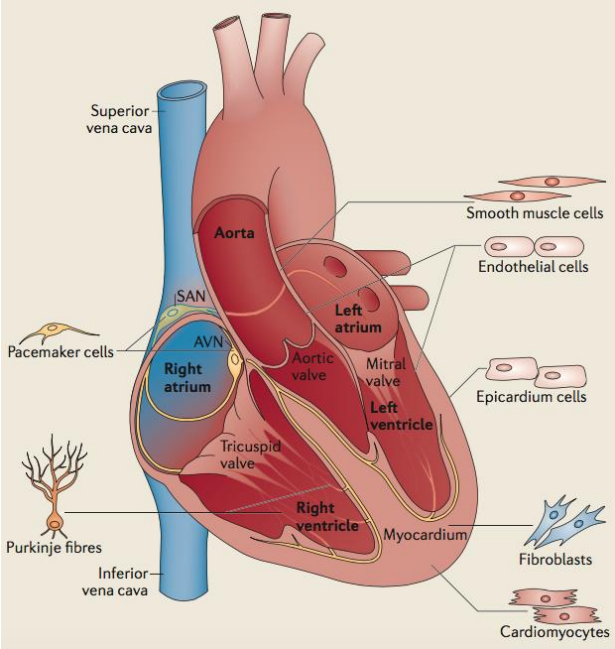

Figure 1. Adult cardiac cell types. A functional heart is composed of different cell types. A and V CMs form the myocardium walls. FBs compose the stromal compartment of the myocardium and cardiac valves (VICs). ECs form the endocardium (inner cell layer of the heart), interior surface of blood vessels and cardiac valves. SMCs contribute to the coronary vasculature and the heart inflow and outflow vasculature (superior and inferior vena cava and aorta). The epicardium is the outer layer of the heart. Pacemaker cells and Purkinje fibers in the conduction system (specialized CMs) generate and conduct electrical impulses. The SAN, composed of a group of pacemaker cells (in the RV), generate impulses to initiate heart contraction. The auriculo-ventricular node (AVN) is located between the atria and ventricles, and it conducts an electrical impulse from the A to the V. A | atria; AVN | auriculo-ventricular node; CMs | cardiomyocytes; ECs | endothelial cells; FBs | fibroblasts; RV | right ventricle; SAN | sino-atrial node; SMCs | smooth muscle cells; V | ventricles; VICs | valvular interstitial cells. Adapted from (Xin et al., 2013).

Fibroblasts are defined by the flat and spindle-shaped morphology with multiple filapodia extensions and by unique features such as the lack of basement membrane. The extensive Golgi apparatus and the large endoplasmic reticulum are structural properties that contribute for central functions of FBs: to synthesize and secrete proteins to the ECM (Howard and Baudino, 2014). Beyond the physiological ECM production, FBs proliferate at the injury environment and are responsible for maintaining myocardium integrity after cardiac injury through ECM remodeling toward replacement of the lost myocardium (Tomasek et al., 2002). Cardiac FBs also participate in the mechano-electrical signaling propagation during myocardium contraction (Kamkin et al., 2005). An important matter regarding this cell type is the

difficulty to define cardiac FBs, largely due to the lack of cell-specific surface markers (Banerjee et al., 2006; Camelliti et al., 2005; Ieda et al., 2009; Norris et al., 2009; Strutz et al., 1995). This has been further worsened by the recognized heterogeneity of the FB cellular population in the heart (Chang et al., 2002).

The combination of ECs and SMCs form the higher caliber coronary vessels and the aorta and pulmonary vessels, while capillaries are mainly constituted by ECs that establish a permeability barrier in the capillary network (Darland and D'Amore, 2001; Davis and Senger, 2005). Coronary vascular system is connected to the ascending aorta, specifically through the left coronary artery, in order to receive the oxygenated blood and distribute it in the myocardium. Arteries travel in well-defined routes along the myocardium surface (epicardial side), giving rise to branches that penetrate the muscle layer. Small muscular arteries continue the branching process and develop the extensive capillary bed that embraces all, or nearly to all, CMs. The venous return occurs again in the myocardium surface accompanying the artery routes (Reese et al., 2002). After injury, neo-angiogenesis and re-vascularization occurs firstly in the transient granulation tissue and then are established in the fibrotic scar (Virag and Murry, 2003).

CMs in the adult become highly specialized increasing their size and complexity of myofibrils organization. Additionally, CMs acquire cell rod-shape (Ehler et al., 1999) (with particular distribution of cell junctions, *i.e.* intercalated discs, at the bipolar ends), increase DNA content (Clubb and Bishop, 1984; Li et al., 1996) and decrease the proliferative activity (Zak, 1974). The highly organized sarcomere proteins observed in the cytoplasm of mature CMs may physically prevent the disassembly and reassembly sequence (process that would require very high levels of energy to complete the breakdown of sarcomeres) that have been described during CMs cell division (Ahuja et al., 2004). CMs replacement in the adult heart has indeed been extensively discussed in recent years (Hsieh et al., 2007; Senyo et al., 2013) (Uchida et al., 2013). The renewal rate and the physiologic conditions that trigger the *de novo* formation of CMs

in the adult are not consensual, therefore questioning its functional relevance. The modest figures for human CMs renewal in the resourceful work by Bergman and colleagues (1% *per annum* at the age of 25 and 0,45% at the age 75) (Bergmann et al., 2009) contrast with the much higher rates observed in a study enrolling patients submitted to radiotherapy (Kajstura et al., 2010). Likewise, mouse CMs turnover was estimated to reach values of approximately 1,3%-4% *per* year (Malliaras et al., 2013). Although some reports favour the *de novo* generation of CMs from division of pre-existing CMs (Bergmann et al., 2009; Bersell et al., 2009; Mollova et al., 2013; Senyo et al., 2013), there is no clear-cut data excluding neither the possibility that the newly formed CMs result from differentiation of adult cardiac progenitor cells (CPCs), nor the simultaneous occurrence of both processes (Hsieh et al., 2007; Malliaras et al., 2013; Uchida et al., 2013; van Berlo et al., 2014).

Immature/Progenitor Cells in the Adult Myocardium: A Critical Review

The possibility that CMs can be generated outside the boundaries of the developing heart emerged back in the 90's from the identification of interstitial cells displaying stem cell-like properties in adult mammalian heart (Warejcka et al., 1996). Since then, self-renewing, multipotent and clonogenic cardiac cells, capable of differentiation, *in vitro* and *in vivo*, into CMs and cells of the vasculature ECs and SMCs, were reported by several authors and grouped under the designation of CPCs (Smith et al., 2007). CPCs have been isolated based on the expression of surface markers (*e.g.* Sca-1 and c-Kit), on functional properties, such as the ability to efflux dyes (*e.g.* rhodamine and Hoechst 33342) – side population (SP) (Hierlihy et al., 2002; Martin et al., 2004; Oyama et al., 2007; Pfister et al., 2005; Yamahara et al., 2008), and on the capacity to migrate out of cardiac explants and grow as 3D multicellular clusters – termed cardiospheres (CSs) (Messina et al., 2004; Ye et al., 2012). The strategy to isolate CPCs by the expression of c-Kit (Beltrami et al., 2003; Gambini et al., 2011) and Sca-1 (Chong et al., 2011; Oh

et al., 2003; Takamiya et al., 2011; Tateishi et al., 2007), two surface proteins also present on hematopoietic stem cells (HSC), coincided with claims that adult hematopoietic progenitors could, under certain conditions, generate cells affiliated with different tissues (neurons and muscle amongst others) (Balsam et al., 2004; Wagers and Weissman, 2004). In the heart, this strategy led to the identification of an apparent multiplicity of CPC subsets (Table 1). It is not clear whether these various CPC subsets represent distinct and perhaps transient physiological states of a single cell progenitor or belong instead to unrelated ancestries (Lyngbæk et al., 2007; Segers and Lee, 2008). The unknown developmental origin of CPCs has also entrenched doubts on whether they constitute remnants of *bona fide* embryonic cardiac progenitors (Bearzi et al., 2007; Eberhard and Jockusch, 2005; Ferreira-Martins et al., 2012), circulating cells from the bone marrow (Fazel et al., 2006; Orlic et al., 2001; Quaini et al., 2002), or simply derive from the surrounding vasculature (Dimmeler et al., 2005; Oh et al., 2003). The multipotency of CPCs has been also questioned because most reports rely on poorly-defined protocols for cardiomyogenic differentiation, *i.e.* cellular exposure to demethylating agents (Oh et al., 2003; van Vliet et al., 2008; Wang et al., 2006b) or co-culture with CMs (Freire et al., 2014a; Martin et al., 2004; Messina et al., 2004; Pfister et al., 2005; Wang et al., 2006b); and on a minimalistic verification of cell differentiation based on the up-regulated expression of a single lineage-affiliated, but not lineage-restricted, protein (Oh et al., 2003; Oyama et al., 2007; Reinecke et al., 2008; Takamiya et al., 2011; Tateishi et al., 2007). Additionally, CPCs on their own are clearly not able to functionally restore the heart in response to an extensive cardiac injury (Lyngbæk et al., 2007; Smith et al., 2007). Nevertheless, they have been viewed as the most promising target for cell-based therapies by authors who favour CPCs as innately prone to generate heart tissue and to respond to cardiac molecular cues (Gonzales and Pedrazzini, 2009). Based on this rationale, at least two clinical trials were established in which c-Kit-expressing cells (SCIPIO) (Bolli et al., 2011) and CS-derived Sca-1^{+} cells (CADUCEUS) (Makkar et al., 2012) have been transplanted in an

autologous setting. Short-term MRI assessment indicates reduction of scar size, increased healthy heart muscle mass and attenuated adverse remodelling. Because of the escalating controversy surrounding part of this work (2011 in *Circulation Journal* (Kajstura et al., 2012) and 2012 in *The Lancet* (Bolli et al., 2011)), which seems to not be reproduced in other independent laboratories, including in our own, we focused our literature synopsis largely in the stem cell antigen-1 (Sca-1)-expressing CPCs.

Oh *et al.* first reported a population of Sca-1$^+$ cells from murine adult myocardium with telomerase activity analogous to that observed in the newborn heart. This Sca-1$^+$ population was distinct from HSCs due to their lack of CD45, CD34, c-Kit, Lmo2, GATA-2 and Tal1/Scl proteins, and also distinct from endothelial progenitor/precursor cells because they do not express CD34, Flk-1 or Flt-1. Although transcripts for cardiomyocytic structural genes were absent, these Sca-1$^+$ cells expressed transcriptional regulators indicative of cardiac commitment, *e.g.* GATA-4, Mef2c and Tef1. Moreover, this population also exhibited the prototypical endothelial marker CD31, possibly as a consequence of contaminating CD31$^+$Sca-1$^+$ ECs. Heart Sca-1$^+$ cells were reported to differentiate in CMs *in vitro,* in response to the demethylating agent 5-azacytidine (5-aza), and *in vivo* following intravenous injection in a myocardial ischemia-reperfusion system (Oh et al., 2003).

In the adult mouse, approximately 70% of heart cells express Sca-1 after depletion of CMs. The majority of these Sca-1$^+$ cells are ECs (Figure 2), a finding common to other organs, such as the liver, the lung and the brain (Kang et al., 2010; Kotton et al., 2003; Luna et al., 2004; Tsuchiya et al., 2008; van de Rijn et al., 1989).

A number of experimental animal systems were used to address Sca-1 function in the heart. Recently, Sca-1 reporter and Sca-1 lineage tracer mouse models were used to investigate the contribution of Sca-1 expressing cells to the adult myocardium. Sca-1 expression was not detected in adult CMs, in healthy or injured heart. However, the descendants of Sca-1$^+$ cells appeared to contribute to the CM compartment. This work provides evidence for a low but continuous replacement of Sca-1-derived CMs in aging

hearts (0,17±0,06 cells/mm^2, 8 months-old) and after MI (0,24±0,04 cells/mm^2, 8 months-old) (Uchida et al., 2013). Nevertheless, the low frequency of Sca-1 traced cells (a maximum of 4,5% of CMs) indicates that most CMs derive from Sca-1$^-$ progenitors. This observation, together with the data indicating that before 2 months of life Sca-1 derived CMs are virtually undetectable, is compatible with the existence of two distinct CM progenitors: one that generates most CMs during fetal life and another that generates the small number of new CMs detected in adult heart (Uchida et al., 2013). Alternatively, a few persisting CM progenitors acquire Sca-1 expression after birth. Nevertheless, a subset of myocardium-resident Sca-1$^+$CD31$^-$ cells was shown to exhibit significant proliferation at 7 days post-MI. While the proliferative response of the endogenous Sca-1$^+$CD31$^-$ appears insufficient to prevent adverse MI remodelling, this process is attenuated, with preservation of the LV contractile performance and improvement of bio-energetic properties, when Sca-1$^+$ cells are expanded *ex vivo* prior to transplantation into the injured myocardium (Wang et al., 2006b).

Table1. Schematic representation of the heart as a mosaic of progenitor cell populations identified in the myocardium (continuation). A variety of procedures have been adopted to isolate and purify a cardiac progenitor cells repertoire, either based on the expression of the stem cell-associated surface markers Sca-1 and c-Kit, on the ability to efflux dyes (eg, rhodamine and Hoechst 33342)—SP, the capacity to grow as 3D multicellular clusters—CSs or by the expression of a specific genetic marker—Wt-1 epicardial progenitors**.** The isolated populations have been subjected to phenotypic characterization and their multipotency, that is, the ability to differentiate in CMs, ECs, and SMCs, has been tested in vitro and/or in vivo, as well as the clonogenic potential. A concise summary of these results is displayed with indication of whether differentiation into a specific cell type was observed (+) in vitro and/or in vivo or if it was not determined (nd) in the specific study.

Table 1. Schematic representation of the heart as a mosaic of progenitor cell population identified in the myocardium.

Ref.	Phenotype	*In vitro* differentiation			*In vivo* differentiation			Clonogenic
		CM	EC	SMC	CM	EC	SMC	
[25]	Sca-1$^+$ Ftl-1$^-$ Flk-1$^-$ CD31$^+$ CD34$^-$ CD45$^-$	4,6%	nd	nd	<1%$^{(a)}$	nd	nd	nd
[22]	Sca-1$^+$ c-Kit$^-$ CD34$^-$ CD31$^-$ CD45$^-$ CD90$^+$ CD105$^+$ CD29$^+$ CD44$^+$ CD106$^+$ CD73$^+$ CD13$^+$	1,24%	12,4%	31,9%	100$^{(b)}$	80$^{(b)}$	120$^{(b)}$	+
[23]	Sca-1$^+$ PDGFRα$^+$ CD31$^-$ CD45$^-$ CD90$^+$ CD105$^+$ CD29$^+$ CD44$^+$ Flk-1$^-$	+	+	+	+	+	+	+
[24]	Sca-1$^+$ c-Kit$^-$ CD34$^-$ CD31$^-$ CD45$^-$ CD29$^+$	<1%	~4,5%	~30%	+	+	nd	+
[39]	Sca-1$^+$ PDGFRα$^+$ CD44$^+$ CD105$^+$CD29$^+$ CD31$^-$ CD45$^-$ Flk-1$^-$c-Kit$^-$ CD34$^-$ CD31$^-$ CD45$^-$ CD90$^-$	+	~1,75%	~27%	~9$^{(c)}$	~4$^{(c)}$	~41$^{(c)}$	+
	Side population							
[13]	Sca-1$^+$ c-Kit$^-$ Flk-2$^-$ CD34$^-$ Thy1.1$^-$	nd	nd	nd	nd	nd	nd	+
[14]	Sca-1$^+$ Abcg2$^+$ c-Kit^{low} CD45^{low} CD34^{low} CD31$^-$	+	nd	nd	nd	nd	nd	nd
[15]	Sca-1$^+$ c-Kit$^-$ CD31$^-$ CD45$^-$ CD44$^-$ CD34$^-$	+	nd	nd	nd	nd	nd	+
[16]	CD29$^+$CD31$^{+/-}$ CD45$^{+/-}$	5,5%	nd	nd	4,4%	6,7%	29%	nd
[17]	Sca-1$^+$ VE-cadherin$^-$ CD34$^+$ CD73$^+$ CD90$^+$ CD105$^+$ CD45$^-$	+	nd	nd	nd	nd	nd	nd
	Epicardial-derived progenitors							
[92]	Sca-1$^+$ c-Kit$^-$ CD31$^-$ Flk-1$^-$	nd	nd	nd	+	nd	nd	nd
	Sphere formation (*cardiospheres*)							
[18]	Sca-1$^+$ c-Kit$^+$ CD31$^+$ CD34$^+$ Flk-1$^+$	+	+	+	+	+	+	+
[19]	Sca-1$^+$ c-Kit$^-$ CD31$^-$ CD34$^-$ CD45$^-$ CD29^{low} CD133$^-$ Flk-1$^-$	~60%	~20%	~34%	~10%	~10%	~10%	+
	c-Kit$^+$ cells							
[20]	c-Kit$^+$ CD45$^-$ CD34$^-$ CD20$^-$ CD45RO$^-$ CD8$^-$ Ter119$^-$	+	+	+	+	+	+	+
[21]	c-Kit$^+$ CD29$^+$ CD44$^+$ CD105$^+$ CD90$^+$	+	+	+	nd	nd	nd	nd

(a) Percentage of diffentiated myocytes; *(b)* Cells/mm^2; *(c)* Cells/heart section

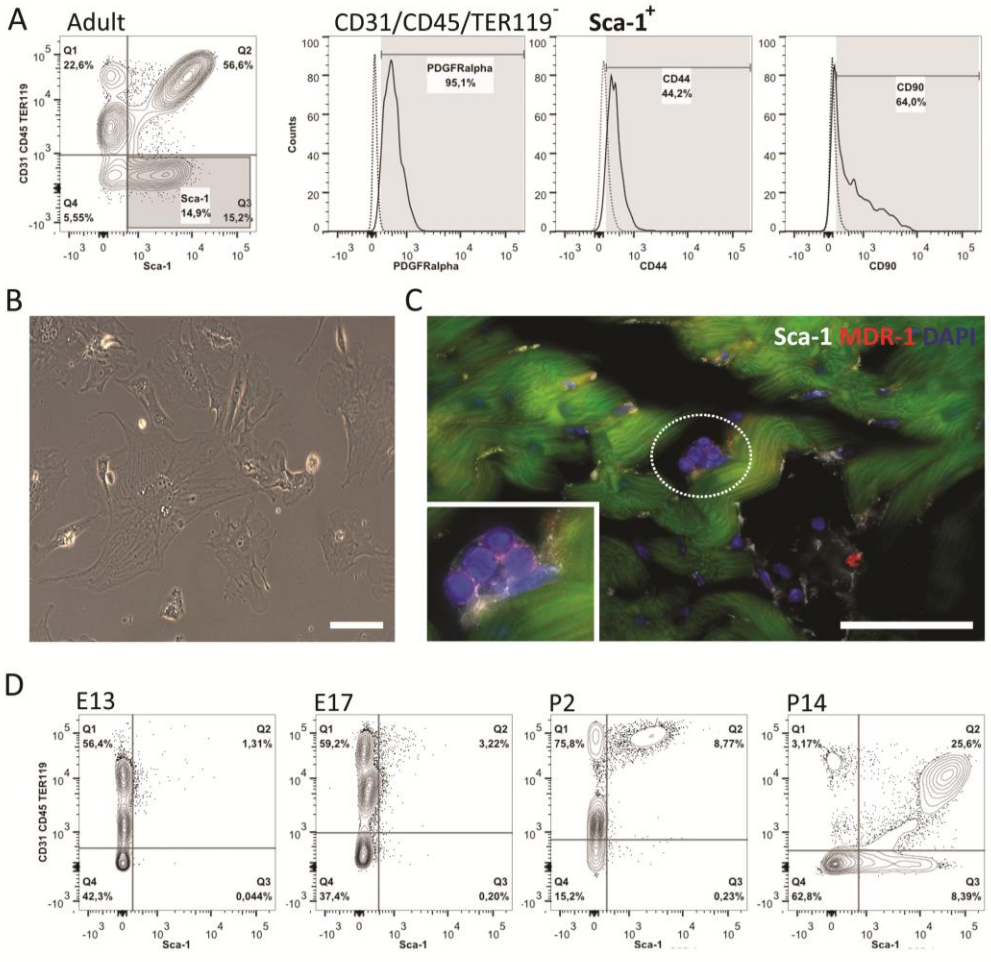

Figure 2. Heart resident Sca-1$^+$ cells – an overview. A. Following collagenase digestion, the adult heart single cell suspension is depleted of CMs. Lin$^-$ (CD31$^-$, CD45$^-$, TER119$^-$) cells constitute a minority of the Sca-1$^+$ population within the heart, which is consistent with the reported expression of this marker also by mature EC. **B.** Lin$^-$ Sca-1$^+$ cells display mesenchymal-affiliated markers (PDGFRα, CD44 and CD90) and plastic-adherence. Scale bar 10 µm. **C.** Sca-1$^+$ cells that do not integrate the vasculature are scattered in small clusters through the myocardium, displaying also the SP-affiliated protein MDR-1. Scale bar 50 µm. **D.** To address the ontogenic origin of the Sca-1$^+$ population we examined the emergence of this population in the heart by flow cytometry of whole-heart single cell suspensions. Lin$^-$Sca-1$^+$ cells appear in the heart around E17 although the establishment of both Sca-1$^+$CD31$^+$ and Sca-1$^+$CD31$^-$ cellular compartments only occurs following birth.

Considering the other possibility, where pre-existing CMs are the potential cell source that contributes to the postnatal myocardium growth, Senyo and collaborators have described that CMs derive from pre-existing CMs at a projected rate of 0.76% per year in young adult mouse and under physiological conditions. This rate decreases with the ageing process but slightly increase after injury. Thus, this model has shown that adult CMs retain some ability to re-enter in cycle but without completion of cell division (Senyo et al., 2013). The postnatal metabolic shift from anaerobic glycolysis to oxidative phosphorylation characteristic of the postnatal breath (*i.e.* hyperoxygenation) mediates CMs cell cycle arrest by DNA damage response (Puente et al., 2014). Following the reasoning that proliferative CMs are under hypoxic conditions thereby protected from the oxidative stress responsible for DNA damage, Kimura *et al.* developed a fate mapping of hypoxic cells and their subsequent progeny in the myocardium. They identified a scarce population of hypoxic, mononucleated, small sized CMs with low levels of DNA damage, which appear to contribute at some extent to adult myocardium (Kimura et al., 2015). Previous studies also drive forward the hypothesis that an immature CM compartment in the adult myocardium is responsible for the muscle cell turnover. Nevertheless, this is not the only possibility under discussion as other perspectives have been highlighted. Work by Naqvi *et al.* claimed that there are two distinct periods of rapid CMs proliferation during mouse postnatal life: a first one between postnatal day (P)1 and P4 and a second period between P14 and P18. The first period of dividing CMs is in accordance with the previous description of Senyo and colleagues, while the second period reports a proliferative burst spatially restricted to the LV and to the subendocardial zone. Additionally, during the second period of proliferation CMs undergoing mitosis (assessed by nuclear Aurora B kinase staining) were from both populations, *i.e.* the mononucleated and the binucleated CMs. Therefore, authors claim that the burst of CMs proliferation at P15, *i.e.* in the pre-adolescence stage, is responsible for the main fraction of heart growth during transition

to the adult size and that part of this proliferation occurs in binucleated CMs (Naqvi et al., 2014). This process seems to be specific of the mouse heart maturation, since such burst of proliferation has not been detected in human adolescents (Mollova et al., 2013). Altogether, these recent reports give at least two prospects for the mechanisms of CMs proliferation: either there is a population of less mature CMs that retain the ability to proliferate and to maintain their pool, or, CMs may proliferate randomly irrespective of their nuclear content.

How to Define Heart Cells and their Progenitors

As described in the previous sections, there is clear heterogeneity in the heart $Lin^{-}Sca\text{-}1^{+}$ population, suggesting that several functionally distinct fractions may co-exist in this cellular compartment. The latter may therefore contain a smaller subset of CPCs responsible for the multipotent phenotype described by many authors (Chong et al., 2011; Freire et al., 2014a; Oh et al., 2003; Takamiya et al., 2011; Tateishi et al., 2007). Cell subsets involved in cardiogenesis have been mainly identified using genetic tracing models. While attempting to correlate the described adult CPCs and cardiovascular embryonic progenitors, Wu and colleagues studied the expression of Sca-1 and c-Kit using a Nkx-2.5-expressing transgenic mouse. These authors reported that cardiac progenitors expressing the transcription factor Nkx-2.5 also display modest levels of c-Kit and Sca-1; although, efforts to clonally expand these cells were unsuccessful (Wu et al., 2006). On the other hand, another work by Chong *et al.* indicated that Sca-1 expression is not detected in the heart before mid-gestation (Chong et al., 2013).

It seems clear that the understanding we had on Cardiovascular Biology is undergoing a conceptual shift in which detailed investigation on the proliferative capacity of the CMs has become a main focus, and thus, a new paradigm brings new questions. One

major question is the identification of proliferating CMs and the characterisation of their source. Several studies have attempted to identify specific surface markers for the isolation of CMs based on the expression of CD106 (or VCAM-1) (Ponten et al., 2013) and CD166 (or ALCAM) (Hirata et al., 2006) in developing murine CMs, SIRPα in human-derived CMs (Dubois et al., 2011) and Caveolin-3 (Parton et al., 1997) in adult CMs. Knowledge on whether these surface markers are co-expressed in the same cell and/or whether each of the markers is represented at different stages of differentiation towards a mature CM is elusive. Of relevance, the selection of a particular cell type based on the expression of a single surface protein is difficult to establish, especially considering that different cell types within an organ-system or from different organs can have a similar surface protein expression. For the heart, in close contact with circulating blood cells (often contaminants in the cellular preparations), a careful discrimination of the hematopoietic cells is mandatory. Even when using genetic tracing experimental systems, accurate knowledge on the spatiotemporal expression pattern of the tracer-gene, and preferentially the monitoring of co-expression of more than one gene, is required to properly interpret the data. Thus, as it has been discussed in this *Thesis*, a consensual strategy to accurately distinguish the cardiac cellular population or their progenitors is not available.

Overview of Mouse Heart Development*

Despite being a highly specialized organ composed of distinct cell types that arise from different embryonic progenitor cells during cardiogenesis, the mammalian heart is the first functional organ during embryogenesis (Lyons, 1996). During heart morphogenesis a series of events occurs to assemble the different sources of cardiac progenitors and reach the final functional structure. Starting at E7.5 the cardiac crescent contains the first progenitor cells that migrate ventrally to form a simple heart tube structure (E8.0). The heart tube loops rightwards in order to reach the four-chambered organ (E14.5) characteristic of mammals (Harvey et al., 2009). This final heart structure is constituted by two A, two V and the auriculo-ventricular junction (AVJ), which includes auriculo-ventricular (AV) valves, great vessels (inflow and outflow) and conduction system (Efimov et al., 2004) (Figure 3).

Molecular mechanisms involved in specifying cardiovascular progenitors into a terminally differentiated cell of the four-chambered fetal heart are not fully disclosed. This knowledge is however crucial to comprehend both, the normal development of the heart, as well as the mechanism subjacent to disease (*e.g.* congenital heart disease, failure of the ischemic heart, etc.).

Cardiac Cell Sources and Early Cardiac Morphogenesis

The majority of cells that compose the heart have a mesodermal origin (Herrmann et al., 1990). Three spatially and temporally distinct progenitor populations contribute to the embryonic heart: cardiogenic mesoderm cells (CMCs) (Kitajima et al., 2006; Saga et al., 1999), proepicardial organ cells (PEO) (Perez-Pomares et al., 2003; Viragh and

* *This section of the General Introduction Chapter contains parts of the review article, from which the full version is available in the Appendix I*

Challice, 1981) and non-mesordermal cardiac neural crest cells (cNCC) (Jiang et al., 2000) (Figure 4).

CMCs are multipotent and, through progressive lineage restriction, contribute to CMs, SMCs and EndoCs (Epstein, 2010; Kattman et al., 2007; Moretti et al., 2006). The first heart structure, the cardiac crescent, is formed at embryonic day (E)7.5 as result of a first wave of CMCs-derived progenitors designated as first heart field (FHF) (Lints et al., 1993; Lyons et al., 1995; Takeuchi et al., 2003). At E8-E8.5, FHF progenitors fuse at the embryo midline, giving rise to the heart tube that initiates the pumping function (Navaratnam et al., 1986; Nishii and Shibata, 2006). At this stage, the heart tube is a simple structure composed by a layer of CMs underlying EndoCs and an interposing proteoglycan-rich ECM – the cardiac jelly (Nakamura and Manasek, 1981). The heart tube is composed by FHF-derived CMs that will mainly contribute to the future left ventricle (LV) (Cai et al., 2003; Srivastava, 2006; Stanley et al., 2002; Wu et al., 2006; Zaffran et al., 2004) (Figure 3).

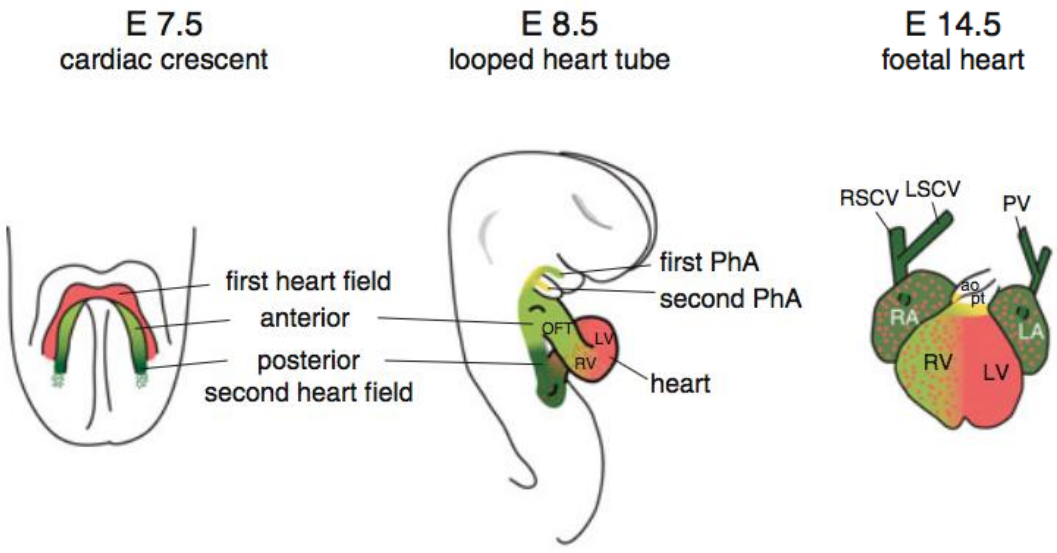

Figure 3. First (FHF) and second (SHF) heart fields and their cellular derivatives. Overview of the heart morphogenesis and the main steps where the color code highlights the location of each cellular progenitor population: the FHF (*in red*) and SHF (*in green*). The latter can be subdivided into anterior (*in light green and yellow*) and posterior (*in dark green*) domain added to the arterial and venous pole (respectively) of the heart tube. ao | aorta; LA | left atrium; LSCV | left superior caval vein; LV | left

ventricle; OFT | outflow tract; PhA | pharyngeal arches; pt | pulmonary trunk; PV | pulmonary vein; RA | right atrium; RSCV | superior caval vein; RV | right ventricle. Adapted from (Lescroart and Meilhac, 2012).

Tbx5 and HCN4 have been suggested as FHF-specific markers (Bruneau et al., 1999; Spater et al., 2013). At the same time, the second heart field (SHF) lineage is determined, in the splanchnic mesoderm dorsally adjacent to the cardiac crescent. These progenitors, characterized by Isl1 expression, migrate then to both poles of the heart tube and contribute for the compartmentalization of the four-chambered heart (anterior/arterial and posterior/venous poles). Genetic lineage-tracing studies have determined the contribution of each SHF domain to the right ventricle (RV, expressing Isl1, Fgf10 (Cai et al., 2003; Zaffran et al., 2004), both A (Isl1, (Cai et al., 2003) and the outflow tract (OFT) (Isl1, Fgf8, Fgf10, Tbx1, (Cai et al., 2003; Kelly et al., 2001; Viragh and Challice, 1973). Despite evidence supporting an early segregation of both myocardial lineages at the primitive streak stage (E6.5) (Tam et al., 1997) lineage tracing analysis of the Isl1 and Nkx2-5 expression suggested the existence of a common origin, demonstrating the contribution of Isl1-expressing cells to CMs of both FHF and SHF (Ma et al., 2008; Prall et al., 2007) (Figure 4).

The endocardium, the inner layer of the heart tube, is composed by EndoCs that also derive from CMCs. In specific regions of the heart tube, namely the auriculo-ventricular canal (AVC) at E9.5 and the OFT at later stages, EndoCs undergo endothelial-to-mesenchymal transition originating the endocardial cushions located between the endocardial and myocardial layers. Endocardial cushions constitute the precursors of the cardiac valves, express Nfatc1 and other endothelial genes (de Lange et al., 2004; Eisenberg and Markwald, 1995; Wu et al., 2011) and are also crucial for septation of the four-chambered heart (Ranger et al., 1998) (Figure 4).

Between E9.5 and E11.5, transient extra-cardiac structures contribute to heart morphogenesis: the PEO and cNCC. PEO-derived cells (coelomic mesenchyme-

derived) express Wt1 (Zhou et al., 2008) and Tbx18 (Cai et al., 2008) (Schulte et al., 2007; Viragh and Challice, 1981) and give rise to the epicardium; they also invade the subepicardial space and the myocardium (Wu et al., 2010), differentiating into interstitial fibroblasts (iFBs) (Ieda et al., 2009; Zhou et al., 2008) and SMCs of the coronary vasculature (Manner, 1999; Mikawa and Gourdie, 1996). Additionally, EpiCs contribute to AV endocardial cushions and to the fibrous annulus, a collagen-rich structure that anchors the valves and separates A from V, promoting a stepwise and synchronized propagation of the electrical impulse (Gittenberger-de Groot et al., 1998). Yet, the contribution of EpiCs to CMs of specific heart regions (Cai et al., 2008; Christoffels et al., 2009; Zhou et al., 2008), as well as to ECs, remains controversial (Cai et al., 2008; Manner, 1999; Mikawa and Gourdie, 1996; Red-Horse et al., 2010; Zhou et al., 2008). cNCC derived from the dorsal neural tube at E9.5, migrate through the 3, 4 and 6 pharyngeal arches, express Pax3, and give rise to SMCs of the distal OFT, the aortico-pulmonary ridge, the ventricular septum, the valves and to the autonomous nervous system of the heart (Jiang et al., 2000; Kirby and Waldo, 1995) (Figure 4).

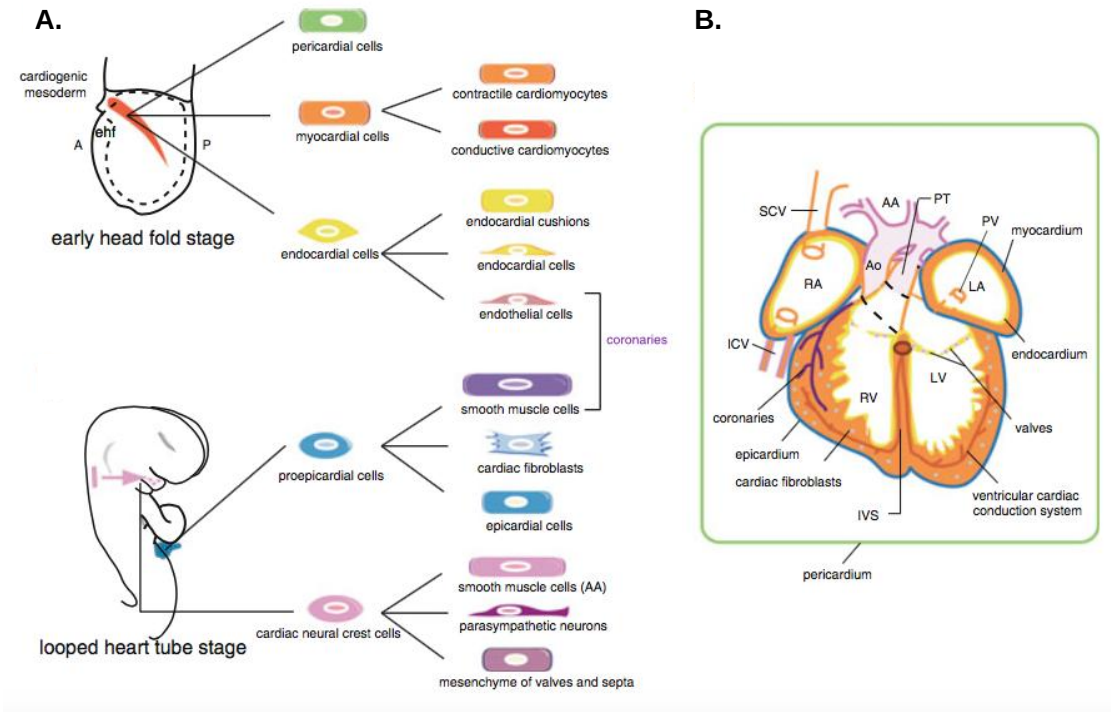

Figure 4. Schematic representation of the cardiac lineages. A. Lineage tree of the distinct cardiac cell types from three origins: i) cardiogenic mesoderm cells (CMCs, *in red*) that give rise to endocardium (*in yellow*), myocardium (in red) and pericardial sac (*in green*) at E6.5; ii) proepicardial organ (PEO, *in blue*); and iii) cardiac neural crest cells (cNCC, *in purple*) at E9.5. **B.** Representative longitudinal section of the fetal heart with the respective color code of each cell type location. A | anterior; AA | arch arteries; Ao | aorta; ehf | early head fold; ICV | inferior caval vein; IVS | interventricular septum; LA | left atrium; LV | left ventricle; P | posterior; PT | pulmonary trunk; PV | pulmonary vein; RA | right atrium; RV | right ventricle; SCV | superior caval vein. Adapted from (Lescroart and Meilhac, 2012).

Development and Growth of the Heart Chambers

Cardiac morphogenesis is a highly dynamic process: migration and colonization of the heart by distinct progenitors occurs at the same time as the organ is gaining its final shape and pumping blood to the whole embryo (Nishii and Shibata, 2006; Nonaka et al., 2002).

CMs of the heart tube are poorly striated, displaying few organized sarcomeres in a polyhedral, sometimes almost round cell shape, where the nucleus occupies the major part of the cell, have immature electrophysiological properties (Perriard et al., 2003;

Sedmera et al., 2003), and express Nkx2.5, Gata4, α-cardiac actin and Mlc2v (Barton et al., 1988; Prall et al., 2007; Sassoon et al., 1988). While the primitive heart tube (around E10.5) undergoes looping, a significant part of the wall growth and thickness results from the expansion of CMs of the outer curvature by a process called ballooning (Christoffels et al., 2000; Sedmera and Thompson, 2011) (Figure 5 and 6).

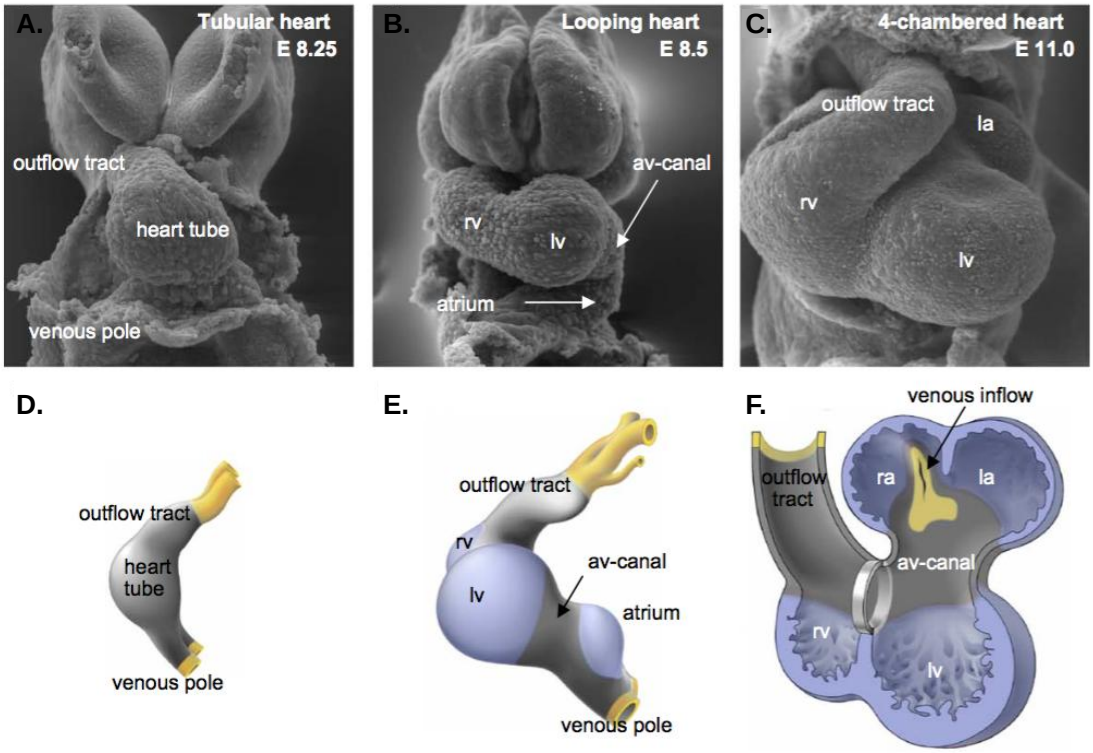

Figure 5. Cardiac chambers development and the model of ballooning process. Top panel - Scanning electron micrographs of mouse embryos ventral view, corresponding to the period from E8.25 to E11.0. **A.** Linear heart tube stage, where the heart is a straight tube at the midline of the embryo. **B.** V chambers of the heart tube during rightward loop. The AVC is located between the V loop and the primitive A. **C.** At E11.0, future cardiac chambers are recognizable, as well as the future A and V septa. **D. – F.** Lower panel – Schematic representation of the same heart morphogenesis stages of the top panel, where the future myocardium is represented in blue; the future non-muscle structures are represented in grey; and in yellow the venous and arterial poles. A | atria; AVC | auriculo-ventricular canal; LV | left ventricle; RV | right ventricle; V | ventricles. Adapted from (Boogerd et al., 2009).

The myocardial architecture of the ventricular wall during ballooning is organized in two distinct layers: the trabeculae, consisting of sheet-like myocardial protrusions into the lumen that allow proper oxygenation of the tissue prior to the establishment of coronary

circulation (Minot, 1900; Van Mierop and Kutsche, 1985); and the compact layer, at the basal portion of the trabeculae (Sedmera et al., 1997). During embryo development, myocardial growth relies mostly on CM cell division (hyperplasia) (Oparil et al., 1984). This hyperplasic growth is highly regionalized (de Boer et al., 2012; Sedmera and Thompson, 2011), as cardiomyocytic proliferation displays a distinct pattern throughout the myocardial wall (Meilhac et al., 2004a; Meilhac et al., 2004b; Meilhac et al., 2003): CMs of the trabecular fraction are more differentiated and display lower mitotic rates (de Boer et al., 2012; Sedmera et al., 2003), whereas their counterparts at the compact zone remain highly proliferative and contribute for a noticeable expansion of the ventricular wall (Sedmera et al., 2003) (Figure 6). This high proliferative ability observed was shown to underlie the great regenerative potential of the organ at the embryonic/fetal heart stage. Drenckhahn and colleagues developed a genetic model of CMs ablation at mid-gestation stage, and observed that this extensive CMs loss is resolved by compensatory growth of the myocardium (Drenckhahn et al., 2008). The majority of the proliferating cells in the mutants were CMs, thus indicating that a cell cycle-based mechanism in differentiated cells is favored in detriment of growth mediated by stem/progenitor cells. This work has thus indicated that the embryonic/fetal heart is capable to regenerate after a significant loss of CMs due to the ability of these cells to proliferate at early developmental stages (Drenckhahn et al., 2008). Contrarily to skeletal muscle cells, in which proliferation and differentiation are mutually exclusive cellular processes (Ahuja et al., 2004), functional CMs are capable to undergo karyokinesis and cytokinesis. This evidence indicates that differentiation and maturation of the CM lineage do not follow the conventional stem cell-based mechanism of organ growth.

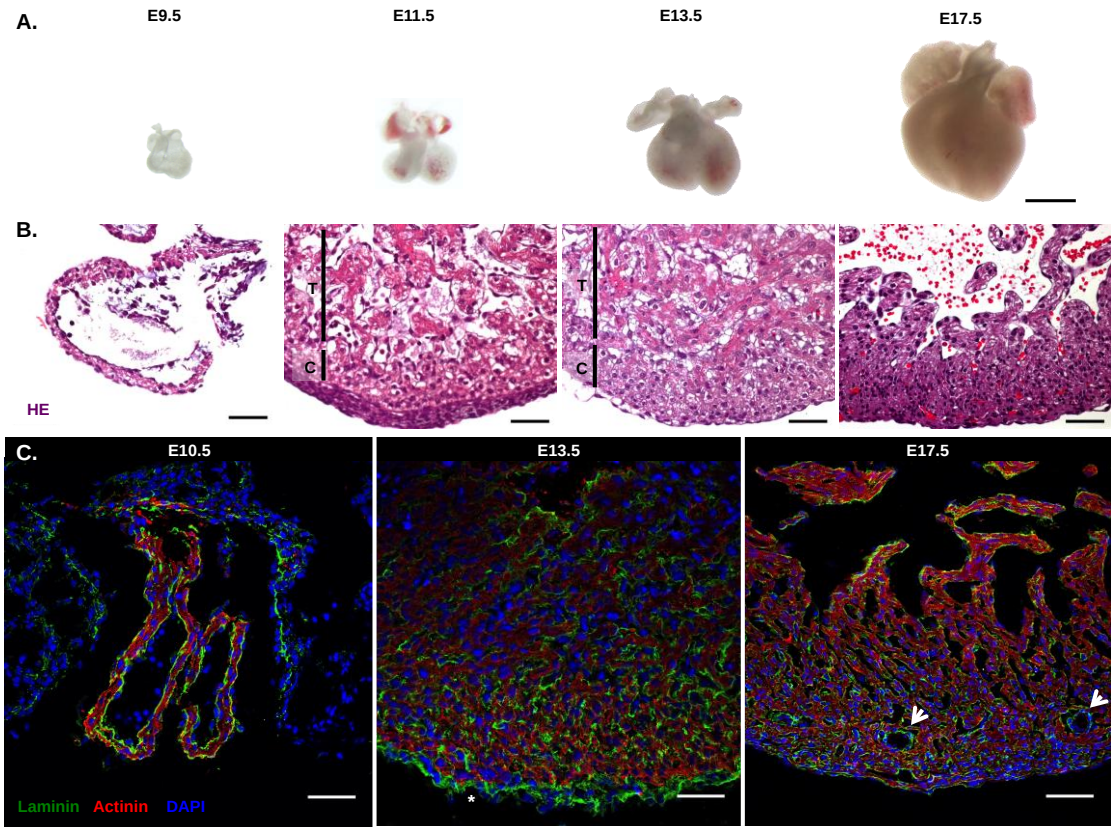

Figure 6. Overview of heart histogenesis throughout development. A. Macroscopic view of cardiac morphogenesis from the folded heart tube (E9.5) until the final four chambered-structure (E17.5). Scale bar 1 mm. **B, C.** Representative images of the heart morphology along development by HE and immunofluorescence staining. The heart evolves from a single myocardial layer (E9.5-E10.5), composed mainly by CMs and ECM (HE, Actinin and Laminin expression) to a multilayer tissue. From E11.5 onwards C and T zones are easily distinguished (HE and Actinin). Absence of Actinin expression and enrichment for Laminin staining allows the identification of the sub-epicardial region on E13.5 (*). At E17.5, the highly organized sarcomeres in the *trabecula* evidence CM maturation; big vessels can also be observed (white arrow). Scale bars: 50 μm. C | compact zone; CMs | cardiomyocytes; ECM | extracellular matrix; HE | hematoxylin-eosin; T | trabecular zone. *Unpublished*.

Along development, and concomitantly with the described morphologic and cellular modifications, V and A chambers acquire a working phenotype characterized by fast conducting and contracting myocardium. Then, A and V myocardium are separated with the formation of a membranous fibrotic tissue called fibrous annulus or AV ring, derived from the epicardium, which contributes to the AVJ formation (Bakker et al., 2012; Sizarov et al., 2011). In the AV ring, the AV node is developed at the posterior

regions of the AV canal (or the future AVJ) (Christoffels et al., 2010; Sizarov et al., 2011), and represents a slow-conducting tissue that synchronizes the electrical impulse in the ventricular walls. The direct communication of the electrical impulse to the V apex is mediated by the bundle of His and two branches endowed with fast conducting properties. These elements assure the contraction of the heart apex before the base, the simultaneous contraction of both V and the consequent ejection of blood through the OFT (Houyel et al., 2013).

Besides CMs proliferation and conduction system formation, proper chamber development relies on important processes (*e.g.* septation, establishment of the coronary vasculature and the definition of the stromal compartment of the myocardium), which are accompanied by the maturation of the different cell lineages. Septation of the heart tube occurs at three levels: A, V and the arterial pole, and can be muscular (between chambers) or valvular (in the AVJ and in the great vessels). Upon septation, connection of the coronary vasculature to the aorta artery is one of the last events taking place in heart development. The coronary vasculature, specifically SMCs, originates from EpiCs (Tian et al., 2013) and connects the subepicardial zone to the myocardium but not to the V lumen. In contrast to the avian heart, mammals lack sinusoids establishing the connection between the coronary circulation and the chamber cavity (Wada et al., 2003). During formation of the coronary arteries, a decreasing gradient of oxygenation is established from the epicardium to the endocardium (Guimaraes-Camboa et al., 2015; Tian et al., 2013). Simultaneously to development of vascularization, FBs increase in number and accumulate in the cardiac *interstitium*, modulating the composition of the ECM (Baudino et al., 2006; Ieda et al., 2009). The multiple cell sources for cardiac FBs may explain their heterogeneity from prenatal stages onwards (Baudino et al., 2006). For example VICs, which are derived from endocardial cushions and thus from EndoCs, are also classified as FBs and contribute to valves formation (membranous-structure enriched in collagen) (Eisenberg and Markwald, 1995; Kovacic et al., 2012; Markwald et al., 1977). On the other hand,

myocardial iFBs are predominantly derived from EpiCs progenitors (Krenning et al., 2010). During ventricular wall growth, iFBs play an important role in the proliferation of CMs in the compact zone (Ieda et al., 2009). In fact, the absence of epicardium results in decreased thickness of the compact layer and defective cardiac function, ultimately leading to embryonic lethality (Manner et al., 2005). It is unclear whether the thin myocardium is unable to compact or if the differentiation into FBs is affected.

Postnatal Growth

Following birth and due to the oxygen demands of the growing organism, the postnatal heart needs to increase in size. The postnatal heart growth can be divided in three phases: hyperplasia (until P4), a transitional phase with simultaneous hyperplasia and hypertrophy (between P5 and P15) and hypertrophy (from P15 onwards) (Clubb and Bishop, 1984; Leu et al., 2001). Although CMs differentiation initiates early in development, terminal differentiation/maturation is only observed after birth (Hirschy et al., 2006; Li et al., 1997a; Li et al., 1997b). Thus, during the first two weeks of life, postnatal murine CMs progressively undergo a final round of DNA synthesis and karyokinesis in the absence of cytokinesis, which culminates in the binucleation of the vast majority of myocytes (approximately 90%) around P14 (Clubb and Bishop, 1984; Li et al., 1997a; Li et al., 1996; Li et al., 1997b; Soonpaa et al., 1996; Walsh et al., 2010). CMs terminal differentiation varies depending on the mammal species. Contrarily to the mouse, humans present a much lower proportion of binucleated CMs (approximately 35%), which is maintained through adulthood, whereas mononucleated CMs can be highly polyploid (Mollova et al., 2013). Terminal differentiation has been related with loss of regenerative capacity. Porrello *et al*. have demonstrated, using cardiac injury models of apex resection (amputation of 15% of the V tip) and myocardial infarction (permanent ligation of left coronary artery), that the neonatal

mouse heart shows complete myocardium restoration at 21 days post-injury (d.p.i.). Interestingly, the ability to efficiently regenerate the heart is lost if the injury is performed after P7 (Porrello et al., 2011; Porrello et al., 2013). This period in postnatal life coincides with the developmental window in which murine CMs lose their proliferative capacity and become multinucleated (Li et al., 1996; Soonpaa et al., 1996). Genetic lineage tracing studies indicated that the majority of regenerated CMs were derived from proliferation of pre-existing cardiac muscle cells (Ali et al., 2014a; Porrello et al., 2013), resembling observations in the zebrafish model of experimentally-induced cardiac injury (Poss et al., 2002).

Despite the proliferative ability of CMs during adaptation of the perinatal heart to the new functional demands (Li et al., 1996; Soonpaa and Field, 1998), the hypertrophic growth acquires a significant importance for the increase in organ size after birth (Clubb and Bishop, 1984). CMs hypertrophic growth consists in the progressive accumulation of sarcomeric proteins in the cytoplasm (Hirschy et al., 2006), which can lead to a 15-fold increase in their size until adulthood (Leu et al., 2001). The hypertrophic growth leads also to the package of myofibriblls strictly aligned in parallel, originating the well-known shape of cardiac muscle cells (*i.e.* rod-shaped, with the bipolar ends composed of intercalated discs) and opposing to the round shape of embryonic CMs (Hirschy et al., 2006) (Perriard et al., 2003).

The formation of the coronary vasculature begins at mid-gestation (Tian et al., 2013) and usually is described as part of a developmental process; however, the postnatal myocardium growth imposes further development of the coronary vasculature. Tian and colleagues (2014) have shown, using genetic lineage tracers, that a significant proportion of the coronary tree is established only after birth. The postnatal coronary vessels derive from the endocardial layer and are localized in the inner half of the ventricular wall. The model proposed by these authors suggests that EndoCs, covering the surface of trabecular myocardium, are induced to form vessels in order to supply the newly compacted myocardium (Tian et al., 2014). Increased FBs density is also an

important process contributing to the growth of the organ size and to the modulation of the stromal cellular compartment and ECM of the postnatal heart, crucial for the re-distribution of the pumping force (Borg et al., 1981; Borg et al., 1984; Miragoli et al., 2006) (Bing et al., 1997). The active remodeling of the stroma takes place during the first week of life and promotes rapid acquisition of the adult heart shape (Norris et al., 2008). Although the source of FBs in the postnatal heart is still elusive, two hypotheses have been proposed: proliferation from pre-existing FB populations (hyperplasic growth) and recruitment of progenitor cells (Bing et al., 1997; David Sedmera, 2000; MacKenna et al., 2000; Norris et al., 2008) (Figure 7).

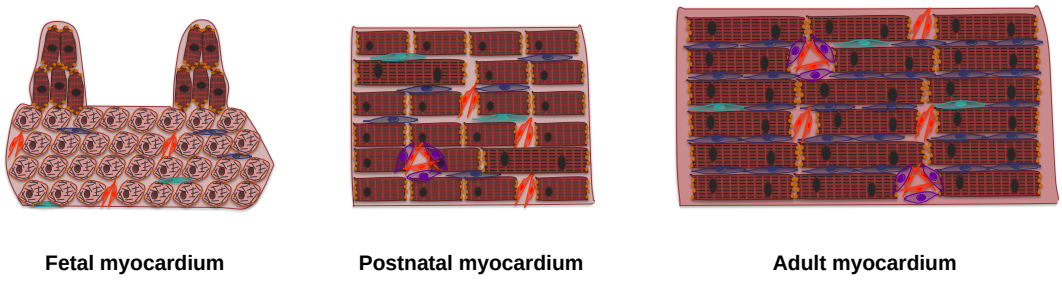

Figure 7. Schematic representation of the ventricular myocardium maturation. Dispersed CMs (dark and light pink), FBs (blue and green) and capillaries (ECs, orange) characterize the fetal myocardium stage. Postnatally, myocardium is characterized by the progressive elongation and polarization of CMs, higher amount of aligned FBs and the maturation of coronary vasculature (SMCs, purple). In the adult stage, CMs are mainly binucleated and surrounded by aligned FBs and coronary vasculature. CMs | cardiomyocytes; ECs | endothelial cells; FBs | fibroblasts; SMCs | smooth muscle cells. *Unpublished*.

Experimental Approaches to the Murine Heart

Besides the importance of a detailed knowledge on heart development and maturation, methodologies used for analysis and “visualization” of the heart are crucial. Hence, this section intends to provide an integrative view from the selection of the appropriated *in vivo* model to assess the functional profile of the cardiac cells and to the selection of the accurate techniques to apply in subsequent analyses. Currently, genetic models for lineage tracing in combination with histological analysis are gold-standard and have

been extensively used to investigate cell differentiation and ancestries under physiological or pathological conditions. Correct interpretation and evaluation of the generated data is a central aspect in these genetic approaches. Among other hurdles, there is a considerable overlap in the expression of a given gene in different cell types thus impairing precise cellular identification based solely on expression of one or two genes. An additional request is the use of appropriate representation and methodologies while analyzing the heart. After selection of the suitable experimental-induced injury model that closely recapitulates clinical relevant features of a particular human disease, the criteria used to select parameters for posterior evaluation are also decisive.

Hence, we have envisaged a strategy to aid on the assigning of unique signatures to the cell populations comprised in the heart, while also enabling prospective identification of cardiovascular progenitors throughout myocardium development. We postulated this could be accomplished by discriminating cell populations, through the use of a panel of cell surface proteins, in combination with detailed analysis of the expression pattern of genes relevant in cardiac development. Subsequent profiling of the discriminated cardiac populations at the single cell level is expected to increase the power of the analysis with information on the heterogeneity of the populations and hierarchical relation between heart cells.

Animal Models to Study Cardiac Disease

The pathophysiology of cardiovascular disease and its repair are complex and multifactorial, requesting an integrative perspective of a living organism. To achieve this, distinct animal models have been developed. Some of the generated models closely mimic the adverse consequences of human cardiac diseases and, indeed, knowledge on the pathogenesis and the current therapies have partially derived from research on experimental animal models (Holmes et al., 2005; Klocke et al., 2007).

Disease-specific animal models have been established to study heart failure (HF), arrhythmias (Nishida et al., 2010), atherosclerosis (Zaragoza et al., 2011), aneurysms (Houser et al., 2012) and myocarditis (Santos Lima and Minoprio, 1996).

Experimental animal models, in which blockage of the coronary blood flow is commonly recreated through the occlusion of the left coronary artery, have been extensively used to study the pathophysiology of the myocardial infarction (MI) or ischemia (Holmes et al., 2005; Klocke et al., 2007; Michael et al., 1995). Following coronary artery occlusion, extensive CMs death and necrosis occur (Dobaczewski et al., 2010; Nah and Rhee, 2009; Sutton and Sharpe, 2000). Next, macrophages and other inflammatory cells phagocyte the necrotic myocardium and stimulate the chemo-attraction to the ischemic zone of myofibroblasts and ECs, which will be pivotal players in the formation of the granulation tissue. This transient structure is enriched in proteoglycans, osteopontin and fibronectin, and prevents rupture of the wall after CMs loss (Dobaczewski et al., 2010; Yano et al., 2005). The maturation phase of the V wall remodeling begins with the accumulation and cross-linking of ECM proteins (in particular type I and III collagen fibers) that mainly align in circumferential direction in accordance to the orientation of cardiac myofibers (Janicki and Brower, 2002; Sun et al., 2002), thus providing mechanical support to the infarcted heart (Dobaczewski et al., 2010). Following the formation of a fibrotic scar, that equilibrates distending and restraining forces, the production of collagen is down-regulated and most myofibroblasts and vascular cells undergo apoptosis, leading to a dramatic thinning of LV wall (Janicki and Brower, 2002; Sutton and Sharpe, 2000). At this stage of the remodeling process, cardiac architectural changes related with scar formation, time-dependent chamber dilatation and hypertrophy of the viable myocyte affect the global LV geometry (Janicki and Brower, 2002; Lutgens et al., 1999; Porter and Turner, 2009; Yang et al., 1999). These geometrical changes of the heart after MI are referred to as cardiac remodeling and are associated with morbidity, higher incidence of arrhythmias and the development of heart failure (Dobaczewski et al., 2010).

Moreover, infections caused by viruses, bacteria, protozoa and fungi, are major etiological factors in clinical myocarditis and progressive HF. Experimental mouse model of Chronic Chagasic cardiomyopathy (CCC) is an example of a setting in which myocarditis is mimicked. CCC is the most prevalent and serious organic failure resultant of systemic infection with the protozoan *Trypanosome cruzi* (*T. cruzi*) and is endemic in Latin America countries (Figure 8). Efficient treatments for infection with *T. cruzi* are restricted to the initial phase of the disease (Chamond et al., 2005). *T. cruzi* has a complex life cycle, involving an insect vector and a mammalian host, in which distinct parasitic developmental stages will take place (Silber et al., 2002) and reviewed in more detail (Machado et al., 2012).

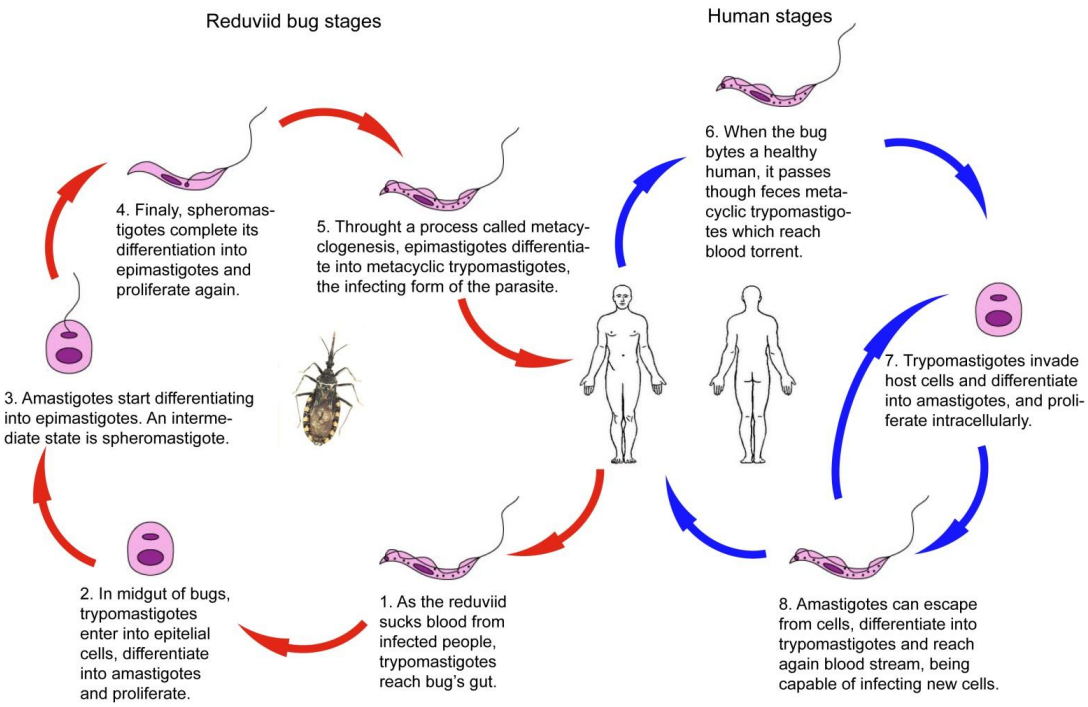

Figure 8. Life cycle of *T. cruzi*. Life cycle of *T. cruzi* parasite consists in four developmental stages. First, bloodform trypomastigotes are ingested when insects feed themselves on an infected mammalian host. Once inside the insect vector, trypomastigotes differentiate into epimastigotes, which after several rounds of division (*i.e.* binary fission) transform into non-dividing but infectious metacyclic trypomastigotes within the gut. The infectious forms are then transmitted in the feces to the mammalian host mucosa or wounded skin, during the insect blood meals. In the mammalian host, the trypomastigotes access the bloodstream

and organs, differentiating into amastigotes that are the dividing intracellular form. Next, amastigotes transform into bloodform trypomastigotes and are released to the blood circulation upon rupture of host mammalian cells. Bloodform trypomastigotes can either infect the surrounding host cells or propagate through the lymphatic or blood circulation, being accessible again to the insect vector. In the mammalian host any nucleated cell can be infected by *T. cruzi* parasite. Adapted from (González et al., 2013).

The infection of the mammal host with *T. cruzi* includes two phases: the acute phase, which is characterized by a transient high concentration of parasites in the blood and tissues, non-specific symptoms and with 5% of patients showing myocardial effects (myocarditis); and the chronic phase that persists lifelong, and can either be asymptomatic or progress to severe HF (Milei et al., 2009; Rassi et al., 2000; Rassi et al., 2010). In the chronic phase, three components are required for the development of CCC: the parasite, the host immune system and fibrosis. These elements of CCC pathogenesis are important players in the damage of the myocardium, conduction system, autonomic ganglia and nerves and microvasculature. The role of *T. cruzi* during chronic stage has long been underestimated due to the low levels of parasites monitored. However, by using distinct technologies, different authors have reported the persistence of vestigial *T. cruzi* antigens, suggesting a prolongation of the cardiac inflammation, still when the parasite is not morphologically detected (Anez et al., 1999; Higuchi Mde et al., 1993; Jones et al., 1993; Schijman et al., 2004). The host immune cells, in particular T lymphocytes and macrophages, persist in the chronic stage of the disease contributing to inflammation, by performing a cytotoxic and cytolytic action. Fibrosis is the most remarkable characteristic of CCC, affecting 8,2% to 49% of the myocardium (Milei et al., 1992). Ultimately, the continued inflammation, necrosis and formation of a scar tissue lead to injury of distinct myocardial components, including the conduction system and microvasculature. Blood form trypomastigotes access CMs after invading ECs, SMCs and the interstitial area of the vasculature (Factor et al., 1993). Inside CMs, *T. cruzi* amastigotes multiply until they are again released to the extracellular space. This process of parasite multiplication provokes the damage of CMs, leading to myocytolysis, myonecrosis and contraction band necrosis (Higuchi et

al., 1999). The inflammation process and CMs damage are followed by ECM degradation, which leads to disintegration of the V muscle layers, to mural thinning and, ultimately, to apical aneurysm. Bands of fibrotic tissue enriched in collagenous matrix replace damaged CMs, defining a prominent hallmark of HF. Interstitial fibrosis progressively leads to heart decompensation, as a result of decreased cardiac output combined with increased workload due to myocardial stiffness (Jalil et al., 1988; Junqueira et al., 1982; Weber et al., 1988; Weber et al., 1989).

Further investigation on the pattern and mechanism underlying myocardial fibrosis in MI and CCC, in combination with quantification of the extent of fibrosis, are needed in order to develop corrective forms of therapy to specifically treat the fibrotic process. Also, despite the acknowledged CMs loss during the progress of myocarditis, the participation of other cardiac population is still missing. Not only in CCC, but also in MI, It is important to understand if and which cells are re-activated in injury settings.

CHAPTER II

AIMS AND CONTEXT OF THIS THESIS

CONTEXT AND AIMS OF THIS THESIS

In the framework of this doctoral *Thesis* collaborative work based in concepts and strategies not commonly applied in the cardiovascular field was established between Pinto-do-Ó & Cumano laboratories.

The focus of Pinto-do-Ó´s research is the identification of mechanisms by which stem/progenitors cells engage in regeneration and/or improved repair in the adult organism. Pinto-do-Ó´s team has been specifically investigating the paradigm of the heart as an organ endowed with resident adult cardiac progenitors and thus with self-regenerating potential. Key unanswered aspects on the biology of the putative adult cardiac progenitors have driven the laboratory focus from the non-regenerating repairing adult heart back to the organ's origin. Thus, a main objective of the team has been to track cardiovascular progenitors in the mouse embryo, and investigate whether/ how such cells relate to the putative adult cardiac progenitors and the rarely renewed cardiomyocytes in the adult heart. In order to surpass drawbacks and disadvantages of more common advanced model-systems already mentioned in the introduction, we have designed a strategy that uses non-genetic models to identify cardiovascular cells.

Cumano's research expertise has contributed through the years for a better understanding of hematopoiesis by the identification of several progenitor populations in the fetal liver, thymus (Ramond et al., 2014) and in the aorta-gonad-mesonephros structure (Cumano et al., 2000) and has also led to the identification and the isolation of other stem/progenitor pools, such as the satellite cells in the muscle (Montarras et al., 2005). Overall, surface signatures have been efficiently used for the identification

and prospective isolation of progenitor cell populations in different organs, which contributed to their in-depth characterization.

Hence, this *Doctoral Thesis* compiles and discusses the results of a combination of research interests of both laboratories, which have been building a strategy to address seemingly opposing views regarding cardiogenesis, *i.e.* the Developmental Biology and the Regenerative Medicine perspectives. The work developed in the herein *Thesis* aimed ultimately at investigating whether the adult mammalian heart harbors precursor/immature cell compartment(s) that participate in response to cardiovascular injury.

The specific aims of the doctoral *Thesis* presented herein were:

To **describe** the state-of-the-art knowledge of heart development and maturation as well as to critically **review** cardiac $Lin^{-}Sca\text{-}1^{+}$ cells in light of what is known for cardiac progenitor cells and cellular compartments with similar phenotypes in other organs. [***Thesis Chapter I*** *(**Appendix I**)*]

To **assign** unique surface signatures (phenotypes) for enabling identification and prospective isolation of the distinct cardiac cell types during mouse heart development and to track the fetal phenotypes in the adult organ. [***Thesis Chapter III***]

To **establish** tools for *in vivo* functional assessment of the cardiac populations in the context of experimental myocardial infarction (murine model): i) **characterize** and **validate** the myocardial ischemia injury model implemented in our laboratory; ii) **develop** strategies to systematize the histological assessment of mouse models of cardiac injury; and iii) **generate** and **validate** an original analytical tool to quantify the extension of myocardial ischemia. [***Thesis Chapter IV*** *(**Appendix II**)*]

To **examine** re-expression of the cell subset phenotypes identified in cardiogenesis in the progression of adult heart injury (ischemia and infection). [***Thesis Chapter V***]

CHAPTER III

SURFACE MARKERS IDENTIFYING DIFFERENT CARDIAC POPULATIONS REVEAL TWO DISTINCT SUBSETS OF CARDIOMYOCYTES IN THE MOUSE FETAL HEART

As previously discussed and further detailed in *Appendix I*, despite an increasing number of reports from independent laboratories on cells with stem/progenitor-like properties within the adult mammalian heart (Beltrami et al., 2003; Oh et al., 2003), these cells have yet not been acknowledged by the scientific community. This resistance is mainly based on the less robust/accurate methodologies originally used to define cardiovascular progenitor and cardiac populations, which do not indeed follow main criteria established for Stem Cell Biology. The cardiac field needs a new strategy to define the distinct cells types that compose the developing heart and their precursors.

Hence, the work developed and presented in this *Chapter* conveys a comprehensive approach novel in the area, *i.e.* the application, in the heart, of a classical method similar to what was used in the hematopoietic (Cumano et al., 2000; Ramond et al., 2014) and skeletal muscle (Montarras et al., 2005) systems, which consists in the definition of new surface signatures by flow cytometry analysis combined with the characterization of their transcriptional profile at the single cell level (multiplex qRT-PCR). This strategy enabled the discrimination and prospective isolation of the main cell fractions engaged in cardiogenesis: CMs, EpiCs, endocardial cushions and valves and FBs. Hence, this work is expected to contribute in future to: i) define culture conditions for the maintenance and differentiation of specific cardiac cell-subsets; ii) develop new *in vivo* assays to assess the functional properties of cardiac cells in their native microenvironment; iii) track embryonic cell phenotypes that may persist in the adult heart during ageing or under the course of disease; iv) search for new candidate genes involved in the differentiation or maturation of cardiac cells; and v) verify the

feasibility of future therapeutic approaches either by targeting CMs replacement or alternatively by modulating the fibroblast cellular compartment following injury or during ageing.

Surface Markers Identifying Different Cardiac Populations Reveal Two Distinct Subsets of Cardiomyocytes in the Mouse Fetal Heart

Mariana Valente*[,1,2,3,4], Tatiana Pinho Resende*[,1,2], Diana Santos Nascimento[1,2], Ana Cumano[§,4,5], Perpétua Pinto-do-Ó[§,1,2,3,4]

[1]Instituto de Investigação e Inovação em Saúde, Universidade do Porto, Portugal.

[2]INEB – Instituto de Engenharia Biomédica, Universidade do Porto, Porto, Portugal.

[3]ICBAS – Instituto de Ciências Biomédicas Abel Salazar, Universidade do Porto, Porto, Portugal.

[4]Unit for Lymphopoiesis | INSERM U668, Immunology Department, Institut Pasteur, [5]Paris, France | University Paris Diderot, Sorbonne Paris Cité, Cellule Pasteur, Paris, France.

*Co-first authors

[§]Co-senior authors

Disclosure of Invention DI 2015-31-HC by Cumano et al. from the Pasteur Institute, Paris, France

Manuscript, unpublished

ABSTRACT

The analysis of the functional properties and proliferative capacity of cardiac cells has been impaired by the lack of a widely accepted combination of surface markers defining the different heart populations. We assembled a multi-parametric phenotypic strategy that, in combination with single-cell multiplex transcriptional analysis, described the major cell types throughout fetal heart development that contribute to the formation of the adult organ. We identified unique phenotypic signatures that allowed tracing epicardial cells and different subsets of fibroblasts, according to location and developmental stages. Importantly, we assigned surface markers to two subsets of cardiomyocytes, corresponding to cells at different stages of maturation. A mature subset characterized by the expression of Caveolin-3 is first detected around E13.5 and persists through adulthood. An immature compartment expressing CD24, CD146 and CD166, but negative for Caveolin-3, proliferates extensively at mid-gestation and decreases in frequency during development to be virtually undetectable shortly after birth.

Highlights:

- Epicardial cells and their progenitors were identified along development.
- We identified surface markers of endocardial cushions, valvular interstitial cells and different subsets of fibroblasts.
- Two populations of cardiomyocyte at different stages of maturation coexist in fetal life.

In Brief:

Valente et al. defined a strategy to identify and isolate the distinct cardiac cell types during mouse development. The combination of surface makers with the transcriptional profiling, at the single cell level, allowed the isolation and characterization of the main fetal cardiac populations and their progenitors. The understanding of the differentiation and maturation processes of cardiomyocytes and heart stromal cells will open new possibilities to study heart physiology and pathology.

INTRODUCTION

In the mammalian heart, the myocardium, composed of cardiomyocytes (CMs) is surrounded by an outer cell layer or epicardium and by an inner cell layer, the endocardium that together shape the four cardiac chambers (two atria (A) and two ventricles (V)). The auriculo-ventricular junction (AVJ) is located at the connection of the four cavities and is composed of connective and membranous tissue that extends to the valves, auriculo-ventricular (AV) conductive components of the pacemaker and His fibers, and to the great vessels (Efimov et al., 2004).

Different cell types (CMs, pacemaker and conductive cells, fibroblasts, endothelial and smooth muscle cells) contribute to the structural, biochemical, mechanical and electrical properties that characterize the cardiac function (Nag, 1980). Moreover, the three distinct layers composing the organ have different developmental origins *i.e.*: i) CMs in the myocardium mainly derive from the first (Lyons et al., 1995; Takeuchi et al., 2003) and second (Cai et al., 2003; Kelly et al., 2001) heart fields, which are cardiogenic mesoderm-derived; ii) the endocardium, also derived from the cardiogenic mesoderm, is composed by endothelial cells and contributes to the formation of the endocardial cushions and the valves with valvular interstitial cells (VICs) and to the endothelial cells of the coronary arteries (de Lange et al., 2004; Eisenberg and Markwald, 1995; Wu et al., 2011); and finally iii) the epicardium, that generates peri-vascular smooth muscle cells and interstitial fibroblasts, and has proepicardial origin, (Cai et al., 2008; Christoffels et al., 2009; Red-Horse et al., 2010; Zhou et al., 2008).

CMs are thought to exit cell cycle over the first week of post-natal life (Porrello et al., 2011; Porrello et al., 2013) growing thereafter by hypertrophy, which coincides in mice

with the bi-nucleation of myocytes (Clubb and Bishop, 1984; Li et al., 1996; Soonpaa et al., 1996; Walsh et al., 2010). The resting state of post-natal CMs has been evoked to explain their poor regenerative response to injury, after post-natal day 7 (Porrello et al., 2011).

The analysis of the proliferative capacity of the cardiovascular populations, their functional properties after injury and the detection of a progenitor cardiomyocytic adult compartment has been impaired by the lack of a recognized combination of surface markers to define the different subsets of cardiac cells. However, several markers have been individually used to define CMs (SIRP□□□□□□□□□ and Caveolin-3 (Cav3)) (Dubois et al.; Parton et al., 1997; Ponten et al., 2013); fibroblasts (Ddr2, CD90) (Goldsmith et al., 2004; Hudon-David et al., 2007; Ieda et al., 2009); smooth muscle cells (PDGFrβ) (Hellstrom et al., 1999), endothelial cells (CD31) (Albelda et al., 1991; Baldwin et al., 1994), and cardiac progenitors (Sca-1 and c-kit) (Beltrami et al., 2003; Oh et al., 2003) and reviewed in (Valente et al., 2014). Because each of these surface markers is expressed in different cell subsets, including in hematopoietic cells, only a multi-parametric surface phenotypic analysis can unambiguously define the cardiovascular populations along development.

Considering that the adult regenerative compartment is generated, in all tissues, during embryonic development (Gros et al., 2005; Weissman et al., 2001) we analyzed the developing mouse heart to identify cardiac progenitors and follow their development up to adulthood. For that end, we combined multi-parametric flow cytometry with single cell multiplex qRT-PCR of purified cell subsets to identify new cell populations and define their lineage affiliation. The expression of CD24, CD54, Sca-1 (Oh et al., 2003), CD90 (Hudon-David et al., 2007), CD146 (Moore-Morris et al., 2014), CD166 (Hirata et al., 2006), PDGFrα (Bax et al., 2010), CD31 (Albelda et al., 1991; Baldwin et al., 1994), cardiac Troponin (Tnnt) (Jin et al., 2008) and Cav3 (Parton et al., 1997) in the non-hematopoietic ($CD45^-Ter119^-$) cell fraction, allowed the isolation of different cardiac cell

subsets, starting from embryonic day (E) 9.5. We found a specific surface phenotype for fibroblasts involved in the formation of valves (AVJ) that differs from that of three other interstitial fibroblast subsets, present in the A or V. Moreover, we identified the phenotype for epicardial components present in all heart regions. In the study herein, surface markers previously assigned to CM progenitors were only expressed in a population of fibroblasts of the AVJ (*i.e.* Sca-1) or in endothelial cells and $CD90^{+}$ fibroblasts (*i.e.* c-kit). Importantly, we found two distinct coexisting subsets of CMs. One immature population characterized by the expression of CD24, CD166, CD146 and Tnnt, but lacking Cav3, a protein only expressed in mature CMs. This CM subset is found at the heart tube stage (E9.5), when CMs are in a proliferative stage and decreases its frequency throughout development, to be almost undetectable after birth. Conversely, the subset of mature CMs, characterized by the expression of Tnnt and Cav3, but lacking CD24, CD146 and CD166 is observed at E13.5, and increases in frequency to be the only CMs found in the adult myocardium. Consistent with this, E17.5 mature CMs do not proliferate and show signs of bi-nucleation. The phenotype corresponding to proliferative embryonic CM was not recognized in the adult heart.

RESULTS

Surface signatures discriminate cell subsets in the fetal heart

To resolve the phenotype of the cellular components in the developing heart, we screened cell suspensions obtained from the three heart regions (*i.e.* A, AVJ and V, Figure 1A) for the expression and relative abundance of more than 30 surface proteins by flow cytometry. The analysis was performed in E17.5 hearts, because at this stage the heart presents its final structure and morphology and the diverse cardiac cellular

populations can be detected. We selected markers discriminating positive and negative subsets in the $CD45^{-}TER119^{-}CD31^{-}$ cell suspension that included proteins that have previously been reported in the heart, such as: Sca-1 (Oh et al., 2003) and reviewed in (Valente et al., 2014) and CD90 (Thy-1) (Hudon-David et al., 2007), as well as proteins that had not been associated with cardiac cells, CD24 (HSA) and CD54 (ICAM-1, Figure 1A and B). CD54-expressing cells were most frequent in A and almost undetectable in V. Similarly, Sca-1 was mainly detected in A (co-expressing CD54, 3.87% ± 0.95%) and in the AVJ (3.78% ± 0.91%) and was less represented in V (1.58% ± 1.04%). CD90 expression was principally observed in the V (20.50% ± 3.99%) and in A and AVJ at lower frequencies. The surface protein CD24 was expressed in the three heart regions: A (17.06% ± 2.85%), AVJ (27.65% ± 4.81%) and V (10.49% ± 2.62%). The negative population for all analyzed markers (Neg) was also found in the three heart regions (A: 16.58 ± 7.47%, AVJ: 47.83% ± 5.92% and V: 48.20% ± 5.48%). As expected, CD31-expressing cells (endothelial and endocardial cells) were detected in the three heart regions with similar frequencies in the chambers (46.73% ± 11.59% in the A and 32.07% in ± 9.25% the V) and at a lower frequency in the AVJ (17.79% ± 3.73%, Figure 1A and B).

Our approach allowed us to correlate within the fetal heart the expression of surface markers with specific cell populations, which were also differentially represented in the distinct cardiac regions.

A.

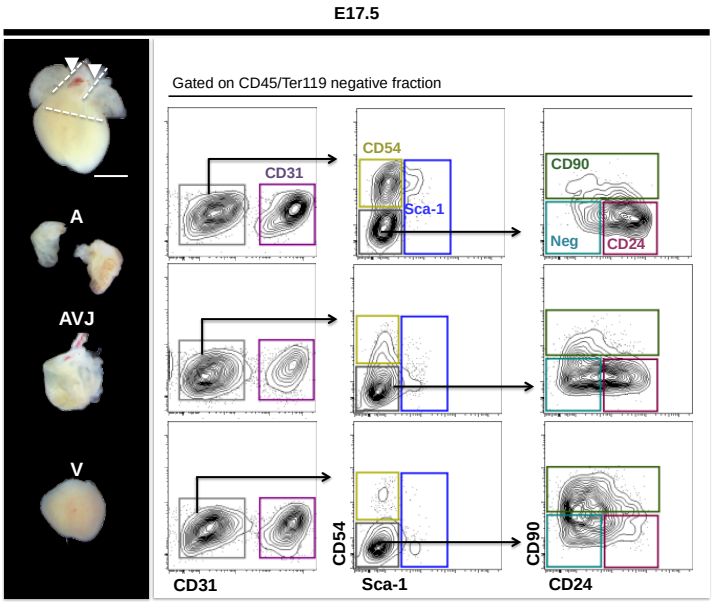

B.

Acronym	*Complete signature*
CD24	CD45$^-$TER119$^-$CD31$^-$CD54$^-$Sca-1$^-$CD90$^-$**CD24$^+$**
Neg	CD45$^-$TER119$^-$CD31$^-$CD54$^-$Sca-1$^-$CD90$^-$CD24$^-$
CD54	CD45$^-$TER119$^-$CD31$^-$**CD54$^+$**Sca-1$^-$ (or Sca-1$^+$A)
Sca-1	CD45$^-$TER119$^-$CD31$^-$CD54$^-$**Sca-1$^+$**
CD90	CD45$^-$TER119$^-$CD31$^-$CD54$^-$Sca-1$^-$**CD90$^+$**CD24$^-$
CD31	CD45$^-$TER119$^-$**CD31$^+$**

Figure 1. Surface signatures define cell subsets with specific anatomic distribution in the fetal heart. A. Macroscopic view of embryonic hearts (E17.5), depicting the distinct regions analyzed: A, AVJ and V. Representative contour plots of flow cytometry analysis (CD45 and Ter119 negative fraction) for the expression of the surface markers CD54 (ICAM-1), Sca-1 (Ly-6 A), CD90 (Thy1), CD24 (HSA) and CD31 (PECAM-1) are shown. Scale bar: 1 mm. **B.** Detailed description of the full surface signature of each isolated population and the respective acronym and color code used along this work. A | Atria; AVJ | Auriculo-ventricular Junction; V | Ventricles.

Transcriptional profiles assign the cell lineage to the newly defined surface signature

To determine the cell identity of the newly defined cardiac populations, we analyzed in 20 cells of each population, sorted to high purity, the expression of more than 40 transcripts defining different cardiac cell types, by multiplex qRT-PCR (Figure S1). Unsupervised hierarchical clustering and principal component analysis (PCA) were used to analyze the multidimensional transcriptional data. The hierarchical clustering grouped the populations in six clusters (Figure 2A). Clusters I and II comprise A and V $CD24^+$ cells, respectively, and express primarily CM-specific proteins (*Nkx2-5*, *Tnnt2*, *Des*). The expression of the specific isoforms of myosin segregated CMs from the A (*Myl2* and *Myh7*) and V (*Myl7* and *Myh6*), supporting the robustness and specificity of our strategy. Cluster V includes CD54-expressing cells and A Sca-1^+ cells. This cluster shows high levels of *Wt1, Gja1* and *Tbx18*, indicative of an epicardial affiliation, as well as *Kdr*, *Tek*, and *S100a4. Kdr*, *Flt1* and *Tek* were found, as expected, in endothelial cells from all regions ($CD31^+$ cells Cluster VI). Clusters III and IV include all AVJ populations ($CD24^+$, Neg, Sca-1^+), which have a fibroblast profile, denoted by the expression of *Nfatc1*, *Gjc1*, *Twist1*, and *Scx* and of *Isl1*, *Tbx3 Snai2*, *Fap*, *Ddr2,* compatible with VICs. The $CD90^+$ V cells are also comprised in cluster III showing a fibroblast profile, although different from that of the VICs in the AVJ and characterized by the expression of *Gata4*, *Tbx20, Tcf21 and Fn1*.

In order to resolve heterogeneity of the cardiac subsets we performed single cell qRT-PCR analysis in the same populations, which revealed that surface signatures have identified homogeneous populations for the analyzed genes (Figure S2). Single cell sorting was performed using the index-sorting tool to record the levels of expression of the all phenotypic parameters for each sorted cell (Figure S3). In contrast with previous reports (Sanada et al., 2014; Uchida et al., 2013; van Berlo et al., 2014), we did not detect c-Kit or Sca-1 expression in CMs. On the other hand, c-Kit expression was

found only in $CD31^+$ endothelial cells and in $CD90^+$ fibroblasts (Figure S4). Interestingly, cells with a transcriptional profile of CMs were also found in the Neg subset. PCA analysis (Figure 2B) summarizes the results obtained in the heat-map hierarchical clustering. Hence, whereas A and V CMs can be identified by the single expression of CD24, CD54 detects epicardial cells mainly represented in A. Ventricular fibroblasts were mostly found in the $CD90^+$ subset, while the AVJ cells share a similar transcriptional profile with interstitial fibroblasts but with additional expression of genes typical of VICs irrespective of their phenotype.

Globally, these results show that our strategy of combining the definition of surface signatures (Figure 1A and B) with transcriptional profile characterization (Figure 2) allowed identifying and prospectively isolating different cell types that constitute the fetal heart. Importantly, CD24 was shown to specifically identify fetal CMs.

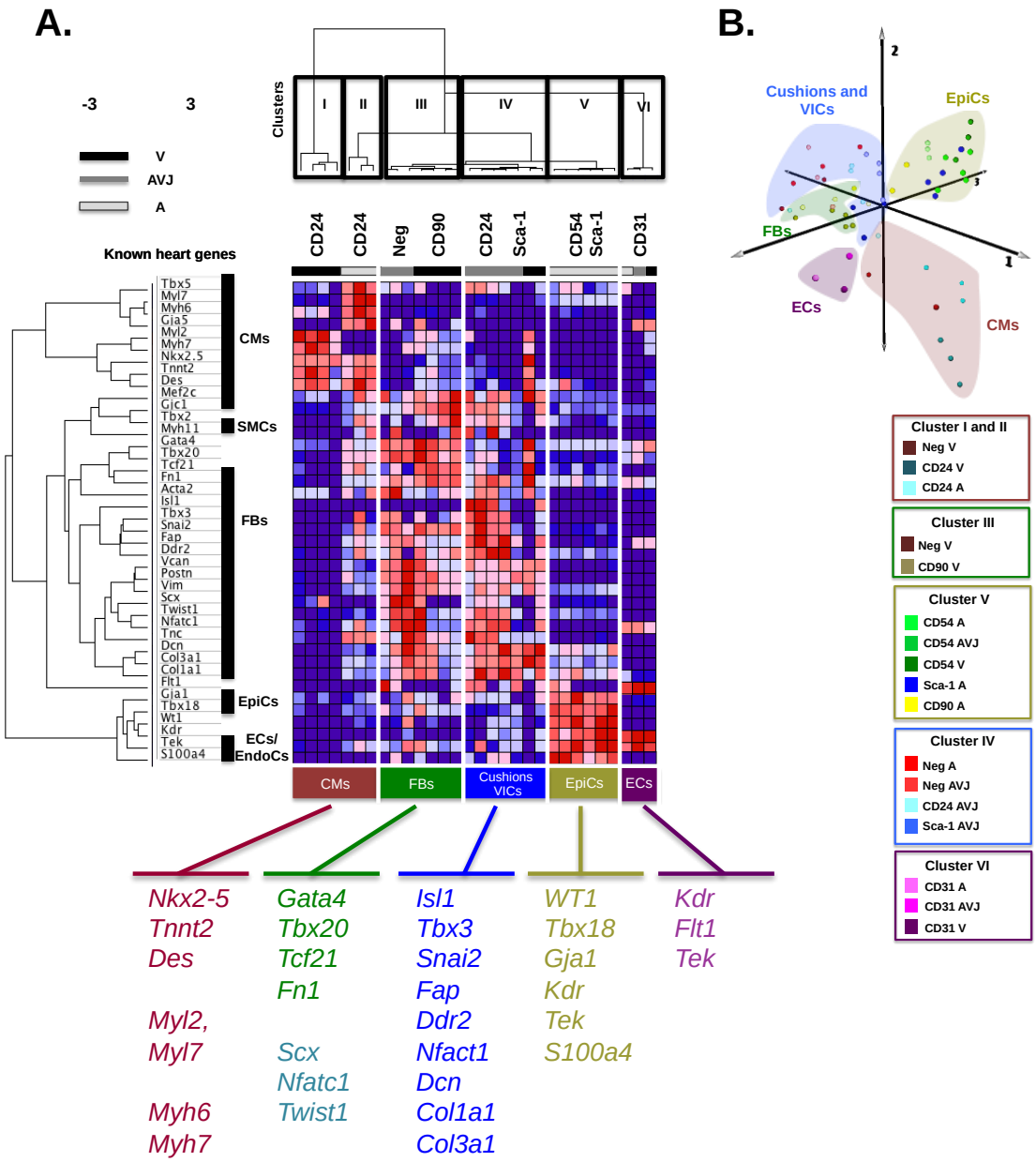

Figure 2. Transcriptional profiles assign a cardiac cell type to each surface signature. A. Hierarchical clustering of the multiplex qRT-PCR data, at the population level (20 sorted cells), of the newly defined cardiac populations (E17.5, n=3). Selected genes are known to be important in cardiovascular development process and main heart cell types; HPRT was used as housekeeping gene. **B.** PCA of the transcriptional profile of the distinct populations (presented on A) allows distinguishing the main clusters observed in the heat map analysis. A | Atria; AVJ | Auriculo-ventricular Junction; V | Ventricles; CMs | Cardiomyocytes; SMCs | Smooth Muscle Cells; FBs | Fibroblasts; Cushions | Endocardial Cushions; VICs | Valvular Interstitial Cells; EpiCs | Epicardial Cells; ECs | Endocardial Cells; EndoCs | Endocardial Cells. See also Figures S1, S2 and S3.

Described surface signatures allows tracking cardiac cell subsets, along mouse development

The capacity to identify distinct cardiac cell types by surface markers at E17.5 prompted us to investigate expression at earlier developmental stages of heart morphogenesis. At the looped heart tube stage, E9.5 (Figure 3A), cardiac cells have an elementary surface profile, expressing only CD31 (48.73% ± 17.18%, 36.36% ± 23.33% and 65.2% ± 24.88%) or CD24 (51,17% ± 17.09%, 63.28% ± 23.59% and 34.56% ± 24.66%) in the primitive atrium (PA), outflow tract (OFT, future AVJ) and primitive V (PV), respectively. From E9.5 to E13.5 substantial morphologic alterations occur in the developing heart and consequently we found increasing complexity in the populations discriminated by phenotyping. A population of cells negative for all analyzed markers (Neg) both in the A (23.14% ± 5.19%) and the V (11.13% ± 1.85%) becomes evident and we detected the emergence of CD54 (1.80% ± 0,59%) and CD90 (3.59%± 1.77%) in the V and Sca-1 (3,07% ± 0.43%) in the A, which will appear as well-defined populations at E17.5 (Figure 3A).

To correlate the phenotype and lineage affiliation of the cellular subsets identified we employed single cell multiplex transcriptional analysis of E9.5 and E13.5 hearts similarly to that of E17.5 cardiac populations. The hierarchical clustering (Figure S4) and PCA analysis (Figure 3B) grouped cells with similar transcriptional profile along development. Our data allowed clustering together the same cell type from the three developmental stages. CD24-expressing cells encompassed CMs of the three stages analyzed and clustered away from the remaining cells types. E9.5 $CD24^+$ cells also comprise a subset expressing transcripts characteristic of endocardial cushion cells (20/40 cells) and few epicardial cells (4/40 cells); no fibroblasts were detected at this developmental stage. E13.5 Neg cells mainly include epicardial cells and a small subset contains interstitial fibroblasts. E17.5 epicardial profile included $CD54^+$ (which in

the A co-expressed Sca-1), whereas fibroblasts were comprised in cells expressing CD90, CD24 and in the negative fraction. The endothelial/endocardium profile was maintained along development in the $CD31^+$ cells. Compatible with their acknowledged origin in the endocardial cells, E9.5 cells expressing an endocardial cushion gene profile were also $CD31^+$ (Figure 3B).

To further confirm the phenotypic expression determined by flow cytometry and to determine their location, we proceeded to analyze the expression of the surface proteins in cardiac tissue sections (Figure 4). The looped heart tube (E9.5) is mainly composed by CMs and endocardial cells. CD24 expression was detected in CMs of the three regions, identified by Actinin expression (asterisks, Figure 4A) and in endocardial cushions, which lack CM-associated proteins (arrowheads, Figure 4A). In E13.5, the majority of A CMs still express CD24, whereas the expression of this protein in V CMs was restricted to the outer ventricular compact zone (asterisks, Figure 4Ba, c); CD24 was also detected in the AVJ endocardial cushions (Figure 4Bb). In E17.5, CMs expressing CD24 were frequently observed in the A, but scarce in the V (asterisks, Figure 4Da, c); consistent with the flow cytometry data, CD24 expression was also found in endocardial cushion mesenchyme in the AVJ (Figure 4Db). CD54 was seen to be expressed by endothelial cells, identified using CD31, in the A endocardium and in the V (Figure 4E). Interestingly, we also detected $CD54^+CD31^-$ cells (white arrowheads, Figure 4E) in the sub-epicardial zone of both chambers. Expression of CD54 in the AVJ was restricted to few non-endothelial cells; CD54 was never detected in CMs. *In situ* expression of the surface markers defined by flow cytometry confirmed the presence of CD24 in a subset of CMs (which is maintained along development) and confirmed CD54 as a marker of epicardial cells. Accordingly, CD54 was also observed in the epicardial layer of the adult murine heart (Figure S6C).

Overall, our data report the increasing cellular complexity that occurs during heart

development. As example, epicardial cells and fibroblasts were barely detected in E9.5 and progressively increased thereafter. Flow cytometry results were corroborated by histological analysis, which allowed the co-localization of the identified surface markers with proteins specific of a given cell type. Interestingly, we identified CD24 as a marker of a subset of CMs that is found in all analyzed developmental stages; Neg CMs emerge only after E13.5 and increase in frequency as development progresses.

Identified cardiac cell populations present differential cell cycle dynamics

Combining the phenotypic markers herein identified with Ki67 and DAPI allowed determining the frequency of cells in G_1 ($Ki67^+$ and $DAPI^{2N}$, top left quadrant), in $S/G_2/M$ ($Ki67^+$ and $DAPI^{>4N}$, top right quadrant) and in G_0 ($Ki67^-$ and $DAPI^{2N}$, bottom left quadrant, Figure 3C). The $CD24^+$ cell fraction at E9.5, which corresponds to CMs, is highly proliferative (48% in G_1 and 26.7% in $S/G_2/M$). As development proceeds, a marked decrease of $CD24^+$ in cells in $S/G_2/M$ (13.2% and 1.7% at E13.5 and E17.5, respectively) is observed, whereas the frequency of cells in G_1 is maintained (42-46%). These observations are consistent with the description of the gradual decline of CMs proliferative capacity along maturation. At the fetal stage E17.5 the most proliferative compartment is the CD90-expressing fibroblasts (27.6% in G_1 and 16.4% in $S/G_2/M$), while most $CD54^+$ epicardial cells are resting cells (G_0 85.9%).

The analysis of the proliferative status of cardiac cells indicates that, despite the diminished proliferative capacity, some CMs are still in G_1 at E17.5. Additionally, at this stage fibroblasts are the most active proliferative compartment in the heart.

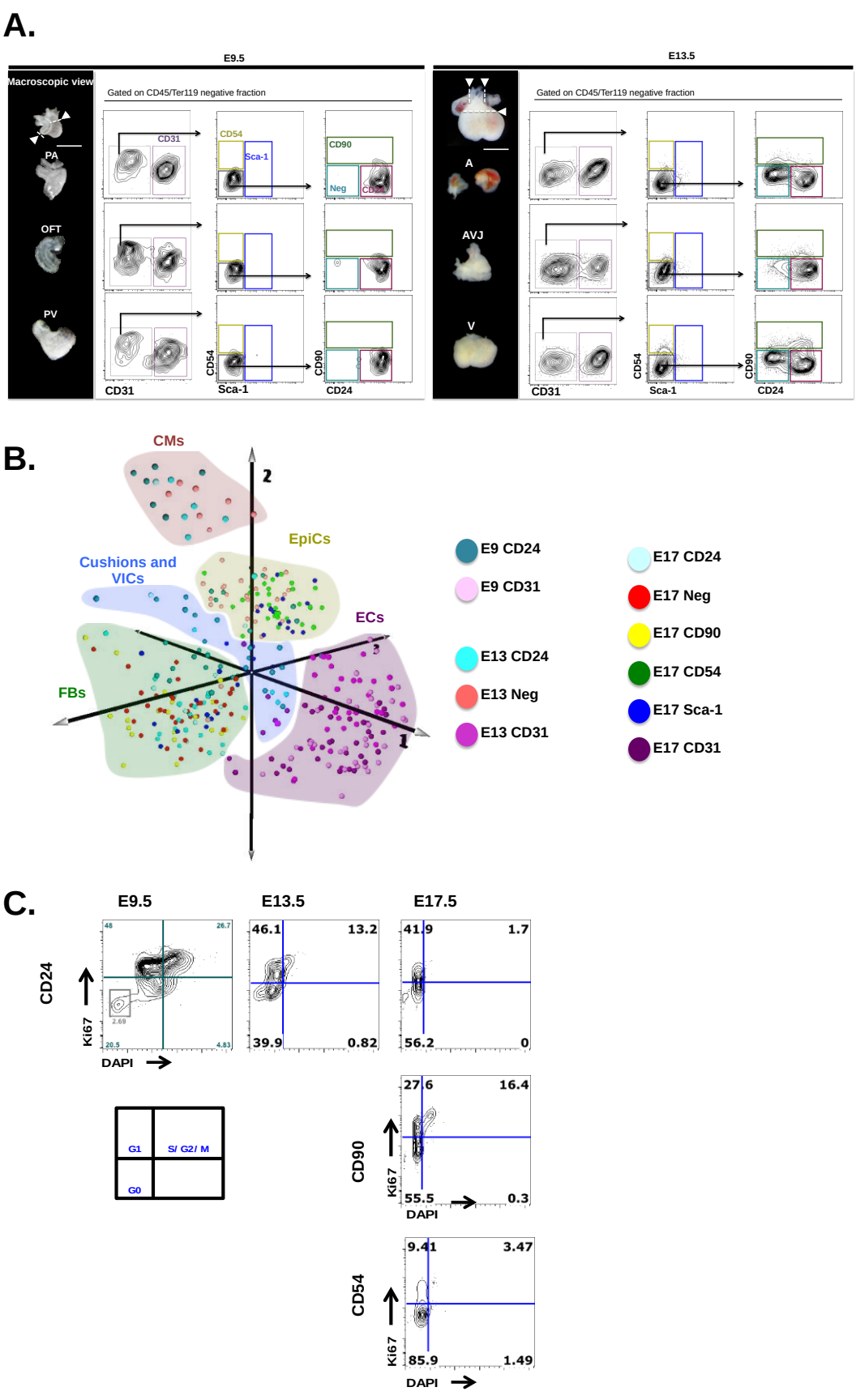
A.
E9.5
E13.5
Macroscopic view
PA
OFT
PV
A
AVJ
V
Gated on CD45/Ter119 negative fraction
CD31
CD54
Sca-1
CD90
CD24
Neg
B.
CMs
EpiCs
Cushions and VICs
ECs
FBs
E9 CD24
E9 CD31
E13 CD24
E13 Neg
E13 CD31
E17 CD24
E17 Neg
E17 CD90
E17 CD54
E17 Sca-1
E17 CD31
C.
E9.5
E13.5
E17.5
CD24
Ki67
DAPI
46.1
13.2
39.9
0.82
41.9
1.7
56.2
0
G1
S/ G2/ M
G0
CD90
27.6
16.4
55.5
0.3
CD54
9.41
3.47
85.9
1.49

Figure 3. Identified surface markers allow tracking cardiac cell types along mouse development (previous page). A. Macroscopic view of embryonic hearts and representative contour plots of flow cytometry analysis on E9.5 and E13.5 heart regions (CD45 and Ter119 negative fractions) for the expression of CD54 (ICAM-1), Sca-1 (Ly-6 A), CD90 (Thy1), CD24 (HSA) and CD31 (PECAM-1). Scale bar: 1 mm. **B.** PCA analysis of single cell qRT-PCR data of the three embryonic time-points analyzed (E9.5, E13.5 and E17.5), revealing the hierarchical relationship of the different cell populations and the dynamics of the surface profile along ontogeny. **C.** Representative contour plots of cell cycle status of $CD24^+$, $CD90^+$ and $CD54^+$ cell populations along development. The frequency of cells in G_0 ($Ki67^+DAPI^{2N}$), G_1 ($Ki67^+$ and $DAPI^{2N}$) and $S/G_2/M$ ($Ki67^+$ and $DAPI^{>4N}$) was obtained by plotting Ki67 (a proliferation marker) versus DAPI (DNA content). A | Atria; PA | Primitive Atria; PV | Primitive Ventricles; OFT | Outflow Tract; AVJ | Auriculo-ventricular Junction; V | Ventricles; CMs | Cardiomyocytes; FBs | Fibroblasts; Cushions | Endocardial Cushions; VICs | Valvular Interstitial Cells; EpiCs | Epicardial Cells; ECs | Endocardial Cells; EndoCs | Endocardial Cells. See also Figure S4.

Identified cardiac cell populations present differential cell cycle dynamics

Combining the phenotypic markers herein identified with Ki67 and DAPI allowed determining the frequency of cells in G_1 ($Ki67^+$ and $DAPI^{2N}$, top left quadrant), in $S/G_2/M$ ($Ki67^+$ and $DAPI^{>4N}$, top right quadrant) and in G_0 ($Ki67^-$ and $DAPI^{2N}$, bottom left quadrant, Figure 3C). The $CD24^+$ cell fraction at E9.5, which corresponds to CMs, is highly proliferative (48% in G_1 and 26.7% in $S/G_2/M$). As development proceeds, a marked decrease of $CD24^+$ in cells in $S/G_2/M$ (13.2% and 1.7% at E13.5 and E17.5, respectively) is observed, whereas the frequency of cells in G_1 is maintained (42-46%). These observations are consistent with the description of the gradual decline of CMs proliferative capacity along maturation. At the fetal stage E17.5 the most proliferative compartment is the CD90-expressing fibroblasts (27.6% in G_1 and 16.4% in $S/G_2/M$), while most $CD54^+$ epicardial cells are resting cells (G_0 85.9%).

The analysis of the proliferative status of cardiac cells indicates that, despite the diminished proliferative capacity, some CMs are still in G_1 at E17.5. Additionally, at this stage fibroblasts are the most active proliferative compartment in the heart.

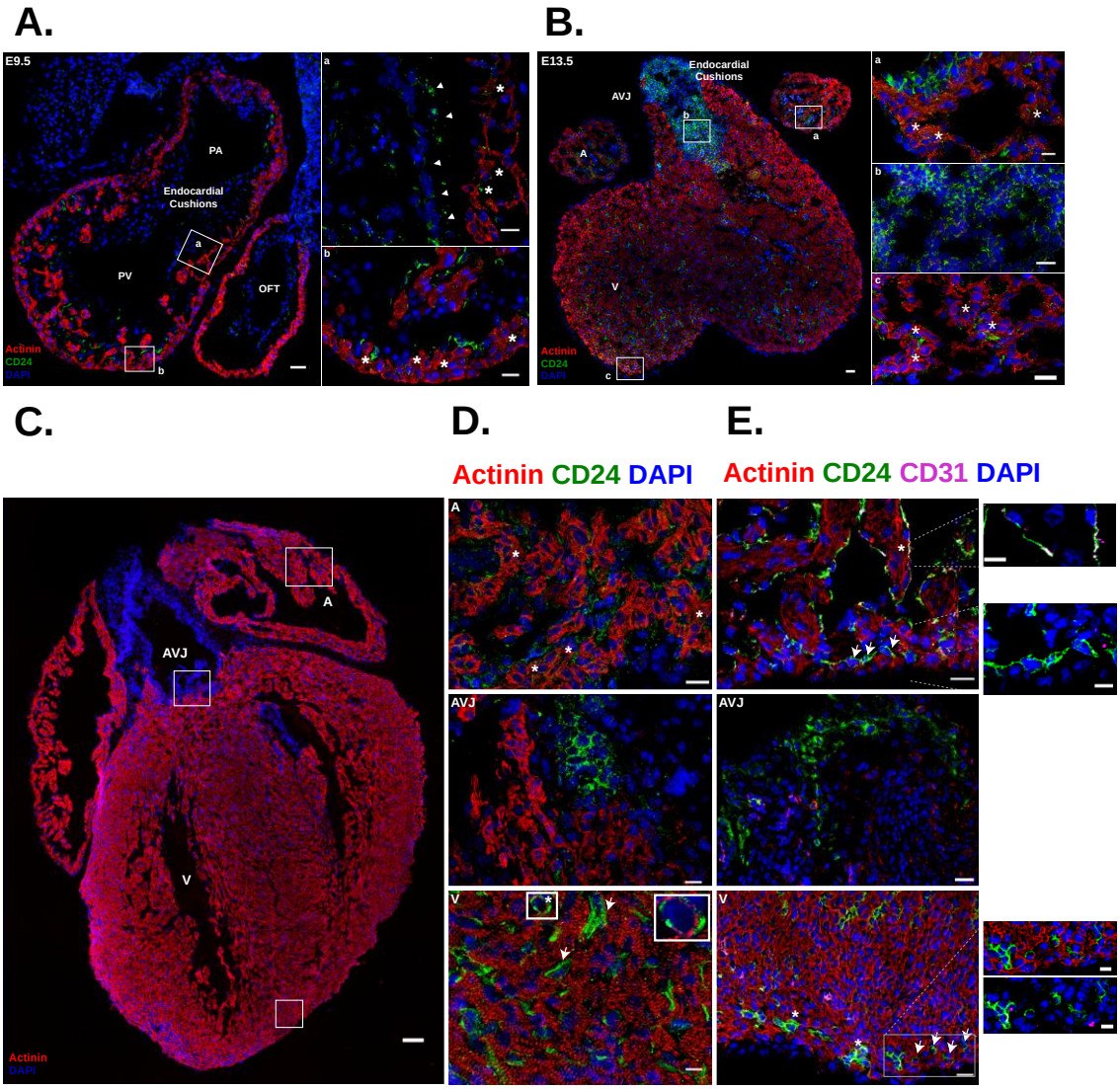

Figure 4. Identified proteins allow spatial characterization of the distinct cell types in the fetal heart (previous page). A-B. *In situ* immunofluorescence analysis of CD24 protein expression in early developmental stages (E9.5 and E13.5). In both stages, the co-expression of CD24 (green) and Actinin (red), *i.e.* in CMs, is shown in A, V and in the outer layer of the OFT; CD24 expression is also present in the endocardial cushions regions (**Aa** and **Bb**). Representative higher magnification images of each region are shown in **Ca** and **b** and **Da**, **b** and **c**. Scale bar: 20 μm. **C.** Section of E17.5 fetal heart stained for Actinin (red) and nuclei (blue) and depicting localization of the area in A, AVJ and V analyzed in more detail for CD24 and CD54 expression. Scale bar: 50 μm. **D.** Representative images of CD24 (green) localization in each cardiac region. The majority of A CMs express CD24, while in the V expression seems to be restricted to small round CMs (*, inset) and mesenchymal cells (arrow); in the AVJ, CD24 is observed only in non-myocytes. **E.** CD54 (green) is expressed by a great portion of A endocardial cells, as indicated by co-localization (white color, upper inset) with CD31 (purple). Atrial layer of sub-epicardial cells, which do not correspond to CMs nor endothelial cells also express CD54 (lower inset). In the V CD54 is detected in small endothelial clusters (*) and also in a sub-epicardial cell layer (arrows and inset). Non-myocytes in the AVJ also express CD54. In the insets, Actinin staining is not shown to highlight CD54 and CD31 co-localization. Scale bars: 20 μm. See also Figure S6. A | Atria; PA | Primitive Atria; PV |

Primitive Ventricles; OFT | Outflow Tract; AVJ | Auriculo-ventricular Junction; V | Ventricles; CMs | Cardiomyocytes; FBs | Fibroblasts.

Additional surface markers refine the definition of cardiomyocytes, fibroblasts and smooth muscle cells in the fetal heart.

Our initial phenotypic characterization using conventional cytometry allowed us identifying diverse cell subsets but a sizable proportion of cardiac cells did not express any of the analyzed surface markers. Moreover, even though CD24 recognized CMs, the frequency of cells expressing this marker decreased with development and was also associated with other cells types, such as endocardial cushions of the AVJ. To further refine the initial analysis (E17.5 hearts) we then used spectral cytometry. Cardiac cells, in particular CMs, display autofluorescence, a recurrent feature that can limit the analytical resolution in conventional flow cytometry. In spectral cytometry, the autofluorescence of the cardiac cells was virtually undetectable. After an initial second round of surface marker screen, we combined three additional antibodies to our panel: CD146 (MCAM) (Moore-Morris et al., 2014), CD166 (ALCAM) (Hirata et al., 2006) and PDGFrα (CD140a) (Bax et al., 2010) (Figure 5A). By combining spectral cytometry with transcriptional profile, we identified a unique surface marker signature to define CMs, *i.e.* CD24 cells co-expressing CD146 and CD166, a population that was only detected on the chambers (Figure 5A upper and lower plots and 5B). $CD90^{+}$ and Neg cell fractions in A and V were further distinguished by the expression of PDGFrα and CD146 that define two mutually exclusive subsets of fibroblasts and exhibit distinct transcriptional profiles: *Tcf21*, *Mef2c* and *Fn1* expressed in the former and *Tbx20*, *Snai2, Postn*, *Col1a1* and *Col3a1* in the latter (Figure 5B). In the AVJ, the expression of PDGFrα is associated with the transcriptional signature for fibroblasts, while CD166 defines a population characterized by the expression of genes affiliated to CMs (*Myl2*), smooth muscle cells (*Acta2* and *Myh11*) and fibroblasts (*Col1a1*, Figure 5B). At this

level of phenotypic characterization less than 10% of cardiac cells remained negative for all analyzed markers.

Thus, by increasing the complexity of the surface protein combination and by eliminating autofluorescence we were able to find a unique signature for a subset of CMs, we could further distinguish two subsets of fibroblasts and we found in the AVJ an intriguing population that co-expresses CM, smooth muscle cells and extracellular matrix transcripts.

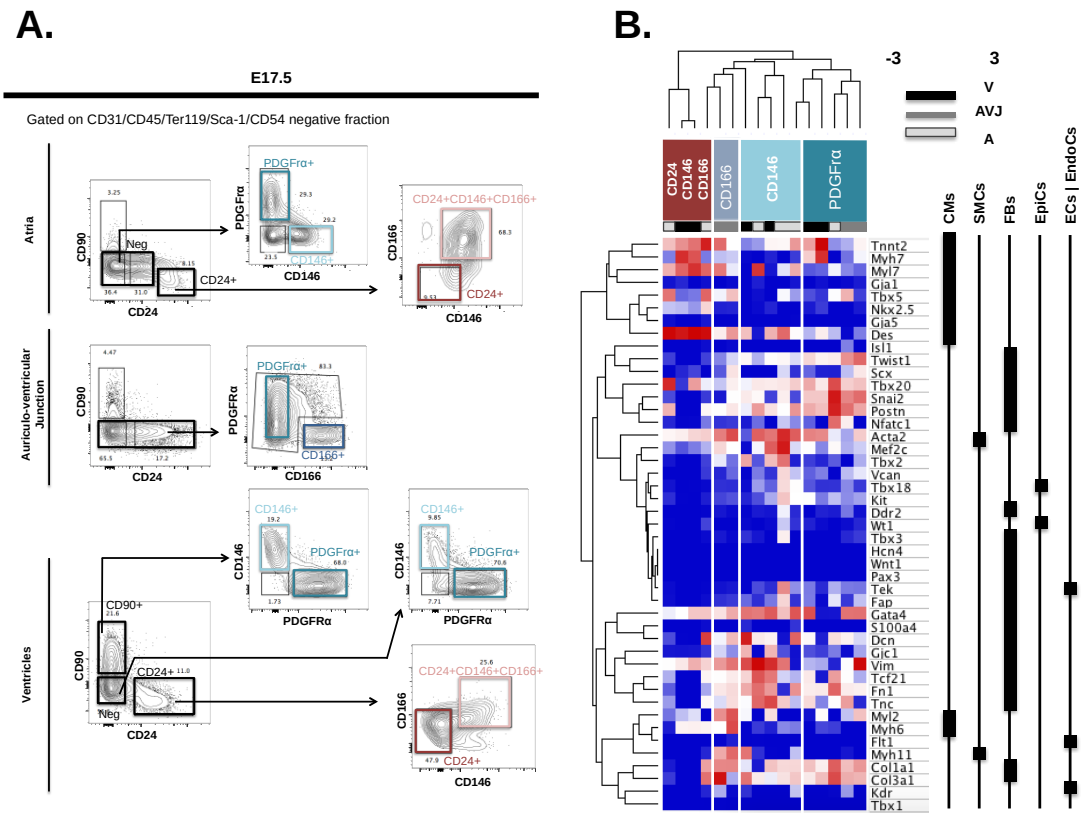

Figure 5. Additional surface proteins refine the definition of cardiomyocytes, and fibroblasts in the fetal heart. A. Representative contour plots of flow cytometry analysis of the three regions studied in E17.5 hearts (CD45, Ter119 CD31, CD54 and Sca-1 negative fraction) for the combined expression of PDGFrα (CD140a), CD146 (MCAM) and CD166 (ALCAM) are presented. **B.** Heat-map of multiplex qRT-PCR data analysis, at the population level (20 sorted cells), showing the global differences on the gene expression of the newly defined populations of CMs (A $CD24^{+}CD146^{+}CD166^{+}$ versus V $CD24^{+}$), fibroblasts (two distinct subsets $CD146^{+}$ and $PDGFR\alpha^{+}$) and a population that shares the transcriptional profile with CM, smooth muscle cell and fibroblast ($CD166^{+}$). HPRT was used as housekeeping gene (n=2). A | Atria; AVJ | Auriculo-ventricular Junction; V | Ventricles.

Distinct surface signatures define two subsets of cardiomyocytes, at different stages of maturation, co-existing in the fetal heart.

Our data shows that early CMs (E9.5) express CD24, while at E17.5 only a small portion of V CMs exhibit this phenotype. To test whether these two subsets corresponded to different stages of cell maturation we included Tnnt (Jin et al., 2008) and Cav3 (Parton et al., 1997) in our analysis. Cav3 was described to be expressed in adult CMs and skeletal muscle cells, but undetectable in immature cells (Parton et al., 1997). Two distinct cell fractions expressing Tnnt (*i.e.* CMs) were detected: one co-expressing CD24, CD146 and CD166 and another negative for these markers (Figure 6A). Expression of Cav3 at the surface membrane was however only identified in the triple negative population (Figure 6B). Our results demonstrated the coexistence, in E17.5 heart, of two subsets of Tnnt-expressing CMs: one more immature that expresses CD24, CD146 and CD166 but not Cav3; and a subset of $CD24^-$ cells, which increases along development, expressing Cav3 and correspond likely to more mature CMs. During maturation, morphological alterations in CMs led to increased sarcomere complexity, increased cell size and, eventually, bi-nucleation (reviewed in (Yang et al., 2014)). Analysis of DNA content using DAPI indicated the occurrence of a cell fraction with double amount of DNA (120K), *i.e.* bi-nucleated (4N), in the $Cav3^+Tnnt^+$ CMs and absent in $Cav^-Tnnt^+CD24^+CD146^+CD166^+$ cells (Figures 6B). This result strengthens the idea that $Cav3^+$ CMs are more mature than the $Cav3^-CD24^+$ subset. $CD24^+$ CMs exhibited the pattern of DNA content, typical of dividing cells, which is a continuum increasing of DAPI intensity, observed during nucleic acid synthesis (Figures 6B, Figure S5). To determine whether similar populations of CMs also co-exist in the adult heart, we analyzed adult cardiac cell suspensions following a similar strategy. Our data revealed that adult cardiac cells are highly enriched for Sca-1-expressing fibroblasts, as well as epicardial cells $CD54^+$ (Figure S6A). A small subset of

$CD24^+CD166^+CD146^+$ cells did not express CM-specific transcripts, which were only found in the cell subset negative for all analyzed markers (Figure S6B).

Altogether, our data demonstrated the co-existence of two populations of fetal CMs in distinct maturation stages, which can be prospectively isolated and further characterized using the specific surface signatures CD24, CD146, CD166 and Cav3 in association with the gating strategy defined in the current work. We did not find any residual population of CMs with a fetal phenotype in the adult myocardium, while the fibroblast populations defined during late heart morphogenesis are well represented in adulthood.

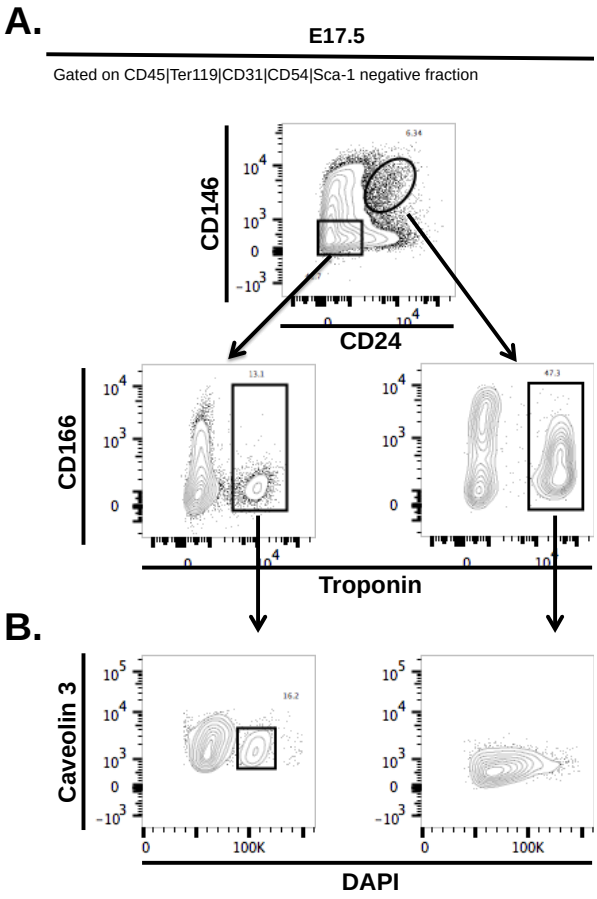

Figure 6. Expression of CD24, CD146, CD166 and Caveolin-3 identify two subsets of fetal cardiomyocytes in different maturation stages. A. Representative contour plots of flow cytometry analysis on E17.5 hearts (CD45, Ter119 CD31, CD54, Sca-1 and CD90 negative fraction) for Tnnt, CD24, CD146 and CD166. Tnnt expression indicates the cardiomyocytic phenotype of the two distinct populations: $CD24^+CD146^+CD166^+$ cells and the Neg subset. **B.** Cav3 expression was only found in CMs of the Neg fraction. DNA content analysis of these of CMs ($CD24^+$ and $Cav3^+$) highlights different maturation states due to the presence of bi-nucleated cells in the $Cav3^+$ fraction. See also Figure S5.

DISCUSSION

The understanding of lineage relationship and characterization of progenitor cell compartments relied in the past on the prospective isolation of cell subsets in different tissues (Cumano et al., 2000; Montarras et al., 2005; Weissman et al., 2001). The absence of a strategy to discriminate and isolate distinct subsets of viable cells in complex tissues, such as the heart, impairs efforts to recognize lineage relationship and the characterization of tissue progenitor compartments that might be involved in regeneration and repair.

We defined phenotypic signatures for cardiac cells in the mouse embryo that combined with multiplex single cell transcriptional profile enabled the distinction of the three main cardiac cell lineages, *i.e.* different subsets of CMs, endocardial and epicardial cells, and allowed us to define their maturation stages along development. Collectively, our findings contributed for the understanding of the population dynamics and hierarchies along cardiac development, as depicted in Figure 7 and further detailed below.

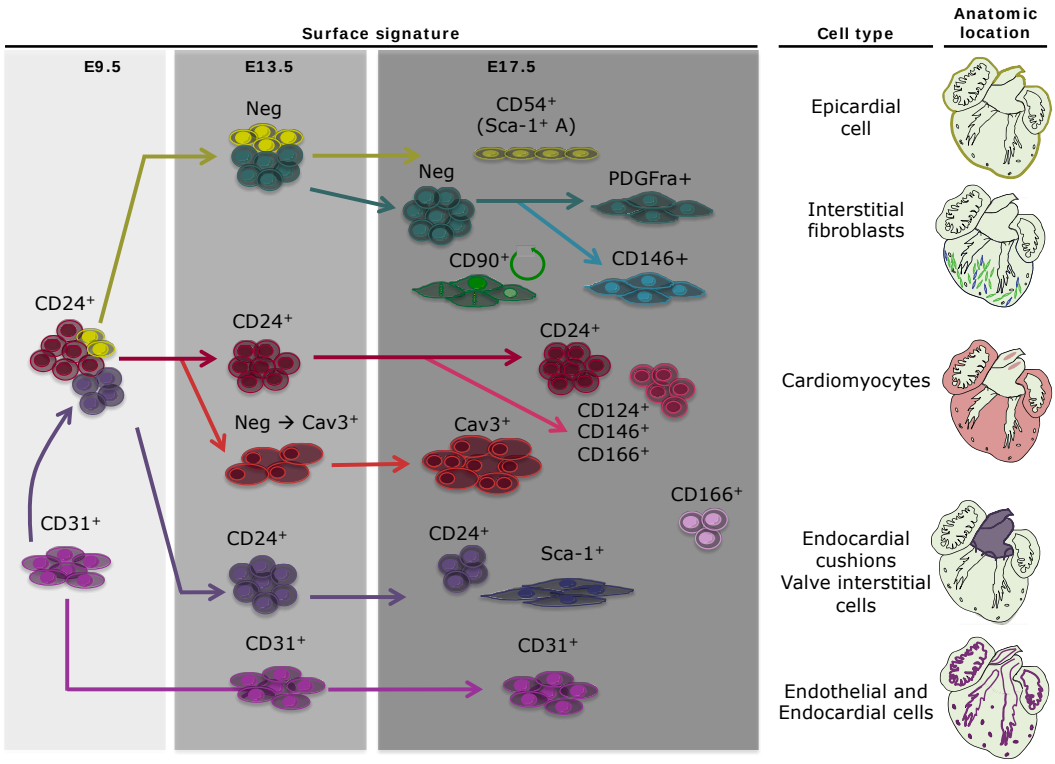

Figure 7. Surface signatures assigned to the distinct cardiac cell types allow establishing their relationship along heart morphogenesis. The dynamics of the surface signatures and their association with specific cell types between E9.5, E13.5 and E17.5 are depicted. We traced epicardial cells, endothelial and endocardial cushion cells and their derivatives, different CM developmental stages and subsets of fibroblasts, leading us to a complete picture of the heart cell types and their kinetics along heart development.

Epicardial maturation: progenitors and mature cells

Epicardial cells derive from the proepicardial organ (extra-cardiac structure) and migrate to the primitive heart tube from E8.5 to E10.5 (Schulte et al., 2007). These cells are recognized by the expression of *Wt1* (Zhou et al., 2008) and *Tbx18* (Cai et al., 2008; Christoffels et al., 2009) during embryonic development and give rise to the smooth muscle cells of coronary vasculature and interstitial fibroblasts (Cai et al., 2008; Christoffels et al., 2009; Red-Horse et al., 2010; Zhou et al., 2008). Both epicardial

cells and fibroblasts are essential for proper heart development (Cai et al., 2008; Christoffels et al., 2009; Kreidberg et al., 1993; Sucov et al., 2009; Zhou et al., 2008) and play a role in adult heart physiology and pathology (Smart et al., 2007; Zhou et al., 2011). A discrete fraction of $CD24^+$ cells co-expresses *Wt1*$^+$ and *Tbx18*$^+$ in the heart tube stage (E9.5), while at mid-gestation (E13.5) epicardial cells are negative for all analyzed surface proteins (Neg). At E17.5 this cell population can be identified using CD54 (ICAM-1) and, adding to *Wt1* and *Tbx18,* also express *Gja1*, *S100a4*, *Kdr* and *Tek* (Figure 3). The same phenotype is found in the adult epicardium (Figure S6). However, while epicardial cells are dividing at E9.5 and E13.5, $CD54^+$ E17.5 cells are quiescent, indicating that they reached a post-mitotic stage of maturation (Figure 3C). This result is corroborating the observations that adult epicardial cells are in a quiescent state, being re-activated in an injury situation (Zhou et al., 2011). The presence of $CD54^+$ cells in the AVJ suggests a contribution of epicardial cells to the development of the valve structures (Figure 4) (Lockhart et al., 2014; Perez-Pomares et al., 2002). Our data also revealed that epicardial cells are a large fraction of the A cell wall, suggesting a significant participation of this population in A morphogenesis, not previously appreciated.

Endocardial cushions and valve subsets

The endocardial cushions derive from the endocardium ($CD31^+$) (Baldwin et al., 1994) and contribute to the formation of the heart septation (AV canal, later the OFT) and valves (Chakraborty et al., 2010; de Lange et al., 2004; Eisenberg and Markwald, 1995; Wu et al., 2013; Wu et al., 2011). Endocardial cushions transcriptional profile (*Nfatc1*$^+$) was first detected on E9.5 in CD24-expressing population (de Lange et al., 2004; Wu et al., 2011). At this developmental stage, some $CD31^+$ cells (endocardium)

displayed the same transcriptional profile as $CD24^{+}CD31^{-}$ endocardial cushion cells. This might represent transitional progenitors between the endocardial cells and the endocardial cushion cells, which at E13.5 are mainly composed of CD24-expressing cells forming a cushion of mesenchyme at the AVJ.

Cardiac valve remodeling takes place later on fetal development and is characterized by the gradual transition from an undifferentiated mesenchyme to specialized VICs (Figure 3). At the fetal stage (E17.5), our results support the increase of complexity of the valves' cellular composition described in the literature (Eisenberg and Markwald, 1995). The cell fraction that maintains CD24 expression in the AVJ denotes, at the histological level, the immature mesenchyme morphology found on E13.5 endocardial cushions, which indicates the reminiscence of an immature mesenchyme on the fetal heart (Figure 4D). Sca-1 expression has been used as a marker of cardiac progenitor cells in the adult heart (reviewed in (Valente et al., 2014)), but our data indicates that this surface protein identifies a population of fibroblasts that integrate the valves (VICs), that emerges only at E17.5 (Figure 1 and 2). $PDGFr\alpha^{+}$ fibroblasts represent an independent subset that is also part of the valve structure (Bax et al., 2010). The great vessels are also included in our dissection strategy for the AVJ. Surprisingly, in this region we found a population of $CD166^{+}$ cells expressing *Myh11* and *Myl2*, *Col1a1*, *Acta2* (Figure 5). This mixed signature of some CM transcripts together with smooth muscle cell and fibroblast transcripts likely correspond to the CM-like cells that that colonize the pulmonary vein (Millino et al., 2000). Overall, we have defined a strategy to distinguish different subsets of VICs in the AVJ, which include immature endocardial cushions mesenchyme cells expressing CD24 and mature VICs expressing $PDGFr\alpha^{+}$ and $Sca\text{-}1^{+}$. The $CD166^{+}$ population is also specific of the AVJ and compatible with CM-like cells of the pulmonary vein.

Interstitial and perivascular fibroblasts' subsets

Like in other tissues, fibroblasts compose the heart stroma, where they play a role in cardiac homeostasis and scaffolding support, organ development, wound healing, inflammation, and fibrosis. Cardiac interstitial fibroblasts derive from epicardial cells (Moore-Morris et al., 2014) and are known to be heterogeneous and thus difficult to define (Ali et al., 2014b; Furtado et al., 2014; Moore-Morris et al., 2014). We show that cells presenting a fibroblast-like transcriptional profile are not found before E13.5 and are more evident at E17.5, representing the cardiac compartment with the highest proliferative activity (Figure 3). Proliferative fibroblasts of the ventricular wall were discriminated by the expression of CD90 at E17.5. Additionally, we discriminated two mutually exclusive fibroblast fractions: $CD146^{+}PDGFr\alpha^{-}$ (*Tcf21*, *Mef2c* and *Fn1*) and $CD146^{-}PDGFr\alpha^{+}$ (*Tbx20*, *Snai2*, *Postn*, *Col1a1* and *Col3a1*, Figure 5). $CD146^{+}$ cells have been identified in several tissues, namely as perivascular fibroblasts following heart injury (Moore-Morris et al., 2014). Our data indicates that $CD146^{+}$ cells are also present in the fetal heart. PDGFrα expression has been described in the myocardial interstitium derived from the epicardial layer (Bax et al., 2010), which corroborates our findings (Figure 5). Thus, our strategy allows identifying and prospectively isolating interstitial $PDGFr\alpha^{+}$ and perivascular $CD146^{+}$ fibroblasts in the fetal heart.

Cardiomyocyte surface profile along development and maturation

During embryonic development, CMs rapidly differentiate (Nishii and Shibata, 2006; Sassoon et al., 1988) and, together with endocardial cells ($CD31^{+}$, the cell types found in the primitive heart tube), they proliferate and contribute to the development of the chambers (A and V) (Christoffels et al., 2004). Two layers of CMs compose the myocardium around mid-gestation (E13.5): the compact zone with CMs actively proliferating; and the trabecular zone, composed by more mature CMs (de Boer et al., 2012; Sedmera et al., 2003). Our results determined that a subset of CMs defined by

the co-expression of *Nkx2-5*, *Myl2*, *Myl7*, *Myh6*, *Myh7*, *Tnnt2*, *Des* and *Acta2* is expressed by a unique $CD45^{-}Ter119^{-}CD31^{-}Sca\text{-}1^{-}CD54^{-}CD90^{-}CD24^{+}CD146^{+}CD166^{+}$ phenotype (Figure 2 and 5). This surface signature that is present starting at the heart tube stage can be found widespread in the A, while in the V decreases during fetal heart maturation, being restricted to rare small *foci* at E17.5 (Figure 1, 3 and 4). Our data indicates a marked decrease in the frequency of $CD24^{+}$ V CMs as development proceeds, and the presence of CMs in the Neg compartment from E13.5 onwards. We thus conclude that there are two populations of CMs that develop in parallel: $Cav3^{-}$ CMs co-expressing CD24, CD146 and CD166, predominant at earlier stages of development; and mature $Cav3^{+}$ CMs (Parton et al., 1997) found in the $CD24^{-}CD146^{-}CD166^{-}$ subset, the major population in E17.5 myocardium. Consistent with an advanced state of maturation, $Cav3^{+}$ CMs are bi-nucleated (Figure 3C, 5 and 6). Together, these results indicate that after mid-gestation two subsets of CMs, at different stages of development, can be distinguished by the expression of the CD24, CD146, CD166 and Cav3 in the fetal heart, allowing their prospective isolation.

The physiological turnover and regenerative capacities of mammalian adult heart have been a matter of extensive debate because strategies to repair injured tissue will vary depending on whether there is an adult progenitor compartment (Hsieh et al., 2007; Uchida et al., 2013; van Berlo et al., 2014) or if mature CMs can divide (Ali et al., 2014a; Bergmann et al., 2009; Bersell et al., 2009; Senyo et al., 2013). Although there are in the literature evidences for both scenarios, the consensus is that only newborn CMs maintain the capacity to proliferate and thus to restore the myocardium after injury (Clubb and Bishop, 1984; Li et al., 1996; Porrello et al., 2011; Porrello et al., 2013; Soonpaa et al., 1996; Walsh et al., 2010). We did not detect c-kit or Sca-1 expression (previously identified as surface markers of cardiac progenitors) in the cardiomyocytic compartment, either in the embryo or in the adult, and we did not find evidence for the

persistence of the fetal phenotype of CMs ($CD24^{+}CD146^{+}CD166^{+}Cav3^{-}$) in the adult heart. We propose that this cardiomyocytic subset, present during uterine life is promptly undetectable after birth, coinciding with the decreased regenerative capacity observed experimentally.

The strategy described herein allows the discrimination and prospective isolation of the main cell fractions of the heart. More specifically, we enabled the future possibility to: i) define culture conditions for the maintenance and differentiation of specific cardiac cell-subsets. *In vitro* assays (e.g. cell culture) are of interest both to test functional properties of the cells and to screen pharmacological compounds; ii) develop *in vivo* assays to assess the functional properties of cardiac cells in their native microenvironment; iii) track embryonic cell phenotypes that may recur in the adult heart during ageing or following disease; iv) search for new candidate genes involved in the differentiation or maturation of cardiac cells; v) verify the feasibility of therapeutic approaches either by targeting CMs replacement or alternatively by modulating the fibroblast cellular compartment following injury or during ageing.

EXTENDED EXPERIMENTAL PROCEDURES

Mice

C57BL/6 mice (Charles River) between 6 and 8 week-old were used as adult mice and timed-pregnant females all embryonic time-points reported. Timed-pregnancies were generated after overnight mating. The next morning, females with vaginal plug were considered to be at E0.5.

All animal procedures at INEB were approved by Instituto de Biologia Molecular e Celular | Instituto de Engenharia Biomédica Animal Ethics Committee and Direcção-

Geral de Veterinária – DGV; at Institut Pasteur according to the Institut Pasteur ethic charter approved by French Agriculture ministry; and to the European Parliament Directive 2010/63/EU at both institutes.

Cardiac Cells Isolation

Surface signatures characterization and transcriptional profile were performed on pooled embryonic/fetal mouse hearts E9.5, E13.5 and E17.5 and on adult hearts.

Embryonic hearts were collected under a stereomicroscope and the three anatomic heart structures (atria, auriculoventricular junction and ventricles) were micro-dissected. Heart tissue was minced into 1 mm^3 fragments and incubated during 15 min at 37ºC in a enzymatic solution: for E13.5 and E17.5 hearts, 0,2mg/mL collagenase (Sigma) in Hank's Balanced Salt Solution with calcium and magnesium cations (HBSS+/+, Invitrogen) was used; for E9.5 hearts, 0,1mg/mL collagenase in HBSS+/+; and for adult heart, 0,2mg/mL collagenase with 60U/mL DNase I (Roche). At the end of each round of incubation in the enzymatic solution, tissue fragments were vigorously re-suspended in the enzymatic solution to complete the enzymatic dissociation. The remaining tissue was let to sediment, the supernatant was collected and enzymatic activity inhibited with 10% FCS (Gibco) HBSS+/+ and kept on ice. These steps were repeated until no more tissue was observed. After digestion, cell suspensions were centrifuged 10 min, 290g at 4ºC, re-suspended in 1%FCS HBSS+/+ and filtered with a 70 µm mesh cell strainer (Fisher).

Flow Cytometry

Heart cell suspensions were stained with conjugated or non-conjugated antibodies against surface proteins (20 minutes, 4ºC in the dark) followed by incubation with conjugated streptavidin for the detection of biotinylated antibodies (10 minutes, 4ºC in the dark). If a non-conjugated antibody was used, a sequential incubation with a

secondary antibody was performed 15 minutes 4ºC in the dark. Dead cells were detected with propidium iodide (PI, 1/40000). Please see the antibodies combination at the **Supplemental Tables**.

For intracellular proteins detection, Foxp3 / Transcription Factor Staining Buffer Set (eBioscience) was used following the manufacturer's instructions. Briefly, cells were fixed 30 minutes at 4ºC in the dark with Fixation/Permeabilization Buffer (diluted 4x in the diluent) and permeabilized in Permeabilization Buffer (diluted 10x in deionized water). Cells were incubated with intracellular antibodies 30 minutes at 4ºC in the dark followed by the conjugated secondary antibody, when using a non-conjugated primary antibody. For DNA staining, fixed cell suspensions were incubated with DAPI 5 minutes at 4ºC in the dark.

Before acquisition, samples were filtered with a 70 µm mesh cell strainer. Conventional flow cytometry data was acquired on a BD FACSCanto™ II (BD Biosciences) and spectral flow cytometry on a Sony SP6800 analyser (Sony). Flow cytometry data were acquired in log scale, except for DNA content analysis, in which linear scale was used. All data was analysed with FlowJo v10.0.8 software.

Cell Sorting

Single cells and 20 cells per well (or 100 cells per well for adult) were sorted on a BD FACSAria™ III with a 70 µm nozzle and under single-cell mask directly into 96 well plates loaded with RT-STA Reaction mix (CellsDirect™ One-Step qRTPCR Kit, Invitrogen, according to the manufacturer's procedures) and 0.2x specific Taqman® Assay mix. After sorting, samples were vigorously mixed, spun down and frozen at -80ºC, at least overnight, to facilitate cell lysis.

For single cell sorting, index sorting tool on BD FACSDiva™ v8.0.1 software (BD Bioscience) was activated to track and record the fluorescence data for each parameter of each individual cell collected in a precise position on the 96-well plate.

This tool allowed the post-sorting correlation of the levels of surface protein expression and the transcriptional profile (Figures S2).

Gates were defined in order to collect cardiac populations with purity higher than 90% (Figures S1).

All data was analysed with FlowJo v10.0.8 software.

Gene Expression Analysis – Microfluidic multiplex qPCR

Lysed samples were thawed, vigorously mixed and directly reverse transcribed and specific target pre-amplified using the following Thermocycler conditions: one cycle of reverse transcription with a gradient of increasing temperature 40°C, 50ºC and 60ºC for 15 minutes each. Reverse transcription enzyme inactivation at 95°C for 2 minutes, followed by 20 cycles for single cell samples and 18 cycles for bulk (20 or 100 cells per well) samples of specific target pre-amplification. Each cycle was composed by denaturation at 95°C for 15 seconds followed by annealing/extension at 60°C for 4 minutes and kept at 4ºC until the dilution.

Pre-amplified samples were diluted 5x with low EDTA TE buffer prior to qPCR analysis using 48.48 Dynamic Array™ IFCs and the BioMark™ HD System (Fluidigm). Processing of the IFCs and operation of the instruments were performed according to the manufacturer's procedures. Prior to loading onto the chip, individual TaqMan® gene expression assays (20x, Life Technologies, see Taqman® Assays' list at the **Supplemental Tables – Table S7**) were diluted 1:1 with 2x assay loading reagent (Fluidigm). Pre-amplified samples (2.9 µL) were combined with 3.25 µL TaqMan Universal Master Mix (Life Technologies) and 0.32 µL 20x GE sample loading reagent (Fluidigm). qPCR cycling conditions were 50°C for 2 minutes, 95°C for 10 minutes, followed by 40 cycles each at 95°C for 15 seconds followed by 60°C for 1 minute.

Bioinformatic Analysis

For bulk analysis, HPRT was used as a housekeeping control to normalize gene expression.

For single cell analysis, a background Ct (non-detected) of 38 was used for all real-time signals. Samples with at least expression of the two housekeeping genes (Actb, Gapdh and HPRT) were considered in the analysis.

Hierarchical clustering was done with MultiExperiment Viewer program. For all hierarchical clustering heatmaps, the rainbow scheme color scale was set from -3 to 3.Principal Component Analysis (PCA) was generated using the MultiExperiment Viewer program.

Histological processing and Immunofluorescence Staining

Either the whole embryo (E9.5) or the hearts (E13.5 and E17.5) were collected, fixed in 0,2% paraformaldehyde (Merk) overnight at 4ºC, dehydrated in a sucrose gradient (4% followed of 15%) prior gelatin (Merk) embedding and freezing. Cryosections (4 µm) were obtained using a cryostat (Leica) and stored at -80ºC. For the immunostaining, sections were washed in 1x PBS and blocked with either 4% FBS/1% BSA or Vector M.O.M.™ basic kit (Vector Laboratories). Incubation with primary antibodies was performed overnight at 4ºC and the following antibodies were used to detect: α-actinin sarcomeric (1:300, Sigma), CD24 (1:250, eBioscience), CD54 (1:100, eBioscience), Sca1 (1:100, BD Pharmingen), CD31 (1:250, Santa Cruz). Alexa Fluor conjugated secondary antibodies (Invitrogen) were used and nuclei were counterstained with DAPI. Representative high-resolution images were acquired from each heart structure (atria, auriculo-ventricular junction and ventricles) at 40x magnification in a confocal microscope (Leica SP5II, Leica). Whole heart acquisitions were obtained using the high-content imaging system (IN Cell Analyzer 2000, GE Healthcare). All acquired images were edited using Image J software.

AUTHOR CONTRIBUTIONS

M.V.: experimental design and execution of the project (embryos dissection, flow cytometry and cell sorting, single cell gene expression, bioinformatics and histology analysis), analysis, interpretation and discussion of the data and manuscript writing; T.P.R.: execution of the project (embryos dissection, histology, confocal imaging and imaging flow cytometry analysis), analysis, interpretation and discussion of the data and critical revising of the manuscript; D.S.N.: interpretation and discussion of the and data critical revising of the manuscript; A.C. experimental and conceptual design of the project, expertise in flow cytometry, analysis, interpretation and discussion of the data and manuscript writing; and P.P.O.: coordination, conceptual and experimental design of the project, interpretation and discussion of the data and manuscript writing.

ACKNOWLEDGMENTS

The authors are grateful to the colleagues from NEWTherapies Group (INEB) and Unitè Lymphopoièse (Institut Pasteur) for the discussions during the project development. The authors are also indebted to the many colleagues who have provided insightful help in several of the procedures herein described, among others, we thank Catarina Leitão (Advanced Flow Cytometry Unit, INEB), María Gómez Lázaro (Confocal microscopy and imaging flow cytometry, INEB - Bioimaging Centre for

Biomaterials and Regenerative Therapies | b.IMAGE), Paula Sampaio (confocal microscopy, Advanced Light Microscopy Unit, IBMC), Sofia Lamas (DVM, IBMC), Isabel Duarte and all the animal caretakers at the IBMC Animal Facility. At Institut Pasteur we are grateful to Sophie Novault and Sandrine Schmutz (at the Flow Cytometry Platform), Koji Futamura and Cédric Ait-Mansour (implementation of the Sony SP6800), Didier Montarras, Sigole Meilhac's lab, and Paola Minoprio and Alain Cosson for sharing scientific expertise and resources.

This work was supported by Fundação para a Ciência e a Tecnologia [SFRH/BD/74218/2010] to M.V., [SFRH/BPD/80588/2011] to T.P.R., QREN/ON.2 [NORTE-07-0124-FEDER-000005] to D.S.N., and by Fundo Europeu de Desenvolvimento Regional, Programa Operacional Factores de Competitividade-COMPETE, Quadro de Referência Estratégico Nacional, Fundo Social Europeu [PEst-C/SAU/LA0002/2013, PTDC/SAU-ORG/118297/2010] and Programa Operacional Regional do Norte (ON.2 – O Novo Norte) [NORTE-07-0124-FEDER-000005 - *Project on Biomedical Engineering for Regenerative Therapies and Cancer*] grants to P.P.O., and the Institut Pasteur, INSERM, ANR [Twothyme] and REVIVE Future Investment Program grants to A.C..

The authors have no conflicting financial interests.

REFERENCES

Please see references at *REFERENCES Chapter*.

SUPPLEMENTAL FIGURES

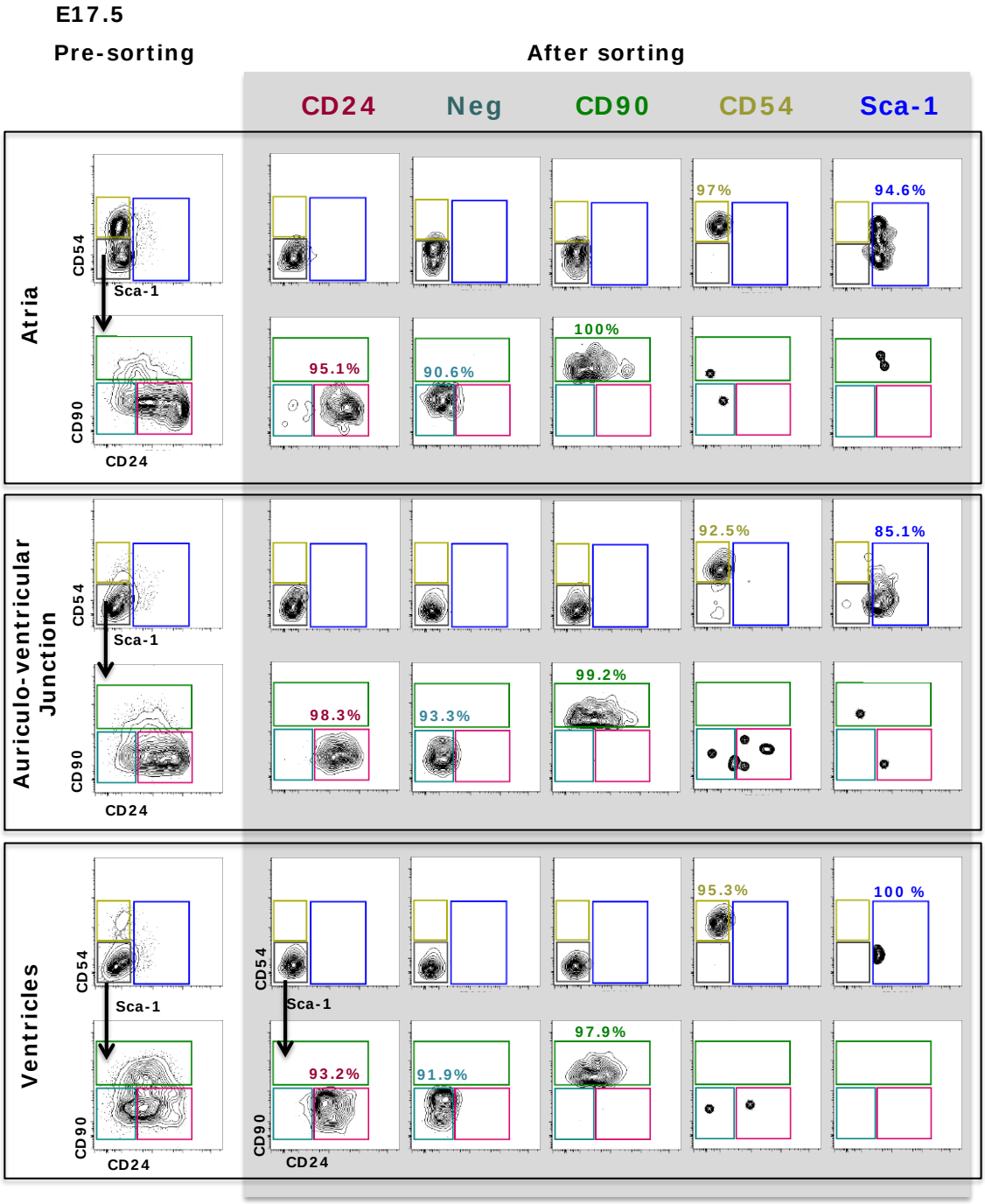

Figure S1, related to Figure 2. Gating strategy and purity analysis of the cardiac cell populations following isolation by FACS. A. Representative contour plot of presorted cardiac cell suspensions, in which the gating strategy is shown. **B.** Flow cytometry analysis of sorted cardiac subsets showing more than 85% purity.

Fqcies	Cluster,1	Cluster,2	Cluster,3	Cluster,4	Cluster,5	Cluster,6	Cluster,7
Dcn	100%	100%	61%	21%	100%	96%	0%
Col1a1	100%	100%	79%	0%	98%	96%	0%
Col3a1	100%	100%	100%	58%	100%	96%	0%
Twist1	63%	90%	46%	6%	47%	74%	0%
Tbx20	100%	100%	18%	12%	66%	96%	80%
Tcf21	100%	20%	21%	0%	60%	96%	0%
Gata4	93%	85%	14%	64%	87%	85%	60%
Acta2	73%	35%	50%	15%	13%	67%	100%
Tnnt2	50%	25%	32%	30%	32%	41%	100%
Myh6	7%	0%	4%	6%	2%	19%	60%
Myh7	37%	5%	7%	6%	0%	15%	100%
Myl2	70%	10%	25%	27%	2%	15%	100%
Des	47%	10%	32%	9%	47%	30%	100%
Nfatc1	60%	60%	21%	70%	9%	44%	20%
Gjc1	47%	50%	50%	18%	28%	44%	20%
Scx	3%	95%	7%	0%	19%	4%	20%
Fap	30%	15%	32%	0%	0%	44%	0%
Gja1	0%	0%	14%	12%	26%	11%	0%
Tbx3	3%	30%	11%	3%	0%	4%	0%
Ddr2	3%	0%	39%	0%	9%	15%	0%
S100a4	0%	5%	14%	0%	30%	0%	0%
Vim	100%	100%	100%	100%	98%	96%	80%
Vcan	83%	60%	46%	9%	13%	48%	0%
Fn1	100%	55%	89%	79%	85%	93%	0%
Mef2c	83%	55%	75%	85%	53%	67%	40%
Snai2	93%	55%	89%	45%	49%	96%	0%
Tnc	83%	70%	75%	21%	19%	85%	0%
Postn	100%	95%	75%	42%	0%	96%	0%
Tek	70%	30%	7%	88%	70%	56%	0%
Kit	77%	10%	14%	79%	0%	30%	0%
Flt1	0%	5%	7%	76%	0%	4%	0%
Kdr	3%	10%	14%	94%	36%	11%	0%
Tbx18	73%	25%	21%	0%	85%	59%	20%
Wt1	33%	0%	18%	24%	96%	7%	0%
Myl7	10%	5%	21%	21%	94%	59%	100%
Tbx5	7%	50%	29%	24%	57%	33%	40%
	FBs	Cushions & VICs		ECs	EPiCs		CMs

Figure S2, related to Figure 2. Frequency of cells expressing each defined transcriptional profile on E17.5 populations at the single cell level. Single cell qRT-PCR rendered a similar transcriptional profile when compared with the bulk analysis (20 sorted cells), indicating that the identified surface signatures define transcriptionally homogenous populations on E17.5 hearts.

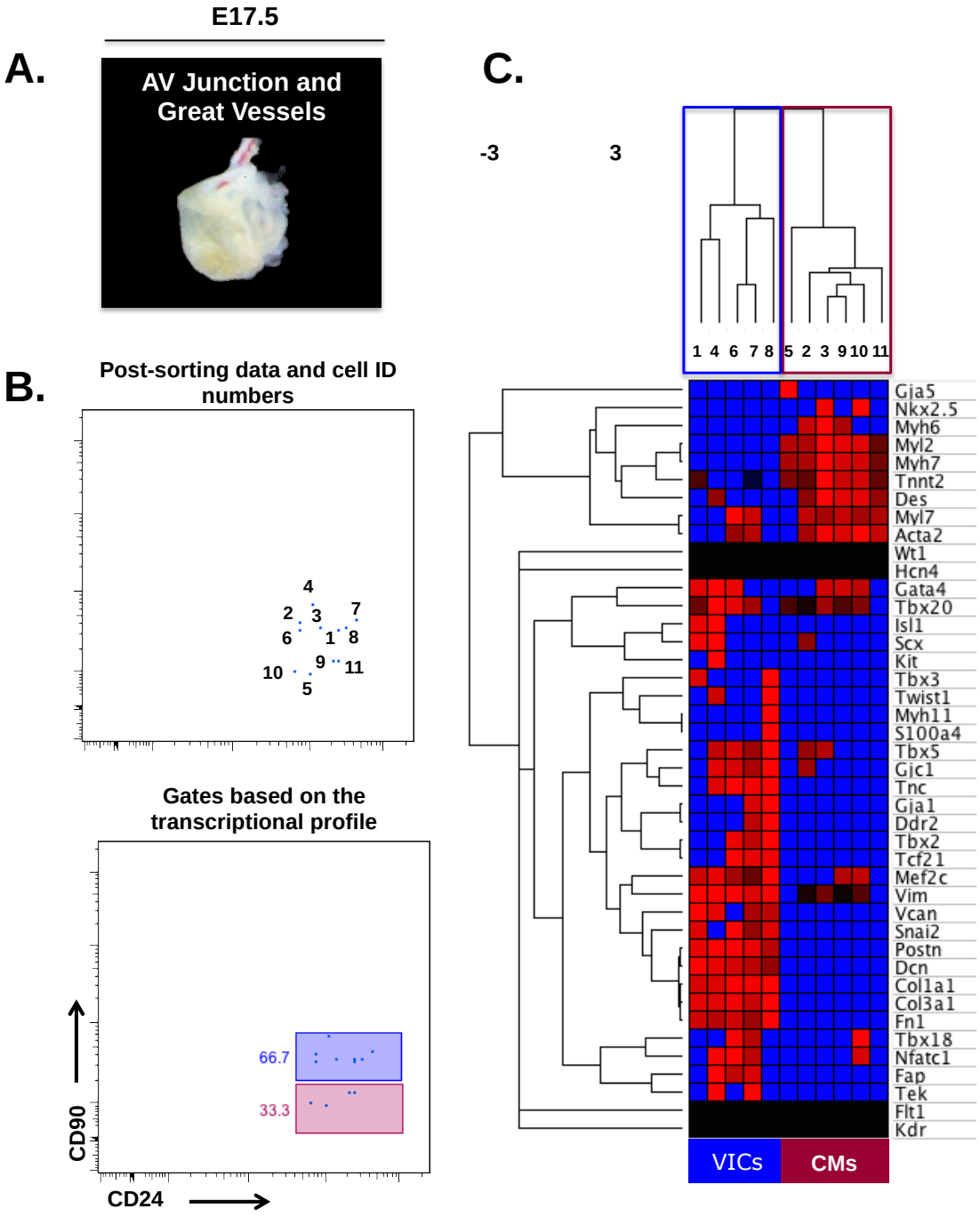

Figure S3, related to Figure 2. Index-sorting of single cell collection of heart populations. An example of the applicability of the index-sorting tool by the correlation of the phenotype of each sorted cell with its transcriptional profile. **A.** Macroscopic view of the dissected E17.5 AVJ, where some ventricular tissue is inevitably included. **B-C.** The correlation of dot plot obtained from index-sorting of $CD24^{+}$ of the AVJ and the heat map resulted from the single cell transcriptional profile, which allowed the discrimination of two subsets of $CD24^{+}$ cells by the different levels of CD90 expression (lower corresponds to the CM profile and the higher to VICs transcripts).

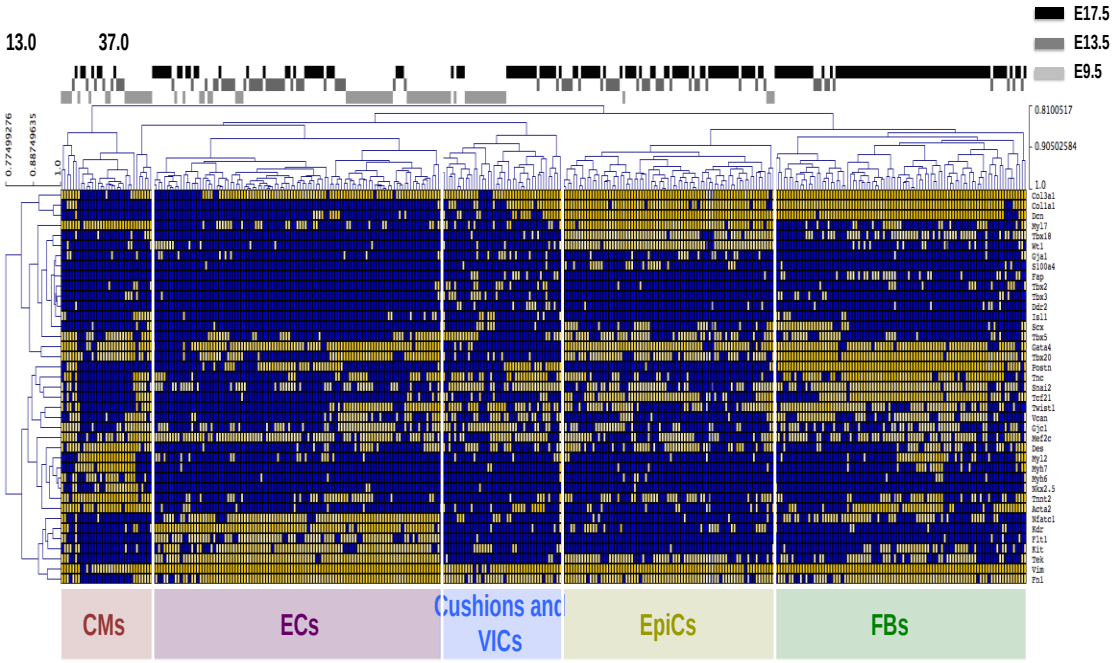

Figure S4, related to Figure 3. Transcriptional profile, at the single cell level, of the distinct cardiac populations. Hierarchical clustering of the single cell qRT-PCR analysis from E9.5, E13.5 and E17.5 cardiac populations highlights the transcriptional relationship of the populations along time.

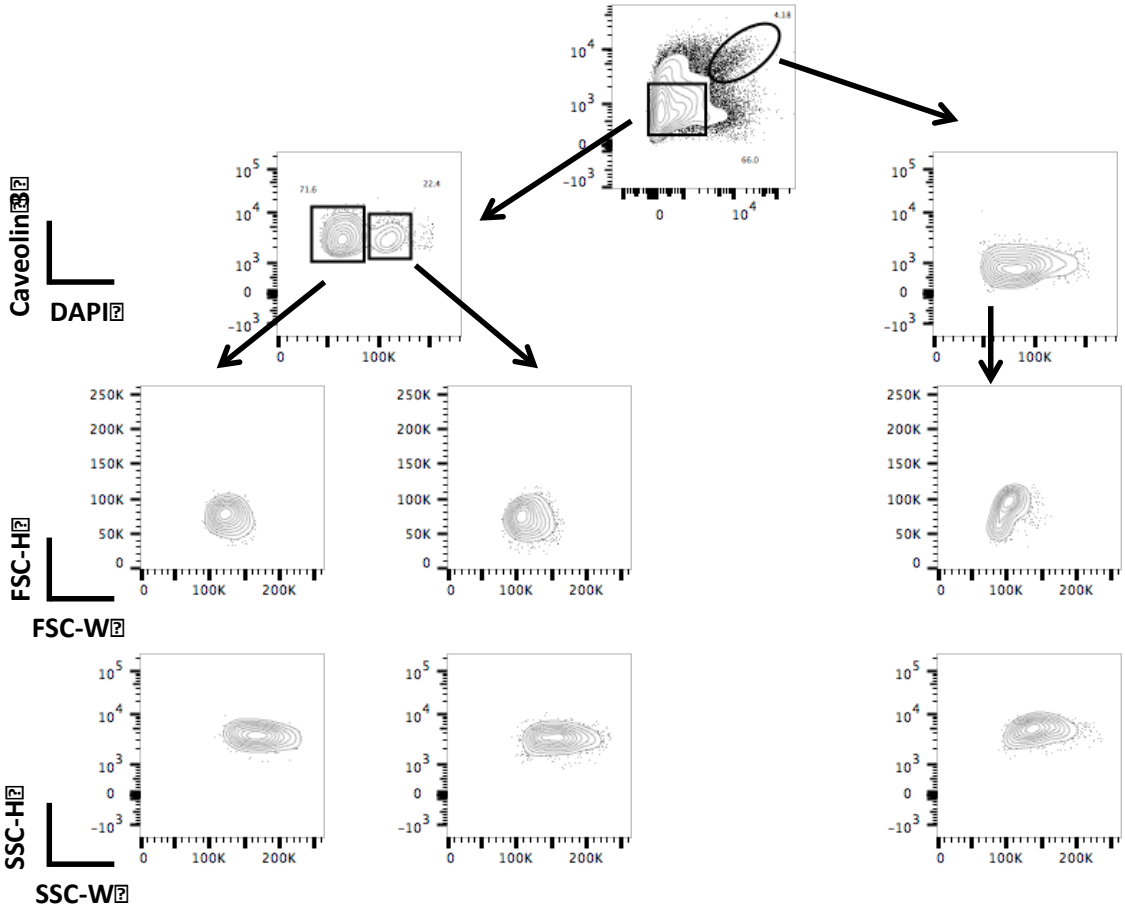

Figure S5, related to Figure 6. Analysis of the doublet discrimination in the two subsets of cardiomyocytes. Representative contour plots of the height versus width in the Forward and Side scatters, excluding the possibility of the binucleation to be result of cell doublets.

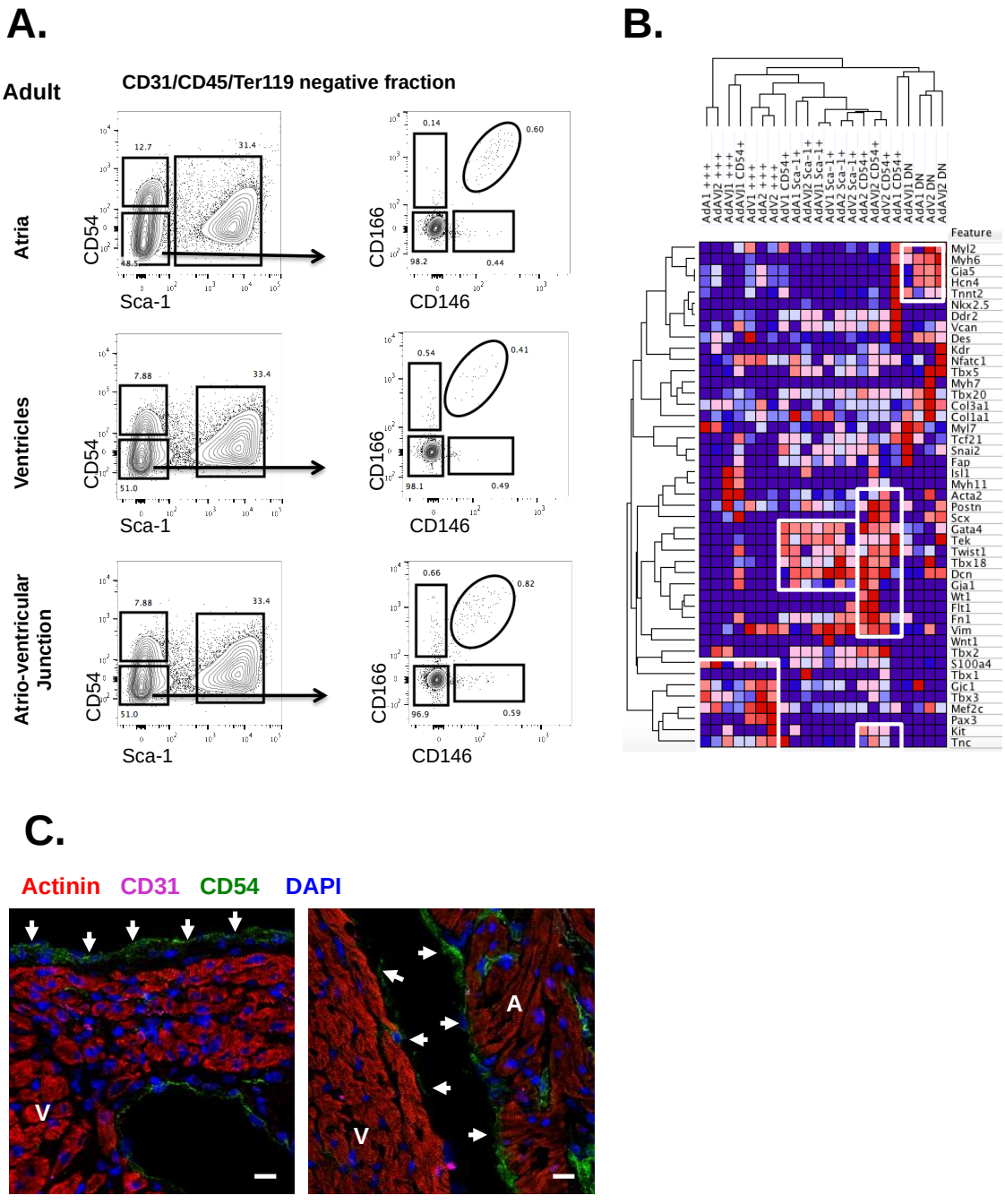

Figure S6. Adult heart cell surface signatures. A. The same analysis strategy was followed for the adult, revealing that the majority of the cell phenotypes identified in the embryo are not observed in the adult heart, except CD54 and Sca-1 which are maintained and increased. **B.** Heat map of multiplex qRT-PCR data analysis, at the population level (20 sorted cells), demonstrating the general differences on the gene expression of the adult populations. HPRT was used as housekeeping gene (n=2). **C.** *In situ* analysis of CD54 signatures delineating epicardial layer (arrows). A | Atria; V | Ventricle. Scale bar: 20 μm.

SUPPLEMENTAL TABLES

Table S1, related to Figure 1A. Panel of antibodies used for embryonic/fetal hearts characterization by flow cytometry and cell sorting.

Panel I	
CD90.2	FITC
CD45	PE
Ter119	PE
Sca-1	PECy5
CD24	PECy7
Dead cells	PI*
CD31	APC
CD54	APCCy7

* PI – propidium iodide

Table S2, related to Figure 1C. Panel of antibodies used for fetal hearts characterization of the cell cycle by flow cytometry.

Panel II-I		**Panel II-II**	
Ki67	FITC	Ki67	FITC
CD45	PE	CD90.2	PE
Ter119	PE	Sca-1	PECy5
Sca-1	PECy5	CD24	PECy7
CD24	PECy7	CD31	APC
CD31	APC	CD45	APCCy7
CD54	APCCy7	Ter119	APCCy7
DNA	DAPI	CD54	APCCy7
		DNA	DAPI

Table S3, related to Figure 4. Panel of antibodies used for the refinement of fetal hearts characterization by flow cytometry and cell sorting.

Panel III (Sony analyzer)		**Panel IV (BD Aria III)**	
CD146	FITC	CD146	FITC
PDGFrα	PE	PDGFrα	PE

Sca-1	PECy5	Sca-1	PECy5
CD24	PECy7	CD24	PECy7
Dead cells	PI	Dead cells	PI
CD166	APC	CD166	APC
CD90.2	BV605	CD90.2	BV605
c-Kit	APCCy7	CD31	BV421
CD45	BV421	CD45	BV421
Ter119	BV421	Ter119	BV421
CD31	BV421	CD54	BV421
CD54	PB		

Table S4, related to Figure 5. Panel of antibodies used for cardiomyocytes phenotyping by flow cytometry.

Panel IV-I		**Panel IV-II**	
CD146	FITC	CD146	FITC
Caveolin3	Cy3	Troponin T	Cy3
CD24	PECy7	CD24	PECy7
CD166	APC	CD166	APC
CD45	APCCy7	CD45	APCCy7
Ter119	APCCy7	Ter119	APCCy7
CD54	APCCy7	CD54	APCCy7
DNA	DAPI	DNA	DAPI

Table S5, related to Figure S5B. Panel of antibodies used for adult hearts cell sorting.

Panel V	
CD146	FITC
CD31	PE
CD45	PE
Ter119	PE
Sca-1	PECy5
CD24	PECy7
Dead cells	PI
CD166	APC

CD54	PB

Table S6, related to Experimental Protocol. List of antibodies used by flow cytometry along this work.

Protein	Clone	Fluorochrome	Source	Reference
CD146	ME-9F1	FITC	Miltenyi biotec	130-102-230
CD90.2	30-H12	FITC	BD Bioscience	553013
Ki67	MOPC-21	FITC	BD Bioscience	556026
CD45	30-F11	PE	BioLegend	103106
Ter119	TER-119	PE	BioLegend	116208
CD31	MEC13.3	PE	BD Bioscience	553373
PDGFrα	APA5	PE	BioLegend	135905
CD90.2	30-H12	PE	BD Bioscience	553014
Sca-1	D7	PECy5	BioLegend	108110
CD24	M1/69	PECy7	BD Bioscience	560536
CD166	eBioALC48	APC	eBiscience	17-1661-82
CD90.2	53-2.1	BV605	BD Bioscience	563008
CD31	MEC13.3	Alexa Fluor® 647	BioLegend	102516
c-Kit	2B8	APCCy7	BioLegend	105825
CD31	MEC13.3	BV421	BD Bioscience	562939
CD54	YN1/1.7.4	PB	BioLegend	116116
CD54	3E2	B	BD Bioscience	553251
CD45	30-F11	B	BioLegend	103104
Ter119	TER-119	B	BD Bioscience	553672
Caveolin 3	-	-	BD Biosciences	610420
TroponinT	13-11	-	Thermo Scientific	MS-295-P0
Donkey Anti-Mouse IgG	-	Cy3	Jackson Immunoreserach Laboratories	715-167-003
SAV	-	APCCy7	BioLegend	405208
SAV	-	BV421	BioLegend	405225

Table S7, related to Experimental Protocol. List of Taqman® Assays used along this work.

Gene	Gene Symbol	Gene ID	Taqman® Assay ID
Islet1	Isl1	16392	Mm00517585_m1
Nkx2.5	Nkx2-5	18091	Mm01309813_s1
Gata4	Gata4	14463	Mm00484689_m1
Mef2c	Mef2c	17260	Mm01340842_m1
Tbx5	Tbx5	21388	Mm00803518_m1
Mlc2v	Myl2	17906	Mm00440384_m1
Mlc2a	Myl7	17898	Mm01183005_g1
cTnt	Tnnt2	21956	Mm01290256_m1
bMHC	Myh7	140781	Mm00600544_m1
aMHC	Myh6	17888	Mm00440359_m1
Connexin 43	Gja1	14609	Mm00439105_m1
Connexin 40	Gja5	14613	Mm01265686_m1
Connexin 45	Gjc1	14615	Mm01253027_m1
Wt-1	Wt1	22431	Mm01337048_m1
Tbx18	Tbx18	76365	Mm00470177_m1
Tbx20	Tbx20	57246	Mm00451515_m1
Tbx3	Tbx3	21386	Mm01195726_m1
Tbx2	Tbx2	21385	Mm00436915_m1
NG2	Vcan	13003	Mm01283063_m1
SMA	Acta2	11475	Mm01546133_m1
sm-MHC	Myh11	17880	Mm00443013_m1
Slug	Snai2	20583	Mm00441531_m1
Twist1	Twist1	22160	Mm04208233_g1
Scleraxis	Scx	20289	Mm01205675_m1
Tcf21	Tcf21	21412	Mm00448961_m1
DDR2	Ddr2	18214	Mm00445615_m1
Fsp1	S100a4	20198	Mm00803371_m1
Vimentin	Vim	22352	Mm01333430_m1
Periostin	Postn	50706	Mm00450111_m1
Decorin	Dcn	13179	Mm00514535_m1
Coll I	Col1a1	12842	Mm00801666_g1
Coll III	Col3a1	12825	Mm01254476_m1

Fap	Fap	14089	Mm01329177_m1
Desmin	Des	13346	Mm00802455_m1
Flk1	Kdr	16542	Mm01222421_m1
Flt1	Flt1	14254	Mm01210866_m1
Nfatc1	Nfatc1	18018	Mm00479445_m1
Tie2	Tek	21687	Mm00443243_m1
Tenascin C	Tnc	21923	Mm00495662_m1
Fibronectin	Fn1	14268	Mm01256744_m1
c-Kit	Kit	16590	Mm00445212_m1
HCN4	Hcn4	330953	Mm01176086_m1
Wnt1 (NCC)	Wnt1	22408	Mm01300555_**g1**
Pax3	Pax3	18505	Mm00435491_m1
Tbx1	Tbx1	21380	Mm00448949_m1
Gapdh	Gapdh	14433	Mm99999915_g1
HPRT	Hprt	15452	Mm01545399_m1
Actin beta	Actb	11461	Mm00607939_s1

CHAPTER IV

ESTABLISHING THE GROUNDS FOR *IN VIVO* FUNCTIONAL EVALUATION OF CARDIAC SUBSETS IN THE CONTEXT OF MYOCARDIAL INFARCTION

MI is one of the most used experimental models of cardiac injury in preclinical studies to dissect the pathophysiological mechanisms of cardiac remodeling and progressive HF at the cellular and molecular level. Tissue alterations and the extension of the lost myocardium are predictors of long-term LV function and geometry and a critical determinant of clinical outcome, even in humans with acute MI. Pathogenesis of the MI is characterized by a series of cellular events that contribute to complete the healing process, as well as the assembly of a collagen-rich ECM, features which we have assessed in the experimental murine model established in our laboratory. Similarly to other works (Virag and Murry, 2003), the permanent ligation of the left coronary artery in the mouse resulted in a trans-mural MI that extends from the apex to the free LV wall (Figure 1). Histochemistry analysis of Hematoxylin-Eosin (HE) stained MI heart demonstrated the cellular progression from coagulative necrosis to scar tissue formation, while Masson's Trichrome (MT) staining evidenced the collagen deposition as part of ECM remodeling (Figure 1). Structural alterations following MI include inflammatory, proliferative and maturation phases, which were found in our MI experimental model (Figure 2). During the first phase, inflammatory cells promote the removal of dead CMs and cellular debris. In our model, the inflammatory phase was detected from 48 hours post-MI until the 4^{th} day after ischemia is established. Seven days after surgery (proliferative phase), we observed granulation tissue (new and transient connective tissue observed in the wound healing process), composed by mononuclear inflammatory cells and by a peak of proliferation, particularly on the vessels' wall and myofibroblasts, *i.e.* activated fibroblast expressing α-smooth muscle actin. These are important players in the MI healing process, because they replace physically the void created by phagocytized CMs and produce and organize the ECM

(Figure 1 and 2). In the maturation phase, we observed a decrease in cellular components and extensive deposition of aligned collagen fibers, leading to the production of resistant scar tissue (Figure 1 and 2). Alongside, the ECM suffers adverse changes due to CMs death and their progressive replacement by fibrotic tissue, resulting in thinning of the LV wall and LV chamber dilation over time – cardiac remodeling. These alteration allow quantifying the extent of the infarction, an essential measure when assessing the morphological and functional consequences of ischemia and a major end-point in clinical trials of emergent therapies (e.g. regenerative potential of cell, genetically and/or pharmacological based-therapies) (Csonka et al., 2010; Takagawa et al., 2007). Despite the widespread application of the histological analysis as a key readout in these studies, there are a number of hurdles associated with the use of this methodology. Potential limitations include time-consuming analysis and high variability amongst studies since the infarct size may, in fact, diverge depending on the method used (Csonka et al., 2010; Takagawa et al., 2007; Zornoff et al., 2009). Likewise, several features of MI size quantification are inconsistent and not yet clearly described, *e.g.* the number of sections used for calculation, the histological staining and the criteria used to identify the ischemic region.

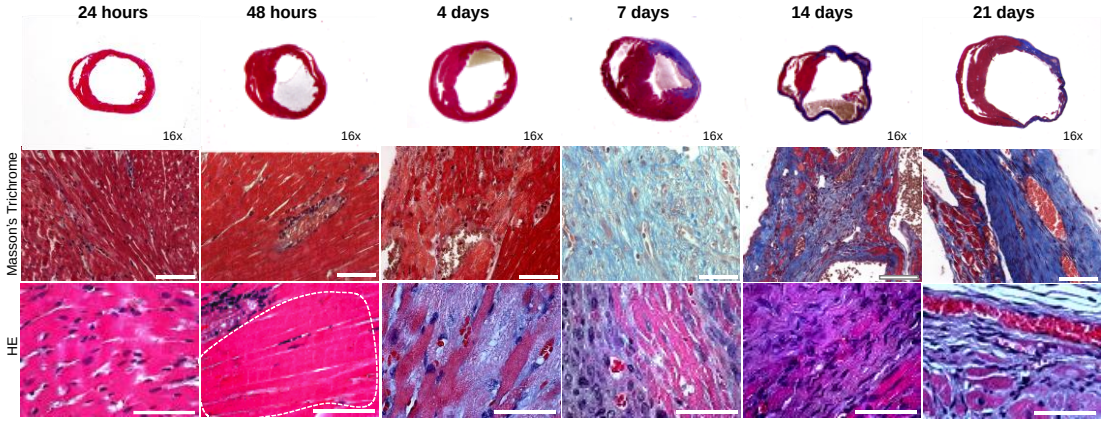

Figure 1. Histopathological evolution of mouse induced myocardial infarction. A. Stereomicroscopic view of representative sections of the LV collected from MI mice at different time-points after surgery, demonstrating the LV remodeling after permanent ligation of the coronary artery with progressive thinning of LV wall, chamber dilation and collagen deposition. Transverse sections were stained with TM, which highlight in red the myocardium and in blue the collagen deposition. Magnification 16x. **B.** In higher magnification, the TM and HE staining showed histological alterations at the cellular level in response to MI. Scale bar 50 µm. (Valente M et al., unpublished)

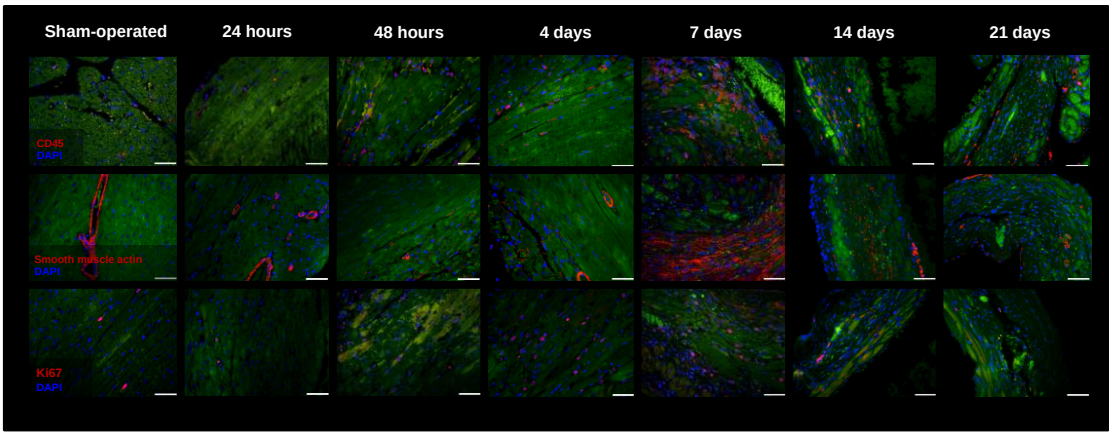

Figure 2. Cellular characterization of induced myocardial infarction. Representative images of the myocardial-infarcted murine heart characterization. The number of inflammatory cells ($CD45^+$), myofibroblasts (SMA^+ cells outside vessels) and proliferating cells ($ki67^+$) increased 48h after coronary occlusion with a peak at 7 days following surgery. At 14 days post-surgery all cell-types related to injury decreased, although the number of $CD45^+$ cells and myofibroblasts where still higher than the ones observed in sham-operated mice at 21 days. Scale bar 50µm. (Valente M et al., unpublished)

Hence, we hereby report the development and validation of *MIQuant,* a user-friendly semi-automated software application that calculates the infarct size on cardiac models of induced-ischemia, as well as a detailed protocol for the representative sampling of the ischemic mouse heart for morphometric analysis of the LV. The extended use of this sampling to other *in situ* analyses will be demonstrated by assessment of neovascularization and exogenous cells engraftment, in the case of cell-based therapies (full version in *Appendix II*).

Although they are not in the scope of this *Thesis*, details on the design i.e. the digital image processing methodology of the software application *MIQuant* (herein available as a freeware) have been published in the following peer-reviewed Proceedings of International Conferences:

Esteves, T., Valente, M., Nascimento, D.S., Pinto-do-Ó, P. and Quelhas P. Automatic and semi-automatic analysis of the extension of myocardial infarction in an experimental murine model. **Pattern Recognition and Image Analysis – Proceedings at 5th Iberian Conference, IbPria 2011 | Lecture notes in Computer Science**, 2011, 6669/2011, 151-158, DOI: 10.1007/978-3-642-21257-4_19.

URL:http://www.ineb.up.pt/docs/marianavalente/Esteves_(2011)_Automated_myocardial_infarction_analysis_in_an_experimental_model_using_image_segmentation_and_model_adaptation.pdf

Esteves, T., Valente, M., Nascimento, D.S., Pinto-do-Ó, P. and Quelhas, P. Automatic Myocardial Infarction Size Extraction in a Experimental Murine Model using an Anatomical Model. **Proceedings at 2012 IEEE International Symposium on Biomedical Imaging (ISBI).** art. No. 6235546, pp. 310-313.

URL:http://www.ineb.up.pt/docs/marianavalente/Esteves(2012)_AUTOMATIC_MYOCARDIAL_INFARCTION_SIZE_EXTRACTION_IN_AN_EXPERIMENTAL_MURINE_MODEL_USING_AN_ANATOMICAL_MODEL.pdf

MIQuant – Semi-automation of Infarct Size Assessment in Models of Cardiac Ischemic Injury

Diana S. Nascimento*[1], Mariana Valente*[1,2], Tiago Esteves[1,3], Maria de Fátima de Pina[1,4], Joana G. Guedes[1], Ana Freire[1,3], Pedro Quelhas[1,3] and Perpétua Pinto-do-Ó[1]

[1]INEB – Instituto de Engenharia Biomédica, Universidade do Porto, Porto, Portugal.

[2]Instituto de Ciências Biomédicas Abel Salazar, Universidade do Porto, Porto, Portugal.

[3]Faculdade de Engenharia, Universidade do Porto, Porto, Portugal.

[4]Departamento de Epidemiologia Clínica, Medicina Preditiva e Saúde Pública, Faculdade de Medicina da Universidade do Porto, Porto, Portugal

*Equally contributing authors.

Corresponding Author: Perpétua Pinto-do-Ó at Stem Cell Biology Team, NEWTherapies Group, INEB - Instituto de Engenharia Biomédica, Universidade do Porto, Rua do Campo Alegre, 823, 4150 - 180 Porto, Portugal; Tel.: 351 226074900; Fax: 351 226094567; E-mail: perpetua@ineb.up.pt.

Article published in ***PLoS ONE***, 2011, 6(9): e25045.

DOI: 10.1371/journal.pone.0025045

ABSTRACT

Background

The cardiac regenerative potential of newly developed therapies is traditionally evaluated in rodent models of surgically-induced myocardial ischemia. A generally accepted key parameter for determining the success of the applied therapy is the infarct size. Although regarded as a gold standard method for infarct size estimation in heart ischemia, histological planimetry is time-consuming and highly variable amongst studies. The purpose of this work is to contribute towards the standardization and simplification of infarct size assessment by providing free access to a novel semi-automated software tool. The acronym *MIQuant* was attributed to this application.

Methodology/Principal Findings

Mice were subject to permanent coronary artery ligation and the size of chronic infarcts was estimated by area and midline-length methods using manual planimetry and with *MIQuant*. Repeatability and reproducibility of *MIQuant* scores were verified. The validation showed high correlation ($r^{midline\ length}$ = 0.981; r^{area} =0.970) and agreement (Bland-Altman analysis), free from bias for midline length and negligible bias of 1.21% to 3.72% for area quantification. Further analysis demonstrated that MIQuant reduced by 4.5-fold the time spent on the analysis and, importantly, *MIQuant* effectiveness is independent of user proficiency. The results indicate that *MIQuant* can be regarded as a better alternative to manual measurement.

Conclusions

We conclude that *MIQuant* is a reliable and an easy-to-use software for infarct size quantification. The widespread use of *MIQuant* will contribute towards the standardization of infarct size assessment across studies and, therefore, to the systematization of the evaluation of cardiac regenerative potential of emerging therapies.

INTRODUCTION

Cardiovascular disease is a leading cause of morbidity and mortality worldwide. Heart failure due to ischemic coronary artery disease is currently the most common cardiac disorder and it correlates with a worse prognosis (Gonzales and Pedrazzini, 2009; Lloyd-Jones et al., 2010). The physiological, histological and molecular changes associated with clinical ischemic heart disease have been clarified with the use of experimental models of myocardial infarction (MI) developed in both large animals, including dogs and swine, as well as in small rodents (Sun, 2009; Zaragoza et al., 2011). The latter are more applicable for high-throughput screening of novel therapeutic approaches, due to the easy maintenance, short reproductive cycle and to the latest advances in gene-targeting and transgenic technologies. In recent years, the evaluation of cardiac regenerative potential of newly developed therapies, as is the case of gene-delivery and transplantation of stem/progenitor-cells, has been primarily explored in rat and mouse models of surgically-induced myocardial ischemia (Ahmed et al., 2010; Gonzales and Pedrazzini, 2009; Ramani et al., 2011; Smits et al., 2009b; Yoon et al., 2005). The so-called left anterior descending (LAD) coronary artery ligation is the prominent model in these studies, and the infarct size has been considered a key parameter for assessing the success of the novel therapy. A strong correlation between the infarction size and the functional and hemodynamic alterations following myocardial infarction is generally observed (Gao et al., 2000; Pfeffer et al., 1979; Takagawa et al., 2007) and therefore considered a fundamental measure in the assessment of the morphological and functional consequences of infarction.

In studies involving an experimental MI setting, the calculation of the infarct size is typically evaluated by histological measurements of either: (a) the endocardial and epicardial length (Patten et al., 1998; Takagawa et al., 2007), (b) the midline length (Takagawa et al., 2007), (c) the endocardial length (Pfeffer et al., 1979) or (d) the area (Michael et al., 1995) of infarcted *versus* non-infarcted left-ventricle (LV) regions. Despite the widespread use of the aforementioned approaches, the infarct size can vary depending on the used method (Minicucci et al., 2007; Takagawa et al., 2007) and therefore no direct comparison can be withdrawn across laboratories. Moreover, several aspects of MI size quantification that can also account for infarct size variation are inconsistent across studies and not always clearly defined, e.g. the number of sections used for the calculation, the histological staining and criteria used to identify the infarcted region. Thus, the purpose of the present work is to contribute towards standardization and simplification of the infarct size assessment in experimental models of MI by making available, as freeware, an easy-to-use semi-automatic software application, which we developed and validated at the “bench”. This tool will contribute for the systematization of the evaluation of cardiac regenerative potential of newly developed therapies. The acronym *MIQuant* that stands for *MI quantification* was attributed to the herein software application.

METHODS

Animals

Male and female C57BL/6 mice aged 8 to 12 weeks were used for this study. All the procedures were subjected to approval by the IBMC-INEB (Instituto de Biologia Molecular e Celular – Instituto de Engenharia Biomédica) Animal Ethics Committee and to the National Direção Geral de Veterinária (permit no: 022793), and are in

conformity with the Directive 2010/63/EU of the European Parliament. Humane endpoints were followed in accordance to the Organisation for Economic Co-operation and Development (OECD) Guidance Document on the Recognition, Assessment, and Use of Clinical Signs as Humane Endpoints for Experimental Animals Used in Safety Evaluation (2000).

Surgical Induction of Myocardial Infarction

MI was experimentally induced by ligation of the LAD coronary artery as described elsewhere (Michael et al., 1995) with minor alterations. Following anesthesia by intraperitoneal injection (ip) of medetomidine (Sededorm, 1mg/Kg) and ketamine (Clorketam, 75mg/kg), animals were subjected to endotracheal intubation and were mechanically ventilated using a small-animal respirator (Minivent 845, Harvard Apparattus). Animals were maintained on warming pads during surgical procedure and until full recovery to prevent hypothermia. Under a stereomicroscope (Leica EZ4, Leica Microsystems) the heart was exposed (Ø 5-7 mm) via left thoracotomy on the third intercostal space and the pericardial sac was gently disrupted. After identification of the LAD coronary artery a non-absorbable 7-0 suture (Silkam®, B. Braun) was passed under the artery and the ligation was performed. The intercostal incision was closed by an absorbable 6-0 suture (Safil®, B. Braun) and surgical staples were used for skin closure. Anesthesia was reverted by atipamezole (ip, Revertor, 5mg/Kg) and analgesia was achieved by butorphanol (ip, Butador, 1mg/Kg). Analgesia and fluid therapy were performed by ip delivery of butorphanol (Butador, 1mg/kg) and 5% glucose physiological saline, respectively. This procedure was repeated every 12h up to 72h post-surgery or until full animal recovery.

For organ collection animals were deeply anesthetized by ip injection of pentobarbital (Eutasil, 70mg/kg). At 21days post-surgery, hearts were harvested, briefly washed in phosphate buffer saline and fixed in 10% Formalin neutral buffer (VWR BDH & Prolabo) up to 24 hours prior to paraffin-embedding. The sampling procedure herein

described results on hearts arrested at variable stages of heart cycle, which may contribute to increased variability of infarct size. Whenever normalization is a requirement, hearts should be arrested in diastole following injection with potassium chloride.

Histological procedures

Representative sampling of the LV (approx. 12 sections) was obtained by transverse sectioning (3μm) from the apex to the base (atrium region) of paraffin-embedded hearts with an interval of 300μm among each section (Figure 1A).

Paraffin sections were stained with modified Masson's trichrome staining (MT). MT staining was performed according to the Trichrome (Masson) Stain kit (Sigma-Aldrich) with the following modifications: nuclei were pre-stained with Celestine Blue solution following staining with Gill's Hematoxylin and incubation for 1 hour in aqueous Bouin's solution to promote a uniform staining.

Myocardial infarct size calculation

For infarct size determination the collagen deposition, highlighted (blue) in MT-stained sections collected at 21 days post-infarction, was used to define the LV scarred region. Images of histological sections were captured with an Olympus SZX10 stereomicroscope and Olympus DP21 camera. The percentage of affected LV wall was calculated by two different and previously validated methods: the *area measurement* (calculated by dividing the infarct area by the total LV area) (Michael et al., 1995) and the *midline length measurement* (calculated by dividing the midline length of the infarcted LV wall by the midline length of total LV wall). Only regions with infarct in >50% of the whole thickness of the myocardium were considered for infarct midline (Takagawa et al., 2007). The MI size determination was performed either manually, by drawing points to outline different anatomical/pathological regions using the Image J 1.42 software (Figure 1B), or by using *MIQuant* (Figure 1C).

Software design

The *MIQuant* software was implemented in MATLAB™ and a MS Windows™ 32-bit compiled version is available online at http://paginas.fe.up.pt/~quelhas/MIQuant/MIQuant.zip. With the objective of developing an approach for automatic infarct size estimation several image processing methodologies were tested (Esteves et al., 2011) and, within all tested semi-supervised methods, region growing was found to work best and also faster, being selected for the final software implementation.

Data and statistical analysis

To validate *MIQuant*, four expert researchers analyzed five hearts (twelve sections *per* heart) using midline and area methods, manually and with *MIQuant*. All *experts* repeated measures at three distanced moments (one month between 1st and 2nd measure and one week between 2nd and 3rd). A one-way repeated measures analysis of variance (ANOVA) was conducted to evaluate repeatability. Seven non-trained *volunteers* measured the same samples using *MIQuant*. The association between manual and *MIQuant* results was investigated using the Pearson product-moment-correlation coefficient (*r*). Additionally, to address agreement amongst methods, the Bland-Altman agreement statistical method was used (Bland and Altman, 1986) following verification of the normal distribution (Gaussian) of results. A two-way between-groups ANOVA was applied to address the impact of observers and heart samples in the results. Post-hoc comparison using the Tukey HSD test was performed. Expert and volunteer results were compared by an independent-samples *t*-test. The time required for manual and *MIQuant*-assisted infarct size calculation was compared by the Mann-Whitney test.

RESULTS

Software overview and availability

MIQuant is a user-friendly software application that assists on the infarct size quantification in an experimental MI-setting. The infarct size, defined as the percentage of the LV affected by coronary artery occlusion, is estimated with representative cross-sections of the LV stained with MT that enables the identification of collagen deposition, a hallmark of established infarction. The software allows the upload of single or multiple images and enables the computation of the MI size of each image, calculated by area(Michael et al., 1995) and midline length (Takagawa et al., 2007) methods, and the total infarct size mean value that can be saved in excel file-format.

MIQuant was designed by applying the region growing image segmentation method, which exploits the spatial context of pixels with similar pixel-color properties. The main criterion for the algorithm of region growing is homogeneity, similar pixels (or regions) that are neighbors are joined together. For each image, region growing requires initial image points (or seeds) that define the region of interest. From these initial points the algorithm grows until no more neighbors can be joined to the region of interest, therefore regions/pixels are merged if they satisfy the chosen criterion and no merging occurs when the criterion is not met (Gonzalez et al., 2004; Wu et al., 1996). In the *MIQuant* software the user is asked to provide input seed points for the LV lumen (if present in the image) and the viable myocardium (if present in the image), prior to automated segmentation. The choice of not requiring the user to select the infarcted LV region has to do with the heterogeneity of the ischemic tissue. The user clicks with the

mouse on the heart section image and gives as many input points as desired. Following selection of the viable myocardium and/or LV lumen the segmentation is generated and displayed on the screen. This will be the support for the infarct size computation. User adjustments to the segmentation are accessible by varying the merging criteria and the segmentation process can be repeated until the user is satisfied with the results. When the segmentation is complete the user can request computation of infarct size results by both midline length and area methods. For the midline length measurement, the *MIQuant* software automatically traces lines from the lumen center outwards and identifies the middle distance between tissue boundaries. The midline of the infarcted region was considered when the LV wall was affected in more than 50% in radial direction. The midline generated by the software can be adjusted by the user prior to MI size calculation.

Commands for image edition are available on the “edit menu”, which permits the removal of tissue regions/artifacts that may interfere with tissue automated segmentation, e.g. the right ventricle or blood within the LV lumen.

The *MIQuant* software was implemented in MATLAB™ and a MS Windows™ 32 bit compiled version is available online at http://paginas.fe.up.pt/~quelhas/MIQuant/MIQuant.zip. The archive should be downloaded and unzipped into a specific folder. The *MIQuant* manual reading is recommended prior to beginning with the software, available at http://www.fe.up.pt/~quelhas/MIQuant/MIQuant_manual.pdf. *MIQuant* requires the installation of MATLAB™ or of the MATLAB™ Component Runtime (MCR) installer (http://paginas.fe.up.pt/~quelhas/MIQuant/MCRInstaller.zip). The application can be initiated by double-click on the executable “MIQuant” file. More information about the software usage and installation is available at the *MIQuant* website http://www.fe.up.pt/~quelhas/MIQuant/.

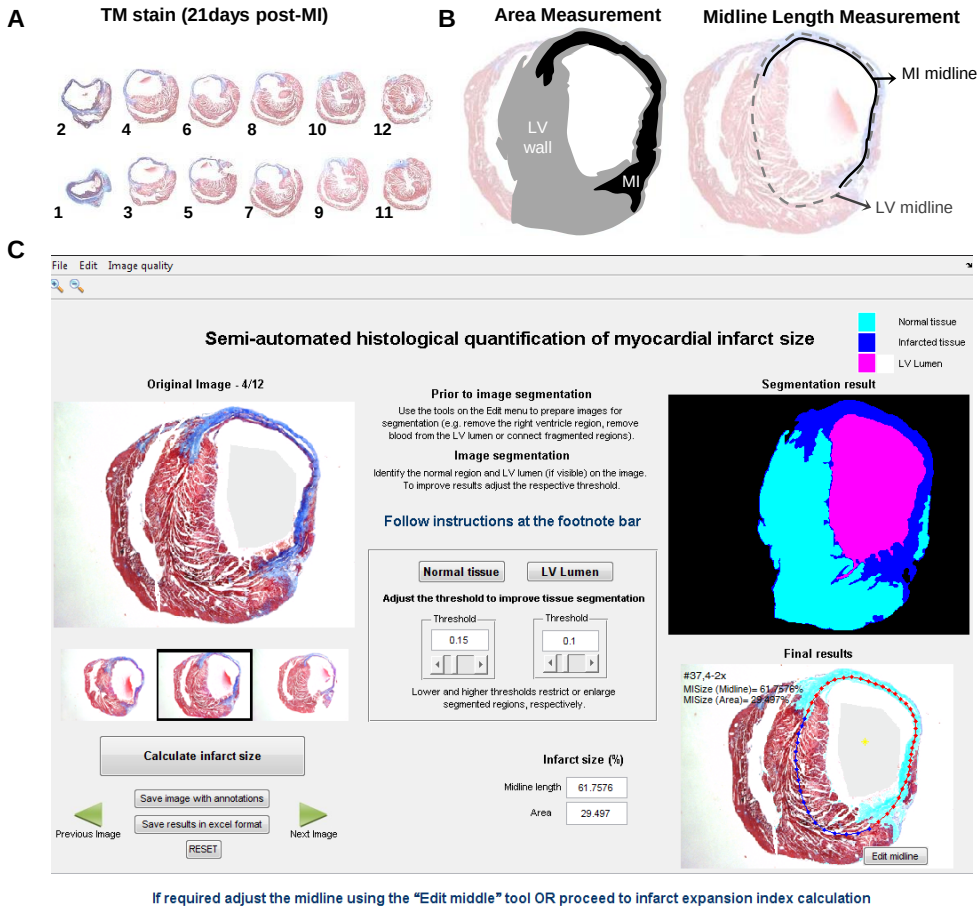

Figure 1. Manual and *MIQuant* semi-automated calculation of MI size in chronic infarcts. (A) LV representative MT stained sections, numbered from the apex to the LV base, were obtained from an infarcted heart harvested at 21 days post-surgery. (B) Histological infarct size calculation by the area method requires manual tracing of the LV myocardium (light gray) and of the scarred LV tissue (black). The infarct size, expressed as a percentage, is the division of the infarct area by the LV area multiplied by 100. For the midline length approach (right) the midline, herein defined as the mid-region between the epicardial and endocardial surfaces, of the total LV (dashed line) and of scarred region (full line) are manually traced. The infarct size, expressed as a percentage, is the division of the infarct midline length by the LV midline length multiplied by 100. The total LV infarct extent is the average of infarct size obtained for the LV representative cross-sections (A). (C) Screen shot of *MIQuant* layout following infarct size calculation. Multiple images can be uploaded in TIFF or JPEG file-formats and the software calculates the intermediate values of infarct size for each image (bottom right). A total MI size is also generated assuming that the uploaded images were representative sections of the LV. For selection of the scarred myocardium (top right) the software requires the user to double-click in a normal tissue region and in the LV lumen, if applicable, over the uploaded image (top left).

MIQuant repeatability and reproducibility

Manual and *MIQuant* infarct size quantification was assessed by two well-validated methods, i.e. the area and the midline length measurement (Figure 2A). Visual inspection of the infarct size scores across methods demonstrate that *MIQuant* results are consistent with the manual assessment, and thus infarct values obtained with the area measurement were significantly smaller than the midline length infarct scores. The similarity between the manual and *MIQuant* approaches demonstrate that the latter might constitute an alternative for the histological quantification of infarct size. Further validation of *MIQuant* is detailed bellow.

Intra-(repeatability) and inter-observer (reproducibility) variability was considered in the experimental design, thus three independent measures were conducted by four different users. Repeated measures one-way ANOVA was applied to compare the repeatability of the area and midline length-based methods, both calculated manually and by using *MIQuant*. The LV infarct size means with standard deviations and ANOVA results are detailed in table 1. No significant effect of the repetition was found on the infarct size obtained *per* section and *per* heart, i.e. mean value of 12 sections representative of the LV, demonstrating the consistency of *MIQuant* measurements obtained at different instances.

Inter-observer variability for each analyzed sample is displayed on Fig. 2B. A two-way ANOVA was conducted to investigate whether the observer influences (inter-observer variability) infarct size measurements manually or using *MIQuant*. Post-hoc comparison using the Tukey HSD test indicated that the mean score of infarct size, for each heart, did not differ significantly ($p > 0.05$) among observers in any of the tested infarct size quantification methods. However, a tendency for increased variability of the manual results when compared to *MIQuant* was observed and was particularly evident on heart C, which is the sample that retrieved more deviation amongst users (Figure 2B).

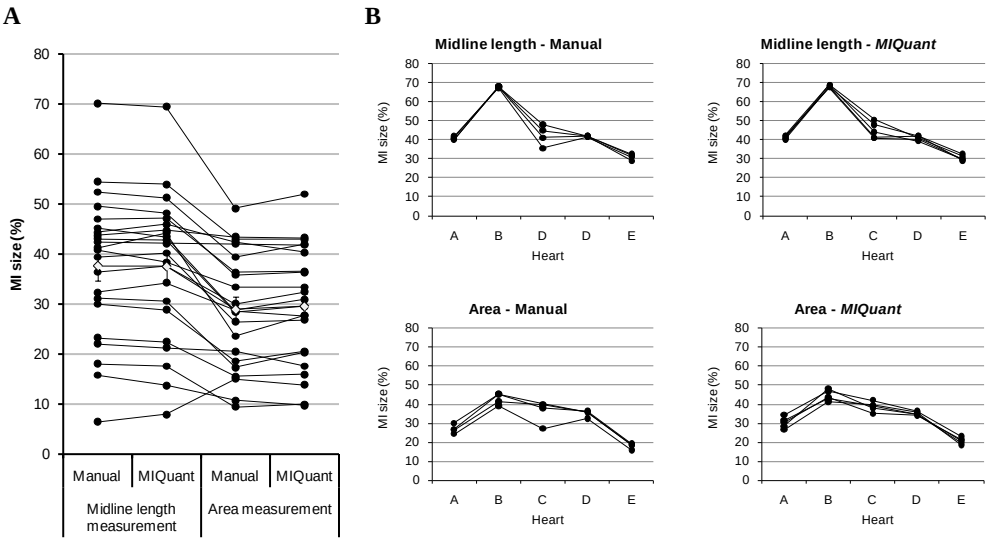

Figure 2. Consistency and reproducibility of *MIQuant infarct size calculation*. (A) Consistency of manual and *MIQuant* infarct size results obtained using the area and midline length measurements. Hearts were harvested at 21 days post-surgery and infarct size determinations are the mean value of 12 cross-sections representative of the LV. Mann-Whitney statistical analysis demonstrated significant differences between the area and midline length methods, as already described by Takagawa (Takagawa et al., 2007). (B) Reproducibility of *MIQuant* measurements. Although ANOVA demonstrated no significant influence of the observer on the LV infarct size scores obtained, neither manually nor using *MIQuant*, the latter displays a tendency for lower discrepancy between operators. ◇ indicates the mean value of each group. * $p < 0.05$.

Validation of *MIQuant* infarct size quantification

A scatter diagram of the infarct size values measured manually and by *MIQuant* is shown in Fig. 3A. The Pearson Product-moment correlation for the individual data points was $r = 0.981$ for the midline length and $r = 0.970$ for the area methods, with a significance level of $p < 0.01$, hence the infarct size values obtained by *MIQuant* are strongly associated to the manual quantification. The strong correlation between manual and *MIQuant* results prompted further analysis to evaluate the magnitude and direction of the differences between methods.

The gold-standard statistical analysis applied to method-comparison studies is the Bland-Altman plot, which determines the agreement of two methods that measure the same variable (Bland and Altman, 1986; Hanneman, 2008). Manual and *MIQuant*

results were subjected to the Bland-Altman agreement statistical method that predicts the bias, i.e. difference in values obtained by the two methods, and the limits of agreement between methods (Figure 3B and C). Bias and concordance limits of ±2% and ±7%, respectively, were established *a priori* as the maximum parameters for acceptance of *MIQuant* regarding *per* heart infarct size quantifications. These values were selected on the basis of acceptance limits addressed for infarct size methods on published studies (Bohl et al., 2009; Dawson et al., 2004; Protti et al., 2010; Yang et al., 2004). The *a priori* establishment of acceptable agreement limits for infarct size *per* section was conditioned by the fact that, to our best knowledge, no previous comparison was performed for single sections. Hence, since it is expected higher degree of discordance across sections, when compared to the mean value, a low-stringency predetermined bias and concordance limits of ±2% and ±15%, respectively, were established.

Bland-Altman analysis was conducted with manual and *MIQuant* results obtained *per* LV section (Figure 3B). The estimated bias is 0.36% with concordance limits of -10.72% and 11.45% for the midline length method, whereas for the area approach the bias is 2.68% with limits of agreement of -7.59% and 12.94% (Figure 3B). Hence, for both methodological approaches, the predicted confidence interval is within acceptance limits and so *MIQuant* is considered equivalent to the established manual quantification method.

The visual inspection of Bland-Altman plot denoted that differences between *MIQuant* and manual measurements are scattered around the bias with no obvious pattern for the midline length results whereas, the area differences appear to increase for higher infarction values (Figure 3B). To determine whether an association exists between the methods discrepancies and the size of infarction, the Pearson coefficient was calculated and a small, non-statistically significant correlation between the two variables was observed ($r = 0.063$; $p = 0.337$).

Measurements of the infarct size *per* heart, i.e. mean value of 12 sections representative of the LV, obtained by the manual and *MIQuant* calculation were also compared accordingly to the Bland-Altman concordance analysis. For the midline length the predicted bias is 0.25% and the limits of agreement are -3.60% and 4.09%, resulting on 7.74% amplitude of concordance (Figure 3C). The analysis of the area measurements retrieves a mean difference of 2.47% (95% confidence interval (CI) from 1.21% to 3.72%), suggesting that *MIQuant* tends to give a higher reading from 1.21% to 3.72% (Figure 3C). The area method concordance interval ranges from -2.79% to 7.72%. Thus, for *MIQuant per* heart infarct size results the confidence interval of the predicted bias and concordance limits are within acceptance limits (bias ±2%, concordance limits ±7%) for both midline length- and area-measurements, which show that the performance of *MIQuant* is equivalent to the manual infarct size calculation.

Although the differences between *MIQuant* and manual measurements are scattered around the bias with no obvious pattern, the association between the two variables was investigated using the Pearson Product-moment-correlation coefficient. Small and non-statistically significant correlations were found for both midline length (r = 0.149; p = 0.531) and area (r = -0.315; p = 0.176) approaches, consequently discrepancies between the manual and semi-automated quantification are independent of the sample infarction size.

Table 1. Repeatability analysis of the manual and *MIQuant* results by repeated measures one-way ANOVA

MI size (%)	Midline length measurement[1]			Area measurement[2]		
	Measurement 1	Measurement 2	Measurement 3	Measurement 1	Measurement 2	Measurement 3
Manual[a]	44.24 ± 13.01	44.84 ± 12.62	45.03 ± 12.82	31.23 ± 9.60	32.51 ± 9.29	31,92 ± 9.25
MIQuant[b]	44.66 ± 13.26	44.58 ± 13.00	45.61 ± 13.01	34.02 ± 8.71	34.00 ± 8.16	35,04 ± 8.72

Values area mean ± STDEV; n = 20; [1, a] ***Per* LV**: Wilks´Lambda = 0.818, F(2, 18) = 2.0001, p = 0.164, multivariate partial eta squared = 0.18; ***Per* section**: Wilks´Lambda = 0.990, F(2, 234) = 2.0001, p = 0.140, multivariate partial eta squared = 0.322; [1, b] ***Per* LV**: Wilks´Lambda = 0.757, F(2, 18) = 2.892, p = 0.081, multivariate partial eta squared = 0.24; ***Per* section**: Wilks´Lambda = 0.977, F(2, 234) = 2.734, p = 0.067, multivariate partial eta squared = 0.023; [2, a] ***Per* LV**: Wilks´Lambda = 0.848, F(2, 18) = 1.617, p = 0.226, multivariate partial eta squared = 0.15; ***Per* section**: Wilks´Lambda = 0.969, F(2, 234) = 3.737, p = 0.025, multivariate partial eta squared = 0.031; [2, b] ***Per* LV**: Wilks´Lambda = 0.827, F(2, 18) = 1.886, p = 0.180, multivariate partial eta squared = 0.17; ***Per* section**: Wilks´Lambda = 0.981, F(2, 234) = 2.286, p = 0.104, multivariate partial eta squared = 0.019

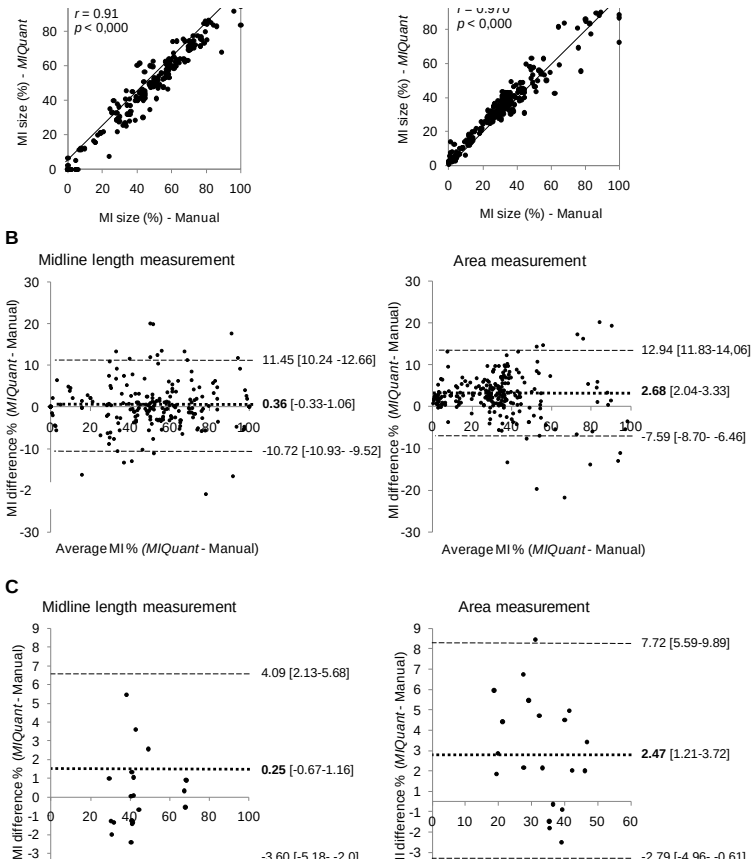

Figure 3. Validation of *MIQuant* for infarct size assessment. (A) Infarct size scatter diagram and the Pearson coefficient demonstrated strong association between manual and *MIQuant* results for area (*right*) and midline length (*left*) approaches. (B) Bland-Altman concordance analysis of the manual and *MIQuant* infarct size measurements demonstrated acceptable limits of agreement between methods. Average values of the three independent measures of infarct size *per* section (B) and *per* heart (C) were subject to the analysis. Differences between the infarct sizes retrieved by each method (*MIQuant*-manual) are displayed in the *y*-axis and the mean infarct size values are plotted in the *x*-axis. The limits of agreement (– –) and bias (▪ ▪ ▪) and respective 95% confidence intervals ([ ]) are shown.

Validation of *MIQuant* by non-trained volunteer-users

To address whether previous experience with the *MIQuant* application and knowledge on infarct size calculation are strict requirements for the correct software usage, a comparison was established between *MIQuant* results obtained by users with distinct proficiency. Five hearts were independently analyzed by four competent users (*experts*), i.e. investigators with extensive training on MI size quantification either manually or using *MIQuant*, and by volunteer-users with no previous experience on MI

size calculation, but to whom free-access to the *MIQuant* manual was provided. An independent-samples *t*-test was conducted and no significant differences were observed on the midline length and area measurements obtained by either *experts* or *volunteers* (Figure 4). In addition, a two–way ANOVA analysis of variance was conducted to explore the impact of the observer type (expert or volunteer) and the heart sample on *MIQuant* infarct size measurement, obtained by either midline length (ML) or area (A) approaches. There was no statistically significant effect for the observer type (ML $p = 0.267$; A $p = 0.77$), whereas the effect of the heart sample was found to be statistically significant ($p < 0.05$).

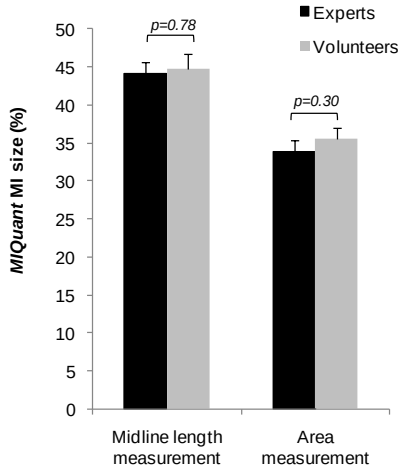

Figure 4. *MIQuant* efficacy is not affected by user proficiency. *MIQuant* infarct size values obtained by competent (*experts*) and non-trained (*volunteer*) users were compared and the mean values are displayed as graph bars. Independent-samples *t*-test showed no significant differences between infarct scores calculated by the *experts vs. volunteers*; furthermore, a two–way ANOVA demonstrated no significant influence of the user on the obtained infarct size value.

Time-efficiency of MIQuant infarct size quantification

The manual quantification of MI size is a time-consuming and laborious endeavor, thus the simplification of this task is highly desired and was a major drive for the development of *MIQuant*. The time required for manual and *MIQuant*-assisted infarct size calculation was compared (Figure 5). The latter was additionally compared for

experts and volunteer operators. Despite the required definition of initial parameters by the user prior to *MIQuant* segmentation, this method resulted on a significant overall 4.5- and 3-fold decrease in the time period spent on the analysis when performed by competent and volunteer users, respectively.

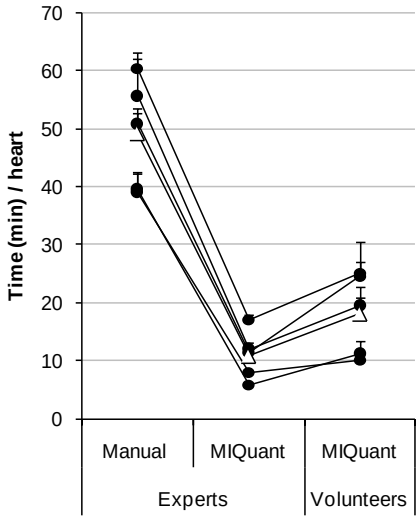

Figure 5. *MIQuant* improves the time-efficiency of infarct size quantification. The time consumption of the infarct size determination *per* heart (mean value of 12 representative sections of the LV) was compared between the manual and *MIQuant* approaches. The Δ indicates the mean value of each group. **p<0.01.

DISCUSSION

In this study, the development and validation of *MIQuant*, a simple and user-friendly software application that calculates the infarct size on cardiac models of induced-ischemia, is reported. To our best knowledge, *MIQuant* constitutes the first computer-assisted tool to ease the arduous and time-consuming endeavor of manual infarct size calculation by classical planimetry.

The view of the heart as a post-mitotic organ has been challenged in recent years by reports of cardiomyocyte renewal in humans (Bergmann et al., 2009), cardiomyocytic-cell replacement after injury in mouse (Hsieh et al., 2007) and of myocardium-resident Sca-1^{+}/c-Kit^{+}/MDR1^{+} progenitor/stem-like cells (Barile et al., 2007; Beltrami et al., 2003; Leri et al., 2005). These findings, together with the fact that cardiovascular diseases are a major cause of morbidity/mortality, have encouraged the publication of studies on the evaluation of cardio-regenerative potential of novel therapies. The latter are commonly tested on rodent models of MI and the infarct size has been regarded as a decisive parameter for the determination of the success of the therapy under test. Although histological planimetry is the gold standard for infarct size quantification, methodological discrepancies are frequent across publications due to a general lack of standardized protocols/methods. The most common methods used to quantify infarct extension are either based on the infarcted area or on the length of the infarction circumference. Both methodologies show limitations related to the infarct size estimation accuracy using parameters that are affected and distorted by cardiac remodeling subsequent to MI (Zornoff et al., 2009). Regarding *MIQuant*, we decided to make available two methods for infarct quantification: the area-based quantification first described by Michael (Michael et al., 1995) and the midline length measurement that was extensively validated recently (Takagawa et al., 2007). In accordance with Takagawa's (Takagawa et al., 2007) observations on manual infarct size quantification, with *MIQuant* we obtained a statistically significant compression of the area results when compared to the midline-length method. Overall, obvious consistency was achieved between manual and *MIQuant* infarct size quantification, which was further illustrated by the excellent correlation between both and by Bland-Altman analysis. Bland-Altman analysis indicated good agreement free from systematic bias for midline-length *MIQuant* infarct scores (0.25±3.84). Regarding the area measurements, although *MIQuant* overestimates infarct size by 1.21-3.27% as compared to the manual quantification, the biological relevance of this overestimation is negligible.

Moreover, a random dispersion of results around the predicted bias was observed, demonstrating that *MIQuant* results are reliable independently of the size of infarction. The repeatability and reproducibility of *MIQuant* results were also confirmed by the use of three independent measures obtained by four independent observers. Overall these results indicate that *MIQuant* is a reliable alternative to the manual quantification of infarct size.

Despite being a determinant factor for an accurate estimation of the infarct size (Takagawa et al., 2007), the number of transverse sections used for such analysis is extremely variable across studies. One of the advantages of *MIQuant* over the classical manual quantification is the 4.5 fold reduction on the time spent on the analysis, thus improving time-efficiency and allowing the investigator to increase the number of sections *per* analysis and consequently the accuracy of results.

MIQuant is available as freeware for research use. The widespread use of *MIQuant* will constitute by itself a major improvement towards normalization of infarct size assessment by restricting the methods to the area and midline length, by standardizing the histological stain used and by restricting the criteria for the identification of the infarcted region. Our results also indicated a tendency, although not statistically significant, for reduced inter-observer variability in *MIQuant* infarct size scores when compared to manual analysis. This may well be underestimated given that the observers in this study were investigators that received similar training on infarct size calculation. It is therefore expected that the diversity of criteria on infarct identification/calculation of observers with different backgrounds will result in increased variability for the manual outcome. In contrast, we demonstrated that *MIQuant* efficacy is independent of previous training with the software and experience on MI size calculation. An interesting experiment would be a comparative analysis between *MIQuant* and manual quantification with experts from different laboratories to therefore undoubtedly clarify whether *MIQuant* contributes to the homogenization of infarct size results. Our attempts to engage in this task *experts* with previous published work on

infarct size histological quantification, met with little success and the intent was therefore aborted.

For the interpretation of this study several limitations should be considered: firstly a single species (mouse) was used for the validation of *MIQuant*, and secondly the only model of cardiac induced-ischemia performed was the permanent LAD coronary artery ligation. However, the pathophysiological and morphological alterations following MI are similar in the rat and the mouse (Fishbein et al., 1978; Pfeffer et al., 1979; Virag and Murry, 2003), supporting the applicability of *MIQuant* for the quantification of rat infarcts. The extension of *MIQuant* to other infarction models, e.g. ischemia-reperfusion or the cryoinjury, is of major interest. Hence, because the software recognizes the infarction region by the collagen deposition, a hallmark of established infarction, we are confident on the software applicability to other models. Indeed, in hearts with non-transmural infarction that very much resembles the reperfusion scenario, *MIQuant* infarct scores were similar to manual quantification (data not shown).

We conclude that *MIQuant* is a valid and easy-to-use software application that assists on infarct size calculation. The widespread use of *MIQuant* will contribute to the reduction of time spent on the analysis and for the standardization of infarct size quantification across studies and, therefore, to a more systematic evaluation of the cardiac regenerative potential of newly developed therapies.

ACKNOWLEDGEMENTS

The authors are indebted to Dr. Dirk J. Duncker for providing mouse cardiac surgical training to DSN at his Laboratory. Dr. Pedro Oliveira is acknowledged by statistical coaching. This work would not have been possible without the collaboration of all those

who volunteered as non-trained operators for the statistical validation of the *MIQuant* software.

REFERENCES

Please see references at *REFERENCES Chapter*.

CHAPTER V

DIFFERENTIAL RE-ACTIVATION OF SPECIFIC EMBRYONIC CELLULAR PHENOTYPES IN THE ADULT MOUSE HEART SUBJECTED TO ISCHEMIA AND INFECTION INJURIES

As previously discussed in the *General Introduction*, the adult heart is not able to regenerate (Ali et al., 2014a; Bergmann et al., 2009; Bersell et al., 2009; Hsieh et al., 2007; Kajstura et al., 2010; Senyo et al., 2013; Uchida et al., 2013; van Berlo et al., 2014), responding to injury with the formation of non-functional scar tissue that replaces the lost myocardium (Virag and Murry, 2003). In neonatal mice, CMs maintain the ability to proliferate and are able to restore the pumping function and myocardial architecture after injury, such as apex resection or MI, if inflicted during the first week of life (Porrello et al., 2011; Porrello et al., 2013). Embryonic and fetal cardiac cells have the natural potential to contribute for heart formation and development. However, as we have shown in *Thesis Chapter III*, populations with the embryonic/fetal phenotype are not found in the adult heart, with the exception of CD54 and Sca-1-expressing cells (which are not related to the cardiomyocytic lineage) (Valente et al., Manuscript). Despite the shift observed in the cellular composition along development and the alterations reported to occur during postnatal growth and maturation, it has been shown that the adult heart is able to reactivate development-associated pathways, which were down-regulated in the physiological state, when subjected to pathological/stress conditions (Oka et al., 2007; Rajabi et al., 2007).

Animal models constitute relevant functional assays to challenge and to retrospectively determine cellular behavior in their native environment *in vivo* (Holmes et al., 2005; Klocke et al., 2007). Several cardiac injury models (*e.g.* MI (Michael et al., 1995), apex resection (Porrello et al., 2011) and myocarditis (Santos Lima and Minoprio, 1996)) have been implemented and may be used to acquire important knowledge about mammalian heart physiology and pathology. To characterize the functional profile of the cardiac phenotypes identified in the developing embryo (*Thesis Chapter III*), we

examined the surface phenotype of adult cardiac cells when challenged in distinct injury settings, *i.e.* MI (*Thesis Chapter IV*) and Chagas heart disease following *T. cruzi* infection (collaboration with Minoprio's Lab | Institut Pasteur).

In this *Thesis Chapter* we come forward with proof-of-principle evidences for a potential role of fetal cardiac phenotypes (*Thesis Chapter III*) in the course of experimental MI and myocarditis.

Differential Re-Activation of Specific Embryonic Cellular Phenotypes in the Adult Mouse Heart Subjected to Ischemia and Infection Injuries

Mariana Valente[1,2,3], Alain Cossan[4], Tatiana Pinho Resende[1], Diana Santos Nascimento1, Tiago Luís Laundos[1], Paola Minoprio[4§], Ana Cumano[3,5*], Perpetua Pinto-do-O[1,2,3,§,*]

[1]Stem-cell microenvironments in repair/regeneration Team, Microenvironment for Newtherapies Group, Instituto de Investigação e Inovação em Saúde & INEB – Instituto de Engenharia Biomédica, Universidade do Porto, 4050-180, Portugal.

[2]ICBAS – Instituto de Ciências Biomédicas Abel Salazar, Universidade do Porto, Porto, 4050-313, Portugal.

[3]Unit for Lymphopoiesis, Immunology Department, INSERM U668, Institut Pasteur, Paris, 75015, France.

[4]Laboratoire d'Immunobiologie des Infections à Trypanosoma, Immunology Department, Institut Pasteur, Paris 75724, France

[5]Université Paris Diderot, Sorbonne Paris Cité, Cellule Pasteur, Paris, 75018, France.

*Co-senior authors

§ Correspondence: perpetua@ineb.up.pt (PPO) and paola.minoprio@pasteur.fr (PM)

Short-report, unpublished.

ABSTRACT

Animal models that recapitulate the clinical manifestation of cardiac diseases are important functional assays for investigation of heart repair/regeneration mechanisms and testing of novel therapies. Myocardial infarction and myocarditis caused by *Trypanosome cruzi* infection have been extensively studied in murine experimental settings. Despite a widely acknowledged lack of regenerative capacity of the adult mammalian heart, re-activation of "fetal programs" during the repair process has been reported. Herein, we investigated whether embryonic cardiogenic subsets previously identified by our team, and which could not be recognized in the adult steady-state heart, would re-emerge under pathological conditions (myocardial infarction and Chagas disease). Interestingly, we found surface signatures (phenotypes) specific of the fetal cardiac populations re-expressed in both experimental cardiac injury models analyzed. This proof-of-principle study indicates that embryonic/fetal phenotypes can be re-activated after injury and demonstrates the importance of the identification of cellular components during heart morphogenesis to understand adult pathologic scenarios.

INTRODUCTION

Heart failure (HF) is a great health and social-economic aging challenge, with a prevalence of 15 million people in Europe (Bui et al., 2011). Adult cardiovascular disorders can arise from long-standing hypertension, myocardial infarction (MI) associated with coronary artery disease, valve insufficiency, myocarditis due to infection, essential hypertrophic and dilated cardiomyopathies and diabetic cardiomyopathy (Klein et al., 2003; Lips et al., 2003). After an acute MI more than 30% of patients develop HF (Bui et al., 2011). The adult myocardium has restricted capacity to generate new cardiomyocytes (CMs) after injury (Ali et al., 2014a; Bergmann et al., 2009; Bersell et al., 2009; Hsieh et al., 2007; Kajstura et al., 2010; Senyo et al., 2013; Uchida et al., 2013; van Berlo et al., 2014), and readily initiates a cascade of reparative events that culminate in the formation of myocardial fibrosis, which is correlated with systolic/diastolic dysfunction. Over the last decade cell-based therapies have emerged as a promising strategy, however, available studies revealed only modest and transient improvement of cardiac function by paracrine mechanisms (Freire et al., 2014a; Laflamme and Murry, 2011; Mercola et al., 2011; Nascimento et al., 2014; Segers and Lee, 2008; Wollert and Drexler, 2010). Indeed, even more recently advanced treatments do not appear capable to promoting myocardium restoration (Fuster, 2014). Therefore, and irrespective of whether or not CM replacement is achieved, alternative therapeutic approaches are necessary to improve/restore cardiac function after injury (Mercola et al., 2011).

Different animal models have been developed to recapitulate the clinical manifestation of a given disorder, contributing to advance our understanding of heart repair and regeneration, as well as to evaluate novel treatments for improving heart function. MI and myocarditis driven by *Trypanosome cruzi* (*T. cruzi*) infection are two relevant conditions for which experimental mouse models of myocardial dysfunction are available. In the MI-induced mouse model, typically through the occlusion of the left coronary artery, an ischemic environment in the downstream myocardium is recreated which has been extensively used to investigate the associated healing processes (Borst et al., 2011; Huang et al., 2006; Michael et al., 1995). In this ischemic setting, CMs undergo cell death by necrosis, and an inflammatory process is promptly triggered, encompassing the infiltration of leukocytes, that will, among other actions, phagocyte cellular debris**.** Fibroblast proliferation and differentiation into myofibroblasts contribute to the resolution of the inflammatory reaction, the formation of a transient ECM (rich in proteoglycans, osteopontin and fibronectin), which leads in a chronic phase to the deposition of collagen fibers that replaces the lost CMs. This sequence of events results in a progressive thinning of LV wall, chamber dilation and, ultimately, in ventricular remodeling (Virag and Murry, 2003). The cellular and histological alterations elicited by an ischemic environment in the experimental setting of MI have been well characterized by many laboratories, including ours (described in detail in *Thesis Chapter IV*). Moreover, within this context, recent innovations such as the software application *MIQuant* ((Nascimento et al., 2011), *Thesis Chapter IV*) have contributed for a faster and more accurate quantification of the inflicted damage, *i.e.* the MI size established.

Whereas MI is an acute event, in which CMs undergo massive death in the first days after coronary occlusion, Chagas' disease induced by systemic *T. cruzi* infection can affect the heart in the chronic phase of disease. *T. cruzi* is a protozoan parasite with a complex life cycle, that includes an insect and mammalian vectors, and with different parasite developmental stages that differ in cell division and infectious ability. Chagas'

cardiomyopathy affects 20-40% of patients in the chronic phase of the infection with HF arrhythmia, heart block, thromboembolism stroke and sudden death. The acute phase of the disease is associated with high parasitemia and intense tissue parasitism (Machado et al., 2012; Rossi and Ramos, 1996). After resolution of the acute phase, chronically infected patients show low or undetectable parasitemia, low tissue parasitism, multifocal mononuclear inflammatory infiltrates and interstitial fibrosis, which leads to chronic chagasic cardiomyopathy (Machado et al., 2012; Rossi, 1991; Rossi and Ramos, 1996).

Clear identification of the distinct cardiac cell populations will enable the investigation of their role in cardiogenesis and adult heart maturation. This is indispensable to comprehend, and likely to aid with resolving therapies, the pathophysiology of heart diseases. Our previous work (detailed in *Thesis Chapter III*) on the phenotypic characterization and surface signatures definition of the cardiac cell compartment allowed the prospective isolation of important contributors for heart development ((Valente et al., Manuscript), *Thesis Chapter III*). We have identified an immature CM population, which co-expresses CD24, CD146 and CD166 and lacks Caveolin-3 at the membrane surface. This population decreases along heart morphogenesis and exhibits high rates of proliferation at midgestation, when CMs are largely responsible for cardiac chambers growth. Our analysis also evidenced the heterogeneity of the stromal cardiac compartment. We described two mutually exclusive populations of fibroblasts, expressing either the surface signature PDGFRα or CD146, present in the atria and ventricles of the embryo. For both cardiac populations (CMs and fibroblasts), the characterized embryonic phenotype was not found in the adult myocardium ((Valente et al., Manuscript), *Thesis Chapter III*). On the other hand, fibroblast populations expressing Sca-1^{+} and $CD54^{+}$ cells appear preserved in the adult myocardium ((Valente et al., Manuscript), *Thesis Chapter III*).

Even though we did not detect fetal-like populations in the adult murine heart, the “fetal program” (namely signaling pathways of cell metabolism and survival) has been shown

to re-activate when exposed to a variety of pathological stimuli (reviewed in (Oka et al., 2007)). Cardiac cells are able to recognize pathological stimuli present in the extracellular milieu either directly, through dedicated biomechanical stretch sensitive receptors, or indirectly through a large array of membrane bound proteins/receptors (Molkentin and Dorn, 2001). Thus, in an injury scenario, the evaluation of the surface proteins profile of cardiac subsets and that of the populations involved in cardiogenesis is fundamental to reveal whether re-activation of earlier development phenotypes is also occurring. Hence, we have investigated the dynamics of the previously identified cardiogenic subsets ((Valente et al., Manuscript), *Thesis Chapter III*) in these two pathological conditions, namely after MI and in Chagas' disease. We herein report the distinct cellular phenotypes, which were re-activated in the two injury models investigated.

MATERIAL AND METHODS

Myocardial Infarction (permanent ligation of coronary artery)

Mice. Adult C57BL/6 mice (8 – 12 weeks-old) were used for this study. All animal procedures at INEB were approved by Instituto de Biologia Molecular e Celular | Instituto de Engenharia Biomédica Animal Ethics Committee and Direcção-Geral de Veterinária – DGV. Humane endpoints were followed in accordance to the OECD Guidance Document on the Recognition, Assessment, and Use of Clinical Signs as Humane Endpoints for Experimental Animals Used in Safety Evaluation (2000).

Myocardial infarction procedure. MI was experimentally induced by permanent ligation of the left coronary artery, as previously described ((Nascimento et al., 2011), *Thesis Chapter IV*).

Echocardiography analysis. Transthoracic echocardiography was performed 21 days after coronary artery ligation using a portable ultrasound apparatus (GE Vivid I, General Electric) equipped with a 12 MHz linear probe (GE 12L-RS Linear Array Transducer, General Electric). Animals were anesthetized with ketamine (Clorketan, 100mg/Kg). Two- dimensional (2D) mode images of short-axis were acquired to position the Motion-mode (M-mode) cursor at level of papillary muscles. To evaluate LV structural changes several parameters from M-mode were measured, *i.e.* the LV internal diameter at diastole (LVIDd) and at systole (LVIDs), and the LV ejection fraction (EF) and fractional shortening (FS) were obtained as the index of systolic function.

Histopathological analysis. Hearts were harvested at 2 and 7 days post-MI, washed in PBS and fixed in 10% Formalin neutral buffer (VWR BDH & Prolabo) to a maximum of 24 hours for paraffin-embedding ((Valente et al., 2015), *Thesis Chapter IV*) or fixed in 0,2% Fixative buffer during 48 hours for gelatin-embedding/freezing. For morphometric analysis, representative heart sampling was obtained as previously ((Valente et al., 2015), *Thesis Chapter IV*). The frozen hearts were longitudinally sectioned (4 µm thickness) from the anterior to posterior heart walls with a 50 µm of interval between each section.

MI quantifications. Paraffin sections were stained with modified Masson's Trichrome (TM) staining to the posterior MI quantification, as previously described ((Nascimento et al., 2011; Valente et al., 2015), *Thesis Chapter IV*). Infarct size measurement was based on the collagen deposition in the ischemic LV wall that is highlighted in blue after MT staining from 14 days post-infarction onwards. The percentage of the affected LV wall was calculated by the area method (Michael et al., 1995) and midline length method (Takagawa et al., 2007) using the semi-automated program *MIQuant* ((Nascimento et al., 2011), *Thesis Chapter IV*).

Immunofluorescence. Gelatin-embedded/frozen sections were washed in 1x PBS and blocked with either 4% FBS/1% BSA or Vector M.O.M.™ basic kit (Vector

Laboratories). Overnight incubation (4ºC) with primary antibodies to detect α-Actinin sarcomeric (1:300, Sigma), CD24 (1:250, eBioscience) and Ph3 (1:800, Cell Signaling) was performed. Alexa Fluor conjugated secondary antibodies (Invitrogen) were used and nuclei counterstained with DAPI. Representative high-resolution images were acquired at 63x magnification in a confocal microscope (Leica SP5II, Leica). Whole heart (long heart axis) images were obtained using MosaiX (AxioVision modules; Carl Zeiss). All acquired images were edited using Image J software.

Statistical analysis. Statistics were performed using SPSW statistic software 18 and $p<0.05$ was considered statistically significant. Values presented in text, tables and figures are the mean ± standard error of the mean (S.E.M.). Correlation between the different parameters of the functional and histological assessment was tested by linear regression.

Chagasic myocarditis (*T. cruzi* infection)

Mice. Eight- to 10-week-old C57BL/6 mice (Charles River, Saint-Aubin-l`es-Elbeuf, France) were used for *T. cruzi* infection experiments; littermates served as control animals. Seven- to 10-week-old C3H/HeJ mice (Charles River, Saint-Aubin-l`es-Elbeuf, France) were used for sequential passage of parasites before infection experiments. All animal procedures were in accordance to the Institut Pasteur ethic charter approved by French Agriculture ministry; and to the European Parliament Directive 2010/63/EU. Humane endpoints were followed in accordance to the OECD Guidance Document on the Recognition, Assessment, and Use of Clinical Signs as Humane Endpoints for Experimental Animals Used in Safety Evaluation (2000).

Parasites and infection procedure. *T. cruzi* (CL Brener clone F11–F5) that stably expresses firefly luciferase (TcTREX-luc) and GFP (TcTREX-GFP) (Goyard et al., 2014) was maintained in the laboratory by sequential passage in C3H/HeJ mice to obtain bloodstream trypomastigote forms. C57BL/6 mice were inoculated in the intraperitoneal cavity (ip) with $2x10^4$ circulating trypomastigote forms *per* mouse.

Parasitemia was scored 3, 4, 8, 16 and 21 days post-infection (d.p.i.) inoculation and mortality was evaluated daily.

***In vivo* bioluminescence imaging**. Mice were shaved ventrally and ip administrated with 150 mg/kg luciferase substrate – luciferin (D-Luciferin potassium salt, Xenogen, California) before any bioluminescence measurements (Goyard et al., 2014). Mice were anaesthetized in a 2.5% isoflurane atmosphere (Aerane, Baxter SA, Maurepas, France) for 5 minutes and kept in the imaging chamber for analysis. Emitted photons were acquired for 5 minutes by a charge couple device (CCD) camera (IVIS Imaging System Lumina, Caliper, Villepinte, France) set in high-resolution mode. The analysis was performed after defining a region of interest (ROI) at the level of the heart. Total photons emitted from the image of each mouse were quantified using Living Image software (Xenogen Corporation, Almeda, California), and results were expressed as number of photons/s/ROI.

***In vitro* fluorescence imaging.** Fluorescent live parasite cultures were analyzed with a system for multicolor fluorescence FLoid^{TM} Cell Imaging Station (Molecular Probes Life Technology) using green fluorescence channel confocal microscopy with a LMS700 (Carl Zeiss).

Heart dissociation. Adult heart tissue was minced into 1 mm^3 fragments and incubated during 15 minutes at 37ºC in a enzymatic solution: 0,2mg/mL collagenase with 60U/mL DNase I (Sigma and Roche, respectively) in Hank's Balanced Salt Solution with calcium and magnesium cations (HBSS+/+, Invitrogen) was used. At the end of each round of incubation, tissue fragments were vigorously re-suspended in the enzymatic solution to complete the dissociation. The remaining tissue was let to sediment, the supernatant was collected and enzymatic activity inhibited with 10% FCS (Gibco) HBSS+/+ and kept on ice. These steps were repeated until no more tissue was observed. After digestion, cell suspensions were centrifuged 10 minutes, 290 g at 4ºC, re-suspended in 1%FCS HBSS+/+ and filtered through a 70 µm mesh cell strainer (Fisher).

Flow Cytometry. Heart cell suspensions were stained with conjugated or biotinylated antibodies against PDGFrα (PE, BioLegend), Sca-1 (PECy5, BioLegend), CD24 (PECy7, BD Bioscience), CD166 (APC, eBiscience), CD90.2 (BV605, BD Bioscience), c-Kit (APCCy7, BioLegend), CD54 (PB, BioLegend), CD31 (BV421, BD Bioscience) 20 minutes, 4ºC in the dark; followed by incubation with BV421 streptavidin for the detection of biotinylated antibodies CD45 (BioLegend) and Ter119 (BD Bioscience) 10 minutes, 4ºC in the dark. Samples were filtered with a 70 µm mesh cell strainer and acquired in a Spectral flow cytometry (Sony SP6800 analyser, Sony). After the definition of the deconvolution matrix with the respective single stains, deconvoluted data was analyzed with FlowJo v10.0.8 software.

RESULTS AND DISCUSSION

Recapitulation of Fetal Cardiomyocyte Phenotype after Myocardial Infarction

To show that the coronary ligation procedure recapitulates the adult heart response to MI**,** size of the established infarction ((Nascimento et al., 2011), *Thesis Chapter IV*), was correlated with systolic function (EF and FS) and cardiac remodeling (LVIDd, LVIDds). Analysis with the *MIQuant* software revealed that 37,49%±3,02 (by midline length method) and 29,57%±2,47 (by area method, mean ± S.E.M.) of the left ventricle (LV) wall were affected. Linear regression analysis showed that both methods of MI quantification are strongly correlated with LVIDd (midline length r=0,952, p<0,05 and area r=0,941, p<0,05) and with LVIDs (midline length r=0,948, p<0,05 and area r=0,919, p<0,05, Figure 1A and C). EF (midline length r=-0,836, p<0,05 and area r=-0,789, p<0,05) and FS (midline length r=-0,822, p<0,05 and area r=-0,791, p<0,05)

were inversely correlated with histological MI size obtained with the two methods (Figure 1B and D). In line with this, both approaches for histological quantification of the fibrotic tissue extension (midline length- and area-based methods) were strongly correlated with functional parameters of the LV chamber dimension and LV wall motion. Our experimental MI setting mimics the main steps of progression of ischemic myocardium and corroborates the severity of heart failure in chronic conditions, constituting therefore a robust model for subsequent examination of the cell subsets implicated in the response to ischemia injury.

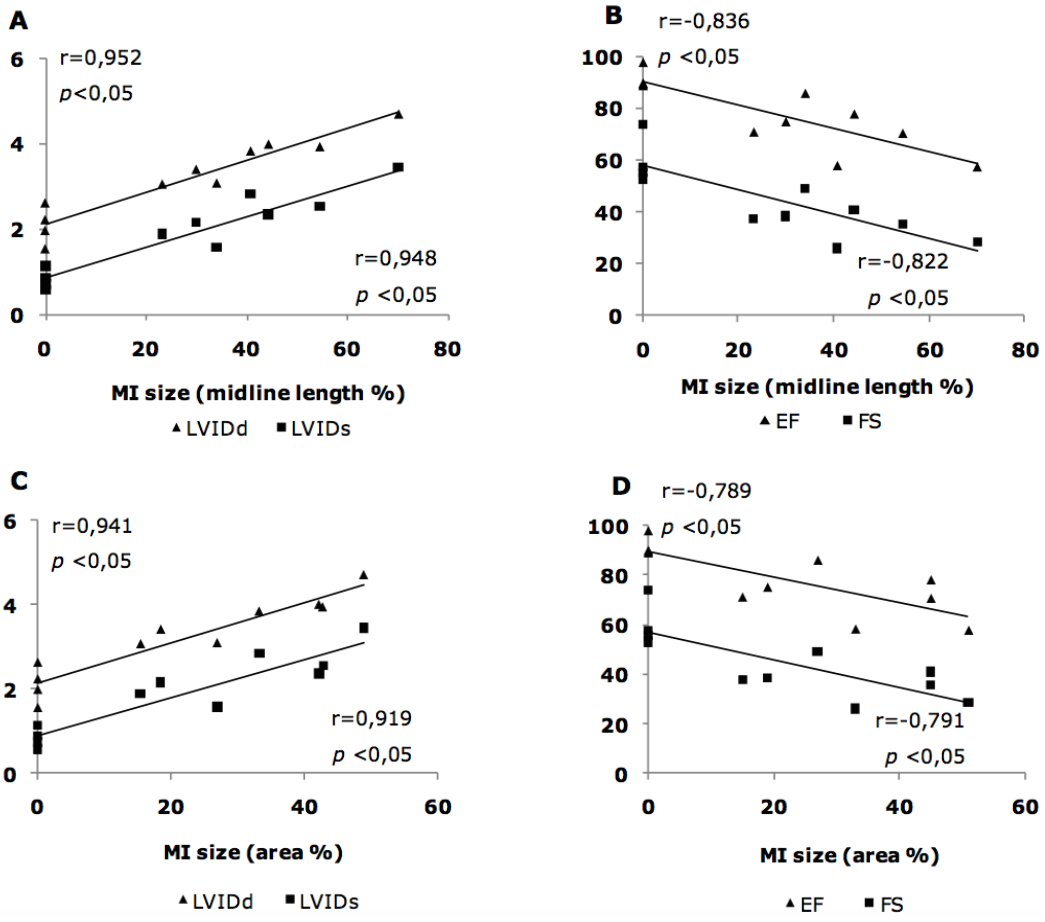

Figure 1. Correlation of histological and functional assessment of mouse model of myocardial infarction. Linear regression between the percentage of the MI size obtained by the histological-based approaches (midline length (**A, B**) and area (**C, D**)) with the echocardiographic parameters (LVIDd and LVIDs (**A, C**) and EF and FS (**B, D**)).

Following the previous identification of surface signatures defining populations of CMs and stromal cells in the developing mouse heart, which we also demonstrated to be no longer recognized in adulthood ((Valente et al., Manuscript), *Thesis Chapter III*), we questioned whether cardiac fetal phenotypes would be re-activated in the adult heart following ischemia. Because the surface marker CD24 was associated with immature CMs during murine development, disappearing as CMs mature to being virtually undetectable in the adult organ ((Valente et al., Manuscript), *Thesis Chapter III*), CD24 and α-Actinin expression were analyzed to confirm a cardiomyocytic lineage association. No CD24 or pH3 expressions were observed in the sham-operated controls throughout the study (Figure 2A and B). Remarkably, in the MI group, CD24 expression was observed two days after MI mainly associated with matrix and widespread in the border zone (Figure 2C, white arrows), whereas in CMs (α-Actinin$^+$ cells) CD24 expression was evident 7 days post-MI (Figure 2D, dashed white line delineates injured tissue and F, white arrows, CD24$^+$ CMs). Interestingly, rare proliferative CD24$^+$ CMs, identified through the expression of phosphorylated histone H3 (pH3) were found at in the vicinity of the MI border zone (Figure 2F, white asterisk). These results demonstrate that, after MI, rare adult CMs can re-express CD24 and proliferate. The modest levels of mitotic activity are compatible with the poor regenerative capacity of adult myocardium.

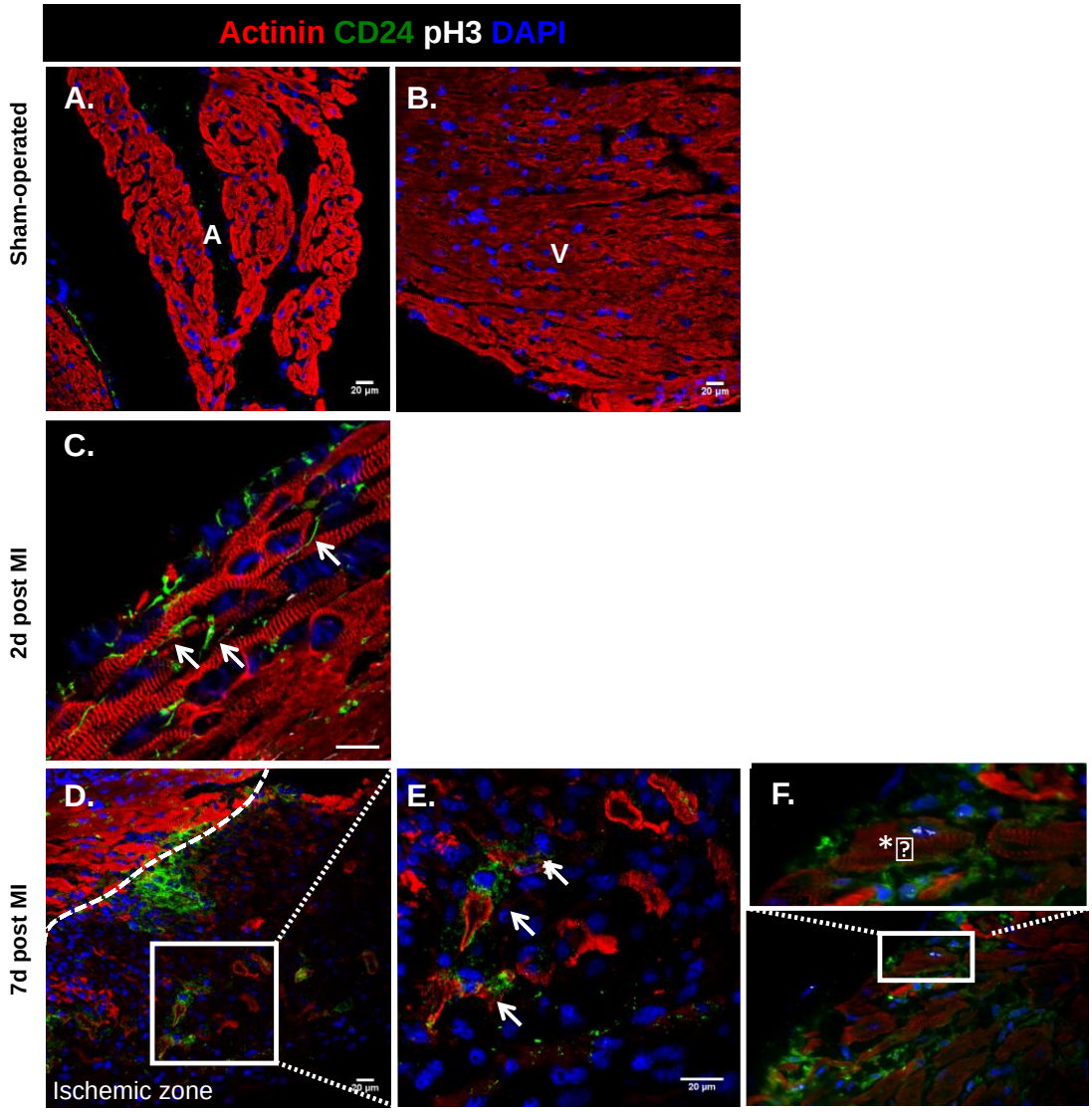

Figure 2. ***In situ*** **characterization of the surface signatures during MI pathogenesis. A-B.** Immunofluorescence analysis of CD24 and Actinin expression in sham-operated myocardium. A | atrium; d | days; V | ventricle. **C.** 2 d post-MI and **D-F.** 7 post-MI, CD24 co-expression with Actinin highlight the presence of $CD24^{+}$ CMs at the ischemic zone of MI mainly 7 days post-MI. **D.** Higher magnification, where a $CD24^{+}$ CM ($Actinin^{+}$) expresses pH3 at the nucleus indicative of cell cycle activity.

These results are of particular interest given the ischemic environment established after coronary ligation and the low oxygen tension in the embryo developing heart, especially in the compact myocardial layer (Guimaraes-Camboa et al., 2015), where the immature $CD24^{+}$ CMs are detected ((Valente et al., Manuscript), *Thesis Chapter*

III). Low oxygen tension (*i.e.* physiological hypoxia) has been described as an enhancer of proliferation of distinct progenitor compartments including skeletal satellite cells (Csete, 2005; Csete et al., 2001; Kook et al., 2008). It is conceivable that CMs capable of reverting their surface phenotype, by re-expressing CD24, are not terminally mature, constituting therefore a putative candidate to improve CM (re-)genesis after injury. Comparative gene expression profile of both cardiomyocytic populations ($CD24^+$ *vs*. $CD24^-$ CMs) would provide a better understanding of the mechanisms underlying the recapitulation of the fetal program and thus contribute to the amelioration of cardiovascular therapeutic approaches. Additionally, other surface proteins can be studied in the MI-induced injury, such as Caveolin-3, which was previously shown to be expressed in more mature CMs. The clear dichotomy between the expression of CD24 and Caveolin-3 found in the two different stages of CM development requires further addressing in the injury scenario. To this end, *in situ* analysis and isolation procedures (laser capture methodology) are underway.

Identification of Cardiac Cell Subsets Engaged in Chagasic Cardiomyopathy in the Adult Mouse

The mouse experimental model of *T. cruzi* infection was established and validated, as reported elsewhere (Santos Lima and Minoprio, 1996). The infection profile was monitored by a survival rate at 22 d.p.i. of 83% (two deaths out of 12 infected mice) and parasitemia levels (number of parasite circulating in the blood, Figure 3). To track parasites and infection progression we used *T. cruzi* stably expressing luciferase and GFP (Goyard et al., 2014), which allowed monitoring parasitemia levels by noninvasive *in vivo* imaging and to detect parasites by fluorescence microscopy (Figure 4A) or flow cytometry (Figure 4B).

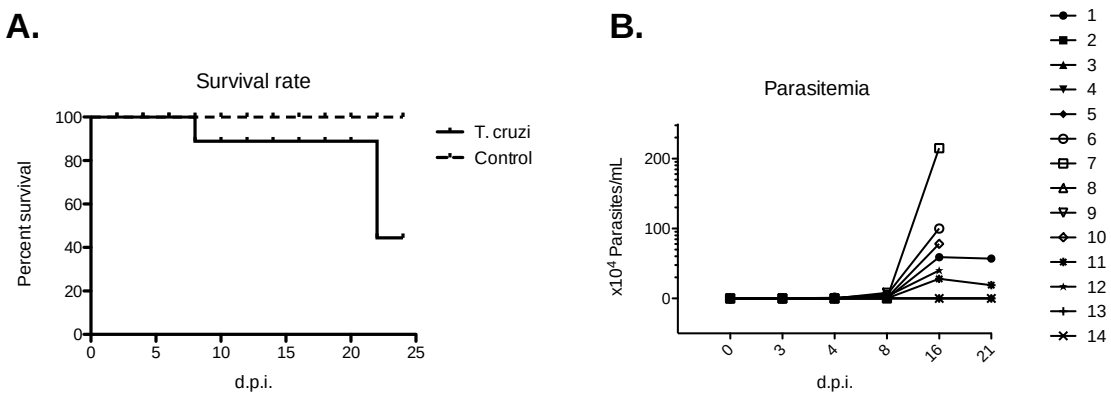

Figure 3. Monitoring of the C57BL/6 mice following *T. cruzi* infection. A. Eight weeks-old C57BL/6 mice were inoculated ip with $2x10^4$ circulating trypomastigote. Survival rate of *T. cruzi* infected and control mice in the course of the experimental time-frame. d.p.i., days post-infection. **B.** Number of circulating parasites (parasitemia, trypomastigote forms) along the course of *T. cruzi* infection in C57BL/6 mice.

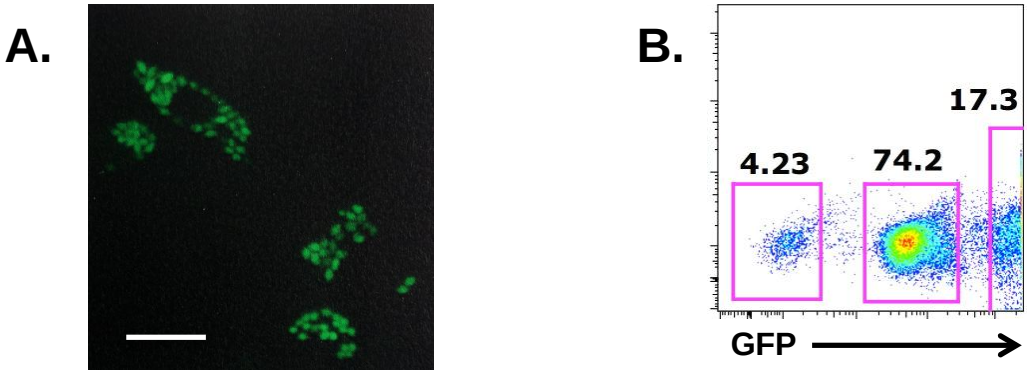

Figure 4. *T. cruzi* strain *CL Roi Glum* (tagged with FITC and luciferase). A. Microscopic view of a VERO cell line (kidney fibroblast-like cells) infected with *T. cruzi CL Roi Glum* (amastigote life cycle stage). Scale bar: 10 µm. **B.** Flow cytometry analysis of *T. cruzi* parasites after fixation procedures to verify the resistance of the parasite fluorescent.

Bioluminescence analysis at different time-points after parasite inoculation evidenced differential tissue distribution of *T. cruzi* and the particular tropism of this parasite to the intestine and heart (Figure 5A). The thorax cavity colonization by *T. cruzi* started around 9 d.p.i. (in animals 3, 4 and 6, with 10^6p/s per ROI), while the substantial

increasing of parasite numbers was observed by 15 d.p.i. (in mice 3, 6, 9 and 10, with almost 10^8p/s per ROI).

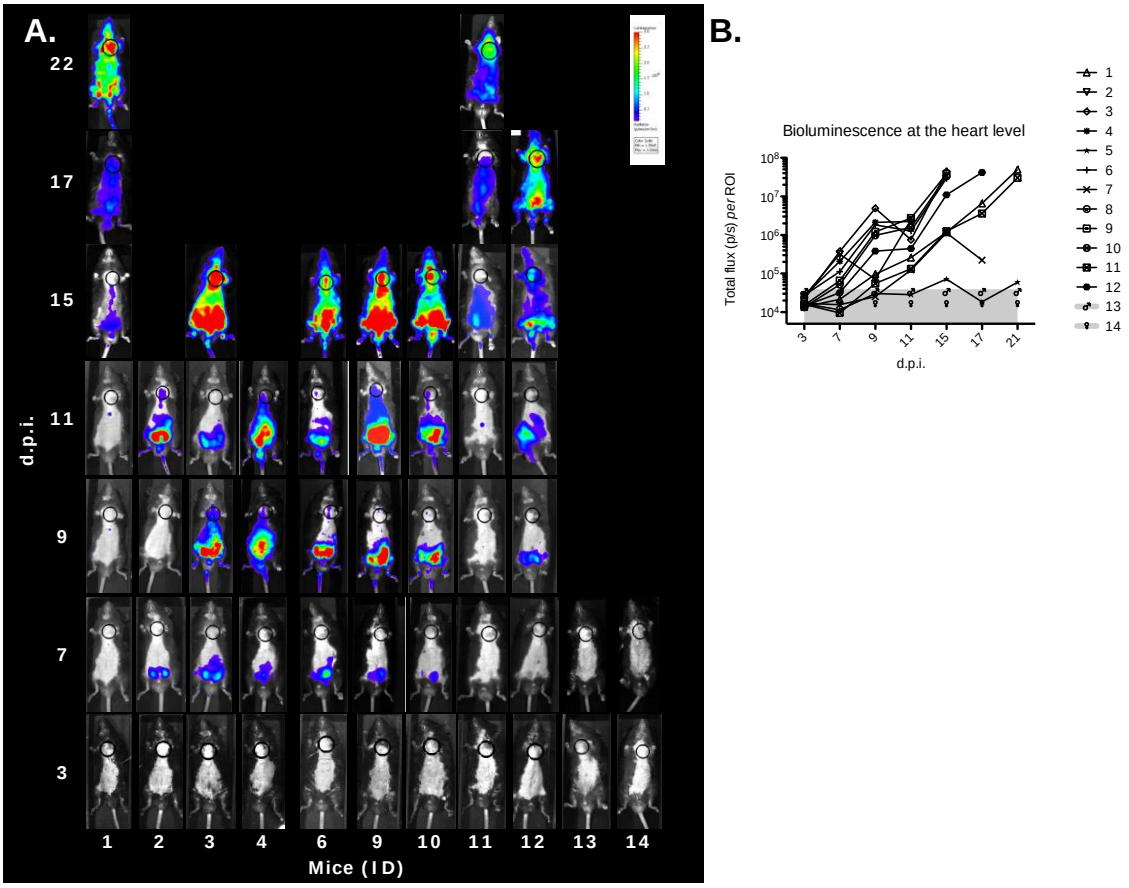

Figure 5. Evaluation of *T. cruzi* infection in C57BL/6 mice (ventral side) by *in vivo* bioluminescence imaging during the time-course of the infection. A. Pseudo-color heat-maps indicate intensity of bioluminescence from low (blue) to high (red) and images were treated with the same log10 scale. ROI (black circle) identifies the location of the heart. **B.** Quantification of the ROI (at the heart level) bioluminescence of mice inoculated trypomastigotes *T. cruzi* parasites. Gey line represents the mean of the background luminescence of control uninfected mice.

To identify the cellular players in cardiac pathogenesis of *T. cruzi*-induced myocarditis, we performed cell phenotyping of *T. cruzi*-infected mouse heart cells at day 11, 15 and 17 post-infection. Phenotyping analysis revealed that most infected cells (*i.e.* GFP^+) are $PDGFR\alpha^+Sca\text{-}1^-CD54^-CD45^-Ter119^-CD31^-$ ($PDGFR\alpha^+$ signature, Figure 6). PDGFRα expression has been reported to identify a fibroblasts subset during fetal life that is

downregulated in the steady-state adult heart ((Valente et al., Manuscript), *Thesis Chapter III*). Fibroblasts are known to be the natural producers of collagen fibers and other ECM proteins (Moore-Morris et al., 2014). Infection of the PDGFrα^{+} cell fraction may constitute the source of the collagen production that leads to the typical scattered dense stellate scars reported in chronic stages of *T. cruzi* infection, leading to HF overtime (Molina et al., 1988). Further analysis, *e.g.* verification of the transcriptional profile of isolated *T. cruzi* infected PDGFrα^{+} cells, as well as the verification of their cell cycle profile, is required to confirm the hypothesis.

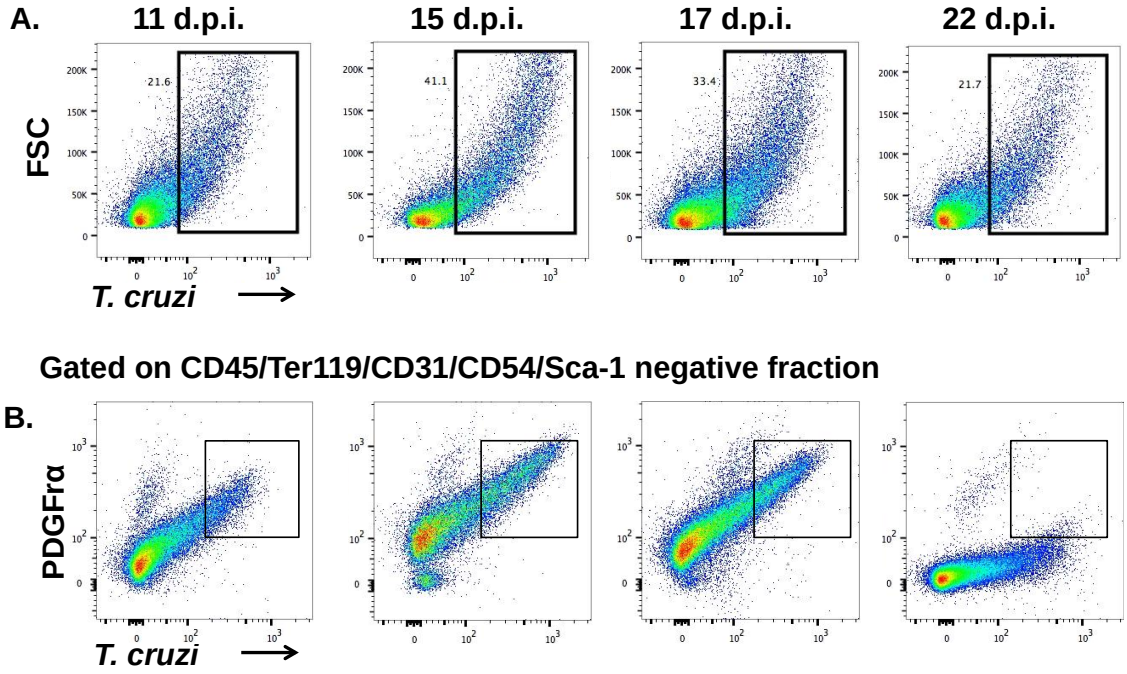

Figure 6. Flow cytometry analysis of *T. cruzi*-infected adult cardiac cells. A. Frequency of cardiac cells infected by *T. cruzi* along the infection time-course. **B.** Representative plots of the PDGFrα expression on infected hearts, where is evident that PDGFrα^{+} cells are infected by *T. cruzi* during a temporal time-window (from 11 – 17 d.p.i.). At later stages of infection (22 d.p.i. chronic phase) the remaining infected cells do not express PDGFrα.

Once *T. cruzi* parasites reach the bloodstream all cell types are susceptive to be infected. However, the striated muscle, namely CMs, is a major target for this parasite

(Andrade et al., 2010). Our analysis did not detect infected cells presenting a phenotype compatible with a CM signature. This is likely explained by the difficulties associated with the enzymatic isolation of adult cardiac cells, which greatly damages mature CMs due to unbalanced calcium levels during isolation (Pinz et al., 2011). Additionally, this limitation is expected to be aggravated following *T. cruzi* infection and subsequent impairment of CM integrity. This limitation may be bettered by performing histological analysis and co-localization of CM-associated markers with *T. cruzi* (underway).

CONCLUSION

Overall, the two injury models employed herein have different etiologies and are therefore likely to activate distinct response mechanisms and impact on different cell subsets. Interestingly, in both experimental settings cardiac injury has activated cellular phenotypes resembling embryonic surface signatures. Following MI we have revealed a fraction of CMs that re-express CD24, whereas in Chagas' disease we observed that *T. cruzi* specifically targets a PDGFrα^{+} fibroblast subset. These two subsets were exclusively found during heart development. Importantly, the two reported cell populations identified by their fetal-associated surface signatures can be prospectively isolated and characterized, either by cell sorting or *in situ* methodologies, such as laser capture, and will certainly contribute to novel knowledge on the pathophysiology of both diseases.

This proof-of-principle study indicates that embryonic/fetal phenotypes can be re-activated after injury and demonstrates the importance of the identification of cellular components during heart morphogenesis to understand adult pathologic scenarios.

REFERENCES

Please see references at *REFERENCES Chapter*.

CHAPTER VI

CONCLUDING REMARKS & FUTURE PERSPECTIVES

CONCLUDING REMARKS

The main propose of the herein *Doctoral Thesis* “At the Embryo’s Heart: Looking for Cardiac Repair/Regenerative Potential” was to contribute for the definition of the cardiac cellular compartments during development, maturation and after injury. This knowledge is expected to strengthen the connection between Cardiovascular Regenerative Medicine and Heart Developmental Biology. Since the beginning of this work several paradigms in cardiac Biology have been challenged and despite the clear lack of regenerative capacity of the adult mammalian heart (Zak, 1974), the possibility to challenge the cardiac cells and to improve the heart function after injury constitutes still a promising approach.

In the framework of this *Thesis* we proposed to study the adult mouse heart in the steady-state and in experimental-induced disease conditions, while also analyzing cardiac development as a mean to elucidate whether the early cellular dynamics at a time the organ is formed may be re-activated or replicated in the adult organ response to injury. In short, we attempted to answer the question as to *whether the mammalian (i.e. mouse) adult heart maintains an immature cell compartment or phenotype that could be stimulated/activated after injury.* To address this, four main goals were defined: i) to critically review the literature about CPCs, *i.e.* cardiac $Lin^{-}Sca\text{-}1^{+}$ cells, and compare it with similar cellular compartments in other organs; ii) to identify and isolate the different cardiac cell types and their progenitors during heart development and track them in the adult organ; iii) to establish the grounds for *in vivo* functional studies in the context of MI, *i.e.* standardization of histological assessment and

development/validation of a software to quantify the extension of ischemic tissue; and finally iv) to investigate re-expression of fetal phenotypes during the progression of adult heart injury. To accomplish the main goal of this work, we delineated a novel strategy in Cardiovascular Experimental Research, previously used with success in other systems like the hematopoietic (Cumano et al., 2000; Ramond et al., 2014) and the skeletal muscle (Montarras et al., 2005), expecting to bring a novel perspective to the field. Additionally, while implementing the models and tools for developing this work, we generated new methodologies to improve standardization in the analysis of the heart as whole organ.

Within the framework of this *Doctoral Thesis* we presented a synopsis that intends to revisit several aspects of the CPCs, as well as to point out aspects of their biology where knowledge is still lacking. For the purpose, we have debated in particular the biological significance of expressing a stem cell associated-marker (Sca-1), which was reported to be a hallmark to the majority of the identified CPC subsets. Despite surmounting reports in this particular theme, the existence of a prototypical stem/progenitor cell(s) entity in the adult mammalian myocardium is a concept that is far from reaching consensus in the scientific community. It seems appropriate to reflect upon the question of *what is or how should we define a heart progenitor?* In other words, *what is expected from an undifferentiated cell of the heart?* (Valente et al., 2014). The answer to this question is quite elusive, if not for other reasons at least for the molecular and morphologic complexity of heart formation, which has been well illustrated in several studies. Several progenitors contribute to building the heart, namely the CMCs (that will give rise to endocardium, ECs, CMs and SMCs) (Kitajima et al., 2006; Saga et al., 1999), PEO (originating iFBs and SMCs of the coronary vasculature) (Perez-Pomares et al., 2003; Viragh and Challice, 1981) and cNCC (distal structures of the OFT) (Jiang et al., 2000). Each of these progenitors contributes differently, at distinct embryonic stages, to the formation of the four-chambered heart.

The enormous complexity of heart development can be easily understood if we consider a given cellular type. For example, SMCs of the coronary vasculature derive from the PEO (Manner, 1999; Mikawa and Gourdie, 1996), while the same cell type present in the inflow and outflow vessels' wall originates from the SHF, and thus are CMCs-derived (Wu et al., 2006). The diversity of cardiovascular progenitors, together with the contribution of distinct cell sources at diverse stages of heart development during embryonic life, hampers the definition of a *heart progenitor*.

Diverse reports (Beltrami et al., 2003; Pfister et al., 2005; Tateishi et al., 2007) and our own experience (Freire et al., 2014a), drive us to postulate that the cardiogenic potential of heart resident Sca-1 CPCs is in general limited. Cardiomyocytic differentiation *in vitro*, usually confirmed by phenotypic (*e.g.* immunofluorescence), genetic (RT-PCR) and/or calcium transient analysis, renders poor evidence of differentiated CMs. Although the latter may as well reflect an absence of appropriate culture conditions (Forte et al., 2008), we are also confronted with *in vivo* results showing lack/insufficient evidence for *de novo* generation of CMs from Sca-1$^+$ CPCs (Uchida et al., 2013). Thus, a common denominator of studies pertaining to experimental models of cardiac injury followed by Sca-1$^+$ and/or c-Kit$^+$ CPCs transplantation, appears to just be the modest replacement of ischemic tissue by newly formed CMs (Hsieh et al., 2007; Uchida et al., 2013). It remains to clarify if the newly formed CMs derive in fact from the transplanted cells or if their paracrine action activates tissue progenitors/precursors. Despite this controversy, the data gathered in the last years does not allow to completely rule out the possibility that undifferentiated Sca-1 heart resident cells may generate CMs. On the other hand, cardiac Sca-1$^+$ cells have been shown to play an important role in the heart repair process mainly by paracrine and angiogenic action (Freire et al., 2014a). It is thus tempting to postulate that Sca-1$^+$ mesenchymal-like cells constitute a population of supportive cells and ECM-producers, likely generating stromal cells, and importantly, critical responders

following tissue injury. This raises diverse questions regarding the nature of Sca-1 cells: *Is the Sca-1 population a mesoderm-derived lineage essential for maintenance of the organ interstitium, as it is assumed for FBs? What would then differentiate Sca-1$^+$ cells from the so-called tissue-specific FBs?* It is known that FBs are a heterogeneous population (Chang et al., 2002); and so: *May Sca-1$^+$ merely correspond to a more immature cell stage, i.e. a precursor of FBs?* The detailed study we have performed along mouse heart development showed that Sca-1 is only found in ECs (CD31$^+$) and in a population of FBs that compose the mature valves (VICs). Additionally, in the fetal heart (E17.5), we also detected Sca-1 in other cellular fractions in the A, co-expressing CD54 and so exhibiting an epicardial gene profile. On the other hand, in the adult myocardium, a large fraction of cells in the three heart regions expresses Sca-1 and maintains the FB gene profile. Importantly, we did not detect c-Kit or Sca-1 expression in the cardiomyocytic compartment either in the embryo or in the adult myocardium (Valente et al., Manuscript). Overall, our results indicate that the Sca-1$^+$ signature does not seem to be associated with a less mature phenotype, but rather to constitute a population that increases in frequency during the maturation process and that presents a FB-like profile. The enzymatic dissociation protocol of the adult heart damages mature CMs but allows maintaining small immature CMs. We thus anticipate that if Sca-1 expression associates also to a CMs progenitor phenotype, our approach would have enabled the identification of such cellular subset during heart embryonic development. This was not the case, suggesting that Sca-1 expressing cells are not immature CMs, but rather a population of cells present in the *interstitium* of the heart, as it was shown in other organs (Driskell et al., 2013; McQualter et al., 2009).

We cannot ignore the fact that several independent studies indicate CMs themselves as major contributors for the limited turnover observed in aging and injured adult mammalian heart (Bergmann et al., 2009; Bersell et al., 2009; Kimura and Sadek, 2012; Mollova et al., 2013; Naqvi et al., 2014; Senyo et al., 2013). These reports are in

accordance with the acknowledged concept that CMs proliferation during heart morphogenesis significantly contributes to the heart chambers growth (de Boer et al., 2012; Drenckhahn et al., 2008; Oparil et al., 1984; Sedmera and Thompson, 2011) and in the neonatal heart to myocardium recovery after injury (Porrello et al., 2011; Porrello et al., 2013). However, we still do not know if adult CMs proliferation is either restricted to a specific CM compartment or if it occurs randomly in any mature myocyte. In other words, *does the mammalian heart contain an immature compartment of CM that is responsible for the low levels of cell proliferation?* Attempting to clarify this question, at least two distinct studies were published, reaching different conclusions. While Kimura *et al.* claim the existence of a population of mononucleated hypoxic CM that preferentially proliferate after injury, the Husain's Laboratory reported that both populations of mono- and bi-nucleated CMs are able to proliferate (Kimura et al., 2015; Naqvi et al., 2014), leaving this question still with the need to be clarified. We decided to approach this issue by characterizing the differentiation/maturation process of CMs using surface markers during mouse heart development. Remarkably, we have discriminated and isolated from the developing mouse heart two populations of CMs that develop in parallel: $Cav3^-$ CMs co-expressing CD24, CD146 and CD166, predominant at earlier stages of development (E9.5 and E13.5); and mature $Cav3^+$ CMs (Parton et al., 1997) found in the $CD24^-CD146^-CD166^-$ subset, which constitutes the major population in E17.5 myocardium. The advanced state of maturation of $Cav3^+$ CMs was confirmed by the presence of two nuclei *per* cell. On the other hand, the immature CM population ($CD24^+CD146^+CD166^+Cav3^-$) displays high frequency of proliferating cells, localizes in the compact myocardial zone and decreases along heart development, being undetectable in the adult heart. Curiously, when the adult myocardium is exposed to ischemia through experimental-induced MI injury (a model previously validated to recapitulate the functional aspects of the disease (Nascimento et al., 2011; Valente et al., Short-report)), CD24 expression was observed in some mononucleated CMs ($Actinin^+$) close to the ischemic border zone. Few of them were

shown to have re-entered the cell cycle, as evidenced by expression of pH3. The re-activation of CD24 expression, associated with the detection of proliferative CMs suggests that these particular CMs might be capable of reverting their phenotype to an embryonic/fetal molecular program. These results are of particular interest given the ischemic environment established after coronary ligation (MI model) and the low oxygen tension observed in the developing embryo tissues, including in the compact myocardial layer (Guimaraes-Camboa et al., 2015), where the proliferating and mononucleated $CD24^{+}$ CMs are detected (Valente et al., Manuscript). Because low oxygen tension, (to some extent a mimetic of ischemic injury), has been shown to boost the proliferation of several progenitor compartments (skeletal satellite cells) (Csete, 2005; Csete et al., 2001; Kook et al., 2008), it is possible that the CMs able to revert their surface phenotype, by re-expressing CD24, are not terminally mature, being a putative candidate to improve CM genesis after injury (Valente et al., Short-report).

Besides enabling us to assign a specific cell surface phenotype to distinct CMs subsets along development, the approach taken to characterize the developing heart allowed gathering phenotypic and molecular information on the distinct cardiac cellular populations. Specifically, and regarding the heterogeneity of the fibroblasts population, our strategy allowed the identification and prospective isolation of distinct fetal FBs subsets. We identified two mutually exclusive stroma populations: interstitial FBs expressing PDGFrα and perivascular FBs, identified by CD146 expression. The surface signature $CD90^{+}$ permitted discriminating the proliferative subset of FBs detected specifically in the ventricular wall. In a proof-of-principle experiment and despite the fact that adult FBs do not exhibit the same phenotype as fetal FBs (Valente et al., Manuscript), we detected a population defined by $PDGFr\alpha^{+}$ surface signature in the adult mouse myocardium after experimental-induced *T. cruzi* infection, as the only cell fraction infected (Valente et al., Short-report). FBs are known to be the natural

producers of collagen fibers and other ECM proteins (Moore-Morris et al., 2014), which might be the explanation for the source of the collagen production that leads to the typical scattered dense stellate scars reported in chronic stages of *T. cruzi* infection (Molina et al., 1988). The PEO is one of the developmental sources of cardiac FBs (Ieda et al., 2009; Zhou et al., 2008). Our results, however did not evidence a population compatible with an epicardial phenotype in the course of *T. cruzi* infection, suggesting that FBs are probably directly infected and revert their phenotype to a fetal stage (Valente et al., Short-report).

Our strategy allowed also the identification of other cardiac cellular compartments, namely the EpiCs. During embryonic heart development EpiCs were found in all heart regions, starting from E9.5 heart tube. The surface signature of this cell population varies along time, starting from expressing CD24 to being negative for all analyzed markers (Neg) at midgestation and acquiring CD54 expression when mature and quiescent. Additionally, EpiCs are a large fraction of the atrial cell wall, suggesting a significant participation of this population in atrial morphogenesis, not previously described (Valente et al., Manuscript).

In the framework of this *Thesis* we also intended to standardize *in vivo* functional studies, which are important to have the proper heart representation in *post-mortem* histological analysis. In fact, the *in vivo* potential of novel therapies for MI, as well as the determination of the cellular participants in the healing process are first assessed in injury mouse models (Ahmed et al., 2010) (Bolli et al., 2011; Gonzales and Pedrazzini, 2009; Makkar et al., 2012; Ramani et al., 2011; Smits et al., 2009a; Takagawa et al., 2007; Weinberger et al., 2012; Yoon et al., 2005). MI size and the percentage of the LV wall affected by collagen deposition are predictors of long-term LV function and geometry and also major end-points in clinical trials of cardio-protective therapies (Csonka et al., 2010; Nascimento et al., 2011; Takagawa et al., 2007). In experimental MI models, measurement of the infarct size is fundamental and is generally combined

with morphometric analysis of the LV (*i.e.* wall thinning and chamber dilation), as well as with functional assays to evaluate the deleterious consequences of MI. Despite the widespread use of the aforementioned methods, the final infarct size value is highly dependent on the methodology used (Csonka et al., 2010; Takagawa et al., 2007; Zornoff et al., 2009). Moreover, several technical aspects that directly impact the reported infarct size are commonly not described by the authors or are inconsistent across studies (Csonka et al., 2010; Takagawa et al., 2007; Zornoff et al., 2009), hampering the direct comparison of results from different laboratories (Valente et al., 2015). Additionally, manual quantification of the infarct size is time-consuming and highly dependent on the operator, as it requires manual contouring of the fibrotic tissue and viable myocardium from each tissue section. In order to ease this task and reduce operator-dependency, we have developed *MIQuant* (which stands for MI Quantification) software that reduces analysis time by 5-fold (Nascimento et al., 2011; Valente et al., 2015). Using MT stained sections, *MIQuant* software provides not only the final average value of the infarct size by the two different described methods – area (Michael et al., 1995) and midline length (Michael et al., 1995) – but also offers the intermediate calculations for each section. Widespread use of *MIQuant* will reduce the time required to quantify the infarct size and, more importantly, will reduce intra-laboratory variability (Nascimento et al., 2011). With the goal of standardizing inter-laboratories quantifications, we have also made available the systematic heart sampling to attain an accurate representation of the different LV regions prior to scar quantification (Valente et al., 2015), even when different quantification methods or tools are preferred over *MIQuant*. Accordingly, beyond the development and validation of the semi-automated software *MIQuant*, we provided a fully detailed protocol for representative sampling of the ischemic mouse heart followed by LV morphometric analysis. Regarding heart sampling, we described a robust methodology that represents different LV regions essential for accurate infarct size calculation and suitable for subsequent biochemical analysis. Our protocol also includes *in situ*

analytical methods to the assessment of neovascularization and cellular engraftment in the setting of cell-based therapies (Valente et al., 2015).

FUTURE PERSPECTIVES

In the herein work, and with the goal of identifying putative cardiac progenitors, we have focused on characterizing and isolating distinct cardiac cell types along mouse development. We have successfully associated surface markers with distinct cellular populations. Additionally, our strategy allowed us to follow cardiac subsets along development and establish their hierarchy. We were however unable to identify the same phenotypic signatures in the adult heart. Specific signaling pathways and molecular mechanisms observed in embryonic development have been reported to be re-activated following injury, both in the heart and in other systems (Freire et al., 2014b). We thus decided to evaluate if the identified cellular populations were re-activated in an injury setting. The use of two distinct injury models, MI and myocarditis caused by *T. cruzi*, allowed us to evaluate cell dynamics in distinct injury-associated responses. Interestingly, in the response to infection setting we observed an increase in the PDGFRα^{+} (Sca1^{-}CD54^{-}CD45^{-}Ter119^{-}CD31^{-}) cell fraction, which identify FBs in the fetal heart and is not detected in the steady-state adult heart. It would be interesting to analyze the transcriptional profile of this cell fraction to evaluate if indeed correspond to the population identified in the fetal heart. It remains to verify if CMs-associated markers (such as CD24) are also re-expressed, which will be performed by histologic analysis of infected hearts. Contrastingly, we report a modest re-expression of CD24 in CMs following MI, some of which were in a proliferative state. The plasticity of these cells, indicated by their capacity to re-express an embryonic/fetal marker, suggest that

they are not terminally mature, constituting a putative candidate to improve CM (re-)genesis after injury. To achieve a better comprehension of the mechanisms underlying recapitulation of the fetal program, it would be interesting to compare the gene expression profile of both cardiomyocytic populations ($CD24^+$ and $CD24^-$) of steady-state and injury animals. Additionally, the expression of Cav3, other surface protein associated with CMs, needs to be evaluated for a better understanding of the dichotomy between the expression of CD24 and Cav3, found to be associated with two different stages of CM development.

Overall, in the present work, we developed and validated tools to standardize the sampling and measurements of the infract size between laboratories. Additionally, we characterized the diverse cellular populations engaged in heart morphogenesis and described surface markers to specifically isolate them. The knowledge attained when studying the embryonic heart was used to analyze the adult heart in steady-state and injury conditions. Together, and even though many questions remain unanswered, the data gathered here will contribute for a better comprehension of the mechanisms underlying cardiogenesis and response to injury.

REFERENCES

Ahmed, R.P., Haider, K.H., Shujia, J., Afzal, M.R., and Ashraf, M. (2010). Sonic Hedgehog gene delivery to the rodent heart promotes angiogenesis via iNOS/netrin-1/PKC pathway. PLoS One *5*, e8576.

Ahn, D., Cheng, L., Moon, C., Spurgeon, H., Lakatta, E.G., and Talan, M.I. (2004). Induction of myocardial infarcts of a predictable size and location by branch pattern probability-assisted coronary ligation in C57BL/6 mice. Am J Physiol Heart Circ Physiol *286*, H1201-1207.

Ahuja, P., Perriard, E., Perriard, J.C., and Ehler, E. (2004). Sequential myofibrillar breakdown accompanies mitotic division of mammalian cardiomyocytes. J Cell Sci *117*, 3295-3306.

Akamatsu, T., Arai, Y., Kosugi, I., Kawasaki, H., Meguro, S., Sakao, M., Shibata, K., Suda, T., Chida, K., and Iwashita, T. (2013). Direct isolation of myofibroblasts and fibroblasts from bleomycin-injured lungs reveals their functional similarities and differences. Fibrogenesis & tissue repair *6*, 15.

Albelda, S.M., Muller, W.A., Buck, C.A., and Newman, P.J. (1991). Molecular and cellular properties of PECAM-1 (endoCAM/CD31): a novel vascular cell-cell adhesion molecule. J Cell Biol *114*, 1059-1068.

Ali, S.R., Hippenmeyer, S., Saadat, L.V., Luo, L., Weissman, I.L., and Ardehali, R. (2014a). Existing cardiomyocytes generate cardiomyocytes at a low rate after birth in mice. Proc Natl Acad Sci U S A *111*, 8850-8855.

Ali, S.R., Ranjbarvaziri, S., Talkhabi, M., Zhao, P., Subat, A., Hojjat, A., Kamran, P., Muller, A.M., Volz, K.S., Tang, Z.*, et al.* (2014b). Developmental heterogeneity of cardiac fibroblasts does not predict pathological proliferation and activation. Circ Res *115*, 625-635.

Andrade, L.O., Galvao, L.M., Meirelles Mde, N., Chiari, E., Pena, S.D., and Macedo, A.M. (2010). Differential tissue tropism of Trypanosoma cruzi strains: an in vitro study. Mem Inst Oswaldo Cruz *105*, 834-837.

Anez, N., Carrasco, H., Parada, H., Crisante, G., Rojas, A., Fuenmayor, C., Gonzalez, N., Percoco, G., Borges, R., Guevara, P*., et al.* (1999). Myocardial parasite persistence in chronic chagasic patients. Am J Trop Med Hyg *60*, 726-732.

Asakura, A., Seale, P., Girgis-Gabardo, A., and Rudnicki, M.A. (2002). Myogenic specification of side population cells in skeletal muscle. J Cell Biol *159*, 123-134.

Bailey, B., Fransioli, J., Gude, N.A., Alvarez, R., Zhan, X., Gustafsson, Å.B., and Sussman, M.A. (2012). Sca-1 Knockout Impairs Myocardial and Cardiac Progenitor Cell Function. Circ Res *111*, 750-760.

Bakker, M.L., Boink, G.J., Boukens, B.J., Verkerk, A.O., van den Boogaard, M., den Haan, A.D., Hoogaars, W.M., Buermans, H.P., de Bakker, J.M., Seppen, J*., et al.* (2012). T-box transcription factor TBX3 reprogrammes mature cardiac myocytes into pacemaker-like cells. Cardiovasc Res *94*, 439-449.

Baldwin, H.S., Shen, H.M., Yan, H.C., DeLisser, H.M., Chung, A., Mickanin, C., Trask, T., Kirschbaum, N.E., Newman, P.J., Albelda, S.M*., et al.* (1994). Platelet endothelial cell adhesion molecule-1 (PECAM-1/CD31): alternatively spliced, functionally distinct isoforms expressed during mammalian cardiovascular development. Development *120*, 2539-2553.

Balsam, L.B., Wagers, A.J., Christensen, J.L., Kofidis, T., Weissman, I.L., and Robbins, R.C. (2004). Haematopoietic stem cells adopt mature haematopoietic fates in ischaemic myocardium. Nature *428*, 668-673.

Bancroft, K.S.S.C.L.J.D. (2013). Bancroft's Theory and Practice of Histological Techniques, 7th edn (London – United Kingdom: Churchill Livingstone).

Banerjee, I., Yekkala, K., Borg, T.K., and Baudino, T.A. (2006). Dynamic Interactions between Myocytes, Fibroblasts, and Extracellular Matrix. Annals of the New York Academy of Sciences *1080*, 76-84.

Barile, L., Chimenti, I., Gaetani, R., Forte, E., Miraldi, F., Frati, G., Messina, E., and Giacomello, A. (2007). Cardiac stem cells: isolation, expansion and experimental use for myocardial regeneration. Nat Clin Pract Cardiovasc Med *4 Suppl 1*, S9-S14.

Barton, P.J., Robert, B., Cohen, A., Garner, I., Sassoon, D., Weydert, A., and Buckingham, M.E. (1988). Structure and sequence of the myosin alkali light chain gene expressed in adult cardiac atria and fetal striated muscle. J Biol Chem *263*, 12669-12676.

Baudino, T.A., Carver, W., Giles, W., and Borg, T.K. (2006). Cardiac fibroblasts: friend or foe? American Journal of Physiology - Heart and Circulatory Physiology *291*, H1015-H1026.

Bax, N.A., Bleyl, S.B., Gallini, R., Wisse, L.J., Hunter, J., Van Oorschot, A.A., Mahtab, E.A., Lie-Venema, H., Goumans, M.J., Betsholtz, C.*, et al.* (2010). Cardiac malformations in Pdgfralpha mutant embryos are associated with increased expression of WT1 and Nkx2.5 in the second heart field. Dev Dyn *239*, 2307-2317.

Bax, N.A., van Marion, M.H., Shah, B., Goumans, M.J., Bouten, C.V., and van der Schaft, D.W. (2012). Matrix production and remodeling capacity of cardiomyocyte progenitor cells during in vitro differentiation. J Mol Cell Cardiol *53*, 497-508.

Bearzi, C., Rota, M., Hosoda, T., Tillmanns, J., Nascimbene, A., De Angelis, A., Yasuzawa-Amano, S., Trofimova, I., Siggins, R.W., Lecapitaine, N.*, et al.* (2007). Human cardiac stem cells. Proc Natl Acad Sci U S A *104*, 14068-14073.

Beltrami, A.P., Barlucchi, L., Torella, D., Baker, M., Limana, F., Chimenti, S., Kasahara, H., Rota, M., Musso, E., Urbanek, K.*, et al.* (2003). Adult Cardiac Stem Cells Are Multipotent and Support Myocardial Regeneration. Cell *114*, 763-776.

Bergmann, O., Bhardwaj, R.D., Bernard, S., Zdunek, S., Barnabe-Heider, F., Walsh, S., Zupicich, J., Alkass, K., Buchholz, B.A., Druid, H.*, et al.* (2009). Evidence for Cardiomyocyte Renewal in Humans. Science *324*, 98-102.

Bersell, K., Arab, S., Haring, B., and Kuhn, B. (2009). Neuregulin1/ErbB4 signaling induces cardiomyocyte proliferation and repair of heart injury. Cell *138*, 257-270.

Bing, O.H., Ngo, H.Q., Humphries, D.E., Robinson, K.G., Lucey, E.C., Carver, W., Brooks, W.W., Conrad, C.H., Hayes, J.A., and Goldstein, R.H. (1997). Localization of alpha1(I) collagen mRNA in myocardium from the spontaneously hypertensive rat during the transition from compensated hypertrophy to failure. J Mol Cell Cardiol *29*, 2335-2344.

Bland, J.M., and Altman, D.G. (1986). Statistical methods for assessing agreement between two methods of clinical measurement. Lancet *1*, 307-310.

Bohl, S., Lygate, C.A., Barnes, H., Medway, D., Stork, L.-A., Schulz-Menger, J., Neubauer, S., and Schneider, J.E. (2009). Advanced methods for quantification of infarct size in mice using three-dimensional high-field late gadolinium enhancement MRI. American Journal of Physiology - Heart and Circulatory Physiology *296*, H1200-H1208.

Bolli, R., Chugh, A.R., D'Amario, D., Loughran, J.H., Stoddard, M.F., Ikram, S., Beache, G.M., Wagner, S.G., Leri, A., Hosoda, T.*, et al.* (2011). Cardiac stem cells in patients with ischaemic cardiomyopathy (SCIPIO): initial results of a randomised phase 1 trial. The Lancet.

Boogerd, C.J., Moorman, A.F., and Barnett, P. (2009). Protein interactions at the heart of cardiac chamber formation. Ann Anat *191*, 505-517.

Borg, T.K., and Caulfield, J.B. (1981). The collagen matrix of the heart. Fed Proc *40*, 2037-2041.

Borg, T.K., Ranson, W.F., Moslehy, F.A., and Caulfield, J.B. (1981). Structural basis of ventricular stiffness. Lab Invest *44*, 49-54.

Borg, T.K., Rubin, K., Lundgren, E., Borg, K., and Obrink, B. (1984). Recognition of extracellular matrix components by neonatal and adult cardiac myocytes. Dev Biol *104*, 86-96.

Borst, O., Ochmann, C., Schonberger, T., Jacoby, C., Stellos, K., Seizer, P., Flogel, U., Lang, F., and Gawaz, M. (2011). Methods employed for induction and analysis of experimental myocardial infarction in mice. Cell Physiol Biochem *28*, 1-12.

Bruneau, B.G., Logan, M., Davis, N., Levi, T., Tabin, C.J., Seidman, J.G., and Seidman, C.E. (1999). Chamber-specific cardiac expression of Tbx5 and heart defects in Holt-Oram syndrome. Dev Biol *211*, 100-108.

Bu, L., Jiang, X., Martin-Puig, S., Caron, L., Zhu, S., Shao, Y., Roberts, D.J., Huang, P.L., Domian, I.J., and Chien, K.R. (2009). Human ISL1 heart progenitors generate diverse multipotent cardiovascular cell lineages. Nature *460*, 113-117.

Bui, A.L., Horwich, T.B., and Fonarow, G.C. (2011). Epidemiology and risk profile of heart failure. Nat Rev Cardiol *8*, 30-41.

Burchfield, J.S., and Dimmeler, S. (2008). Role of paracrine factors in stem and progenitor cell mediated cardiac repair and tissue fibrosis. Fibrogenesis & tissue repair *1*, 4.

Cai, C.L., Liang, X., Shi, Y., Chu, P.H., Pfaff, S.L., Chen, J., and Evans, S. (2003). Isl1 identifies a cardiac progenitor population that proliferates prior to differentiation and contributes a majority of cells to the heart. Dev Cell *5*, 877-889.

Cai, C.L., Martin, J.C., Sun, Y., Cui, L., Wang, L., Ouyang, K., Yang, L., Bu, L., Liang, X., Zhang, X.*, et al.* (2008). A myocardial lineage derives from Tbx18 epicardial cells. Nature *454*, 104-108.

Camelliti, P., Borg, T.K., and Kohl, P. (2005). Structural and functional characterisation of cardiac fibroblasts. Cardiovascular Research *65*, 40-51.

Carson, F. (1997). Histotechnology: a self-instructional text, Second edn (Dallas, Texas – USA: ASCP Press).

Chakraborty, S., Combs, M.D., and Yutzey, K.E. (2010). Transcriptional regulation of heart valve progenitor cells. Pediatr Cardiol *31*, 414-421.

Challen, G.A., and Little, M.H. (2006). A Side Order of Stem Cells: The SP Phenotype. Stem Cells *24*, 3-12.

Chamond, N., Goytia, M., Coatnoan, N., Barale, J.C., Cosson, A., Degrave, W.M., and Minoprio, P. (2005). Trypanosoma cruzi proline racemases are involved in parasite differentiation and infectivity. Mol Microbiol *58*, 46-60.

Chang, H.Y., Chi, J.T., Dudoit, S., Bondre, C., van de Rijn, M., Botstein, D., and Brown, P.O. (2002). Diversity, topographic differentiation, and positional memory in human fibroblasts. Proc Natl Acad Sci U S A *99*, 12877-12882.

Chong, J.J., Chandrakanthan, V., Xaymardan, M., Asli, N.S., Li, J., Ahmed, I., Heffernan, C., Menon, M.K., Scarlett, C.J., Rashidianfar, A.*, et al.* (2011). Adult cardiac-resident MSC-like stem cells with a proepicardial origin. Cell Stem Cell *9*, 527-540.

Chong, J.J., Reinecke, H., Iwata, M., Torok-Storb, B., Stempien-Otero, A., and Murry, C.E. (2013). Progenitor cells identified by PDGFR-alpha expression in the developing and diseased human heart. Stem Cells Dev *22*, 1932-1943.

Christoffels, V.M., Grieskamp, T., Norden, J., Mommersteeg, M.T., Rudat, C., and Kispert, A. (2009). Tbx18 and the fate of epicardial progenitors. Nature *458*, E8-9; discussion E9-10.

Christoffels, V.M., Habets, P.E., Franco, D., Campione, M., de Jong, F., Lamers, W.H., Bao, Z.Z., Palmer, S., Biben, C., Harvey, R.P.*, et al.* (2000). Chamber formation and morphogenesis in the developing mammalian heart. Dev Biol *223*, 266-278.

Christoffels, V.M., Hoogaars, W.M., Tessari, A., Clout, D.E., Moorman, A.F., and Campione, M. (2004). T-box transcription factor Tbx2 represses differentiation and formation of the cardiac chambers. Dev Dyn *229*, 763-770.

Christoffels, V.M., Smits, G.J., Kispert, A., and Moorman, A.F. (2010). Development of the pacemaker tissues of the heart. Circ Res *106*, 240-254.

Clayton, E., and Forbes, S.J. (2009). The isolation and in vitro expansion of hepatic Sca-1 progenitor cells. Biochem Biophys Res Commun *381*, 549-553.

Clubb, F.J., Jr., and Bishop, S.P. (1984). Formation of binucleated myocardial cells in the neonatal rat. An index for growth hypertrophy. Lab Invest *50*, 571-577.

Csete, M. (2005). Oxygen in the cultivation of stem cells. Ann N Y Acad Sci *1049*, 1-8.

Csete, M., Walikonis, J., Slawny, N., Wei, Y., Korsnes, S., Doyle, J.C., and Wold, B. (2001). Oxygen-mediated regulation of skeletal muscle satellite cell proliferation and adipogenesis in culture. J Cell Physiol *189*, 189-196.

Csonka, C., Kupai, K., Kocsis, G.F., Novak, G., Fekete, V., Bencsik, P., Csont, T., and Ferdinandy, P. (2010). Measurement of myocardial infarct size in preclinical studies. Journal of pharmacological and toxicological methods *61*, 163-170.

Cumano, A., Dieterlen-Lievre, F., and Godin, I. (2000). The splanchnopleura/AGM region is the prime site for the generation of multipotent hemopoietic precursors, in the mouse embryo. Vaccine *18*, 1621-1623.

Darland, D.C., and D'Amore, P.A. (2001). Cell-cell interactions in vascular development. Curr Top Dev Biol *52*, 107-149.

David Sedmera, T.P.M.V.R.P.T.R.H.A. (2000). Developmental patterning of the myocardium. The Anatomical Record *258*, 319-337.

Davis, G.E., and Senger, D.R. (2005). Endothelial extracellular matrix: biosynthesis, remodeling, and functions during vascular morphogenesis and neovessel stabilization. Circ Res *97*, 1093-1107.

Dawson, D., Lygate, C.A., Saunders, J., Schneider, J.E., Ye, X., Hulbert, K., Noble, J.A., and Neubauer, S. (2004). Quantitative 3-Dimensional Echocardiography for Accurate and Rapid Cardiac Phenotype Characterization in Mice. Circulation *110*, 1632-1637.

de Boer, B.A., van den Berg, G., de Boer, P.A., Moorman, A.F., and Ruijter, J.M. (2012). Growth of the developing mouse heart: an interactive qualitative and quantitative 3D atlas. Dev Biol *368*, 203-213.

de Lange, F.J., Moorman, A.F., Anderson, R.H., Manner, J., Soufan, A.T., de Gier-de Vries, C., Schneider, M.D., Webb, S., van den Hoff, M.J., and Christoffels, V.M. (2004). Lineage and morphogenetic analysis of the cardiac valves. Circ Res *95*, 645-654.

Dekel, B., Zangi, L., Shezen, E., Reich-Zeliger, S., Eventov-Friedman, S., Katchman, H., Jacob-Hirsch, J., Amariglio, N., Rechavi, G., Margalit, R.*, et al.* (2006). Isolation and characterization of nontubular sca-1+lin- multipotent stem/progenitor cells from adult mouse kidney. J Am Soc Nephrol *17*, 3300-3314.

Dettman, R.W., Denetclaw, W., Jr., Ordahl, C.P., and Bristow, J. (1998). Common epicardial origin of coronary vascular smooth muscle, perivascular fibroblasts, and intermyocardial fibroblasts in the avian heart. Dev Biol *193*, 169-181.

Dimmeler, S., Zeiher, A.M., and Schneider, M.D. (2005). Unchain my heart: the scientific foundations of cardiac repair. J Clin Invest *115*, 572-583.

Dobaczewski, M., Chen, W., and Frangogiannis, N.G. (2010). Transforming growth factor (TGF)-[beta] signaling in cardiac remodeling. Journal of Molecular and Cellular Cardiology *In Press, Corrected Proof*.

Drenckhahn, J.-D., Schwarz, Q.P., Gray, S., Laskowski, A., Kiriazis, H., Ming, Z., Harvey, R.P., Du, X.-J., Thorburn, D.R., and Cox, T.C. (2008). Compensatory Growth of Healthy Cardiac Cells in the Presence of Diseased Cells Restores Tissue Homeostasis during Heart Development. Developmental cell *15*, 521-533.

Driskell, R.R., Lichtenberger, B.M., Hoste, E., Kretzschmar, K., Simons, B.D., Charalambous, M., Ferron, S.R., Herault, Y., Pavlovic, G., Ferguson-Smith, A.C., *et al.* (2013). Distinct fibroblast lineages determine dermal architecture in skin development and repair. Nature *504*, 277-281.

Dubois, N.C., Craft, A.M., Sharma, P., Elliott, D.A., Stanley, E.G., Elefanty, A.G., Gramolini, A., and Keller, G. (2011). SIRPA is a specific cell-surface marker for isolating cardiomyocytes derived from human pluripotent stem cells. Nat Biotechnol *29*, 1011-1018.

Eberhard, D., and Jockusch, H. (2005). Patterns of myocardial histogenesis as revealed by mouse chimeras. Dev Biol *278*, 336-346.

Efimov, I.R., Nikolski, V.P., Rothenberg, F., Greener, I.D., Li, J., Dobrzynski, H., and Boyett, M. (2004). Structure-function relationship in the AV junction. Anat Rec A Discov Mol Cell Evol Biol *280*, 952-965.

Ehler, E., Rothen, B.M., Hammerle, S.P., Komiyama, M., and Perriard, J.C. (1999). Myofibrillogenesis in the developing chicken heart: assembly of Z-disk, M-line and the thick filaments. J Cell Sci *112 (Pt 10)*, 1529-1539.

Eisenberg, L.M., and Markwald, R.R. (1995). Molecular regulation of atrioventricular valvuloseptal morphogenesis. Circ Res *77*, 1-6.

Epstein, J.A. (2010). Franklin H. Epstein Lecture. Cardiac development and implications for heart disease. N Engl J Med *363*, 1638-1647.

Esteves, T., Valente, M., Nascimento, D., Pinto-do-Ó, P., and Quelhas, P. (2011). Automatic and Semi-automatic Analysis of the Extension of Myocardial Infarction in an Experimental Murine Model

Pattern Recognition and Image Analysis. In, J. Vitrià, J. Sanches, and M. Hernández, eds. (Springer Berlin / Heidelberg), pp. 151-158.

Factor, S.M., Tanowitz, H., Wittner, M., and Ventura, M.C. (1993). Interstitial connective tissue matrix alterations in acute murine Chagas' disease. Clin Immunol Immunopathol *68*, 147-152.

Fazel, S., Cimini, M., Chen, L., Li, S., Angoulvant, D., Fedak, P., Verma, S., Weisel, R.D., Keating, A., and Li, R.-K. (2006). Cardioprotective c-kit+ cells are from the bone marrow and regulate the myocardial balance of angiogenic cytokines. J Clin Invest *116*, 1865-1877.

Ferreira-Martins, J., Ogorek, B., Cappetta, D., Matsuda, A., Signore, S., D'Amario, D., Kostyla, J., Steadman, E., Ide-Iwata, N., Sanada, F., *et al.* (2012). Cardiomyogenesis in the developing heart is regulated by c-kit-positive cardiac stem cells. Circ Res *110*, 701-715.

Fishbein, M.C., Maclean, D., and Maroko, P.R. (1978). The histopathologic evolution of myocardial infarction. Chest *73*, 843-849.

Forte, G., Carotenuto, F., Pagliari, F., Pagliari, S., Cossa, P., Fiaccavento, R., Ahluwalia, A., Vozzi, G., Vinci, B., Serafino, A.*, et al.* (2008). Criticality of the biological and physical stimuli array inducing resident cardiac stem cell determination. Stem Cells *26*, 2093-2103.

Freire, A.G., Nascimento, D.S., Forte, G., Valente, M., Resende, T.P., Pagliari, S., Abreu, C., Carvalho, I., Di Nardo, P., and Pinto-do, O.P. (2014a). Stable phenotype and function of immortalized Lin-Sca-1+ cardiac progenitor cells in long-term culture: a step closer to standardization. Stem Cells Dev *23*, 1012-1026.

Freire, A.G., Resende, T.P., and Pinto-do, O.P. (2014b). Building and repairing the heart: what can we learn from embryonic development? Biomed Res Int *2014*, 679168.

Frenzel, H., Schwartzkopff, B., Holtermann, W., Schnurch, H.G., Novi, A., and Hort, W. (1988). Regression of cardiac hypertrophy: morphometric and biochemical studies in rat heart after swimming training. J Mol Cell Cardiol *20*, 737-751.

Furtado, M.B., Costa, M.W., Pranoto, E.A., Salimova, E., Pinto, A.R., Lam, N.T., Park, A., Snider, P., Chandran, A., Harvey, R.P.*, et al.* (2014). Cardiogenic genes expressed in cardiac fibroblasts contribute to heart development and repair. Circ Res *114*, 1422-1434.

Fuster, V. (2014). Top 10 cardiovascular therapies and interventions for the next decade. Nat Rev Cardiol *11*, 671-683.

Gambini, E., Pompilio, G., Biondi, A., Alamanni, F., Capogrossi, M.C., Agrifoglio, M., and Pesce, M. (2011). C-kit+ cardiac progenitors exhibit mesenchymal markers and preferential cardiovascular commitment. Cardiovasc Res *89*, 362-373.

Gao, X.-M., Dart, A.M., Dewar, E., Jennings, G., and Du, X.-J. (2000). Serial echocardiographic assessment of left ventricular dimensions and function after myocardial infarction in mice. Cardiovascular Research *45*, 330-338.

Gittenberger-de Groot, A.C., Vrancken Peeters, M.P., Mentink, M.M., Gourdie, R.G., and Poelmann, R.E. (1998). Epicardium-derived cells contribute a novel population to the myocardial wall and the atrioventricular cushions. Circ Res *82*, 1043-1052.

Gnecchi, M., Zhang, Z., Ni, A., and Dzau, V.J. (2008). Paracrine Mechanisms in Adult Stem Cell Signaling and Therapy. Circ Res *103*, 1204-1219.

Goldman, S. (2005). Stem and progenitor cell-based therapy of the human central nervous system. Nat Biotechnol *23*, 862-871.

Goldsmith, E.C., Hoffman, A., Morales, M.O., Potts, J.D., Price, R.L., McFadden, A., Rice, M., and Borg, T.K. (2004). Organization of fibroblasts in the heart. Dev Dyn *230*, 787-794.

Gonzales, C., and Pedrazzini, T. (2009). Progenitor cell therapy for heart disease. Exp Cell Res *315*, 3077-3085.

Gonzalez, A.M., Osorio, J.C., Manlhiot, C., Gruber, D., Homma, S., and Mital, S. (2007). Hypertrophy signaling during peripartum cardiac remodeling. Am J Physiol Heart Circ Physiol *293*, H3008-3013.

González, J., Azzato, F., Ambrosio, G., and Milei, J. (2013). Pathogenesis of Chronic Chagasic Myocarditis, Diagnosis and Treatment of Myocarditis. Available from: http://wwwintechopencom/books/diagnosis-and-treatment-of-myocarditis/pathogenesis-of-chronic-chagasic-myocarditis, .

Gonzalez, R., Woods, R., and Eddins, S. (2004). Digital Image Processing Using MAT-LAB (Pearson Education).

Goyard, S., Dutra, P.L., Deolindo, P., Autheman, D., D'Archivio, S., and Minoprio, P. (2014). In vivo imaging of trypanosomes for a better assessment of host-parasite relationships and drug efficacy. Parasitol Int *63*, 260-268.

Gros, J., Manceau, M., Thome, V., and Marcelle, C. (2005). A common somitic origin for embryonic muscle progenitors and satellite cells. Nature *435*, 954-958.

Guimaraes-Camboa, N., Stowe, J., Aneas, I., Sakabe, N., Cattaneo, P., Henderson, L., Kilberg, M.S., Johnson, R.S., Chen, J., McCulloch, A.D.*, et al.* (2015). HIF1alpha Represses Cell Stress Pathways to Allow Proliferation of Hypoxic Fetal Cardiomyocytes. Dev Cell *33*, 507-521.

Hanneman, S.K. (2008). Design, analysis, and interpretation of method-comparison studies. AACN Adv Crit Care *19*, 223-234.

Harvey, R.P., Meilhac, S.M., and Buckingham, M.E. (2009). Landmarks and Lineages in the Developing Heart. Circ Res *104*, 1235-1237.

Heineke, J., and Molkentin, J.D. (2006). Regulation of cardiac hypertrophy by intracellular signalling pathways. Nat Rev Mol Cell Biol *7*, 589-600.

Hellstrom, M., Kalen, M., Lindahl, P., Abramsson, A., and Betsholtz, C. (1999). Role of PDGF-B and PDGFR-beta in recruitment of vascular smooth muscle cells and pericytes during embryonic blood vessel formation in the mouse. Development *126*, 3047-3055.

Herrmann, B.G., Labeit, S., Poustka, A., King, T.R., and Lehrach, H. (1990). Cloning of the T gene required in mesoderm formation in the mouse. Nature *343*, 617-622.

Hertz, M.I., Aurora, P., Christie, J.D., Dobbels, F., Edwards, L.B., Kirk, R., Kucheryavaya, A.Y., Rahmel, A.O., Rowe, A.W., and Stehlik, J. (2010). Scientific

Registry of the International Society for Heart and Lung Transplantation: introduction to the 2010 annual reports. The Journal of heart and lung transplantation : the official publication of the International Society for Heart Transplantation *29*, 1083-1088.

Hierlihy, A.M., Seale, P., Lobe, C.G., Rudnicki, M.A., and Megeney, L.A. (2002). The post-natal heart contains a myocardial stem cell population. FEBS Letters *530*, 239-243.

Higuchi Mde, L., De Brito, T., Martins Reis, M., Barbosa, A., Bellotti, G., Pereira-Barreto, A.C., and Pileggi, F. (1993). Correlation between Trypanosoma cruzi parasitism and myocardial inflammatory infiltrate in human chronic chagasic myocarditis: Light microscopy and immunohistochemical findings. Cardiovasc Pathol *2*, 101-106.

Higuchi, M.L., Fukasawa, S., De Brito, T., Parzianello, L.C., Bellotti, G., and Ramires, J.A. (1999). Different microcirculatory and interstitial matrix patterns in idiopathic dilated cardiomyopathy and Chagas' disease: a three dimensional confocal microscopy study. Heart *82*, 279-285.

Hill, J.A., and Olson, E.N. (2008). Cardiac plasticity. N Engl J Med *358*, 1370-1380.

Hirata, H., Murakami, Y., Miyamoto, Y., Tosaka, M., Inoue, K., Nagahashi, A., Jakt, L.M., Asahara, T., Iwata, H., Sawa, Y.*, et al.* (2006). ALCAM (CD166) is a surface marker for early murine cardiomyocytes. Cells Tissues Organs *184*, 172-180.

Hirschy, A., Schatzmann, F., Ehler, E., and Perriard, J.C. (2006). Establishment of cardiac cytoarchitecture in the developing mouse heart. Dev Biol *289*, 430-441.

Holmes, C., and Stanford, W.L. (2007). Concise Review: Stem Cell Antigen-1: Expression, Function, and Enigma. Stem Cells *25*, 1339-1347.

Holmes, J.W., Borg, T.K., and Covell, J.W. (2005). Structure and mechanics of healing myocardial infarcts. Annu Rev Biomed Eng *7*, 223-253.

Houser, S.R., Margulies, K.B., Murphy, A.M., Spinale, F.G., Francis, G.S., Prabhu, S.D., Rockman, H.A., Kass, D.A., Molkentin, J.D., Sussman, M.A.*, et al.* (2012). Animal models of heart failure: a scientific statement from the American Heart Association. Circ Res *111*, 131-150.

Houyel, L., Bajolle, F., Capderou, A., Laux, D., Parisot, P., and Bonnet, D. (2013). The pattern of the coronary arterial orifices in hearts with congenital malformations of the outflow tracts: a marker of rotation of the outflow tract during cardiac development? J Anat *222*, 349-357.

Howard, C.M., and Baudino, T.A. (2014). Dynamic cell-cell and cell-ECM interactions in the heart. J Mol Cell Cardiol *70*, 19-26.

Hsieh, P.C.H., Segers, V.F.M., Davis, M.E., MacGillivray, C., Gannon, J., Molkentin, J.D., Robbins, J., and Lee, R.T. (2007). Evidence from a genetic fate-mapping study that stem cells refresh adult mammalian cardiomyocytes after injury. Nat Med *13*, 970-974.

Huang, C., Gu, H., Yu, Q., Manukyan, M.C., Poynter, J.A., and Wang, M. (2011). Sca-1+ cardiac stem cells mediate acute cardioprotection via paracrine factor SDF-1 following myocardial ischemia/reperfusion. PLoS One *6*, e29246.

Huang, N.F., Sievers, R.E., Park, J.S., Fang, Q., Li, S., and Lee, R.J. (2006). A rodent model of myocardial infarction for testing the efficacy of cells and polymers for myocardial reconstruction. Nat Protoc *1*, 1596-1609.

Hudon-David, F., Bouzeghrane, F., Couture, P., and Thibault, G. (2007). Thy-1 expression by cardiac fibroblasts: lack of association with myofibroblast contractile markers. J Mol Cell Cardiol *42*, 991-1000.

Ieda, M., Tsuchihashi, T., Ivey, K.N., Ross, R.S., Hong, T.T., Shaw, R.M., and Srivastava, D. (2009). Cardiac fibroblasts regulate myocardial proliferation through beta1 integrin signaling. Dev Cell *16*, 233-244.

Ito, C.Y., Li, C.Y.J., Bernstein, A., Dick, J.E., and Stanford, W.L. (2003). Hematopoietic stem cell and progenitor defects in Sca-1/Ly-6A-null mice. Blood *101*, 517-523.

Jacobs, T.W., Prioleau, J.E., Stillman, I.E., and Schnitt, S.J. (1996). Loss of tumor marker-immunostaining intensity on stored paraffin slides of breast cancer. Journal of the National Cancer Institute *88*, 1054-1059.

Jalil, J.E., Doering, C.W., Janicki, J.S., Pick, R., Clark, W.A., Abrahams, C., and Weber, K.T. (1988). Structural vs. contractile protein remodeling and myocardial stiffness in hypertrophied rat left ventricle. J Mol Cell Cardiol *20*, 1179-1187.

Janicki, J.S., and Brower, G.L. (2002). The role of myocardial fibrillar collagen in ventricular remodeling and function. J Card Fail *8*, S319-325.

Jiang, X., Rowitch, D.H., Soriano, P., McMahon, A.P., and Sucov, H.M. (2000). Fate of the mammalian cardiac neural crest. Development *127*, 1607-1616.

Jin, J.P., Zhang, Z., and Bautista, J.A. (2008). Isoform diversity, regulation, and functional adaptation of troponin and calponin. Crit Rev Eukaryot Gene Expr *18*, 93-124.

Jones, E.M., Colley, D.G., Tostes, S., Lopes, E.R., Vnencak-Jones, C.L., and McCurley, T.L. (1993). Amplification of a Trypanosoma cruzi DNA sequence from inflammatory lesions in human chagasic cardiomyopathy. Am J Trop Med Hyg *48*, 348-357.

Junqueira, L.C., Montes, G.S., and Sanchez, E.M. (1982). The influence of tissue section thickness on the study of collagen by the Picrosirius-polarization method. Histochemistry *74*, 153-156.

Kafadar, K.A., Yi, L., Ahmad, Y., So, L., Rossi, F., and Pavlath, G.K. (2009). Sca-1 expression is required for efficient remodeling of the extracellular matrix during skeletal muscle regeneration. Dev Biol *326*, 47-59.

Kajstura, J., Rota, M., Cappetta, D., Ogorek, B., Arranto, C., Bai, Y., Ferreira-Martins, J., Signore, S., Sanada, F., Matsuda, A.*, et al.* (2012). Cardiomyogenesis in the aging and failing human heart. Circulation *126*, 1869-1881.

Kajstura, J., Urbanek, K., Perl, S., Hosoda, T., Zheng, H., Ogorek, B., Ferreira-Martins, J., Goichberg, P., Rondon-Clavo, C., Sanada, F.*, et al.* (2010). Cardiomyogenesis in the adult human heart. Circ Res *107*, 305-315.

Kamkin, A., Kiseleva, I., Lozinsky, I., and Scholz, H. (2005). Electrical interaction of mechanosensitive fibroblasts and myocytes in the heart. Basic Res Cardiol *100*, 337-345.

Kang, S.G., Shinojima, N., Hossain, A., Gumin, J., Yong, R.L., Colman, H., Marini, F., Andreeff, M., and Lang, F.F. (2010). Isolation and perivascular localization of mesenchymal stem cells from mouse brain. Neurosurgery *67*, 711-720.

Karlsson, C., and Karlsson, M.G. (2011). Effects of long-term storage on the detection of proteins, DNA, and mRNA in tissue microarray slides. The journal of histochemistry and cytochemistry : official journal of the Histochemistry Society *59*, 1113-1121.

Kattman, S.J., Adler, E.D., and Keller, G.M. (2007). Specification of multipotential cardiovascular progenitor cells during embryonic stem cell differentiation and embryonic development. Trends Cardiovasc Med *17*, 240-246.

Kelly, R.G., Brown, N.A., and Buckingham, M.E. (2001). The arterial pole of the mouse heart forms from Fgf10-expressing cells in pharyngeal mesoderm. Dev Cell *1*, 435-440.

Kimura, W., and Sadek, H.A. (2012). The cardiac hypoxic niche: emerging role of hypoxic microenvironment in cardiac progenitors. Cardiovasc Diagn Ther *2*, 278-289.

Kimura, W., Xiao, F., Canseco, D.C., Muralidhar, S., Thet, S., Zhang, H.M., Abderrahman, Y., Chen, R., Garcia, J.A., Shelton, J.M.*, et al.* (2015). Hypoxia fate mapping identifies cycling cardiomyocytes in the adult heart. Nature *523*, 226-230.

Kirby, M.L., and Waldo, K.L. (1995). Neural crest and cardiovascular patterning. Circ Res *77*, 211-215.

Kitajima, T., Nishii, K., Ueoka, H., Shibayama, T., Gemba, K., Kodani, T., Kiura, K., Tabata, M., Hotta, K., Tanimoto, M.*, et al.* (2006). Recent improvement in lung cancer screening: a comparison of the results carried out in two different time periods. Acta Med Okayama *60*, 173-179.

Klein, L., O'Connor, C.M., Gattis, W.A., Zampino, M., de Luca, L., Vitarelli, A., Fedele, F., and Gheorghiade, M. (2003). Pharmacologic therapy for patients with chronic heart failure and reduced systolic function: review of trials and practical considerations. Am J Cardiol *91*, 18F-40F.

Klocke, R., Tian, W., Kuhlmann, M.T., and Nikol, S. (2007). Surgical animal models of heart failure related to coronary heart disease. Cardiovasc Res *74*, 29-38.

Kobayashi, S., Yoshikawa, Y., Sakata, S., Takenaka, C., Hagihara, H., Ohga, Y., Abe, T., Taniguchi, S., and Takaki, M. (2004). Left ventricular mechanoenergetics after hyperpolarized cardioplegic arrest by nicorandil and after depolarized cardioplegic arrest by KCl. American Journal of Physiology - Heart and Circulatory Physiology *287*, H1072-H1080.

Kook, S.H., Son, Y.O., Lee, K.Y., Lee, H.J., Chung, W.T., Choi, K.C., and Lee, J.C. (2008). Hypoxia affects positively the proliferation of bovine satellite cells and their myogenic differentiation through up-regulation of MyoD. Cell Biol Int *32*, 871-878.

Kotton, D.N., Summer, R.S., Sun, X., Ma, B.Y., and Fine, A. (2003). Stem cell antigen-1 expression in the pulmonary vascular endothelium. Am J Physiol Lung Cell Mol Physiol *284*, L990-L996.

Kovacic, J.C., Mercader, N., Torres, M., Boehm, M., and Fuster, V. (2012). Epithelial-to-mesenchymal and endothelial-to-mesenchymal transition: from cardiovascular development to disease. Circulation *125*, 1795-1808.

Kreidberg, J.A., Sariola, H., Loring, J.M., Maeda, M., Pelletier, J., Housman, D., and Jaenisch, R. (1993). WT-1 is required for early kidney development. Cell *74*, 679-691.

Krenning, G., Zeisberg, E.M., and Kalluri, R. (2010). The origin of fibroblasts and mechanism of cardiac fibrosis. J Cell Physiol *225*, 631-637.

Kubalak, S.W., Miller-Hance, W.C., O'Brien, T.X., Dyson, E., and Chien, K.R. (1994). Chamber specification of atrial myosin light chain-2 expression precedes septation during murine cardiogenesis. J Biol Chem *269*, 16961-16970.

Laflamme, M.A., and Murry, C.E. (2011). Heart regeneration. Nature *473*, 326-335.

Lajiness, J.D., and Conway, S.J. (2013). Origin, development, and differentiation of cardiac fibroblasts. J Mol Cell Cardiol.

Leri, A., Kajstura, J., and Anversa, P. (2005). Cardiac stem cells and mechanisms of myocardial regeneration. Physiol Rev *85*, 1373-1416.

Lescroart, F., and Meilhac, S.M. (2012). Cell lineages, growth and repair of the mouse heart. Results Probl Cell Differ *55*, 263-289.

Leu, M., Ehler, E., and Perriard, J.C. (2001). Characterisation of postnatal growth of the murine heart. Anat Embryol (Berl) *204*, 217-224.

Li, F., Wang, X., Bunger, P.C., and Gerdes, A.M. (1997a). Formation of binucleated cardiac myocytes in rat heart: I. Role of actin-myosin contractile ring. J Mol Cell Cardiol *29*, 1541-1551.

Li, F., Wang, X., Capasso, J.M., and Gerdes, A.M. (1996). Rapid Transition of Cardiac Myocytes from Hyperplasia to Hypertrophy During Postnatal Development. Journal of Molecular and Cellular Cardiology *28*, 1737-1746.

Li, F., Wang, X., and Gerdes, A.M. (1997b). Formation of binucleated cardiac myocytes in rat heart: II. Cytoskeletal organisation. J Mol Cell Cardiol *29*, 1553-1565.

Lints, T.J., Parsons, L.M., Hartley, L., Lyons, I., and Harvey, R.P. (1993). Nkx-2.5: a novel murine homeobox gene expressed in early heart progenitor cells and their myogenic descendants. Development *119*, 419-431.

Lips, D.J., deWindt, L.J., van Kraaij, D.J., and Doevendans, P.A. (2003). Molecular determinants of myocardial hypertrophy and failure: alternative pathways for beneficial and maladaptive hypertrophy. Eur Heart J *24*, 883-896.

Lloyd-Jones, D., Adams, R.J., Brown, T.M., Carnethon, M., Dai, S., De Simone, G., Ferguson, T.B., Ford, E., Furie, K., Gillespie, C.*, et al.* (2010). Executive summary: heart disease and stroke statistics--2010 update: a report from the American Heart Association. Circulation *121*, 948-954.

Lockhart, M.M., Phelps, A.L., van den Hoff, M.J., and Wessels, A. (2014). The Epicardium and the Development of the Atrioventricular Junction in the Murine Heart. J Dev Biol *2*, 1-17.

Luna, G., Paez, J., and Cardier, J.E. (2004). Expression of the hematopoietic stem cell antigen Sca-1 (LY-6A/E) in liver sinusoidal endothelial cells: possible function of Sca-1 in endothelial cells. Stem Cells Dev *13*, 528-535.

Lutgens, E., Daemen, M.J., de Muinck, E.D., Debets, J., Leenders, P., and Smits, J.F. (1999). Chronic myocardial infarction in the mouse: cardiac structural and functional changes. Cardiovasc Res *41*, 586-593.

Lyngbæk, S., Schneider, M., Hansen, J., and Sheikh, S. (2007). Cardiac regeneration by resident stem and progenitor cells in the adult heart. Basic Res Cardiol *102*, 101-114.

Lyons, G.E. (1996). Vertebrate heart development. Curr Opin Genet Dev *6*, 454-460.

Lyons, I., Parsons, L.M., Hartley, L., Li, R., Andrews, J.E., Robb, L., and Harvey, R.P. (1995). Myogenic and morphogenetic defects in the heart tubes of murine embryos lacking the homeo box gene Nkx2-5. Genes Dev *9*, 1654-1666.

Ma, Q., Zhou, B., and Pu, W.T. (2008). Reassessment of Isl1 and Nkx2-5 cardiac fate maps using a Gata4-based reporter of Cre activity. Dev Biol *323*, 98-104.

Machado, F.S., Jelicks, L.A., Kirchhoff, L.V., Shirani, J., Nagajyothi, F., Mukherjee, S., Nelson, R., Coyle, C.M., Spray, D.C., de Carvalho, A.C.*, et al.* (2012). Chagas heart disease: report on recent developments. Cardiol Rev *20*, 53-65.

MacKenna, D., Summerour, S.R., and Villarreal, F.J. (2000). Role of mechanical factors in modulating cardiac fibroblast function and extracellular matrix synthesis. Cardiovasc Res *46*, 257-263.

Makkar, R.R., Smith, R.R., Cheng, K., Malliaras, K., Thomson, L.E., Berman, D., Czer, L.S., Marban, L., Mendizabal, A., Johnston, P.V.*, et al.* (2012). Intracoronary cardiosphere-derived cells for heart regeneration after myocardial infarction (CADUCEUS): a prospective, randomised phase 1 trial. Lancet *379*, 895-904.

Malliaras, K., Zhang, Y., Seinfeld, J., Galang, G., Tseliou, E., Cheng, K., Sun, B., Aminzadeh, M., and Marban, E. (2013). Cardiomyocyte proliferation and progenitor cell recruitment underlie therapeutic regeneration after myocardial infarction in the adult mouse heart. EMBO Mol Med *5*, 191-209.

Manasek, F.J. (1969). Embryonic development of the heart. II. Formation of the epicardium. J Embryol Exp Morphol *22*, 333-348.

Manner, J. (1999). Does the subepicardial mesenchyme contribute myocardioblasts to the myocardium of the chick embryo heart? A quail-chick chimera study tracing the fate of the epicardial primordium. Anat Rec *255*, 212-226.

Manner, J., Schlueter, J., and Brand, T. (2005). Experimental analyses of the function of the proepicardium using a new microsurgical procedure to induce loss-of-proepicardial-function in chick embryos. Dev Dyn *233*, 1454-1463.

Markwald, R.R., Fitzharris, T.P., and Manasek, F.J. (1977). Structural development of endocardial cushions. Am J Anat *148*, 85-119.

Martin, C.M., Meeson, A.P., Robertson, S.M., Hawke, T.J., Richardson, J.A., Bates, S., Goetsch, S.C., Gallardo, T.D., and Garry, D.J. (2004). Persistent expression of the ATP-binding cassette transporter, Abcg2, identifies cardiac SP cells in the developing and adult heart. Dev Biol *265*, 262-275.

Matsuura, K., Honda, A., Nagai, T., Fukushima, N., Iwanaga, K., Tokunaga, M., Shimizu, T., Okano, T., Kasanuki, H., Hagiwara, N.*, et al.* (2009). Transplantation of cardiac progenitor cells ameliorates cardiac dysfunction after myocardial infarction in mice. J Clin Invest *119*, 2204-2217.

Maxeiner, H., Krehbiehl, N., Muller, A., Woitasky, N., Akinturk, H., Muller, M., Weigand, M.A., Abdallah, Y., Kasseckert, S., Schreckenberg, R.*, et al.* (2010). New insights into paracrine mechanisms of human cardiac progenitor cells. Eur J Heart Fail *12*, 730-737.

McQualter, J.L., Brouard, N., Williams, B., Baird, B.N., Sims-Lucas, S., Yuen, K., Nilsson, S.K., Simmons, P.J., and Bertoncello, I. (2009). Endogenous Fibroblastic Progenitor Cells in the Adult Mouse Lung Are Highly Enriched in the Sca-1 Positive Cell Fraction. Stem Cells *27*, 623-633.

Meilhac, S.M., Esner, M., Kelly, R.G., Nicolas, J.F., and Buckingham, M.E. (2004a). The clonal origin of myocardial cells in different regions of the embryonic mouse heart. Dev Cell *6*, 685-698.

Meilhac, S.M., Esner, M., Kerszberg, M., Moss, J.E., and Buckingham, M.E. (2004b). Oriented clonal cell growth in the developing mouse myocardium underlies cardiac morphogenesis. J Cell Biol *164*, 97-109.

Meilhac, S.M., Kelly, R.G., Rocancourt, D., Eloy-Trinquet, S., Nicolas, J.F., and Buckingham, M.E. (2003). A retrospective clonal analysis of the myocardium reveals two phases of clonal growth in the developing mouse heart. Development *130*, 3877-3889.

Mercola, M., Ruiz-Lozano, P., and Schneider, M.D. (2011). Cardiac muscle regeneration: lessons from development. Genes & Development *25*, 299-309.

Messina, E., De Angelis, L., Frati, G., Morrone, S., Chimenti, S., Fiordaliso, F., Salio, M., Battaglia, M., Latronico, M.V.G., Coletta, M.*, et al.* (2004). Isolation and Expansion of Adult Cardiac Stem Cells From Human and Murine Heart. Circ Res *95*, 911-921.

Michael, L.H., Entman, M.L., Hartley, C.J., Youker, K.A., Zhu, J., Hall, S.R., Hawkins, H.K., Berens, K., and Ballantyne, C.M. (1995). Myocardial ischemia and reperfusion: a murine model. Am J Physiol *269*, H2147-2154.

Mikawa, T., and Gourdie, R.G. (1996). Pericardial mesoderm generates a population of coronary smooth muscle cells migrating into the heart along with ingrowth of the epicardial organ. Dev Biol *174*, 221-232.

Milei, J., Guerri-Guttenberg, R.A., Grana, D.R., and Storino, R. (2009). Prognostic impact of Chagas disease in the United States. Am Heart J *157*, 22-29.

Milei, J., Mautner, B., Storino, R., Sanchez, J.A., and Ferrans, V.J. (1992). Does Chagas' disease exist as an undiagnosed form of cardiomyopathy in the United States? Am Heart J *123*, 1732-1735.

Millino, C., Sarinella, F., Tiveron, C., Villa, A., Sartore, S., and Ausoni, S. (2000). Cardiac and smooth muscle cell contribution to the formation of the murine pulmonary veins. Dev Dyn *218*, 414-425.

Minicucci, M.F., Azevedo, P.S., Duarte, D.R., Matsubara, B.B., Matsubara, L.S., Campana, Ã.I.O., Paiva, S.A.R., and Zornoff, L.A.M. (2007). Comparison of Different Methods to Measure Experimental Chronic Infarction Size in the Rat Model. Arquivos Brasileiros de Cardiologia *89*, 93-98.

Minot, C.S. (1900). On a Hitherto Unrecognized Form of Blood Circulation without Capillaries in the Organs of Vertebrates. J Boston Soc Med Sci *4*, 133-134.

Miragoli, M., Gaudesius, G., and Rohr, S. (2006). Electrotonic modulation of cardiac impulse conduction by myofibroblasts. Circ Res *98*, 801-810.

Molina, H.A., Milei, J., Rimoldi, M.T., Gonzalez Cappa, S.M., and Storino, R.A. (1988). Histopathology of the heart conducting system in experimental Chagas disease in mice. Trans R Soc Trop Med Hyg *82*, 241-246.

Molkentin, J.D., and Dorn, G.W., 2nd (2001). Cytoplasmic signaling pathways that regulate cardiac hypertrophy. Annu Rev Physiol *63*, 391-426.

Mollova, M., Bersell, K., Walsh, S., Savla, J., Das, L.T., Park, S.Y., Silberstein, L.E., Dos Remedios, C.G., Graham, D., Colan, S.*, et al.* (2013). Cardiomyocyte proliferation contributes to heart growth in young humans. Proc Natl Acad Sci U S A *110*, 1446-1451.

Montarras, D., Morgan, J., Collins, C., Relaix, F., Zaffran, S., Cumano, A., Partridge, T., and Buckingham, M. (2005). Direct isolation of satellite cells for skeletal muscle regeneration. Science *309*, 2064-2067.

Moore-Morris, T., Guimaraes-Camboa, N., Banerjee, I., Zambon, A.C., Kisseleva, T., Velayoudon, A., Stallcup, W.B., Gu, Y., Dalton, N.D., Cedenilla, M.*, et al.* (2014). Resident fibroblast lineages mediate pressure overload-induced cardiac fibrosis. J Clin Invest *124*, 2921-2934.

Moorman, A.F., and Christoffels, V.M. (2003). Cardiac chamber formation: development, genes, and evolution. Physiol Rev *83*, 1223-1267.

Moretti, A., Caron, L., Nakano, A., Lam, J.T., Bernshausen, A., Chen, Y., Qyang, Y., Bu, L., Sasaki, M., Martin-Puig, S.*, et al.* (2006). Multipotent Embryonic Isl1+ Progenitor Cells Lead to Cardiac, Smooth Muscle, and Endothelial Cell Diversification. Cell *127*, 1151-1165.

Mosqueira, D., Pagliari, S., Uto, K., Ebara, M., Romanazzo, S., Escobedo-Lucea, C., Nakanishi, J., Taniguchi, A., Franzese, O., Di Nardo, P.*, et al.* (2014). Hippo Pathway Effectors Control Cardiac Progenitor Cell Fate by Acting as Dynamic Sensors of Substrate Mechanics and Nanostructure. ACS nano *8*, 2033-2047.

Mozaffarian, D., Benjamin, E.J., Go, A.S., Arnett, D.K., Blaha, M.J., Cushman, M., de Ferranti, S., Despres, J.P., Fullerton, H.J., Howard, V.J., *et al.* (2015). Heart disease and stroke statistics--2015 update: a report from the American Heart Association. Circulation *131*, e29-322.

Nag, A.C. (1980). Study of non-muscle cells of the adult mammalian heart: a fine structural analysis and distribution. Cytobios *28*, 41-61.

Nah, D.Y., and Rhee, M.Y. (2009). The inflammatory response and cardiac repair after myocardial infarction. Korean Circ J *39*, 393-398.

Nakamura, A., and Manasek, F.J. (1981). An experimental study of the relation of cardiac jelly to the shape of the early chick embryonic heart. J Embryol Exp Morphol *65*, 235-256.

Naqvi, N., Li, M., Calvert, J.W., Tejada, T., Lambert, J.P., Wu, J., Kesteven, S.H., Holman, S.R., Matsuda, T., Lovelock, J.D., *et al.* (2014). A proliferative burst during preadolescence establishes the final cardiomyocyte number. Cell *157*, 795-807.

Nascimento, D.S., Mosqueira, D., Sousa, L.M., Teixeira, M., Filipe, M., Resende, T.P., Araujo, A.F., Valente, M., Almeida, J., Martins, J.P., *et al.* (2014). Human umbilical cord tissue-derived mesenchymal stromal cells attenuate remodeling following myocardial infarction by pro-angiogenic, anti-apoptotic and endogenous cell activation mechanisms. Stem cell research & therapy *5*, 5.

Nascimento, D.S., Valente, M., Esteves, T., de Pina, M.d.F.t., Guedes, J.G., Freire, A., Quelhas, P., and Pinto-do-Ã“, P.t. (2011). MIQuant - Semi-Automation of Infarct Size Assessment in Models of Cardiac Ischemic Injury. PLoS ONE *6*, e25045.

Navaratnam, V., Kaufman, M.H., Skepper, J.N., Barton, S., and Guttridge, K.M. (1986). Differentiation of the myocardial rudiment of mouse embryos: an ultrastructural study including freeze-fracture replication. J Anat *146*, 65-85.

Nishida, K., Michael, G., Dobrev, D., and Nattel, S. (2010). Animal models for atrial fibrillation: clinical insights and scientific opportunities. Europace *12*, 160-172.

Nishii, K., and Shibata, Y. (2006). Mode and determination of the initial contraction stage in the mouse embryo heart. Anat Embryol (Berl) *211*, 95-100.

Nonaka, S., Shiratori, H., Saijoh, Y., and Hamada, H. (2002). Determination of left-right patterning of the mouse embryo by artificial nodal flow. Nature *418*, 96-99.

Norris, R.A., Borg, T.K., Butcher, J.T., Baudino, T.A., Banerjee, I., and Markwald, R.R. (2008). Neonatal and adult cardiovascular pathophysiological remodeling and repair: developmental role of periostin. Ann N Y Acad Sci *1123*, 30-40.

Norris, R.A., Potts, J.D., Yost, M.J., Junor, L., Brooks, T., Tan, H., Hoffman, S., Hart, M.M., Kern, M.J., Damon, B., *et al.* (2009). Periostin promotes a fibroblastic

lineage pathway in atrioventricular valve progenitor cells. Dev Dyn *238*, 1052-1063.

Oh, H., Bradfute, S.B., Gallardo, T.D., Nakamura, T., Gaussin, V., Mishina, Y., Pocius, J., Michael, L.H., Behringer, R.R., Garry, D.J.*, et al.* (2003). Cardiac progenitor cells from adult myocardium: Homing, differentiation, and fusion after infarction. Proc Natl Acad Sci U S A *100*, 12313-12318.

Oh, H., Chi, X., Bradfute, S.B., Mishina, Y., Pocius, J., Michael, L.H., Behringer, R.R., Schwartz, R.J., Entman, M.L., and Schneider, M.D. (2004). Cardiac muscle plasticity in adult and embryo by heart-derived progenitor cells. Ann N Y Acad Sci *1015*, 182-189.

Oka, T., Xu, J., and Molkentin, J.D. (2007). Re-employment of developmental transcription factors in adult heart disease. Semin Cell Dev Biol *18*, 117-131.

Oparil, S., Bishop, S.P., and Clubb, F.J., Jr. (1984). Myocardial cell hypertrophy or hyperplasia. Hypertension *6*, III38-43.

Orlic, D., Kajstura, J., Chimenti, S., Limana, F., Jakoniuk, I., Quaini, F., Nadal-Ginard, B., Bodine, D.M., Leri, A., and Anversa, P. (2001). Mobilized bone marrow cells repair the infarcted heart, improving function and survival. Proc Natl Acad Sci U S A *98*, 10344-10349.

Oyama, T., Nagai, T., Wada, H., Naito, A.T., Matsuura, K., Iwanaga, K., Takahashi, T., Goto, M., Mikami, Y., Yasuda, N.*, et al.* (2007). Cardiac side population cells have a potential to migrate and differentiate into cardiomyocytes in vitro and in vivo. J Cell Biol *176*, 329-341.

Parton, R.G., Way, M., Zorzi, N., and Stang, E. (1997). Caveolin-3 associates with developing T-tubules during muscle differentiation. J Cell Biol *136*, 137-154.

Patten, R.D., Aronovitz, M.J., Deras-Mejia, L., Pandian, N.G., Hanak, G.G., Smith, J.J., Mendelsohn, M.E., and Konstam, M.A. (1998). Ventricular remodeling in a mouse model of myocardial infarction. American Journal of Physiology - Heart and Circulatory Physiology *274*, H1812-H1820.

Paylor, B., Fernandes, J., McManus, B., and Rossi, F. (2013). Tissue-resident Sca1+ PDGFRalpha+ mesenchymal progenitors are the cellular source of fibrofatty infiltration in arrhythmogenic cardiomyopathy. F1000Research *2*, 141.

Perez-Pomares, J.M., Phelps, A., Sedmerova, M., Carmona, R., Gonzalez-Iriarte, M., Munoz-Chapuli, R., and Wessels, A. (2002). Experimental studies on the spatiotemporal expression of WT1 and RALDH2 in the embryonic avian heart: a model for the regulation of myocardial and valvuloseptal development by epicardially derived cells (EPDCs). Dev Biol *247*, 307-326.

Perez-Pomares, J.M., Phelps, A., Sedmerova, M., and Wessels, A. (2003). Epicardial-like cells on the distal arterial end of the cardiac outflow tract do not derive from the proepicardium but are derivatives of the cephalic pericardium. Dev Dyn *227*, 56-68.

Perriard, J.C., Hirschy, A., and Ehler, E. (2003). Dilated cardiomyopathy: a disease of the intercalated disc? Trends Cardiovasc Med *13*, 30-38.

Pfeffer, M.A., Pfeffer, J.M., Fishbein, M.C., Fletcher, P.J., Spadaro, J., Kloner, R.A., and Braunwald, E. (1979). Myocardial infarct size and ventricular function in rats. Circ Res *44*, 503-512.

Pfister, O., Mouquet, F., Jain, M., Summer, R., Helmes, M., Fine, A., Colucci, W.S., and Liao, R. (2005). CD31- but Not CD31+ Cardiac Side Population Cells Exhibit Functional Cardiomyogenic Differentiation. Circ Res *97*, 52-61.

Pinz, I., Zhu, M., Mende, U., and Ingwall, J.S. (2011). An improved isolation procedure for adult mouse cardiomyocytes. Cell Biochem Biophys *61*, 93-101.

Ponten, A., Walsh, S., Malan, D., Xian, X., Scheele, S., Tarnawski, L., Fleischmann, B.K., and Jovinge, S. (2013). FACS-based isolation, propagation and characterization of mouse embryonic cardiomyocytes based on VCAM-1 surface marker expression. PLoS One *8*, e82403.

Porrello, E.R., Mahmoud, A.I., Simpson, E., Hill, J.A., Richardson, J.A., Olson, E.N., and Sadek, H.A. (2011). Transient regenerative potential of the neonatal mouse heart. Science *331*, 1078-1080.

Porrello, E.R., Mahmoud, A.I., Simpson, E., Johnson, B.A., Grinsfelder, D., Canseco, D., Mammen, P.P., Rothermel, B.A., Olson, E.N., and Sadek, H.A. (2013). Regulation of neonatal and adult mammalian heart regeneration by the miR-15 family. Proc Natl Acad Sci U S A *110*, 187-192.

Porter, K.E., and Turner, N.A. (2009). Cardiac fibroblasts: At the heart of myocardial remodeling. Pharmacology & Therapeutics *123*, 255-278.

Poss, K.D., Wilson, L.G., and Keating, M.T. (2002). Heart regeneration in zebrafish. Science *298*, 2188-2190.

Prall, O.W., Menon, M.K., Solloway, M.J., Watanabe, Y., Zaffran, S., Bajolle, F., Biben, C., McBride, J.J., Robertson, B.R., Chaulet, H.*, et al.* (2007). An Nkx2-5/Bmp2/Smad1 negative feedback loop controls heart progenitor specification and proliferation. Cell *128*, 947-959.

Protti, A., Sirker, A., Shah, A.M., and Botnar, R. (2010). Late gadolinium enhancement of acute myocardial infarction in mice at 7T: Cine-FLASH versus inversion recovery. Journal of Magnetic Resonance Imaging *32*, 878-886.

Puente, B.N., Kimura, W., Muralidhar, S.A., Moon, J., Amatruda, J.F., Phelps, K.L., Grinsfelder, D., Rothermel, B.A., Chen, R., Garcia, J.A.*, et al.* (2014). The oxygen-rich postnatal environment induces cardiomyocyte cell-cycle arrest through DNA damage response. Cell *157*, 565-579.

Quaini, F., Urbanek, K., Beltrami, A.P., Finato, N., Beltrami, C.A., Nadal-Ginard, B., Kajstura, J., Leri, A., and Anversa, P. (2002). Chimerism of the Transplanted Heart. N Engl J Med *346*, 5-15.

Rajabi, M., Kassiotis, C., Razeghi, P., and Taegtmeyer, H. (2007). Return to the fetal gene program protects the stressed heart: a strong hypothesis. Heart Fail Rev *12*, 331-343.

Ramani, R., Nilles, K., Gibson, G., Burkhead, B., Mathier, M., McNamara, D., and McTiernan, C.F. (2011). Tissue Inhibitor of Metalloproteinase-2 Gene Delivery Ameliorates Postinfarction Cardiac Remodeling. Clinical and Translational Science *4*, 24-31.

Ramond, C., Berthault, C., Burlen-Defranoux, O., de Sousa, A.P., Guy-Grand, D., Vieira, P., Pereira, P., and Cumano, A. (2014). Two waves of distinct hematopoietic progenitor cells colonize the fetal thymus. Nat Immunol *15*, 27-35.

Ranger, A.M., Grusby, M.J., Hodge, M.R., Gravallese, E.M., de la Brousse, F.C., Hoey, T., Mickanin, C., Baldwin, H.S., and Glimcher, L.H. (1998). The transcription factor NF-ATc is essential for cardiac valve formation. Nature *392*, 186-190.

Rassi, A., Jr., Rassi, A., and Little, W.C. (2000). Chagas' heart disease. Clin Cardiol *23*, 883-889.

Rassi, A., Jr., Rassi, A., and Marin-Neto, J.A. (2010). Chagas disease. Lancet *375*, 1388-1402.

Red-Horse, K., Ueno, H., Weissman, I.L., and Krasnow, M.A. (2010). Coronary arteries form by developmental reprogramming of venous cells. Nature *464*, 549-553.

Reese, D.E., Mikawa, T., and Bader, D.M. (2002). Development of the coronary vessel system. Circ Res *91*, 761-768.

Reinecke, H., Minami, E., Zhu, W.-Z., and Laflamme, M.A. (2008). Cardiogenic Differentiation and Transdifferentiation of Progenitor Cells. Circ Res *103*, 1058-1071.

Rosenblatt-Velin, N., Ogay, S., Felley, A., Stanford, W.L., and Pedrazzini, T. (2012). Cardiac dysfunction and impaired compensatory response to pressure overload in mice deficient in stem cell antigen-1. FASEB J *26*, 229-239.

Rosenthal, N., and Harvey, R.P. (2010). Heart Development and Regeneration (London, UK: Elsevier).

Rossi, M.A. (1991). The pattern of myocardial fibrosis in chronic Chagas' heart disease. Int J Cardiol *30*, 335-340.

Rossi, M.A., and Ramos, S.G. (1996). Pathogenesis of chronic Chagas' myocarditis: An overview. Cardiovasc Pathol *5*, 197-202.

Ryzhov, S., Goldstein, A.E., Novitskiy, S.V., Blackburn, M.R., Biaggioni, I., and Feoktistov, I. (2012). Role of A2B adenosine receptors in regulation of paracrine functions of stem cell antigen 1-positive cardiac stromal cells. J Pharmacol Exp Ther *341*, 764-774.

Saga, Y., Miyagawa-Tomita, S., Takagi, A., Kitajima, S., Miyazaki, J., and Inoue, T. (1999). MesP1 is expressed in the heart precursor cells and required for the formation of a single heart tube. Development *126*, 3437-3447.

Sanada, F., Kim, J., Czarna, A., Chan, N.Y., Signore, S., Ogorek, B., Isobe, K., Wybieralska, E., Borghetti, G., Pesapane, A.*, et al.* (2014). c-Kit-positive cardiac stem cells nested in hypoxic niches are activated by stem cell factor reversing the aging myopathy. Circ Res *114*, 41-55.

Santos Lima, E.C., and Minoprio, P. (1996). Chagas' disease is attenuated in mice lacking gamma delta T cells. Infect Immun *64*, 215-221.

Sassoon, D.A., Garner, I., and Buckingham, M. (1988). Transcripts of alpha-cardiac and alpha-skeletal actins are early markers for myogenesis in the mouse embryo. Development *104*, 155-164.

Schijman, A.G., Vigliano, C.A., Viotti, R.J., Burgos, J.M., Brandariz, S., Lococo, B.E., Leze, M.I., Armenti, H.A., and Levin, M.J. (2004). Trypanosoma cruzi DNA in cardiac lesions of Argentinean patients with end-stage chronic chagas heart disease. Am J Trop Med Hyg *70*, 210-220.

Schulte, I., Schlueter, J., Abu-Issa, R., Brand, T., and Manner, J. (2007). Morphological and molecular left-right asymmetries in the development of the proepicardium: a comparative analysis on mouse and chick embryos. Dev Dyn *236*, 684-695.

Sedmera, D., Misek, I., and Klima, M. (1997). On the development of Cetacean extremities: I. Hind limb rudimentation in the Spotted dolphin (Stenella attenuata). Eur J Morphol *35*, 25-30.

Sedmera, D., Reckova, M., DeAlmeida, A., Coppen, S.R., Kubalak, S.W., Gourdie, R.G., and Thompson, R.P. (2003). Spatiotemporal pattern of commitment to slowed proliferation in the embryonic mouse heart indicates progressive differentiation of the cardiac conduction system. Anat Rec A Discov Mol Cell Evol Biol *274*, 773-777.

Sedmera, D., and Thompson, R.P. (2011). Myocyte proliferation in the developing heart. Dev Dyn *240*, 1322-1334.

Segers, V.F.M., and Lee, R.T. (2008). Stem-cell therapy for cardiac disease. Nature *451*, 937-942.

Senyo, S.E., Steinhauser, M.L., Pizzimenti, C.L., Yang, V.K., Cai, L., Wang, M., Wu, T.D., Guerquin-Kern, J.L., Lechene, C.P., and Lee, R.T. (2013). Mammalian heart renewal by pre-existing cardiomyocytes. Nature *493*, 433-436.

Silber, A.M., Tonelli, R.R., Martinelli, M., Colli, W., and Alves, M.J. (2002). Active transport of L-proline in Trypanosoma cruzi. J Eukaryot Microbiol *49*, 441-446.

Sizarov, A., Devalla, H.D., Anderson, R.H., Passier, R., Christoffels, V.M., and Moorman, A.F. (2011). Molecular analysis of patterning of conduction tissues in the developing human heart. Circ Arrhythm Electrophysiol *4*, 532-542.

Smart, N., Bollini, S., Dube, K.N., Vieira, J.M., Zhou, B., Davidson, S., Yellon, D., Riegler, J., Price, A.N., Lythgoe, M.F.*, et al.* (2011). De novo cardiomyocytes from within the activated adult heart after injury. Nature.

Smart, N., Risebro, C.A., Melville, A.A.D., Moses, K., Schwartz, R.J., Chien, K.R., and Riley, P.R. (2007). Thymosin [bgr]4 induces adult epicardial progenitor mobilization and neovascularization. Nature *445*, 177-182.

Smith, R.R., Barile, L., Cho, H.C., Leppo, M.K., Hare, J.M., Messina, E., Giacomello, A., Abraham, M.R., and Marban, E. (2007). Regenerative potential of cardiosphere-derived cells expanded from percutaneous endomyocardial biopsy specimens. Circulation *115*, 896-908.

Smits, A.M., van den Hengel, L.G., van den Brink, S., Metz, C.H., Doevendans, P.A., and Goumans, M.-J. (2009a). A new in vitro model for stem cell differentiation and interaction. Stem cell research *2*, 108-112.

Smits, A.M., van Laake, L.W., den Ouden, K., Schreurs, C., Szuhai, K., van Echteld, C.J., Mummery, C.L., Doevendans, P.A., and Goumans, M.J. (2009b). Human cardiomyocyte progenitor cell transplantation preserves long-term function of the infarcted mouse myocardium. Cardiovasc Res *83*, 527-535.

Smits, A.M., van Vliet, P., Metz, C.H., Korfage, T., Sluijter, J.P., Doevendans, P.A., and Goumans, M.J. (2009c). Human cardiomyocyte progenitor cells differentiate into functional mature cardiomyocytes: an in vitro model for studying human cardiac physiology and pathophysiology. Nat Protoc *4*, 232-243.

Soonpaa, M.H., and Field, L.J. (1998). Survey of studies examining mammalian cardiomyocyte DNA synthesis. Circ Res *83*, 15-26.

Soonpaa, M.H., Kim, K.K., Pajak, L., Franklin, M., and Field, L.J. (1996). Cardiomyocyte DNA synthesis and binucleation during murine development. Am J Physiol *271*, H2183-2189.

Spater, D., Abramczuk, M.K., Buac, K., Zangi, L., Stachel, M.W., Clarke, J., Sahara, M., Ludwig, A., and Chien, K.R. (2013). A HCN4+ cardiomyogenic progenitor derived from the first heart field and human pluripotent stem cells. Nat Cell Biol *15*, 1098-1106.

Srivastava, D. (2006). Making or breaking the heart: from lineage determination to morphogenesis. Cell *126*, 1037-1048.

Stanley, E.G., Biben, C., Elefanty, A., Barnett, L., Koentgen, F., Robb, L., and Harvey, R.P. (2002). Efficient Cre-mediated deletion in cardiac progenitor cells conferred by a 3'UTR-ires-Cre allele of the homeobox gene Nkx2-5. Int J Dev Biol *46*, 431-439.

Strutz, F., Okada, H., Lo, C.W., Danoff, T., Carone, R.L., Tomaszewski, J.E., and Neilson, E.G. (1995). Identification and characterization of a fibroblast marker: FSP1. J Cell Biol *130*, 393-405.

Sucov, H.M., Gu, Y., Thomas, S., Li, P., and Pashmforoush, M. (2009). Epicardial control of myocardial proliferation and morphogenesis. Pediatr Cardiol *30*, 617-625.

Sun, Y. (2009). Myocardial repair/remodelling following infarction: roles of local factors. Cardiovasc Res *81*, 482-490.

Sun, Y., Kiani, M.F., Postlethwaite, A.E., and Weber, K.T. (2002). Infarct scar as living tissue. Basic Res Cardiol *97*, 343-347.

Sutton, M.G.S.J., and Sharpe, N. (2000). Left Ventricular Remodeling After Myocardial Infarction : Pathophysiology and Therapy. Circulation *101*, 2981-2988.

Takagawa, J., Zhang, Y., Wong, M.L., Sievers, R.E., Kapasi, N.K., Wang, Y., Yeghiazarians, Y., Lee, R.J., Grossman, W., and Springer, M.L. (2007). Myocardial infarct size measurement in the mouse chronic infarction model: comparison of area- and length-based approaches. J Appl Physiol *102*, 2104-2111.

Takamiya, M., Haider, K.H., and Ashraf, M. (2011). Identification and characterization of a novel multipotent sub-population of Sca-1(+) cardiac progenitor cells for myocardial regeneration. PLoS One *6*, e25265.

Takeuchi, J.K., Ohgi, M., Koshiba-Takeuchi, K., Shiratori, H., Sakaki, I., Ogura, K., Saijoh, Y., and Ogura, T. (2003). Tbx5 specifies the left/right ventricles and ventricular septum position during cardiogenesis. Development *130*, 5953-5964.

Tam, P.P., Parameswaran, M., Kinder, S.J., and Weinberger, R.P. (1997). The allocation of epiblast cells to the embryonic heart and other mesodermal lineages: the role of ingression and tissue movement during gastrulation. Development *124*, 1631-1642.

Tateishi, K., Ashihara, E., Takehara, N., Nomura, T., Honsho, S., Nakagami, T., Morikawa, S., Takahashi, T., Ueyama, T., Matsubara, H.*, et al.* (2007). Clonally amplified cardiac stem cells are regulated by Sca-1 signaling for efficient cardiovascular regeneration. J Cell Sci *120*, 1791-1800.

Thannickal, V.J., Lee, D.Y., White, E.S., Cui, Z., Larios, J.M., Chacon, R., Horowitz, J.C., Day, R.M., and Thomas, P.E. (2003). Myofibroblast differentiation by transforming growth factor-beta1 is dependent on cell adhesion and integrin signaling via focal adhesion kinase. J Biol Chem *278*, 12384-12389.

Tian, X., Hu, T., Zhang, H., He, L., Huang, X., Liu, Q., Yu, W., He, L., Yang, Z., Yan, Y.*, et al.* (2014). Vessel formation. De novo formation of a distinct coronary vascular population in neonatal heart. Science *345*, 90-94.

Tian, X., Hu, T., Zhang, H., He, L., Huang, X., Liu, Q., Yu, W., He, L., Yang, Z., Zhang, Z.*, et al.* (2013). Subepicardial endothelial cells invade the embryonic ventricle wall to form coronary arteries. Cell Res *23*, 1075-1090.

Tomasek, J.J., Gabbiani, G., Hinz, B., Chaponnier, C., and Brown, R.A. (2002). Myofibroblasts and mechano-regulation of connective tissue remodelling. Nat Rev Mol Cell Biol *3*, 349-363.

Tsuchiya, A., Heike, T., Baba, S., Fujino, H., Umeda, K., Matsuda, Y., Nomoto, M., Ichida, T., Aoyagi, Y., and Nakahata, T. (2008). Sca-1+ endothelial cells (SPECs) reside in the portal area of the liver and contribute to rapid recovery from acute liver disease. Biochem Biophys Res Commun *365*, 595-601.

Uchida, S., De Gaspari, P., Kostin, S., Jenniches, K., Kilic, A., Izumiya, Y., Shiojima, I., grosse Kreymborg, K., Renz, H., Walsh, K.*, et al.* (2013). Sca1-Derived Cells Are a Source of Myocardial Renewal in the Murine Adult Heart. Stem Cell Reports *1*, 397-410.

Valente, M., Araujo, A., Esteves, T., Laundo, T.L., Freire, A.G., Quelhas, P., Pinto-do-O, P., and Nascimento, D.S. (2015). Optimized Heart Sampling and Systematic Evaluation of Cardiac Therapies in Mouse Models of Ischemic Injury: Assessment of Cardiac Remodeling and Semi-automated Quantification of Myocardial Infarct Size. Current Protocols in Mouse Biology *5*.

Valente, M., Cossan, A., Resende, T.P., Laundos, T.L., Nascimento, D.S., Minoprio, P., Cumano, A., and Pinto-do-O, P. (Short-report). Differential re-activation of specific embryonic cellular phenotypes in the adult mouse heart subjected to ischemia and infection injuries.

Valente, M., Nascimento, D.S., Cumano, A., and Pinto-do, O.P. (2014). Sca-1+ cardiac progenitor cells and heart-making: a critical synopsis. Stem Cells Dev *23*, 2263-2273.

Valente, M., Resende, T.P., Nascimento, D.S., Cumano, A., and Pinto-do-O, P. (Manuscript). Surface Markers Identifying Different Cardiac Populations Reveal Two Distinct Subsets of Cardiomyocytes in the Mouse Fetal Heart.

van Berlo, J.H., Kanisicak, O., Maillet, M., Vagnozzi, R.J., Karch, J., Lin, S.C., Middleton, R.C., Marban, E., and Molkentin, J.D. (2014). c-kit+ cells minimally contribute cardiomyocytes to the heart. Nature *509*, 337-341.

van de Rijn, M., Heimfeld, S., Spangrude, G.J., and Weissman, I.L. (1989). Mouse hematopoietic stem-cell antigen Sca-1 is a member of the Ly-6 antigen family. Proc Natl Acad Sci U S A *86*, 4634-4638.

Van Mierop, L.H., and Kutsche, L.M. (1985). Development of the ventricular septum of the heart. Heart Vessels *1*, 114-119.

van Vliet, P., Roccio, M., Smits, A., van Oorschot, A., Metz, C., van Veen, T., Sluijter, J., Doevendans, P., and Goumans, M.J. (2008). Progenitor cells isolated from the human heart: a potential cell source for regenerative therapy. Neth Heart J *16*, 163-169.

Vikstrom, K.L., Bohlmeyer, T., Factor, S.M., and Leinwand, L.A. (1998). Hypertrophy, pathology, and molecular markers of cardiac pathogenesis. Circ Res *82*, 773-778.

Vincent, S.D., and Buckingham, M.E. (2010). How to make a heart: the origin and regulation of cardiac progenitor cells. Curr Top Dev Biol *90*, 1-41.

Virag, J.I., and Murry, C.E. (2003). Myofibroblast and Endothelial Cell Proliferation during Murine Myocardial Infarct Repair. Am J Pathol *163*, 2433-2440.

Viragh, S., and Challice, C.E. (1973). Origin and differentiation of cardiac muscle cells in the mouse. J Ultrastruct Res *42*, 1-24.

Viragh, S., and Challice, C.E. (1981). The origin of the epicardium and the embryonic myocardial circulation in the mouse. Anat Rec *201*, 157-168.

Wada, A.M., Willet, S.G., and Bader, D. (2003). Coronary vessel development: a unique form of vasculogenesis. Arterioscler Thromb Vasc Biol *23*, 2138-2145.

Wagers, A.J., and Weissman, I.L. (2004). Plasticity of adult stem cells. Cell *116*, 639-648.

Walsh, S., Pontén, A., Fleischmann, B.K., and Jovinge, S. (2010). Cardiomyocyte cell cycle control and growth estimation in vivo—an analysis based on cardiomyocyte nuclei. Cardiovascular Research *86*, 365-373.

Wang, J., Bo, H., Meng, X., Wu, Y., Bao, Y., and Li, Y. (2006a). A simple and fast experimental model of myocardial infarction in the mouse. Tex Heart Inst J *33*, 290-293.

Wang, X., Hu, Q., Nakamura, Y., Lee, J., Zhang, G., From, A.H., and Zhang, J. (2006b). The role of the sca-1+/CD31- cardiac progenitor cell population in postinfarction left ventricular remodeling. Stem cells *24*, 1779-1788.

Warejcka, D.J., Harvey, R., Taylor, B.J., Young, H.E., and Lucas, P.A. (1996). A Population of Cells Isolated from Rat Heart Capable of Differentiating into Several Mesodermal Phenotypes. J Surg Res *62*, 233-242.

Weber, K.T., and Brilla, C.G. (1991). Pathological hypertrophy and cardiac interstitium. Fibrosis and renin-angiotensin-aldosterone system. Circulation *83*, 1849-1865.

Weber, K.T., Janicki, J.S., Shroff, S.G., Pick, R., Chen, R.M., and Bashey, R.I. (1988). Collagen remodeling of the pressure-overloaded, hypertrophied nonhuman primate myocardium. Circ Res *62*, 757-765.

Weber, K.T., Pick, R., Jalil, J.E., Janicki, J.S., and Carroll, E.P. (1989). Patterns of myocardial fibrosis. J Mol Cell Cardiol *21 Suppl 5*, 121-131.

Weinberger, F., Mehrkens, D., Friedrich, F.W., Stubbendorff, M., Hua, X., Muller, J.C., Schrepfer, S., Evans, S., Carrier, L., and Eschenhagen, T. (2012). Localization of Islet-1-Positive Cells in the Healthy and Infarcted Adult Murine Heart. Circ Res.

Weissman, I.L., Anderson, D.J., and Gage, F. (2001). Stem and progenitor cells: origins, phenotypes, lineage commitments, and transdifferentiations. Annu Rev Cell Dev Biol *17*, 387-403.

Welm, B.E., Tepera, S.B., Venezia, T., Graubert, T.A., Rosen, J.M., and Goodell, M.A. (2002). Sca-1(pos) cells in the mouse mammary gland represent an enriched progenitor cell population. Dev Biol *245*, 42-56.

Wollert, K.C., and Drexler, H. (2010). Cell therapy for the treatment of coronary heart disease: a critical appraisal. Nat Rev Cardiol *7*, 204-215.

Wu, B., Baldwin, H.S., and Zhou, B. (2013). Nfatc1 directs the endocardial progenitor cells to make heart valve primordium. Trends Cardiovasc Med *23*, 294-300.

Wu, B., Wang, Y., Lui, W., Langworthy, M., Tompkins, K.L., Hatzopoulos, A.K., Baldwin, H.S., and Zhou, B. (2011). Nfatc1 coordinates valve endocardial cell lineage development required for heart valve formation. Circ Res *109*, 183-192.

Wu, M., Smith, C.L., Hall, J.A., Lee, I., Luby-Phelps, K., and Tallquist, M.D. (2010). Epicardial spindle orientation controls cell entry into the myocardium. Dev Cell *19*, 114-125.

Wu, Q., Merchant, F., and Castleman, K. (1996). Microscope Image Processing (USA: Elsevier).

Wu, S.M., Chien, K.R., and Mummery, C. (2008). Origins and fates of cardiovascular progenitor cells. Cell *132*, 537-543.

Wu, S.M., Fujiwara, Y., Cibulsky, S.M., Clapham, D.E., Lien, C.-l., Schultheiss, T.M., and Orkin, S.H. (2006). Developmental Origin of a Bipotential Myocardial and Smooth Muscle Cell Precursor in the Mammalian Heart. Cell *127*, 1137-1150.

Xin, L., Lawson, D.A., and Witte, O.N. (2005). The Sca-1 cell surface marker enriches for a prostate-regenerating cell subpopulation that can initiate prostate tumorigenesis. Proc Natl Acad Sci U S A *102*, 6942-6947.

Xin, M., Olson, E.N., and Bassel-Duby, R. (2013). Mending broken hearts: cardiac development as a basis for adult heart regeneration and repair. Nat Rev Mol Cell Biol.

Yamahara, K., Fukushima, S., Coppen, S.R., Felkin, L.E., Varela-Carver, A., Barton, P.J.R., Yacoub, M.H., and Suzuki, K. (2008). Heterogeneic nature of adult cardiac side population cells. Biochem Biophys Res Commun *371*, 615-620.

Yang, X., Pabon, L., and Murry, C.E. (2014). Engineering adolescence: maturation of human pluripotent stem cell-derived cardiomyocytes. Circ Res *114*, 511-523.

Yang, X.-P., Liu, Y.-H., Rhaleb, N.-E., Kurihara, N., Kim, H.E., and Carretero, O.A. (1999). Echocardiographic assessment of cardiac function in conscious and anesthetized mice. American Journal of Physiology - Heart and Circulatory Physiology *277*, H1967-H1974.

Yang, Z., Berr, S.S., Gilson, W.D., Toufektsian, M.-C., and French, B.A. (2004). Simultaneous Evaluation of Infarct Size and Cardiac Function in Intact Mice by Contrast-Enhanced Cardiac Magnetic Resonance Imaging Reveals Contractile Dysfunction in Noninfarcted Regions Early After Myocardial Infarction. Circulation *109*, 1161-1167.

Yano, T., Miura, T., Ikeda, Y., Matsuda, E., Saito, K., Miki, T., Kobayashi, H., Nishino, Y., Ohtani, S., and Shimamoto, K. (2005). Intracardiac fibroblasts, but not bone marrow derived cells, are the origin of myofibroblasts in myocardial infarct repair. Cardiovascular Pathology *14*, 241-246.

Ye, J., Boyle, A., Shih, H., Sievers, R.E., Zhang, Y., Prasad, M., Su, H., Zhou, Y., Grossman, W., Bernstein, H.S.*, et al.* (2012). Sca-1+ Cardiosphere-Derived Cells Are Enriched for Isl1-Expressing Cardiac Precursors and Improve Cardiac Function after Myocardial Injury. PLoS One *7*, e30329.

Yoon, Y.S., Wecker, A., Heyd, L., Park, J.S., Tkebuchava, T., Kusano, K., Hanley, A., Scadova, H., Qin, G., Cha, D.H.*, et al.* (2005). Clonally expanded novel multipotent stem cells from human bone marrow regenerate myocardium after myocardial infarction. J Clin Invest *115*, 326-338.

Zaffran, S., Kelly, R.G., Meilhac, S.M., Buckingham, M.E., and Brown, N.A. (2004). Right ventricular myocardium derives from the anterior heart field. Circ Res *95*, 261-268.

Zak, R. (1974). Development and proliferative capacity of cardiac muscle cells. Circ Res *35*, suppl II:17-26.

Zaragoza, C., Gomez-Guerrero, C., Martin-Ventura, J.L., Blanco-Colio, L., Lavin, B., Mallavia, B., Tarin, C., Mas, S., Ortiz, A., and Egido, J. (2011). Animal models of cardiovascular diseases. J Biomed Biotechnol, 497841.

Zhou, B., Honor, L.B., He, H., Ma, Q., Oh, J.H., Butterfield, C., Lin, R.Z., Melero-Martin, J.M., Dolmatova, E., Duffy, H.S.*, et al.* (2011). Adult mouse epicardium modulates myocardial injury by secreting paracrine factors. J Clin Invest *121*, 1894-1904.

Zhou, B., Ma, Q., Rajagopal, S., Wu, S.M., Domian, I., Rivera-Feliciano, J., Jiang, D., von Gise, A., Ikeda, S., Chien, K.R.*, et al.* (2008). Epicardial progenitors contribute to the cardiomyocyte lineage in the developing heart. Nature *454*, 109-113.

Zhou, H., Bian, Z.-Y., Zong, J., Deng, W., Yan, L., Shen, D.-F., Guo, H., Dai, J., Yuan, Y., Zhang, R.*, et al.* (2012). Stem Cell Antigen 1 Protects Against Cardiac Hypertrophy and Fibrosis After Pressure Overload. Hypertension *60*, 802-809.

Zornoff, L.A., Paiva, S.A., Minicucci, M.F., and Spadaro, J. (2009). Experimental myocardium infarction in rats: analysis of the model. Arq Bras Cardiol *93*, 434-440, 426-432.

APPENDIX I

SCA-1^{+} CARDIAC PROGENITOR CELLS AND HEART-MAKING: A CRITICAL SYNOPSIS

Sca-1^{+} Cardiac Progenitor Cells and Heart-Making: A Critical Synopsis

Mariana Valente[1,2,3], Diana Santos Nascimento[1], Ana Cumano[3], Perpétua Pinto-do-Ó[1,2]

[1]Stem-cell microenvironments in repair/regeneration Team, Microenvironments for NewTherapies Group, INEB - Instituto Nacional de Engenharia Biomédica, Universidade do Porto, Rua do Campo Alegre, n.º 823, 4150-180 Porto, Portugal.

[2]ICBAS - Instituto de Ciências Biomédicas Abel Salazar, Universidade do Porto, Rua de Jorge Viterbo Ferreira n.º 228, 4050-313 Porto, Portugal.

[3]Unité Lymphopoïèse, Département d'Immunologie, Institut Pasteur, 25 Rue du Docteur Roux, 75724 Paris Cedex 15, France.

Corresponding Author: Perpétua Pinto do Ó; INEB – Instituto de Engenharia Biomédica, Universidade do Porto, Rua do Campo Alegre, 823, P-4150-180 Porto, Portugal; email address: perpetua@ineb.up.pt; phone: +351 226 094 567; fax: +351 226 094 567.

Article published in **Stem Cells and Development**, 2014, 23(19):2263-2273.
DOI: 10.1089/scd.2014.0197

ABSTRACT

The identification, in the adult, of cardiomyocyte (CM) turnover events and of cardiac progenitor cells (CPCs) has revolutionized the field of cardiovascular medicine. However, the low rate of CPCs differentiation events reported both *in vitro* and *in vivo*, even after injury, raised concerns on the biological significance of these subsets. In this *Comprehensive Review*, we discuss the current understanding of cardiac Lin^{-}Sca-1^{+} cells in light of what is also known for cellular compartments with similar phenotypes in other organs.

HIGHLIGHTS

- The Lin^{-}Sca-1^{+} heart subset is heterogeneous and displays a mesenchymal profile, characterized by a limited ability to generate CMs *in vitro* and *in vivo*, even after injury.
- There is no evidence for Sca-1 expression in embryonic cardiovascular progenitors.
- In other organs, Sca-1 expression is mainly observed on mesoderm-derived cells, although it is not restricted to stem/progenitor cell populations.
- It is urgent to determine, at a single cell level, to which extent cardiac Lin^{-}Sca-1^{+} cells overlap with the fibroblast compartment.

INTRODUCTION

Cardiomyocyte (CM) replacement in the adult heart, via the expansion of pre- existing CMs and/or the differentiation of endogenous progenitors, has been extensively discussed (Hsieh et al., 2007; Senyo et al., 2013). The renewal rate and the physiologic conditions that trigger adult CM formation, and therefore its functional relevance, are not consensual.

The modest figures for human CMs renewal derived from the resourceful work by Bergman and colleagues, 1% *per annum* at the age of 25 and 0,45% at the age 75 (Bergmann et al., 2009), contrast with the much higher rates observed in a study enrolling patients submitted to radiotherapy (Kajstura et al., 2010). Likewise, mouse CMs turnover was estimated to reach values of approximately 1,3%-4% *per* year (Malliaras et al., 2013).

Recent groundbreaking experiments showed that a massive CMs loss, secondary to experimental heart injury (mechanical and ischemic), inflicted during the first 6 days of life is fully restored in a process that we would designate as myocardial re-genesis. However, starting at day 7 post-birth, this capacity is lost and, like in the adult heart, a fibrotic scar is formed (Porrello et al., 2011; Porrello et al., 2013). The loss of regenerative capacity coincides with post-natal maturation and cell-cycle arrest of CMs (Clubb and Bishop, 1984; Soonpaa et al., 1996), suggesting that the identification of the underlying regulators is crucial to unlock the boundaries of cardiac regeneration-repair mechanisms.

In the current state of knowledge it is possible that heart regeneration is more complex than the intrinsic (cell-autonomous) capacity of any cell subset to expand and/or differentiate into functional elements. The reciprocal modulation of cells and of the embedding extracellular matrix (ECM) might be a major process governing regeneration and/or repair of the damaged tissue, at different stages of post-natal life. Having said this, it should also be noted that the apparent loss of regenerative capacity in the adult heart cannot be used as an argument to contest the existence of adult CPCs, in the same manner that limited adult neurogenesis is not invoked to refute the recognized stem cell activity in some territories of the central nervous system (Goldman, 2005). What are then the major concerns in the stem cell biology field when discussing the properties of CPCs? What is the basis for the heated dispute concerning the nature and function of the adult CPCs?

This *Comprehensive Review* critically revisits several aspects of CPC's biology, debating in particular the CPC-subsets that express the stem cell associated-marker Stem Cell Antigen-1 (Sca-1). Sca-1$^+$ CPCs display a mesenchymal phenotype, have limited cardiogenic potential, and are able to improve cardiac remodelling following myocardial infarction (MI) mainly by paracrine mechanisms. The analysis of other organs containing mesodermal derivatives with similar phenotype (Lin$^-$Sca-1$^+$) highlighted the possible fibroblastic nature of this compartment and stressed the need to clarify the eventual overlapping of Sca-1$^+$ CPCs with other Lin$^-$Sca-1$^+$ stromal cells of the heart.

ABBREVIATIONS

cCFU – cardiac colony-forming units; CM – cardiomyocyte; CPC – cardiac progenitor cell; CS – cardiosphere; E – embryonic day; EC – endothelial cell; ECM – extracellular

matrix; EPDC – epicardial-derived cell; FHF – first heart field; HSC – hematopoietic stem cell; Lin – lineage; MI – myocardial infarction; MMP – metalloproteinase; P – postnatal day; SHF – second heart field; SMC – smooth muscle cell; SP – side population; Tβ4 – thymosin β4; 5-aza – 5-azacytidine.

1. How have heart resident stem/progenitor cells been defined?

The possibility that CMs can be generated outside the boundaries of the developing heart emerged back in the 1990's from the identification of interstitial cells displaying stem cell-like properties in adult mammalian heart (Warejcka et al., 1996). Since then, self-renewing, multipotent and clonogenic cardiac cells, capable of differentiation, *in vitro* and *in vivo*, into CMs and cells of the vasculature (endothelial (ECs) and smooth muscle cells (SMCs)), were reported by several authors and grouped under the designation of CPCs (Smith et al., 2007). CPCs have been isolated based on the expression of surface markers (*e.g.* Sca-1 and c-Kit), on functional properties, such as the ability to efflux dyes (*e.g.* rhodamine and Hoechst 33342) – side population (SP) (Hierlihy et al., 2002; Martin et al., 2004; Oyama et al., 2007; Pfister et al., 2005; Yamahara et al., 2008), and on the capacity to migrate out of cardiac explants and grow as 3D multicellular clusters – termed cardiospheres (CSs) (Messina et al., 2004; Ye et al., 2012).

The strategy to isolate CPCs by the expression of c-Kit (Beltrami et al., 2003; Gambini et al., 2011) and Sca-1 (Chong et al., 2011; Oh et al., 2003; Takamiya et al., 2011; Tateishi et al., 2007), two surface proteins also present on hematopoietic stem cells (HSC), coincided with claims that adult hematopoietic progenitors could, under certain conditions, generate cells affiliated with different tissues (neurons and muscle amongst others) (Balsam et al., 2004; Wagers and Weissman, 2004). Despite subsequent evidence that un-manipulated HSCs can only regenerate the hematopoietic system, the notion that c-Kit and Sca-1 could be useful markers to identify the adult stem/progenitor compartment in multiple tissues persisted in the scientific community.

In the heart, this strategy led to the identification of an apparent multiplicity of CPC subsets (Table 1). It is not clear whether these various CPC subsets represent distinct and perhaps transient physiological states of a single cell type or belong instead to unrelated lineages (Lyngbæk et al., 2007; Segers and Lee, 2008). The unknown developmental origin of CPCs has also entrenched doubts on whether they constitute remnants of *bona fide* embryonic cardiac progenitors (Bearzi et al., 2007; Eberhard and Jockusch, 2005; Ferreira-Martins et al., 2012), circulating cells from the bone marrow (Fazel et al., 2006; Orlic et al., 2001; Quaini et al., 2002), or simply derive from the surrounding vasculature (Dimmeler et al., 2005; Oh et al., 2003). The multipotency of CPCs has been also questioned because most reports rely on poorly-defined protocols of cardiomyogenic differentiation, *i.e.* cellular exposure to demethylating agents (Oh et al., 2003; van Vliet et al., 2008; Wang et al., 2006b) or co-culture with CMs (Freire et al., 2014a; Martin et al., 2004; Messina et al., 2004; Pfister et al., 2005; Wang et al., 2006b); and on a minimalistic verification of cell differentiation based on the up-regulated expression of a single lineage-affiliated, but not lineage-restricted, protein (Oh et al., 2003; Oyama et al., 2007; Reinecke et al., 2008; Takamiya et al., 2011; Tateishi et al., 2007). Additionally, CPCs on their own are clearly not able to functionally restore the heart in response to an extensive cardiac injury (Lyngbæk et al., 2007; Smith et al., 2007). Nevertheless, they have been viewed as the most promising target for cell-based therapies by authors who favour CPCs as innately prone to generate heart tissue and to respond to cardiac molecular cues (Gonzales and Pedrazzini, 2009). Based on this rationale, at least two clinical trials were established in which c-Kit-expressing cells (SCIPIO) (Bolli et al., 2011) and CS-derived Sca-1$^+$ cells (CADUCEUS) (Makkar et al., 2012) have been transplanted in an autologous setting. Short-term MRI assessment indicates reduction of scar size, increased healthy heart muscle mass and attenuated adverse remodelling.

Despite extensive reports on this particular topic, the existence of a prototypical stem/progenitor cell(s) entity in the adult mammalian myocardium is a concept that is far from being consensual.

Table1. Schematic representation of the heart as a mosaic of progenitor cell population identified in the myocardium (continuation). A variety of procedures have been adopted to isolate and purify a cardiac progenitor cells panoply, either based on the expression of the stemness-associated surface markers Sca-1 and c-Kit, the ability to efflux dyes (eg, rhodamine and Hoechst 33342)—SP, to grow as 3D multicellular clusters—CSs or by the expression of a specific genetic marker—Wt-1 epicardial progenitors**.** The isolated population have been subjected to phenotypic characterization and their multipotency, that is, the ability to differentiate in CMs, ECs, and SMCs, has been tested in vitro and/or in vivo, as well as the clonogenic potential. A concise summary of these results is displayed with indication of whether differentiation into a specific cell type was observed (+) in vitro and/or in vivo or if it was nd in the specific study.

Table 1. Schematic representation of the heart as a mosaic of progenitor cell population identified in the myocardium.

		In vitro differentiation			*In vivo* differentiation			Clonogenic
Ref.	**Phenotype**	**CM**	**EC**	**SMC**	**CM**	**EC**	**SMC**	
[25]	Sca-1$^+$ Ftl-1$^-$ Flk-1$^-$ CD31$^+$ CD34$^-$ CD45$^-$	4,6%	nd	nd	<1%$^{(a)}$	nd	nd	nd
[22]	Sca-1$^+$ c-Kit$^-$ CD34$^-$ CD31$^-$ CD45$^-$ CD90$^+$ CD105$^+$ CD29$^+$ CD44$^+$ CD106$^+$ CD73$^+$ CD13$^+$	1,24%	12,4%	31,9%	100$^{(b)}$	80$^{(b)}$	120$^{(b)}$	+
[23]	Sca-1$^+$ PDGFRα$^+$ CD31$^-$ CD45$^-$ CD90$^+$ CD105$^+$ CD29$^+$ CD44$^+$ Flk-1$^-$	+	+	+	+	+	+	+
[24]	Sca-1$^+$ c-Kit$^-$ CD34$^-$ CD31$^-$ CD45$^-$ CD29$^+$	<1%	~4,5%	~30%	+	+	nd	+
[39]	Sca-1$^+$ PDGFRα$^+$ CD44$^+$ CD105$^+$CD29$^+$ CD31$^-$ CD45$^-$ Flk-1$^-$c-Kit$^-$ CD34$^-$ CD31$^-$ CD45$^-$ CD90$^-$	+	~1,75%	~27%	~9$^{(c)}$	~4$^{(c)}$	~41$^{(c)}$	+
	Side population							
[13]	Sca-1$^+$ c-Kit$^-$ Flk-2$^-$ CD34$^-$ Thy1.1$^-$	nd	nd	nd	nd	nd	nd	+
[14]	Sca-1$^+$ Abcg2$^+$ c-Kit^{low} CD45^{low} CD34^{low} CD31$^-$	+	nd	nd	nd	nd	nd	nd
[15]	Sca-1$^+$ c-Kit$^-$ CD31$^-$ CD45$^-$ CD44$^-$ CD34$^-$	+	nd	nd	nd	nd	nd	+
[16]	CD29$^+$CD31$^{+/-}$ CD45$^{+/-}$	5,5%	nd	nd	4,4%	6,7%	29%	nd
[17]	Sca-1$^+$ VE-cadherin$^-$ CD34$^+$ CD73$^+$ CD90$^+$ CD105$^+$ CD45$^-$	+	nd	nd	nd	nd	nd	nd
	Epicardial-derived progenitors							
[92]	Sca-1$^+$ c-Kit$^-$ CD31$^-$ Flk-1$^-$	nd	nd	nd	+	nd	nd	nd
	Sphere formation (*cardiospheres*)							
[18]	Sca-1$^+$ c-Kit$^+$ CD31$^+$ CD34$^+$ Flk-1$^+$	+	+	+	+	+	+	+
[19]	Sca-1$^+$ c-Kit$^-$ CD31$^-$ CD34$^-$ CD45$^-$ CD29^{low} CD133$^-$ Flk-1$^-$	~60%	~20%	~34%	~10%	~10%	~10%	+
	c-Kit$^+$ cells							
[20]	c-Kit$^+$ CD45$^-$ CD34$^-$ CD20$^-$ CD45RO$^-$ CD8$^-$ Ter119$^-$	+	+	+	+	+	+	+
[21]	c-Kit$^+$ CD29$^+$ CD44$^+$ CD105$^+$ CD90$^+$	+	+	+	nd	nd	nd	nd

(a) Percentage of diffentiated myocytes; *(b)* Cells/mm^2; *(c)* Cells/heart section

Figure 1

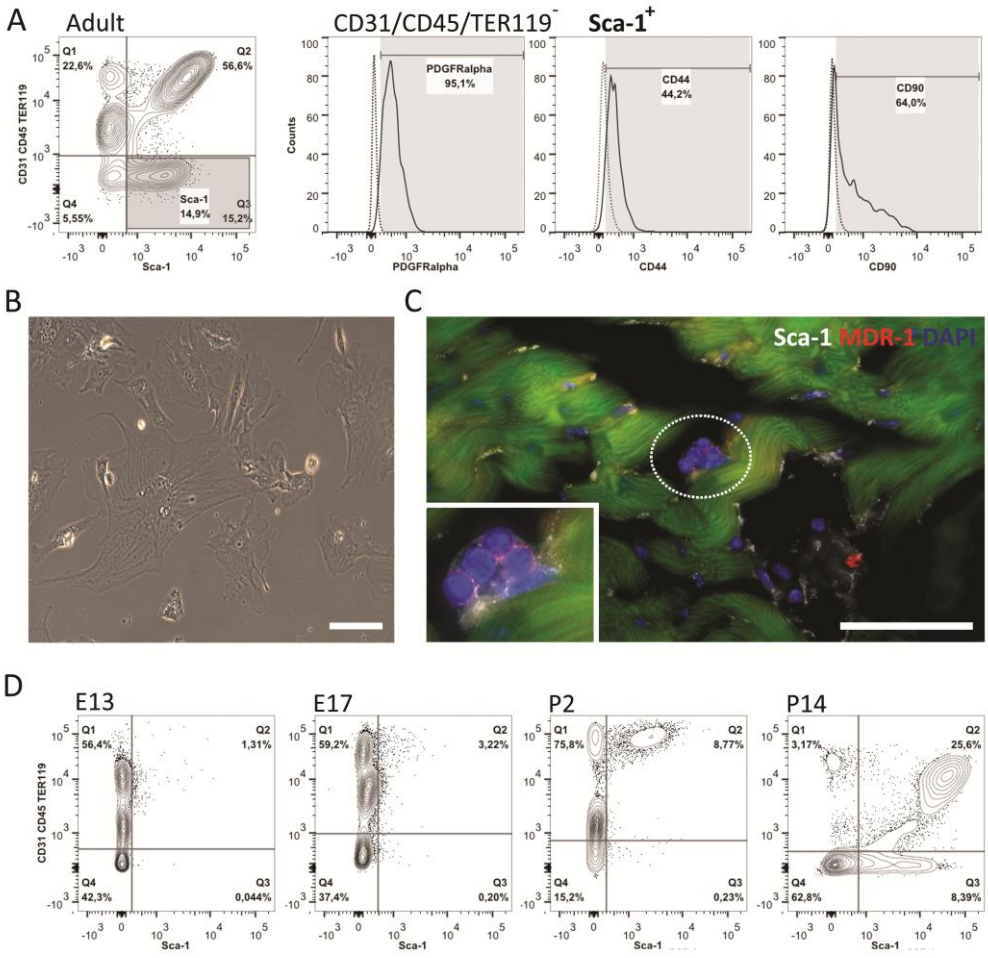

Figure 1. Heart resident Sca-1^{+} cells – an overview. Following collagenase digestion, the adult heart single cell suspension is depleted from CMs. Lin^{-} (CD31^{-}, CD45^{-}, TER119^{-}) cells constitute a minority of the Sca-1^{+} population within the heart (A) which is consistent with the reported expression of this marker also by mature EC. Lin^{-} Sca-1^{+} cells display mesenchymal-affiliated markers (PDGFRα, CD44 and CD90) and plastic-adherence (B). Scale bar 10 µm. Sca-1^{+} cells that do not integrate the vasculature are scattered in small clusters through the myocardium also displaying the SP-affiliated protein MDR-1 (C). Scale bar 50 µm. To address the ontogenic origin of the Sca-1^{+} population we are addressing the emergence of this population within the heart (D) by flow cytometry of whole-heart single cell suspensions. Lin^{-}Sca-1^{+} cells appear in the heart around E17 although the establishment of both Sca-1^{+}CD31^{+} and Sca-1^{+}CD31^{-} cellular compartments only occurs following birth.

2. What is known about the role and the cardiovascular potential of Sca-1$^+$ CPCs?

In the adult mouse, approximately 70% of heart cells express Sca-1 after depletion of CMs. The majority of these Sca-1$^+$ cells are ECs (Figure 1A), a finding common to other organs, such as the liver, the lung and the brain (Kang et al., 2010; Kotton et al., 2003; Luna et al., 2004; Tsuchiya et al., 2008; van de Rijn et al., 1989). Oh *et al.* first reported a population of Sca-1$^+$ cells from murine adult myocardium with telomerase activity analogous to that observed in newborn heart. This Sca-1$^+$ population was considered distinct from HSCs due to their lack of CD45, CD34, c-Kit, Lmo2, GATA-2 and Tal1/Scl proteins, and also distinct from endothelial progenitor/precursor cells since they do not express CD34, Flk-1 or Flt-1. Although transcripts for cardiomyocytic structural genes were absent, these Sca-1$^+$ cells expressed transcriptional regulators indicative of cardiac commitment, *e.g.* GATA-4, Mef2c and Tef1. Moreover, this population also exhibited the prototypical endothelial marker CD31, possibly due to the presence of contaminating endothelial CD31$^+$Sca-1$^+$ cells. Be that as it may, the Sca-1$^+$ cells were reported to differentiate in CMs, *in vitro* in response to the demethylating agent 5-azacytidine (5-aza), and *in vivo* following intravenous injection in a myocardial ischemia-reperfusion system (Oh et al., 2003).

Following Oh and colleagues, several other authors isolated and characterized heart-derived CPCs on the basis of Sca-1 expression (Table 1). These subsets lack expression of the endothelial- (CD31) and hematopoietic-affiliated (CD45) markers (hereafter referred as lineage negative (Lin$^-$)), display a mesenchymal cell-surface profile (CD34$^-$, CD29$^+$, CD90$^+$, CD105$^+$ and CD44$^+$) and were generally reported to be able to differentiate, to a certain extent, into CM-, endothelial- and smooth muscle-like cells (Chong et al., 2011; Freire et al., 2014a; Takamiya et al., 2011; Tateishi et al., 2007).

Although a human ortholog of the Sca-1 protein has not so far been identified, Sca-1$^+$-like cells have been isolated from the adult human heart using an anti-mouse Sca-1

antibody. Human Sca-1$^+$-like cells were shown to express early cardiac transcription factors (GATA-4, Mef2c, Isl-1 and Nkx-2.5) and to differentiate into contractile CMs. Notably, the authors reported that CM differentiation was more robust when cells were subjected to 5-aza pre-treatment (Smits et al., 2009c).

Cells with the capacity to extrude metabolic dyes through overproduction of ATP-binding cassette transporters (*e.g.* Abcg2 and MDR-1), called SP, were described in several organs as being able to undergo tissue-specific differentiation (Asakura et al., 2002). Different authors identified SP cells (Challen and Little, 2006; Martin et al., 2004; Pfister et al., 2005; Smith et al., 2007) expressing Sca-1 (93,3%) and lacking c-Kit (Oh et al., 2004) in the heart (Table 1). The cardiac SP was shown to be heterogeneous and composed of ECs, SMCs and a mesenchymal stromal cell-fraction. Thus, similarly to the results obtained using Sca-1$^+$ cells, the vast majority of the Sca-1$^+$ cardiac SP were described as being endothelium-affiliated, while the cardiomyogenic potential appeared restricted to the Lin$^-$ mesenchymal subset (Pfister et al., 2005; Yamahara et al., 2008).

Additionally, isolation and *ex vivo* expansion of CPCs also revealed the ability of progenitor cells to form spheres, designated as CSs. CSs are characterized by a mixed population growing *in vitro* as 3D clusters, containing Sca-1$^+$ CPCs that are either c-Kit$^+$ (Messina et al., 2004) or c-Kit$^-$ (Ye et al., 2012), and spontaneously differentiating into CM- and vascular-like cells, depending on the size of the sphere and on the length of time in culture (Table 1). This specific isolation protocol has the advantage of allowing substantial *in vitro* cell expansion, a critical requirement to obtain enough cells for therapeutic use (Messina et al., 2004).

A number of experimental animal systems were used to address Sca-1 function in the heart. Recently, Sca-1 reporter and Sca-1 lineage tracer mouse models were used to investigate the contribution of Sca-1 expressing cells to the adult myocardium. Sca-1 expression was not detected in adult CMs, in healthy or injured heart. However, the descendants of Sca-1$^+$ cells appeared to contribute to the CM compartment. This work

provides evidence for a low but continuous replacement of Sca-1-derived CMs in aging hearts (0,17±0,06 cells/mm^2, 8 months-old) and after MI (0,24±0,04 cells/mm^2, 8 months-old) (Uchida et al., 2013). Nevertheless, the low frequency of Sca-1 traced cells (a maximum of 4,5% of CMs) indicates that most CMs derive from Sca-1$^-$ progenitors. This observation, together with the data indicating that before 2 months of life Sca-1 derived CMs are virtually undetectable, is compatible with the existence of two distinct CM progenitors: one that generates most CMs during foetal life and another that generates the small number of new CMs detected in adult heart (Uchida et al., 2013). Alternatively, a few persisting CM progenitors acquire Sca-1 expression after birth. Irrespective of their origin, the adult Sca-1$^+$ CM progenitors did not significantly contribute to myocardial regeneration in the injured heart.

Although the role of Sca-1 in heart repair is still elusive, different models of Sca-1 KO mice consistently reported age-related cardiac hypertrophy and impaired response to damage. Less clear is the role of Sca-1 in the CPCs compartment, owing to the opposing effects on proliferation/differentiation of these cell subsets that have been claimed (Bailey et al., 2012; Rosenblatt-Velin et al., 2012; Zhou et al., 2012). Nevertheless, a subset of myocardium-resident Sca-1$^+$CD31$^-$ cells was shown to exhibit significant proliferation at 7 days post-MI. While the proliferative response of the endogenous Sca-1$^+$CD31$^-$ appears insufficient to prevent adverse MI remodelling, this process is attenuated, with preservation of the left ventricle contractile performance and improvement of bioenergetic properties, when Sca-1$^+$ cells are expanded *ex vivo* prior to transplantation into the injured myocardium (Wang et al., 2006b). Furthermore, transplantation of clonally expanded Sca-1$^+$ cell sheets, *i.e.* spontaneously detached monolayer cell grafts, improved cardiac function and attenuated cardiac remodelling following MI. Donor-derived Sca-1$^+$ cells differentiated in CM- and endothelial-like cells and secreted a battery of cytokines and growth factors, including soluble VCAM-1 (CD106), which in its turn promoted angiogenesis, cardioprotection, and CPC migration/survival via VLA-4 binding (Matsuura et al., 2009). The role of the Sca-1$^+$

CPCs secretome in improving cardiac repair at the onset of MI has been emphasized in a series of *in vitro* and *in vivo* studies (Freire et al., 2014a; Huang et al., 2011; Maxeiner et al., 2010; Ryzhov et al., 2012). In 2012, Ryzhov and colleagues showed that the accumulation of adenosine in the injured myocardium might activate Sca-1$^+$CD31$^-$ cells. These cells exhibit high adenosine receptor density at their surface and secrete pro-angiogenic factors such as VEGF, CXCL1 and IL-6 via adenosine-dependent activation. At the present time, the beneficial effect of most cell-based therapies for cardiac repair has been assigned to paracrine effects, irrespectively of the cell origin. The reported mechanisms encompass a decrease in hypoxia-induced apoptosis, increase of CMs proliferation, enhancement of neovascularization, restraining of the granulation and scar tissue formation and recruitment of endogenous progenitor cells (reviewed in (Burchfield and Dimmeler, 2008; Gnecchi et al., 2008)). Further work is needed to address whether the secretome of CPCs outperform that of, for instance, mesenchymal stem/stromal cells of extra-cardiac origin. It is also conceivable that growth factors and cytokines produced by transplanted cells in general might play a role in the proliferation, mobilization, differentiation and/or survival of endogenous CPCs. We have recently demonstrated that non-cardiac Wharton's jelly mesenchymal stem/stromal cells are able to stimulate Sca-1$^+$ CPCs proliferation and to activate a cardiomyogenic program through secreted factors (Nascimento et al., 2014). Comprehensive investigations are also lacking on the ability of Sca-1$^+$ CPCs to modulate their nesting microenvironment. On this point, there are indications that CPCs produce fibronectin as well as collagens I, III and IV, and also matrix metalloproteinases (MMPs) and their inhibitors (Bax et al., 2012). The production of ECM and remodelling proteins was further enhanced following stimulation with TGF-β1 (Smits et al., 2009c), which is commonly used to stimulate CM differentiation by CPCs. Remarkably, this cytokine is also a known myofibroblast activator (Thannickal et al., 2003).

In summary, different Sca-1$^+$ cell subsets have been identified by using a set of cell

surface markers and/or based on functional properties, resulting in the isolation of diverse collections of Sca-1$^+$ cells, which are difficult to directly compare. As mentioned previously, this is a recurrent problem in the field of CPCs. The common characteristics of Sca-1$^+$ CPCs are: (i) CPCs belong to the CD31$^-$CD45$^-$ compartment; (ii) CPCs display mesenchymal affiliated markers (Figure 1A and B); and/or (iii) express proteins whose function is to extrude metabolic dyes (Figure 1C). Significantly, the cardiomyocytic differentiation of CPCs *in vitro* has been generally evaluated by methods that, when used separately, are insufficient to assign a cell to the CM pool, *e.g.* immunofluorescence, qPCR and calcium transient analysis. Nevertheless, it is clear that the cardiogenic potential of heart resident Sca-1$^+$ CPCs is either limited or masked by the heterogeneous nature of the isolated subsets (Table 1). Alternatively, the low cardiogenic potential of this population simply reflects the absence of appropriate *in vitro* culture conditions (Forte et al., 2008; Mosqueira et al., 2014). Also *in vivo* Sca-1$^+$ CPCs exhibit a low capacity for *de novo* CMs generation, even following injury (Uchida et al., 2013). Likewise, the collective results obtained in the Sca-1$^+$ transplantation experiments, during the initial phases of MI, appear to be a modest replacement of ischemic tissue by newly formed CMs (Freire et al., 2014a; Oh et al., 2003; Takamiya et al., 2011). Additionally, their capacity to differentiate into cells with SMC-like phenotype has been frequently reported as being more efficient than that of ECs and CMs (Table 1 (Freire et al., 2014a; Oh et al., 2003; Oyama et al., 2007; Takamiya et al., 2011; Tateishi et al., 2007)). Of note, some of the proteins used to identify SMC differentiation (*e.g.* Smooth Muscle Actin, Calponin and SM22) are also expressed by myofibroblasts, and thus further discrimination is required to precisely assess whether Sca-1$^+$ CPCs undergo SMC differentiation or acquire a fibroblasts/myofibroblast phenotype.

At this point, it appears too speculative to assume that Sca-1$^+$ CPCs are a source for CMs, ECs and SMCs either in the steady state or following injury.

3. Is there a correlation of Sca-1 expression and the distinct cardiac cell-types emerging during embryonic development?

The identification of the embryonic origin of the cell subsets that make the heart will certainly provide us with knowledge of potential biomedical impact. After the isolation of putative CPCs from the adult heart it was imperative to enquire their origin and how they correlate with other already known players in cardiogenesis. Thus, we will briefly revisit heart development, with the aim of contextualizing a few pertinent findings.

The heart is essentially a mesodermal organ. During embryonic morphogenesis the heart progenitors shape a horseshoe-like structure, the cardiac crescent, which progresses to the linear heart tube, elongates and loops rightward until it reaches the complex four-chambered heart structure. The heart tube starts beating at around embryonic day (E)8.0 (Navaratnam et al., 1986), while the organ is still under construction.

The first and second heart fields (FHF and SHF, respectively) originate sequentially from early mesodermal progenitors. Current knowledge in cardiovascular development supports the divergence of CM-, SMC- and EC-lineages from a common progenitor (Kattman et al., 2007; Moretti et al., 2006). At the onset of the cardiac program, around E7.5, the FHF progenitors colonize the cardiac crescent and immediately differentiate into CMs (Kattman et al., 2007; Prall et al., 2007). These primitive CMs are functional, express sarcomeric proteins (Nishii and Shibata, 2006; Sassoon et al., 1988) and later contribute to the formation of the left ventricle (Kubalak et al., 1994; Lints et al., 1993). SHF multipotent cells migrate to both poles of the heart tube, express Isl-1, Nkx-2.5 and Flk-1 and are able to give rise both to CMs and vascular cells (ECs and SMCs) (Bu et al., 2009; Moretti et al., 2006). This population contributes to the majority of the right ventricle, atria (left and right) and the outflow tract (Cai et al., 2003; Kelly et al., 2001).

The myocardium of the looped tube (E9.5-11.5) is highly regionalized and the length and thickness of the wall-tissue increases dramatically, by expansion and migration of

progenitor cells as well as proliferation of CMs (de Boer et al., 2012). What will become the heart chambers suffer a balloon-like growth through the proliferation of CMs, particularly from the compact layer. In contrast, the inner myocardial layer is trabecular, more differentiated, and displays a lower mitotic rate (de Boer et al., 2012; Moorman and Christoffels, 2003; Sedmera et al., 2003). Noteworthy, E9.5 is the later-stage at which a progenitor, originated from cardiogenic mesoderm, was isolated. These cells are bipotent, express Nkx-2.5 and show spontaneous differentiation into CM- and SMC-like cells, suggesting that they are more committed to a muscle fate. Nkx-2.5^{+} progenitors display modest levels of the c-Kit and Sca-1, surface-markers used to isolate adult CPCs; however, attempts to clonally expand these cells were unsuccessful (Wu et al., 2006).

Although the myocardium is the most relevant tissue for heart pumping function, the survival and proper functional maturation of developing CMs would be compromised without signals emanating from both the endocardium (specialized vascular endothelium) (Bersell et al., 2009) and the epicardium (epithelial layer that covers the myocardium) (Dettman et al., 1998; Manasek, 1969; Vincent and Buckingham, 2010). Indeed, both non-myocardial layers are crucial, contributing with new cell subsets and soluble signals that modulate the progress of myocardial histogenesis (Rosenthal and Harvey, 2010). However, as the myocardium becomes thicker, it is unlikely that the signals from both layers can reach all myocardial cells. The epicardial cells arise around E10.5 from a cluster of cells, the proepicardial organ, which are recognized by Tbx18 (Cai et al., 2008) and Wt-1 expression (Zhou et al., 2008). After wrapping the myocardial layer, epicardial cells undergo epithelial to mesenchymal transition and contribute to the EPDCs that migrate and colonize the muscle wall. EPDCs give rise to cells of myocardial stroma, *i.e.* fibroblasts, pericytes and coronary vasculature cells (SMCs and ECs) (Dettman et al., 1998; Ieda et al., 2009); contributing also to the production of ECM components that create the propitious environment for maturation of the late-foetal heart (Ieda et al., 2009). Irrespective of the well-established

contribution of the epicardium to the stromal heart fraction, signs of epicardial-derived CM differentiation have also been reported (Cai et al., 2008; Zhou et al., 2008).

The ontogenic origin of Sca-1$^+$ CPCs remains largely unknown although is currently under scrutiny by several laboratories, including our own (unpublished work), and conjectures in the field stem from the so far slim body of data available (Chong et al., 2011; Wu et al., 2008).

Smart and colleagues showed that a progenitor population resident in the adult heart can be activated with thymosin β4 (Tβ4) to re-express the embryonic epicardial gene Wt-1. The Wt-1$^+$ cell subset expresses Sca-1 (80%) and, when treated with Tβ4 prior to injury, a small fraction of the Tβ4-primed cells (~0,59±0,18%) displays a CM phenotype 14 days post-MI. Of note, *de novo* CMs formation is only observed if the injury is inflicted after Tβ4 priming. Conversely, Tβ4 pre-treatment in otherwise healthy hearts appears to lead to an increase in the frequency of Isl1$^+$ cells at the subepicardial zone (Smart et al., 2011). Less exciting, from the therapeutic viewpoint, is that Tβ4 administration following MI is not seen to either mobilize or differentiate the EPDCs (Zhou et al., 2012). Although the authors were unable to unequivocally disregard a non-epicardial source for the Tβ4-primed Wt-1$^+$ progenitors, the evident restriction of Wt1 expression in the epicardium and subepicardial region is indicative of an EPDC origin. Harvey and colleagues tracked-back to an epicardial origin the PDGFRα$^+$Sca-1$^+$ population of multipotent cells with colony-forming units (cCFU) properties (adherent, clonogenic and non-phagocytic) (Chong et al., 2011; Chong et al., 2013). While adult cCFU appear to be confined to the PDGFRα$^+$Sca-1$^+$ subset, it is of interest that the authors based the genetic tracing analysis solely in PDGFRα given that Sca-1 expression is not detected in the heart before mid-gestation. This is in agreement with our data when analysing cardiac cell-populations from E13.5, all through post-natal day (P)2, P14 and adult hearts; Sca-1 cells appears late in cardiac development (from E17.5 onwards), and both CD31$^+$Sca-1$^+$ and CD31$^-$Sca-1$^+$ subsets increase in frequency after birth (Figure 1A and D). Therefore, a prominent role for a CPC subset,

in this case Sca-1$^+$ CPCs, which emerges after the establishment of the four-chambered heart, is difficult to substantiate. Here again, it is formally possible that an embryonic cardiovascular progenitor acquires Sca-1 expression only after birth to lose it again as it differentiates (discussed in section 2.). We find this possibility worth considering but unlikely.

4. Is Sca-1 a pan-marker for stem/progenitor cell activity in mesodermal derivatives?

Sca-1, or lymphocyte activation protein-6A (Ly-6A) belongs to Ly6 gene family and is a glycosyl phosphatidylinositol-anchored cell surface protein (GPI-AP). Sca-1 was first reported as a cell surface marker of HSCs and, in combination with c-kit, allows the definition of a population that contains the vast majority of HSCs, although they are still present at low frequency (around 10%) (Holmes and Stanford, 2007; van de Rijn et al., 1989). It has also been claimed that Sca-1 is expressed by the progenitor compartment of a number of other tissues, such as the skeletal muscle (Asakura et al., 2002; Holmes and Stanford, 2007), mammary gland (Holmes and Stanford, 2007; Welm et al., 2002), kidney (Dekel et al., 2006; Holmes and Stanford, 2007), liver (Clayton and Forbes, 2009) and prostate (Holmes and Stanford, 2007; Xin et al., 2005). While some of these reports are not consensually accepted, others remain unchallenged. It should also be kept in mind that protocols used to identify progenitors frequently rely on a previous period of cell expansion *in vitro*. In culture, cell expansion might result in a population that is not representative of the cell input and cells can also acquire new surface markers due to differentiation or stress in the culture. Therefore, conclusions based on the analysis of cells after culture, rather than on their isolation *ex vivo*, should be critically evaluated.

Additionally, Sca-1 expression has been observed in the resident fibroblast population of several organs. In the skin, Sca-1$^+$ fibroblasts are restricted to the hypodermal lineage (Sca-1$^+$PDGFRα$^+$Dlk1$^{+/-}$), display adipogenic potential and are of mesenchymal

origin. After injury, these cells participate in the first wave of dermal regeneration, characterized by the production of high levels of collagenous-based ECM (Driskell et al., 2013). In the lung, Lin^{-}Sca-1^{+} cells appear to be highly enriched in fibroblast progenitors located in perivascular areas. The latter population expands post-birth and co-express markers typical of mesenchymal affiliation, *i.e.* CD34, PDGFRα and CD90 (McQualter et al., 2009). Furthermore, after an injury stimulus, lung fibroblasts (Sca-1^{high}) can differentiate into myofibroblasts (Sca-1^{low}) and increase the ECM production towards a more efficient repair process (Akamatsu et al., 2013).

Nevertheless, and surprisingly in view of the *quasi* ubiquitous expression of this protein (present in a wide array of cells, including mature types and distinct stem/progenitor cell systems), the mechanisms and signalling pathways through which Sca-1 acts remain unclear. Sca-1 protein regulates and activates cell signalling via receptor-ligand binding and protein-protein interactions, playing a role in cell adhesion in the hematopoietic system (Holmes and Stanford, 2007). It has been reported to play a part in the self-renewal of hematopoietic and mesenchymal progenitors (Holmes and Stanford, 2007; Ito et al., 2003; Welm et al., 2002) and, in skeletal muscle, Sca-1^{+} cells were shown to up-regulate directly or indirectly the activity of MMPs, thereby promoting breakdown of the ECM and thus supporting muscle regeneration (Kafadar et al., 2009). To the best of our knowledge, all revised Sca-1 cell subsets are indicative of a mesodermal origin, even considering organs from distinct germ layers, *e.g.* ectoderm (skin) and endoderm (lung). Thus, the answer to the original question is that, while Sca-1 expression is confined to mesoderm-derivatives it is not restricted to a stem/progenitor compartment.

5. Does the Lin^{-}Sca-1^{+} population in the heart overlap with fibroblasts?

The adult cardiac tissue is composed of a syncytial network of CMs and of a non-cardiomyocytic fraction, in which fibroblasts are a major constituent. Fibroblasts are recognized mediators of the heart repair response to MI and to other pathological

conditions. Several other functions have also been attributed to cardiac fibroblasts, including (i) production of mitogenic stimuli during heart development, (ii) secretion of growth factors, ECM and ECM-remodelling proteins throughout life, and (iii) electrical coupling with CMs (Lajiness and Conway, 2013). Despite all this, it is still difficult to define a "fibroblast" mainly because the designation is given to a heterogeneous population (Chang et al., 2002) with a largely undefined molecular signature. While a definitive lineage marker is not established, cardiac fibroblasts are commonly identified by the expression of DDR-2, Fsp-1, PDGFRα, Periostin, CD90, and Vimentin (Lajiness and Conway, 2013).

Lin$^-$Sca-1$^+$ cells in different organs seem to overlap with the population of tissue-resident fibroblasts (Akamatsu et al., 2013; Driskell et al., 2013; McQualter et al., 2009). In the heart, Sca-1 expression has not been ascribed to a population of cardiac fibroblasts, although the evidence is that Sca-1-expressing cells are present in the myocardial interstitium. What are then the similarities between cardiac Lin$^-$Sca-1$^+$ cells and fibroblasts? Similarly to fibroblasts, Lin$^-$Sca-1$^+$ heart cells (i) display the typical mesenchymal proteins PDGFRα, CD90, CD44 and CD105 (Chong et al., 2011; Freire et al., 2014a; Tateishi et al., 2007); (ii) appear to be more prone to differentiate in smooth muscle actin-expressing cells (Freire et al., 2014a; Oyama et al., 2007; Tateishi et al., 2007); (iii) augment the production of ECM and MMPs following TGF-β stimulation (Thannickal et al., 2003); (iv) appear to derive from the epicardium late in development, although the population expands mainly after birth (Chong et al., 2011); and (v) play an important role in heart repair mainly by paracrine and pro-angiogenic actions (Matsuura et al., 2009; Wang et al., 2006a). Thus, it is tempting to postulate that Lin$^-$Sca-1$^+$ heart cells constitute/generate stromal cell producers of ECM and, importantly, are the main responders following tissue injury. Indeed, this hypothesis has recently been put forward together with the suggestion that cardiac-resident Sca-1$^+$PDGFRα$^+$ mesenchymal progenitors, as defined by Chong and colleagues (Chong et

al., 2011), could be a source for fibroblasts and adipocytes, characteristic of a fibro-fatty heart condition (Paylor et al., 2013).

Of note, and because of the clear heterogeneity of the heart Lin$^-$Sca-1$^+$ compartment, it is conceivable that several functionally distinct fractions may be present in this population. The latter may possibly embrace a smaller subset of CPCs that are actually responsible for the multipotent phenotype described by many authors (Chong et al., 2011; Freire et al., 2014a; Oh et al., 2003; Takamiya et al., 2011; Tateishi et al., 2007). In our view, a direct comparison between heart-derived Lin$^-$Sca-1$^+$ cells and fibroblasts, at the single cell level, is urgently needed, in order to establish the functional and phenotypic differences, if they exist, of these populations *in vitro* and *in vivo.*

CONCLUSION

The urge to manage the burden of an escalating number of severe cardiovascular disorders led to the premature therapeutic use of CPCs. CPC-based therapy was initiated even before a consensus was reached in the scientific community to the function of CPCs in the healthy and diseased heart.

The cardiac Lin$^-$Sca-1$^+$ compartment, which has been considered as a multipotent population of CPCs (capable of differentiating in CMs, ECs and SMCs *in vitro* and *in vivo),* is heterogeneous and displays some characteristics commonly associated with fibroblasts. A combination of reporter and lineage-tracer animal models recently demonstrated Sca-1 contribution to the low, but continuous, myocardial turnover during adulthood and after injury. This work supports the potential of Sca-1-expressing cells in heart regeneration. Thus, it is of major importance to study the differences that may exist between Sca-1$^+$ CPCs and other Lin$^-$Sca-1$^+$ stromal cells of the heart. This will be only possible with a detailed characterization (at the single cell level) of Lin$^-$Sca-1$^+$

heart-resident cells, combined with robust clonal assays to test stem cell activity, both *in vitro* and *in vivo*.

ACKNOWLEDGMENTS

This work was supported by Fundação para a Ciência e a Tecnologia [SFRH/BD/74218/2010 to M.V., [SFRH/BPD/42254/2007] and QREN/ON.2 [NORTE-07-0124-FEDER-000005] to D.S.N., and Fundo Europeu de Desenvolvimento Regional, Programa Operacional Factores de Competitividade-COMPETE, Quadro de Referência Estratégico Nacional, Fundo Social Europeu [PEst-C/SAU/LA0002/2013, PTDC/SAU-ORG/118297/2010 and NORTE-07-0124-FEDER-000005]. By the Pasteur Institute, INSERM, ANR through a grant “Lymphopoiesis” and through the REVIVE Future Investment Program, La Ligue contre le Cancer with grants to AC. The authors are thankful to Dr. Tatiana P. Resende for critical discussion during the manuscript preparation and to Dr. Paulo Vieira for the fine editing work.

Author Disclosure Statement

No competing financial interests exist.

REFERENCES

Please see references at *REFERENCES Chapter*.

APPENDIX II

OPTIMIZED HEART SAMPLING AND SYSTEMATIC EVALUATION OF CARDIAC THERAPIES IN MOUSE MODELS OF ISCHEMIC INJURY: ASSESSMENT OF CARDIAC REMODELING AND SEMI- AUTOMATED QUANTIFICATION OF MYOCARDIAL INFARCT SIZE

Optimized heart sampling and systematic evaluation of cardiac therapies in mouse models of ischemic injury: assessment of cardiac remodeling and semi-automated quantification of myocardial infarct size

Mariana Valente[1,2,3,4], Ana Araújo[1,2], Tiago Esteves[1,2,5], Tiago L. Laundos[1,2], Ana G. Freire[1,2,5,6], Pedro Quelhas[1,2,5], Perpétua Pinto-do-Ó[1,2,3,4,*] and Diana S. Nascimento[1,2,*,§]

[1]INEB – Instituto de Engenharia Biomédica, Universidade do Porto, Porto, Portugal.

[2]Instituto de Investigação e Inovação em Saúde, Universidade do Porto, Portugal.

[3]ICBAS – Instituto de Ciências Biomédicas Abel Salazar, Universidade do Porto, Porto, Portugal.

[4]Unit for Lymphopoiesis, Immunology Department, INSERM U668, University Paris Diderot, Sorbonne Paris Cité, Cellule Pasteur, Institut Pasteur, Paris, France.

[5]FEUP – Faculdade de Engenharia da Universidade do Porto, Universidade do Porto, Porto, Portugal.

[6]Department of Developmental and Regenerative Biology and The Black Family Stem Cell Institute, Icahn School of Medicine at Mount Sinai, New York, USA.

*Equally contributing authors.

[§]Corresponding Author: Diana S. Nascimento; INEB – Instituto de Engenharia Biomédica, Universidade do Porto, Rua do Campo Alegre, 823, 4150-180 Porto, Portugal; Tel.: +351 226074900; Fax: +351 226094567.

In Press in **Current Protocols in Mouse Biology**, 2015, 5(4).

ABSTRACT

Cardiac therapies are commonly tested pre-clinically in small animal models of myocardial infarction. Following functional evaluation, *post-mortem* histological analysis is essential to assess morphological and molecular alterations underlying the treatment's effectiveness. However, non-methodical and inadequate sampling of the left ventricle often leads to misinterpretations and variability making direct study comparisons untrustworthy. Herein, this *Unit* details protocols for representative sampling of the ischemic mouse heart followed by morphometric analysis of the left ventricle. Extending the use of this sampling to other types of *in situ* analysis is also illustrated through the assessment of neovascularization and cellular engraftment in a cell-based therapy setting. This is of interest to the general cardiovascular research community as it details methods for standardization and simplification of histo-morphometric evaluation of emergent heart therapies.

Keywords: Mouse-models of myocardial infarction; Systematic evaluation of cardiac therapies; Representative heart sampling; Quantification of infarct size; Software *MIQuant*.

INTRODUCTION

For many years, coronary artery diseases have been regarded as the most prominent cause of mortality and morbidity worldwide. Despite available pharmacological and device-based therapies, prognosis remains poor. Currently, the only efficient long-term treatment is through heart transplantation, yet is mainly impaired by organ shortage and immunosuppression requirements (Hertz et al., 2010). Consequently, new therapeutic approaches aimed at more efficient repair and/or functional myocardial restoration are needed, and the *in vivo* potential of these novel therapies for myocardial infarction (MI) is first assessed in mouse models (Ahmed et al., 2010; Bolli et al., 2011; Gonzales and Pedrazzini, 2009; Makkar et al., 2012; Ramani et al., 2011; Smits et al., 2009b; Takagawa et al., 2007; Yoon et al., 2005).

In humans as well as in rodents, cardiac remodeling after an ischemic injury is a dynamic and time-dependent process that affects the necrotic, as well as adjacent, myocardial regions. Cardiac remodeling is initiated with an inflammatory response. Granulation tissue is then formed and replaced with non-functional fibrotic tissue (Virag and Murry, 2003). This collagen-rich scar is evident at 14 days postMI and thus collagen deposition can be quantified from this time-point onwards (Nascimento et al., 2011). MI size, the percentage of the left ventricle (LV) wall affected by collagen deposition, is a predictor of long-term LV function and geometry and is a major end-point in clinical trials of cardio-protective therapies (Csonka et al., 2010; Nascimento et al., 2011; Takagawa et al., 2007). In experimental MI models, measurement of the infarct size is fundamental and is generally combined with morphometric analysis of the

LV (*i.e.* wall thinning and chamber dilation) as well as with functional assays to evaluate the deleterious consequences of MI. Despite the widespread use of the aforementioned methods, the final infarct size value is highly dependent on the methodology used (Csonka et al., 2010; Takagawa et al., 2007; Zornoff et al., 2009). Moreover, several technical aspects that directly impact the reported infarct size are commonly not described by the authors or are inconsistent across studies (Csonka et al., 2010; Takagawa et al., 2007; Zornoff et al., 2009), and therefore no direct comparison can be withdrawn between laboratories.

Herein, we provide a fully detailed protocol for representative sampling of the ischemic mouse heart followed by LV morphometric analysis and infarct size quantification either manually or assisted by the freeware *MIQuant*. Extending the use of this sampling to a larger repertoire of *in situ* analytical methods will be demonstrated with the assessment of neovascularization and cellular engraftment in the setting of cell-based therapies (Fig. 1, see Support Protocol 1 and 2).

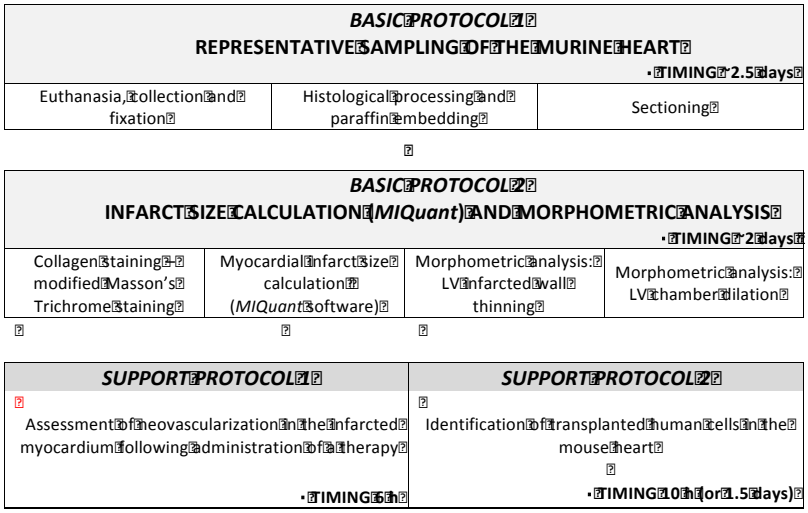

Figure 1 Flowchart outlining the timeline of the described experimental procedures.

NOTE: All protocols using live animals must first be reviewed and licensed by an Institutional Animal Care and Use Committee (IACUC) and conform to national or institutional guidelines.

BASIC PROTOCOL 1

REPRESENTATIVE SAMPLING OF THE MURINE HEART

Following functional evaluation, histological analysis is essential to assess morphological and molecular alterations relating to the treatment's effectiveness. At least seven histological sections obtained from different regions of LV were required for an accurate representation of the chamber, because the collagen deposition and cardiac remodeling (*e.g.* aneurysm formation) regionally and heterogeneously affect the ventricular wall (Takagawa et al., 2007). Additionally, the coronary artery ligation model results in a diverse range of infarct sizes and scar distribution owing to different branching patterns observed even between syngeneic animals (Ahn et al., 2004). Despite these variables, *in situ* analysis of the heart is frequently reported on the basis of only one single tissue section of the papillary muscle, and is assumed to be an accurate representation. Thus, a correct representation of the different anatomical regions of LV, prior to the quantification of parameters to estimate the entire chamber, is clearly needed.

In Basic Protocol 1, we have combined stepwise guidelines for the fixation and histological processing of whole mouse hearts that are suitable for both histochemical

analysis (*i.e.* Masson's Trichrome staining) and detection of proteins (immunostaining, see Support Protocol 1 and 2). With regards to heart sampling, we describe a robust methodology that represents different LV regions essential for accurate infarct size calculation and suitable for subsequent biochemical analysis (Fig. 1).

Materials

Samples

NOTE: All protocols using live animals must first be reviewed and licensed by an Institutional Animal Care and Use Committee (IACUC) and conform to national or institutional guidelines for the care and use of animals, that cover the research

Young adult (8-12 weeks old) C57BL/6 mice (*Mus musculus*) sacrificed at 14 days post-MI (Virag and Murry, 2003).

Solutions

CAUTION: Take care as most of the solutions used on Basic Protocol 1 are inflammable and harmful by inhalation and/or skin contact. Always be acquainted with the hazards of the reagents PRIOR to their usage. Work in a safety biohazard hood and wear gloves and protective eyewear.

Pentobarbital, 400 mg kg^{-1}

99.8% (v/v) Ethanol (see recipe)

4M KCl (Potassium Chloride, see recipe)

PBS (Phosphate-Buffered Saline)

10% (v/v) Neutral Buffered Formalin pH 7.0 at 25 ºC

Clear-Rite™ 3 (Thermo Scientific, 6901) or other clearing agent (*e.g.* xylene)

Paraffin wax (56 to 57°C)

Distilled water (18.2 MΩ.cm dH_2O)

Equipment

CAUTION: Handle surgical instruments with care to avoid puncture and incision wounds. There is also a danger of burning the skin on the hot (~60°C) or cold (~ -15°C) surfaces.

Safety biohazard hood

1 ml syringes with inserted 26-gauge ½" – 0.45 x 13 mm needle

Dissection tools:

Dissection holder (styrofoam plaque home-made)

21-gauge ½" - 0.8 x 40 mm needles

Fine scissors (Fine Iris Scissors - Curved 10.5 cm, Fine Science Tools, 14095-11)

Gross forceps (Narrow Pattern Forceps - Curved 12 cm, Fine Science Tools, 11003-12)

Fine forceps (Dumont #7 Forceps, Fine Science Tools, 11272-30)

Standard plastic labware: Petri dish 100 x 15 mm non-TC; 15 ml conical tubes

Histological cassettes

500 ml glass beaker

Tissue Processor

Paraffin Embedding Center

Stainless Steel Molds 60 x 45 x 15 mm

Cooling plate

Single edge razor blade

Rotary Microtome

Disposable microtome blade

Set of brushes for microtome

APES coated slides (see recipe)

Transparent plastic container (dark bottom) with approximately 200 mm x 100 mm

Slide staining holders

Water bath (stable temperature at 45°C)

Slide boxes

Refrigerator (at 4°C)

Euthanasia, collection and fixation

1. Deeply anesthetize the animal by intra-peritoneal injection of 400 mg kg^{-1} Pentobarbital with a 1 ml syringe and 26-gauge ½" needle.

Verify that the animal is unresponsive applying pressure on the mouse paw (toe-pinch reflex) before starting dissection.

2. Place the animal in supine position and immobilize with 21-gauge needles on the dissection holder. Spray and wipe the thorax surface with 70% ethanol (also preventing further spread of the mouse hair).

Steps 2 – 6 can be either performed on a safety biohazard hood or on the bench.

3. Remove the mouse skin (with Fine scissors and Gross forceps) at the thorax level.
4. Open the chest cavity by pulling the inferior tip of the sternum (gross forceps) and carefully cutting the diaphragm muscle with fine scissors.
5. Expose the heart (apical view) and inject 100 µl of 4M KCl (with 1 ml syringe and 26-gauge ½" needle) into the LV wall to arrest the heart in diastole.

Morphometric quantifications are highly dependent on tissue size and shape, and therefore, hearts must be at the same stage of cardiac cycle for reliable comparison. Intra-wall injection of KCl promotes cardioplegia allowing the hearts to be harvested in diastole (Kobayashi et al., 2004) (see Critical Parameters).

6. Harvest the heart by dissecting the great vessels (with Fine scissors and Fine forceps), and transfer it to a 100 x 15 mm Petri dish containing PBS. Remove most of the blood from the heart cavities by gently pressing the organ.
7. Fix the entire heart in a 15 ml Falcon tube containing 10 ml of Neutral Buffered Formalin for 12-16 h at room temperature.

The fixation step should be done immediately after organ harvesting. The volume of fixative must be 20 times greater than the heart volume to promote correct fixation. Do not fix the tissue for more than 16 h because aldehyde-based fixatives cause tissue shrinkage, hardening and mask antigenic epitopes volume (see Critical Parameters).

Histological processing and paraffin embedding

8. In a fume hood, transfer each heart to a labeled histological cassette and collect all cassettes in a container with PBS (500 ml glass beaker).
9. For automated processing, collect all cassettes into the apparatus' basket and program Tissue Processor for 1 h immersion in each of the following solutions:

The following histological procedure details a standard processing for mouse tissue. Whenever using a different protocol be certain of its suitability for subsequent analysis, such as immunofluorescence.

a. PBS (first bath).
b. 70% Ethanol (second bath).
c. 80% Ethanol (third bath).
d. 90% Ethanol (fourth bath).
e. 96% Ethanol (fifth bath).
f. 2 times 99.8% ethanol (sixth and seventh bath).
g. 3 times Clear-Rite^{TM} 3 (eighth, ninth and tenth bath).

h. 2 times melted paraffin wax at 56°C (eleventh and twelfth bath).

Tissue Processor solutions can be reused several times; however it is mandatory to confirm they are clear and non-saturated before each processing round. Do not incubate more than 1 h on each bath (standard size samples, i.e. within histological cassettes), except in the PBS bath. Ensure the solution volume is 10 times greater than the sample volume. If using an automated machine, ensure the basket is immersed in paraffin at the end of processing (see Critical Parameters and Troubleshooting – Table 2).

10. Transfer histological cassettes to the Paraffin Embedding Center.
11. Embed hearts in paraffin vertically in order to get transverse sections by following the next steps:

a. Fill an appropriate warmed mold with freshly melted paraffin at 56°C (Fig. 2A).

   The metallic mold must have enough depth to allow vertical heart embedding .

b. Transfer the mold to the cold surface of the Embedding Center to allow a thin layer of paraffin to solidify in the bottom of the mold.
c. Immediately place the heart on the solid paraffin layer, vertically oriented with the apex down (Fig. 2B).
d. Hold the heart in the same position for 30 s to allow paraffin block solidification prior to any movement (Fig. 2C).
e. While paraffin at the surface of the block/mold is still liquid, cover the mold with the bottom of the pre-labeled cassette (Fig. 2D).

   The bottom of the cassette must be properly positioned in the mold to prevent any misalignment of the paraffin block.

f. Carefully transfer the mold to the Cooling Plate and wait until the embedding medium is fully hardened.

Once paraffin blocks are solidified they can be stored in a dry place, protected from direct light at room temperature.

Manipulate paraffin-impregnated hearts as fast as possible with warmed forceps and under a warm plate. Embedding (Step 11) can be repeated if the heart was incorrectly oriented.

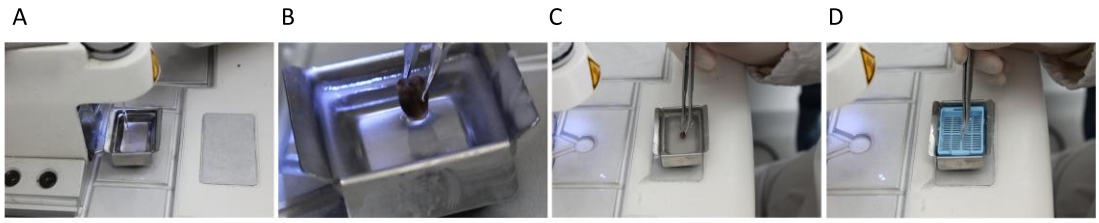

Figure 2 Overview of the paraffin embedding procedure. (**A**) Fill the mold with new paraffin over the hot surface. (**B**) On the cold surface, adjust the position and hold the heart vertically (apex down). (**C**) Immobilize the heart as the paraffin starts to solidify (paraffin becomes white). (**D**) Cover the mold with the bottom of the pre-labeled cassette while the paraffin surface of the block/mold is still liquid.

Sectioning

For any doubt, please consult Critical Parameters and/or Troubleshooting – Table 2.

12. Sectioning station setup:

a. Turn on the cooling plate and adjust the temperature of the water bath to 45°C.

b. Prepare the cold dH_2O in a plastic container with few drops of 99.8% ethanol (to decrease the surface tension) – cold dH_2O-Ethanol.

Place the transparent plastic container over a dark surface to increase the contrast of paraffin sections.

c. Label APES slides according to the scheme in Fig. 3.

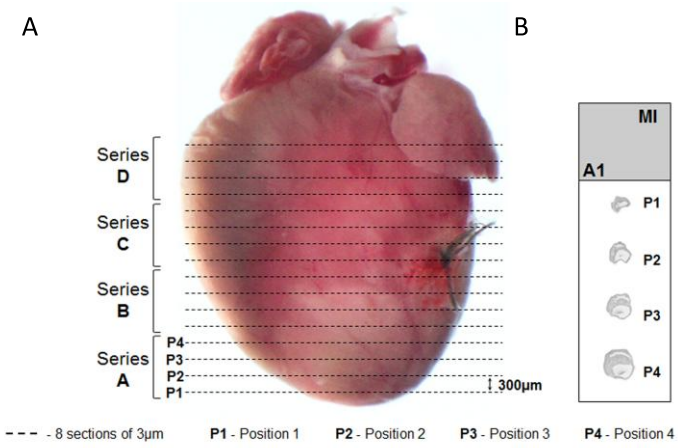

Figure 3 Schematic representation of the systematic left ventricle (LV) sampling. (**A**) Sectioning starts in the apical region, and 8 adjacent sections are collected from 12 – 14 equally distant (300 µm) regions. (**B**) Schematic illustration of the first replicate of the apical region (A1: series A, slide 1), which contains 4 sections distanced 300 µm apart. Replicates should be numbered from A1 to A8.

13. Shape the paraffin block to a rectangle by trimming the excess paraffin from the edges of the block using a single edge razor blade (Fig. 4A-D) until a width compatible with collection of at least 4 tissue sections *per* slide is reached.

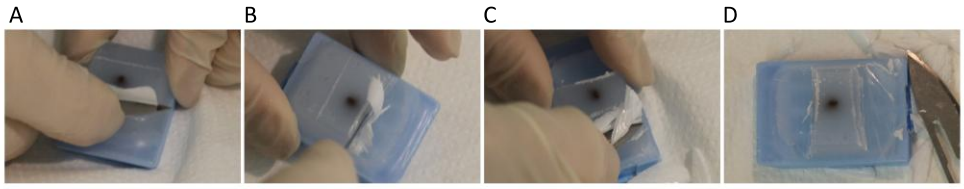

Figure 4. Molding the paraffin block to a rectangular shape. (**A – D**) Trim the excess paraffin by removing small portions of paraffin on both sides of the block.

14. The following procedure was adapted to obtain 8 replicate slides of 12 – 14 regions of the heart with 300 µm of interval between sections (Fig. 3), if another heart sampling is required adjust the sectioning steps according to Table 1.

15. Assemble the Microtome with a disposable microtome blade (position 1) and adjust cutting thickness to 10 µm.
16. With the block at room temperature, trim the excess paraffin until the tissue is visible at the block surface (see Troubleshooting – Table 2).
17. Cool down the trimmed surface of the paraffin block in a Cooling Plate for a few minutes and adjust the microtome blade to a non-used position (position 2) and cutting thickness to 3 µm (see Troubleshooting – Table 2).
18. Assemble the cold trimmed block in the microtome and immediately cut 8-10 sections of 3 µm thickness. Sections will naturally form a ribbon (Fig. 5A).

a. While holding with a thin brush (Fig. 5B), transfer the ribbon (shiny side down) to the cold dH_2O-Ethanol (transparent plastic container with dark bottom, Fig. 5C). Meanwhile, cool down the paraffin block surface in the Cooling Plate.
b. Gently remove any folds and/or wrinkles in the paraffin sections with a thin brush.

Paraffin ribbons are easily blown away and lost, therefore avoid rapid air movements during Step 18. In order to recognize the orientation of the ribbon, make a mark to discriminate the beginning from the end. Be careful because sometimes the ribbons break when they are placed on the cold dH_2O-Ethanol.

Table 1 Representative sampling of the adult mouse left ventricle (LV) (12 – 14 equidistant sections). The protocol describes representative sampling of the mouse LV in which the user is expected to obtain 8 replicates of 12 to 14 equidistant sections. Whenever the user requires a different number of replicate slides, trimming thickness between regions has to be adjusted accordingly. To facilitate protocol adjustments Table 1 details the best-suited trimming for a wide range of replicates.

Number of slide replicates	Approximated trimming between region
1	335 µm
2	330 µm
3	325 µm
4	320 µm
5	315 µm
6	310 µm
7	305 µm
8	300 µm
9	295 µm
10	290 µm
20	250 µm
40	100 µm

c. Transfer the first section to the respective APES-coated slide (near the frost side) (Fig. 5D).
d. Immerse the slide in the water bath just enough to allow section expansion and flattening (Fig. 5E-F, see Troubleshooting – Table 2).
e. Firmly shake the slide to drain the excess of water.
f. Repeat *Step 18c-f* until 8 cuts of the ribbon are adhered to the 8 replicate slides.

19. In the microtome, place the blade to position 1 for trimming and adjust the cutting thickness to 25 µm.

To prevent a crack in the block, do not trim more than 25 µm at a time (see Troubleshooting – Table 2).

20. Trim the heart, with paraffin block surface at room temperature, 12 consecutive times to discard 300 µm (25 µm x 12) of tissue.

The more replicates are required per series, the less tissue is trimmed between regions (Table 1).

21. To obtain replicate sections of the following heart regions repeat *Steps 18 – 20* until no more tissue is observed in the block (Fig. 5).
22. Transfer APES slides to a Slide Staining Holder and dry overnight at 37°C (or 1-2 h at 60°C for histochemistry) in order to evaporate the water trapped between the paraffin section and the slide glass, and to improve tissue adherence to the slide.

Once paraffin-embedded sections are properly adhered and completely dried, the slides can be stored in slide trays or boxes protected from direct light at 4°C. Storage at 4°C will preserve tissue antigenicity which is valuable when immunolabelling experiments are planned (Jacobs et al., 1996; Karlsson and Karlsson, 2011).

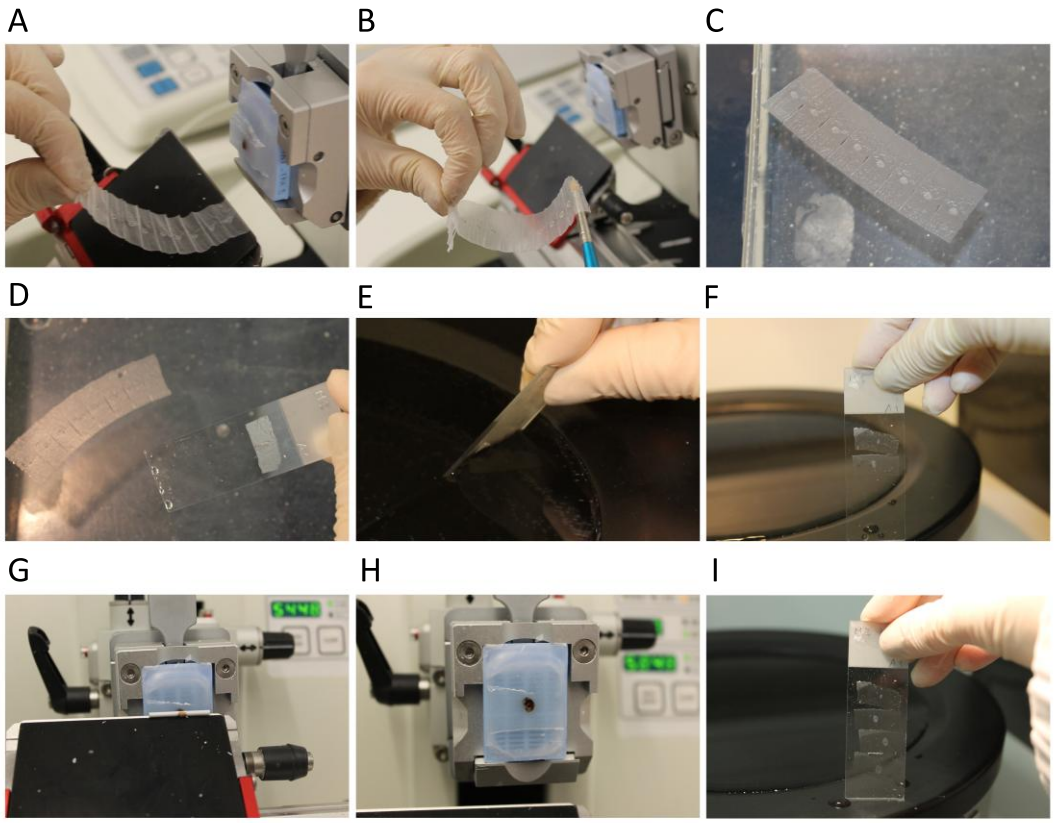

Figure 5. Overview of systematic sectioning of the left ventricle (LV). (**A**) Following exposure of the apex at the surface of the block, cut 3 µm-thick sections, making a ribbon of 8 – 10 sequential sections. The white spot in the center of the section is the heart tissue (apex region). (**B**) Transfer the ribbon of adjacent sections to cold dH_2O-Ethanol with a thin brush. (**C**) Check and remove any folds and/or wrinkles in the paraffin sections. (**D**) Collect the first section near the frosted side of the APES-coated slide. (**E**) Immerse the slide with the section in the water bath to expand and smooth the paraffin section. Remove slide from the water bath by inclining the bottom edge up to decrease the amount of water in between the paraffin and the glass slide. (**F**) Detail of the extended and flattened sections. (**G**) Sectioning of 25 µm-thick cuts during trimming in order to attain 300 µm of interval between heart regions. (**H-I**) Detail of the paraffin block after sectioning and of the A1 slide (series A, replicate 1) after the collection of 4 sections.

BASIC PROTOCOL 2

INFARCT SIZE CALCULATION AND MORPHOMETRIC ANALYSIS

The infarct size, percentage of the LV affected by extensive collagen deposition, is considered a key parameter when assessing the potential of cardiac therapies in rodent models of MI; as there is a general correlation between infarct size and functional and hemodynamic alterations (Csonka et al., 2010; Nascimento et al., 2011; Takagawa et al., 2007).

Calculation of infarct size is typically evaluated by histological measurements, such as the midline length (Takagawa et al., 2007) and the area (Michael et al., 1995) of infarcted *versus* non-infarcted LV regions. Manual quantification of the infarct size is time-consuming and highly dependent on the user, as it requires manual contouring of the fibrotic tissue and viable myocardium from each tissue section. In order to ease this task and to reduce the user-dependency, we have developed the *MIQuant* (stands for MI Quantification) software that reduces analysis time 5-fold (Nascimento et al., 2011). Using Masson's Trichrome stained sections, *MIQuant* software provides not only the final average value of the infarct size by the two different described methods – area (Michael et al., 1995) and midline length (Takagawa et al., 2007) – but also offers the intermediate calculations for each section. In more detail, area measurement is

calculated by dividing the infarct area by the total LV area, and the midline measurement is determined by dividing the midline length of the infarcted LV wall (only regions with infarct in 50% of the whole thickness of the myocardial wall) by the midline length of total LV wall. Although the area and midline length measurements have been previously validated, both display some limitations. The infarct size measurement by area can underestimate infarction size because of the retraction of infarcted area and the hypertrophy of non-infarcted region that are associated with cardiac remodeling. In contrast, the midline measurement overestimates the infarct size in cases of substantial cardiac remodeling and aneurism formation. Accordingly, infarct size results calculated by the area method are significantly smaller than those calculated by the midline length (Takagawa et al., 2007; Zornoff et al., 2009).

Widespread use of *MIQuant* will reduce the time required to quantify the infarct size and, more importantly, will reduce intra-laboratory variability (Nascimento et al., 2011). However, when different quantification methods or tools are preferred over *MIQuant*, we encourage the use of the systematic heart sampling described in Basic Protocol 1 to attain an accurate representation of the different LV regions prior to scar quantification.

Basic Protocol 2 describes the assessment of MI size, using the *MIQuant* software, and of the LV remodeling following MI, by morphometric analysis of LV chamber dilation and wall thinning, using the representative sections obtained in the Basic Protocol 1 (Fig. 1). Guidelines concerning image acquisition and manual infarct size quantification are also outlined.

Materials

Samples

Representative sections of the LV of infarcted hearts (see Basic Protocol 1)

Solutions

CAUTION: Take care as most of the solutions used on Basic Protocol 1 are inflammable and harmful by inhalation and/or skin contact. Always be acquainted with the hazards of the reagents PRIOR to their usage. Work in a safety biohazard hood and wear gloves and protective eyewear.

Xylene

50%, 70%, 96% and 99.8% Ethanol dilutions (see recipe)

Distilled water (18.2 MΩ.cm dH_2O)

Tap water

Celestine Blue Solution (see recipe)

Gill's Hematoxylin Solution

Masson's Trichrome Kit (Sigma, HT15, see recipe)

Bouin Solution

Mounting media

Equipment

Slide Staining Holders

Slide Staining Set (Staining jars)

Coverslips

Stereomicroscope with a digital camera

Software ImageJ1.42®

Computer with the operative system MS Windows™ and Internet access.

Collagen staining – modified Masson's Trichrome staining

Masson´s Trichrome staining must be performed on coated slides and at room temperature to prevent detachment of the tissue.

In case of doubt, please consult Critical Parameters and/or Troubleshooting – Table 2.

1. In a fume hood, bring tissue sections to room temperature.
2. Perform the staining steps by soaking slides in staining jars as follows:

a. Dewax tissue sections in xylene (a series of 3 containers, 10 min each).

b. Hydrate tissue sections in a decreasing ethanol series (2 min each with stirring): 99.8% ethanol twice, 96% ethanol, 70% ethanol, 50% ethanol and tap water.
c. Rinse in dH_2O.

Solutions from the dewax and hydration steps and subsequent dehydration and clearing steps (Step 13) can be reused several times; however, it is mandatory to confirm they are clear and non-saturated before each round of staining. Never confuse dewax/hydration solutions with dehydration/clearing ones; although they are of the same composition, they have different functions and are subjected to a different sequence of solutions.

3. Nuclei staining: Dip slides in Celestine Blue Solution 5 min for nuclei pre-staining. Rinse in dH_2O, followed by Gill's Hematoxylin Solution for 5 min.
4. Rinse in running tap water for 2 min, followed by a quick wash in dH_2O.
5. Immerse slides for 1 h in Bouin solution.
6. Rinse in dH_2O for 1 min with stirring.
7. Muscle tissue and cytoplasm staining: Immerse slides in Biebrich Scarlet-Acid Fuchsin Solution for 5 min.
8. Rinse in dH_2O for 1 min with stirring.
9. Immerse slides in freshly prepared working solution of Phosphomolybdic Acid/Phosphotungstic Acid Solution for 5 min.
10. Drain the excess Phosphomolybdic Acid/Phosphotungstic Acid Solution. Do not rinse.
11. Collagen fibers staining: immerse slides in Aniline Blue for 5 min.

With the exception of Phosphomolybdic Acid/Phosphotungstic Acid working solution, dye solutions can be reused if properly stored at room temperature in the dark. If a film

of oxidized dye is formed at the dye surface, filter dye solutions prior to use to avoid non-specific staining of samples.

12. Rinse in dH_2O for 1 min with stirring.
13. Dehydrate in fresh 99.9% ethanol twice for 1 min with stirring and clear in xylene 3 times for 2 min each. Optionally, instead of ethanol dehydration, samples can be dried for 2 h at 37°C and then processed in xylene.
14. Mount Masson's Trichrome-stained slides with one drop of mounting medium at the center of the coverslip. Carefully place the coverslip on the slide by starting from one edge and slowly lowering the opposite side until it reaches the slide to avoid the formation of bubbles.
15. Allow mounting medium to dry partially for 5 min and then squeeze out any entrapped bubbles.

Be careful and avoid any contact between slides after mounting because mounting medium needs at least 12 h to completely solidify. Masson's Trichrome-stained heart slides can be stored in slide boxes at room temperature.

16. With a stereomicroscope coupled to a camera acquire images of all Masson's Trichrome-stained heart sections at a low magnification (capturing the full cross-section) for posterior infarct size quantification and morphometric analysis (Fig. 6).
17. Save images in either .jpg or .tiff (suitable for *MIQuant* and ImageJ; when other analysis tools will be used, ensure that a compatible image type is selected).

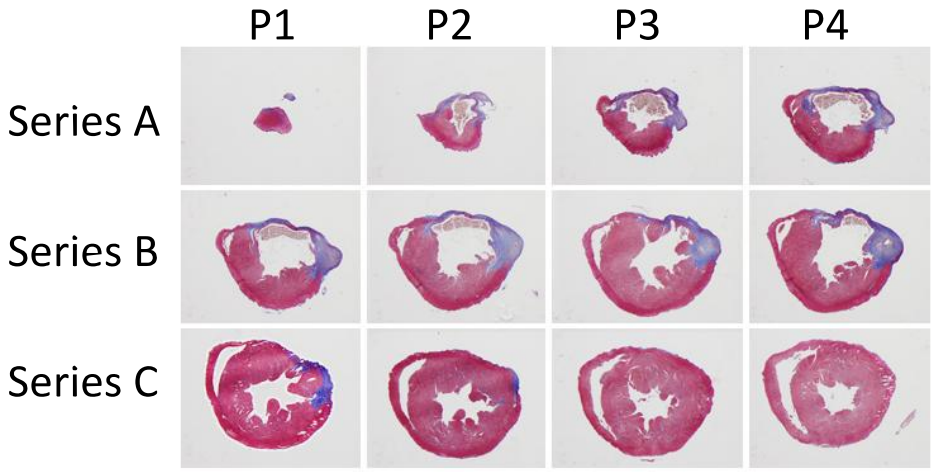

Figure 6. Overview of representative left ventricle (LV) cross-sections obtained with herein described heart sampling. Low-magnification photographs of heart sections stained with Masson's Trichrome from an infarcted mouse (permanent ligation of the left coronary artery) collected 21 days post-injury. Muscle is stained in red, collagen deposition in blue and erythrocytes in brown-reddish. Series A represents the apical region of the heart, series B represents the middle zone and series C corresponds to the base of the heart.

Myocardial infarct size calculation with MIQuant

18. *MIQuant* software and manual, with installation and user instructions, are available at (http://paginas.fe.up.pt/~quelhas/MIQuant/). Download and install *MIQuant* following the website instructions.

a. If MATLAB™ is not present, install the MCRInstaller, available at the "MATLAB™ Runtime Install" hyperlink.

b. Download *MIQuant* software available at the "MIQuant Install" hyperlink and execute "MIQuant.exe".

19. Initiate the application by double-clicking on the "MIQuant" file (Fig. 7A).

A footnote bar exhibited in the bottom of the layout displays important instructions and/or the available options to assist MI size calculation (Fig. 7A1).

For any doubt, please consult Critical Parameters and/or Troubleshooting – Table 2.

20. Upload an image or multiple images in .jpg or .tiff, acquired from *Step 17*, in the commands "File" and "Open images" (Fig. 7A2 and 7B).

MIQuant software retrieves the MI size of each image as well as the average value for all the images.

21. During image upload, automatic pre-processing aimed at image color and contrast enhancement is performed.

a. Remove this option in the “Image quality” section if it is not facilitating tissue segmentation (Fig. 7A2 and 7C).

Pre-processing is useful for uneven or non-white backgrounds.

22. If necessary, edit original images before MI size calculation in the “Edit” menu command (Fig. 7A2 and 7D).

a. Remove the right ventricle at the “Remove tissue” command (Fig. 7A2 and 7D).

    i. Click to define a line path and double-click/ENTER to complete the line drawing that will introduce a cut to separate the tissue to be removed from the analysis (*e.g.* right ventricle, Fig. 7A3 and 7E-F).

b. Delete undesired staining artifacts or blood from the LV lumen that can interfere with tissue segmentation at the “Clean LV lumen” command (Fig. 7A2 and 7D).

    i. Click to define the path of the region to be cleared and double-click/ENTER to complete the area definition (Fig. 7A3 and 7E).

c. Link heart tissue regions by using the “Connect tissue regions” command. (Fig. 7A2 and 7D).

    i. Click sequentially on the two regions of the tissue to be connected (Fig. 7A3 and 7F).

d. Click “Undo” if you need to erase all previous modifications to the original image (Fig. 7A2 and 7D).

e. If necessary select  and  applications to enlarge or decrease, respectively, a selected image field (Fig. 7A2).

23. Selection of normal LV muscle and lumen for automatic tissue segmentation:

a. Press “Normal tissue” button (Fig. 7A5) and then click over the viable myocardium (red stained, Fig. 7A3) of the Masson’s Trichrome stained section, several regions can be selected, double-click to end the selection (Fig. 7G).

b. Press “LV lumen” button (Fig. 7A5), and then click over the LV lumen of the Masson’s Trichrome stained section (Fig. 7A3), double-click to end the selection (Fig. 7G).

The objective of image segmentation, as applied here, is to obtain tissue delineation that correctly estimates normal, infarcted and lumen regions in the original image. When different shades of red exist within the viable myocardium, it is important to click on these regions (usually 3-4 regions is sufficient) for “normal tissue” selection to improve automated segmentation. The same procedure should be applied if 2 non-contiguous infarcted regions are present.

24. Verify if the obtained segmented figure is equivalent to the original photograph (Fig. 7G-H). If not, either repeat *Step 23* and select different regions, or adjust the thresholds accordingly; *i.e.* increase or decrease the threshold (Fig. 7A5) to obtain a less restricted or a wider selection, respectively, and followed by *Step 23*.

Segmentation can be repeated until accurate results are obtained.

25. Calculate MI size by pressing “Calculate Infarct Size” button. Infarct size results calculated using the midline length and the area methods will be visible on the software interface (Fig. 7I-J).

The predicted midline can be corrected by the user on "Edit midline" button (Fig. 7I). For that, click on the dot to be corrected and then on the preferred final position. The MI size will be automatically re-calculated. Use the commands  and  *to enlarge or decrease the image during the edition. To abort the analysis press the "Reset" button at any time (see Troubleshooting – Table 2).*

26. Save the final segmented image ("Save image with annotations") and/or the excel file with the retrieved values ("Save results in excel", Fig. 7A7).

27. When working with multiple images, press  to proceed to the next image and repeat *Steps 21 – 26*. Press "End analysis" button to obtain the average MI for all uploaded images.

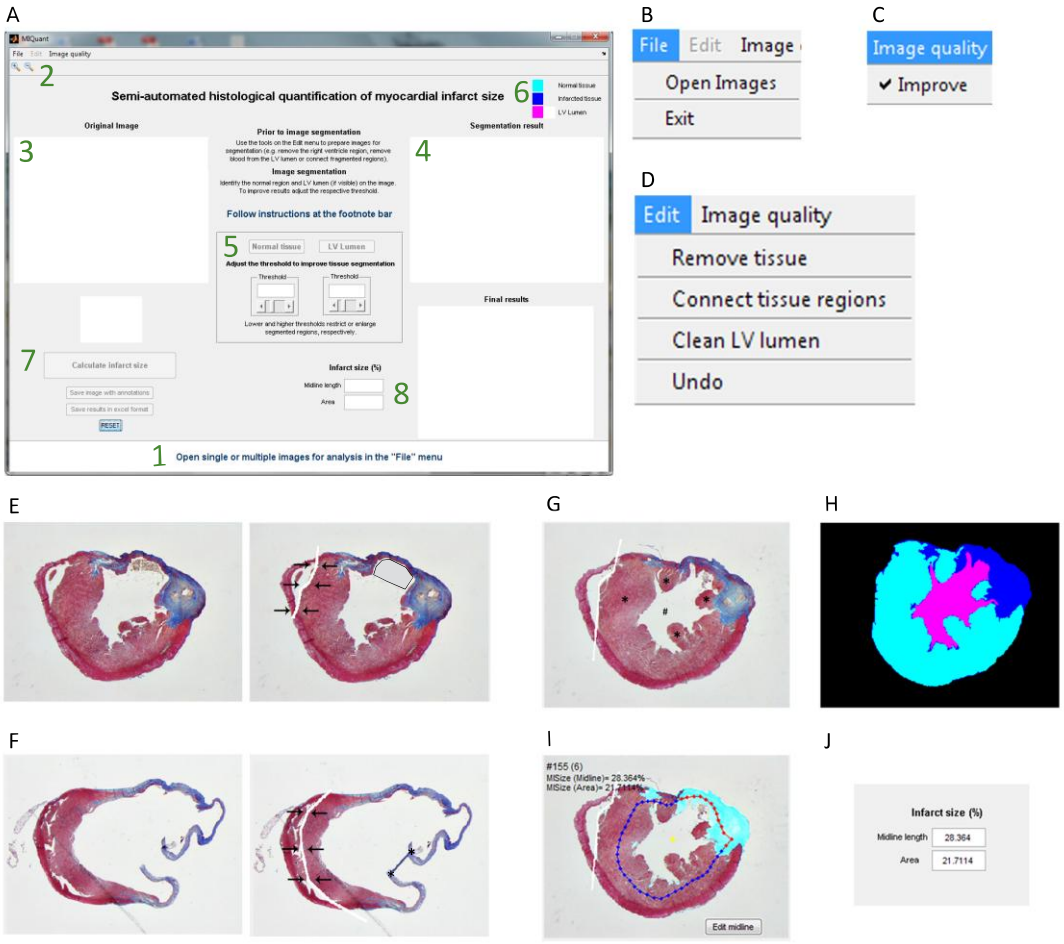

Figure 7. Overview of the *MIQuant* software interface and tools. (**A**) Layout of the *MIQuant* software, where a footnote bar (**1**) displays important instructions and/or the available options at each step. All the editing tools are available on the top left (**2**). Briefly, the original image is displayed on the left (**3**) and its corresponding segmentation is immediately available on the right side (**4**); including all image editing. The obtained segmentation can be tuned by adjusting the threshold value for both “Normal tissue” and “LV lumen” (**5**). A color legend is available to ease the analysis of the segmented image (**6**). Calculation of the MI size is obtained with the command “Calculate infarct size” (**7** and **8**). (**B**) One or more images can be uploaded in the software at the same time, enabling MI calculation based on one image or on the average of multiple images, respectively. (**C**) During image upload, the software automatically adjusts the quality of the image. This pre-processing step can be removed on the “Image quality” option by clicking on the check symbol. (**D**) All the editing tools are displayed in the “Edit” command, including the “Undo” step. (**E-F**) Editing scenarios that include the use of different editing tools such as “Remove tissue” (arrows, **E-F**), “Clean LV lumen” (delimited area, **E**) and “Connect tissue regions” (*, **F**). (**G**) Selection of the Normal tissue (*) and the LV lumen (#) required for image segmentation. (**H**) Segmented image that is used by *MIQuant* for subsequent automated measurements. (**I**) Final results overlaying the infarcted area, the estimated midline and the MI size using the area and midline length methods. (**J**) MI size is displayed on the interface as the percentage of LV affected by collagen deposition, calculated on the basis of both methods.

Morphometric analysis LV infarcted wall thinning

For further information please consult Critical Parameters.

28. Upload images of Masson's Trichrome stained heart sections obtained on *Step 17* to the ImageJ1.42® software.
    a. Select only images that contain both LV lumen and infarcted region for the analysis.
29. Draw at least 5 equidistant lines from the epicardial to the endocardial border of the infarcted LV wall using the "Straight Line" tool.

Annotation of the length of the straight lines is obtained in pixels and should be collected in an excel file.

30. Repeat *Step 29* for each image.
31. Convert pixels values to the appropriate units applying the correct image scale (*e.g.* conversion of pixels to mm).
32. Calculate the average of infarcted LV wall thickness (lines length) for all sections that contain LV lumen and calculate the average index value.

Morphometric analysis: LV chamber dilation with MIQuant retrieved data

The MIQuant excel file saved after calculation of infarct size contains all the measurements required for this quantification.

For further information please consult Critical Parameters.

33. Assess LV chamber dilation as the ratio between the LV lumen area and the total LV area:

a. Consult the excel file retrieved during MI quantification (*Step 26*, Fig. 7A7) with the *MIQuant* software.

b. Use area values obtained for "LV Lumen Area", "Normal Area" and "Infarcted Area".

c. First calculate the total LV area by the sum of “LV Lumen Area”, “Normal Area” and “Infarcted Area”.

d. Divide the “LV Lumen Area” by the total LV area (*Step 33c*).

e. Multiply by 100 to show results as a percentage.

34. Repeat *Step 33* for all sections that contain LV lumen and calculate the average index value.

CAUTION: In the case of aneurism formation, LV dilation cannot be estimated by this method, as the area of the LV lumen will not be easily assessed if LV wall becomes highly irregular.

Only sections (Step 17) containing LV lumen should be considered to estimate LV dilation.

Manual quantification of infarct size and LV chamber dilation calculation

For further information please consult Critical Parameters.

35. Assess LV infarct size by the area method (Michael et al., 1995) as the ratio between the LV infarcted area and the total LV area:

a. Upload an image or multiple images to an image processing tool (e.g. Image J).

b. Determine the LV total area.

   i. Draw a close line circumscribing the LV.

   ii. Determine the area of the drawn polygon using appropriate function.

c. Determine the LV lumen area.

   iii. Draw a close line circumscribing the LV endocardium.

   iv. Determine the area of the drawn polygon using appropriate function.

d. Determine the LV infarcted region area.

    i. Draw a close line circumscribing the LV region where collagen deposition is observed (blue staining).

    ii. Determine the area of the drawn polygon using appropriate function.

For non-contiguous collagen deposition regions, circumscribe the different regions with separate polygons. The LV infarcted area will be the sum of the areas of the different drawn regions.

e. Calculate the LV tissue area, by subtracting the LV lumen area (step 35c) from the LV total area (Step35b).

f. Calculate the infarct size (area), by dividing LV infarcted region area by the LV tissue area.

g. Multiply by 100 to show results as a percentage.

36. Repeat Step 35 for all sections that contain LV lumen and calculate the average LV infarct size (area) value for the whole heart.

37. Assess LV chamber dilation as the ratio between the LV total area and the LV lumen area. Multiply by 100 to express results as a percentage

38. Repeat Step 36 for all sections that contain LV lumen and calculate the average LV chamber dilation value for the whole heart.

39. Assess LV myocardial infarct size by midline-length method (Takagawa et al., 2007) as the ratio between the LV infarcted midline length and the total LV midline length:

a. Upload an image or multiple images to the processing tool with a compatible image type.

b. Determine the LV midline length.

    i. Delineate LV infarcted midline on regions in which more than 50% of the LV wall is affected by collagen deposition

ii. Determine the length of the LV infarcted midline using appropriate function.

iii. Delineate the total LV midline.

iv. Determine the length of the total LV midline using an appropriate function.

v. Divide the length of the LV infarcted midline by the total LV midline and multiply by 100 to show the results as a percentage.

40. Repeat Step 39 for all sections that contain LV lumen and calculate the average LV infarct size (midline-length) value for the whole heart.

SUPPORT PROTOCOL 1

ASSESSMENT OF NEOVASCULARIZATION IN THE INFARCTED MYOCARDIUM FOLLOWING ADMINISTRATION OF A THERAPY

Most novel, cardiovascular therapies aim to improve the formation of new vessels (neovascularization) at the ischemic site in order to support the viability of the remaining functional tissue as well as the hypothetically newly formed tissue. The most common assessment of neovascularization involves the quantification of CD31 (PECAM-1, a marker of endothelial cells)-expressing cells in the infarcted/peri-infarcted myocardium. The comparison is performed between the treated and vehicle control group (Freire et al., 2014a; Nascimento et al., 2014).

The assessment of neovascularization is particularly dependent on the selected region; therefore, heart sampling should be performed in accordance to Basic Protocol 1.

In the Support Protocol 1 provided here, we detail the procedure for CD31 immunostaining and quantification of CD31-expressing cells in paraffin embedded sections obtained from Basic Protocol 1.

Materials

Samples

Slides with representative tissue sections of the LV (see Basic Protocol 1) from treated and control groups.

Be aware to include appropriate controls, i.e. a section incubated with an irrelevant isotype matched antibody replacing the primary antibody, to detect non-specific antibody staining.

Reagents

Xylene

50%, 70%, 96% and 99.8% Ethanol dilutions (see recipe)

Tap water

Distilled water (dH_2O, Synergy® UV system Millipore with a resistivity of 18.2 MΩ.cm)

PBS (Phosphate-Buffered Saline)

10 mM Tris/1 mM EDTA pH 9.0 (see recipe)

0.2% (v/v) Triton X-100 (see recipe)

4% FBS/1% BSA Blocking solution (see recipe)

0.8 µg/ml Goat anti-mouse CD31 IgG (Santa Cruz Biotechnology, sc-1506, see recipe)

0.8 µg/ml Normal goat IgG (Santa Cruz Biotechnology, sc-2028, see recipe)

2 µg/ml Donkey anti-goat IgG Alexa Fluor 568 (Life Technologies, A11057, see recipe)

Vectashield with DAPI® (Vector Laboratories, H-1200)

Equipment

Water bath (stable temperature at 98°C)

Plastic cuvette

PAP pen (hydrophobic pen)

StainTray™ Slide Staining System (Humidity chamber, eBioscience, 44-0404-10)

Refrigerator (at 4°C)

Coverslips

Dark Slides Boxes

Inverted fluorescence microscope with MosaiX AxioVision module (Zeiss)

NOTE: Microscope needs to be equipped with emission light sources and filter sets to excite and detect DAPI and Alexa 568, as well as a monochrome high-resolution sensitive camera for image acquisition.

In case the MosaiX AxioVision module (Zeiss) is not available, the users must acquire a random selection of LV fields, i.e. 10 fields of infarcted and 10 fields of peri-infarcted regions per heart section (as described in Step 15) without MosaiX AxioVision module (Zeiss).

Software ImageJ1.42®

For further information please consult Critical Parameters and/or Troubleshooting – Table 2.

41. Select paraffin sections that contain infarcted myocardium (check for collagen deposition in the Masson's Trichrome stained samples, Basic Protocol 2) obtained in Basic Protocol 1.
42. Dewax and hydrate paraffin sections according to *Steps 1 – 2* of the Basic Protocol 2.
43. Rinse slides in PBS.
44. Perform antigen retrieval:

After formaldehyde-based fixation, antigen retrieval of masked epitope is often required for efficient antigen-antibody coupling.

a. Pre-warm the water bath to 98°C with the plastic cuvettes filled with 10 mM Tris/1 mM EDTA pH 9.0. Once bubbles are seen on the inner surfaces of the plastic cuvettes, proceed to the next step.
b. Place 4 slides *per* plastic cuvette (slides side-by-side, with sections in direct contact with the solution, and 2 pairs of slides separated to increase available solution).

In order to keep conditions constant between experiments add empty slides to complete the 2 pairs of slides in the plastic cuvette.

c. Immerse sections in 10 mM Tris/1 mM EDTA pH 9.0 for 35 min at 98°C.

CAUTION: Be careful with the boiling solution.

d. Cool down the solution for 20 min at room temperature.
e. Wash slides by immersion 3 times in PBS for 5 min at room temperature.
45. Permeabilize tissue sections by incubating in 0.2% Triton X-100 solution for 5 min at room temperature.
46. Wash slides by immersion 3 times in PBS for 5 min at room temperature.
47. Delineate each section with a hydrophobic PAP pen in order to reduce the amount of antibody solution required to cover the section.
48. Block non-specific staining with 4% FBS/1% BSA Blocking solution for 1 h in a humidity chamber at room temperature. Discard only the excess and do not rinse.
49. Cover each section with diluted primary antibody or negative control antibody (0.8 µg/ml Goat anti-mouse CD31 IgG or 0.8 µg/ml Normal goat IgG) and incubate for 2 h in a humidity chamber at room temperature or overnight at 4°C.

50. Wash slides by immersion 3 times in PBS for 5 min at room temperature.
51. Cover each section with diluted secondary antibody (2 µg/ml Donkey anti-goat IgG Alexa Fluor 568) and incubate for 1 h in a dark humidity chamber at room temperature.
52. Wash slides by immersion 3 times in PBS for 5 min at room temperature.
53. Counterstain nuclei and mount slides with Vectashield with DAPI®.

Slides should be analyzed as soon as possible to prevent fluorochrome fading. Meanwhile, slides should be kept in a dark slide box at 4°C or at -20°C for longer periods.

54. Capture high magnification microphotographs (63X objective) from the peri-infarct and infarcted region using the MosaiX AxioVision module of the inverted fluorescence microscope Zeiss Axiovert 200 (see equipment description).
55. Using the ImageJ 1.42® software with "Cell Counting" plugin, count CD31-expressing cells:

a. Select at least 10 fields of infarcted and 10 fields of peri-infarcted regions *per* heart section (Fig. 8).

The analyzed regions should be representative and systematically selected from the MosaiX AxioVision composite microphotograph (Fig. 8).

b. Quantify CD31-expressing cells in at least 3 sections *per* heart using the same strategy as *Step 15a*.

56. Represent the neovascularization density as CD31-expressing cells *per* square millimeter (mm^2).

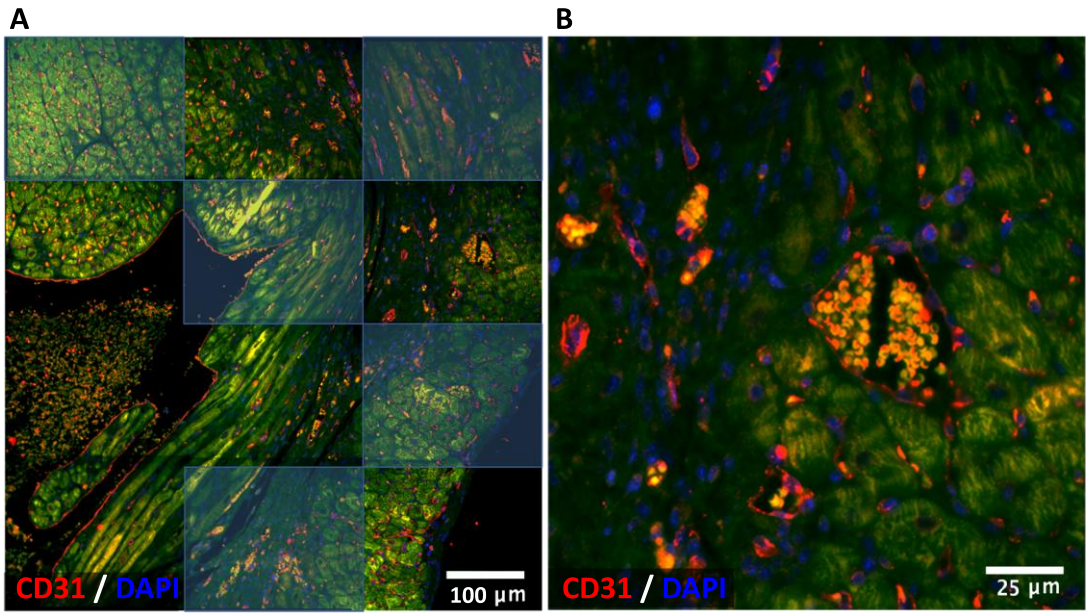

Figure 8. Assessment of neovascularization. (**A**) Composite image of the LV wall obtained with the MosaiX software (63X objective). Systematic selection of fields is represented (blue rectangles). (**B**) High magnification detail of the CD31 immunostaining. Endothelial cells of big vessels and capillaries are stained in red (CD31), nuclei in blue (DAPI) and the background is green (autofluorescence). Scale bars: 100 µm (A) and 25 µm (B).

SUPPORT PROTOCOL 2

IDENTIFICATION OF TRANSPLANTED HUMAN CELLS IN THE MOUSE HEART

The therapeutic potential of a diversity of cell types is under investigation for the treatment of MI. Mouse experimental models of MI are considered valuable tools for the evaluation of human cells, either in an immuno-compromised or -competent setting. In line with this, assessing engraftment of human cells in the myocardium is an important parameter.

Herein, we detail the discrimination of human cells by immunostaining with an anti-human nucleus antibody (Nascimento et al., 2014). Detection of human cells throughout the mouse heart requires representative sampling according to Basic Protocol 1.

Materials

Samples

Slides with adherent paraffin tissue sections (see Basic Protocol 1) from treated and control groups

Be aware to include appropriate controls, i.e. a section incubated with an irrelevant isotype matched antibody replacing the primary antibody, to detect non-specific staining of the secondary antibody.

Reagents

Xylene

50%, 70%, 96% and 99.8% Ethanol dilutions (see recipe)

Tap water

Distilled water (dH_2O, Synergy® UV system Millipore with a resistivity of 18.2 MΩ.cm)

PBS (Phosphate-Buffered Saline)

10 mM Citrate pH 6.0 solution (see recipe)

0.4% (v/v) Triton X-100 solution (see recipe)

Vector® M.O.M.™ kit (Vector Laboratories, BMK-2202, see recipe)

2.5 µg/ml Anti-Nuclei Antibody (Millipore, MAB4383, see recipe)

2.5 µg/ml Mouse IgG1 negative control (Millipore, MABC002, see recipe)

2 µg/ml Donkey anti-mouse IgG Alexa Fluor 594 (Life Technologies, A21203, see recipe)

Vectashield with DAPI® (Vector Laboratories, H-1200)

Equipment

Plastic cuvette

Water bath (stable temperature at 98°C)

PAP pen (hydrophobic pen)

StainTray™ Slide Staining System (Humidity chamber, eBioscience, 44-0404-10)

Refrigerator (at 4°C)

Coverslips

Dark slides boxes

Inverted fluorescence microscope

NOTE: Microscope needs to be equipped with emission light sources and filter sets to excite and detect DAPI and Alexa 594, as well as a monochrome high-resolution sensible camera for image acquisition.

For further information please consult Critical Parameters and/or Troubleshooting – Table 2.

57. Select paraffin sections obtained from Basic Protocol 1.
58. Dewax and hydrate paraffin sections following *Steps 1 – 2* of Basic Protocol 2.
59. Rinse slides in PBS.
60. Perform antigen retrieval:

After formaldehyde-based fixation, antigen retrieval of masked epitopes is generally required for efficient antigen-antibody binding.

a. Pre-warm the water bath at 98°C with the plastic cuvettes filled with 10 mM Citrate pH 6.0. Once bubbles are evident on the inner surface of the plastic cuvette, proceed to the next step.
b. Place 4 slides *per* plastic cuvette (slides side-by-side, with sections in direct contact with the solution, and 2 pairs of slides separated to increase available solution).

In order to keep conditions constant between experiments, add empty slides to complete the 2 pairs of slides in the plastic cuvette.

c. Immerse sections in 10 mM Citrate pH 6.0 for 35 min at 98°C.

CAUTION: Be careful with the boiling solution.

d. Cool down the solution for 20 min at room temperature.
e. Wash slides 3 times by immersion in PBS for 5 min at room temperature.

61. Permeabilize tissue sections by incubating in 0.4% Triton X-100 solution for 5 min at room temperature.

62. Wash slides 3 times by immersion in PBS for 5 min at room temperature.
63. Delineate each section with a hydrophobic PAP pen in order to reduce the amount of antibody solution required to cover the section.
64. Block unspecific staining with Vector® M.O.M.™ kit:

a. Cover each section with Mouse Ig Blocking solution and incubate for 1 h in a humidity chamber at room temperature.
b. Wash slides 3 times by immersion in PBS for 2 min at room temperature.

65. Cover each section with M.O.M.™ Diluent and incubate for 5 min in a humidity chamber at room temperature. Discard only the excess and do not rinse.
66. Cover each section with diluted primary antibody or negative control antibody (2.5 µg/ml mouse anti-human nuclei IgG1 or 2.5 µg/ml mouse IgG1 negative control) and incubate for 4 h in a humidity chamber at room temperature or overnight at 4°C followed by 2 h at room temperature.
67. Wash the slides 3 times by immersion in PBS for 5 min at room temperature.
68. Cover each section with diluted secondary antibody (2 µg/ml Donkey anti-mouse IgG Alexa Fluor 568) and incubate for 1 h in a dark humidity chamber at room temperature.
69. Wash the slides 3 times by immersion in PBS for 5 min at room temperature.
70. Counterstain nuclei and mount slides with Vectashield with DAPI®.

Slides should be analyzed as soon as possible to prevent fluorochrome fading. Meanwhile, slides should be kept at 4°C, or for a longer period of time at -20°C in a dark slides box.

71. Capture high magnification images (63X objective) representative of the peri-infarct and infarcted region using an inverted fluorescence microscope and compare with the controls (Fig. 9).

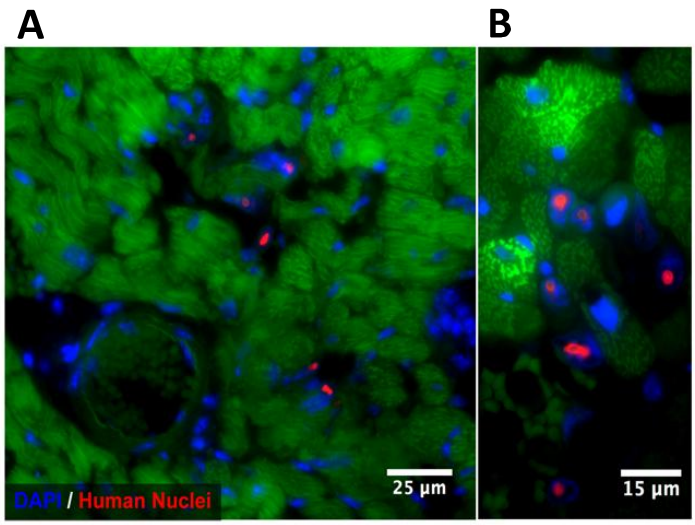

Figure 9. Detection of human cells in the mouse heart. (**A-B**) Transplanted human cells are observed in the myocardial interstitial space. Human nuclei are highlighted in red, mouse nuclei are counterstained in blue (DAPI) and the background is green (autofluorescence). Scale bar: 25 µm.

REAGENTS AND SOLUTIONS

CAUTION: Be careful. Most of the solutions required for this *Unit* are flammable, and harmful by inhalation and/or in skin contact. Always be acquainted with the hazards of reagents prior to use. Work in a safety biohazard hood and wear gloves.

Use distilled water (Synergy® UV system Millipore with a resistivity of 18.2 MΩ.cm) when dH_2O is indicated.

APES slides coating

CAUTION: Work in a safety biohazard hood, wear gloves and use protective eyewear.

Ready-to-use Poly-L-Lysine- or silane-coated slides (e.g. VWR, 100490-312 or 100501-000) are also commercially available.

APES (3-Aminopropyltriethoxysilane-Silane), 5 ml

dH_2O

Methanol

Equipment

Microscope Slides 76 x 26 x 1 mm

Oven (stable at 60°C)

4 Plastic containers

Slides boxes

Slides staining holders

Insert the microscope slides in slides staining holders (fill 2 holders at each time). Distribute the solutions in the 4 plastic containers using the following order: 2% APES solution (5 ml of APES in 250 ml methanol, freshly prepared), absolute methanol and the last two containers with dH_2O. Immerse slides in 2% APES solution for 5 min at room temperature. Rinse the slides in absolute methanol followed by 2 rinses in dH_2O. Completely dry APES-coated slides (APES slides) for at least 12 h at 60°C (in slides boxes with the lid opened). Solution should be freshly prepared before each coating session.

NOTE: Coating prevents loss of tissue sections during histological staining. It is convenient to keep the original microscope slides boxes in order to save APES slides after coating. Ensure APES slides are completely dried before storing and that original microscope slides boxes are correctly identified with the APES designation.

Celestine Blue Solution

Ammonium iron (II) sulphate hexahydrate, 5 g

Celestine Blue, 0.5 g

dH_2O, 100 ml

Glycerol, 14 ml

After dissolving 5 g of Ammonium iron (II) sulphate hexahydrate in 100 ml dH_2O, add 0.5 g of Celestine Blue. Boil the solution for 3 min then cool it down until reaching room temperature, filter the dye solution and add 14 ml of glycerol. Solution is stable in the dark at room temperature for 3 months.

In case a thin film of oxidative dye is formed at the solution surface, filter the dye before use to avoid non-specific staining.

10 mM Citrate Solution pH 6.0

dH_2O, 1000 ml

Sodium citrate, 2.94 g

Mix 2.94 g of Sodium citrate in 800 ml of dH_2O in a stirrer and dissolve. Adjust pH to 6.0 and bring volume to 1000 ml. Autoclave the solution and store up to 6 months at room temperature.

Ethanol dilutions

50% ethanol:

500 ml of 99.8% (v/v) ethanol in 500 ml dH_2O

70% ethanol:

700 ml of 99.8% (v/v) ethanol in 300 ml dH_2O

80% ethanol:

800 ml of 99.8% (v/v) ethanol in 200 ml dH_2O

90% ethanol:

900 ml of 99.8% (v/v) ethanol in 100 ml dH_2O

96% ethanol:

960 ml of 99.8% (v/v) ethanol in 40 ml dH_2O

Diluted ethanol is stable at room temperature for several months.

4% FBS/1% BSA Blocking Solution

Bovine Serum Albumin (BSA), 1 g

Fetal Bovine Serum (FBS), 4 ml

Dilute both components in 100 ml of PBS. Can be stored at -20°C for several months.

4 M KCl

KCl, 14.91 g

dH_2O, 50 ml

Dissolve 14.91 g of KCl in 50 ml of dH_2O. Solution of KCl should be autoclaved and is stable at room temperature for several months.

Masson's Trichrome Kit (Sigma, HT15)

Phosphomolybdic/Phosphotungstic Acid working solution

dH_2O, 2 volumes

Phosphomolybdic Acid Solution, 1 volume

Phosphotungstic Acid Solution, 1 volume

Mix 1 volume of Phosphotungstic Acid Solution and 1 volume of Phosphomolybdic Acid Solution with 2 volumes of dH_2O. Solution should be freshly prepared before each staining session.

The formation of precipitates in the Phosphomolybdic Acid Solution does not affect the mordent properties.

Primary antibodies dilution:

0.8 µg/ml Goat anti-mouse CD31 IgG

4% FBS/1% BSA Blocking solution (see recipe), 996 µl

Goat anti-mouse CD31 IgG (Santa Cruz Biotechnology, sc-1506), 4 µl

Dilute 4 µl of Goat anti-mouse CD31 IgG in 996 µl of 4% FBS/1% BSA Blocking solution to obtain a 0.8 µg/ml final dilution. Prepare a fresh dilution prior to use.

0.8 µg/ml normal goat IgG

4% FBS/1% BSA Blocking solution (see recipe), 996 µl

Normal goat IgG (Santa Cruz Biotechnology, sc-2028), 4 µl

Dilute 4 µl of Normal goat IgG in 996 µl of 4% FBS/1% BSA Blocking solution to obtain a 0.8 µg/ml final dilution. Prepare a fresh dilution prior to use.

2.5 µg/ml mouse anti-human nuclei IgG1

M.O.M.™ Diluent (see recipe), 997 µl

Mouse anti-human nuclei IgG1 (Millipore, MAB4383), 2.5 µl

Dilute 2.5 µl of Mouse anti-human nuclei IgG1 in 997 µl of M.O.M.™ Diluent to obtain a 2.5 µg/ml final dilution. Prepare a fresh dilution prior to use.

2.5 µg/ml mouse IgG1 negative control (Millipore, MABC002)

M.O.M.™ Diluent (see recipe), 997 µl

Mouse IgG1 negative control (Millipore, MABC002), 2.5 µl

Dilute 2.5 µl of mouse IgG1 negative control in 997 µl of M.O.M.™ Diluent to obtain a 2.5 µg/ml final dilution. Prepare a fresh dilution prior to use.

Secondary antibodies dilution:

2 µg/ml donkey anti-goat IgG Alexa Fluor 568

4% FBS/1% BSA Blocking solution (see recipe), 999 µl

Donkey anti-goat IgG Alexa 568 (Life Technologies, A11057), 1 µl

Dilute 1 µl of donkey anti-goat IgG Alexa 568 in 999 µl of 4% FBS/1% BSA Blocking solution to obtain a 2 µg/ml final dilution. Prepare a fresh dilution prior to use.

2 µg/ml donkey anti-mouse IgG Alexa Fluor 568

M.O.M.™ Diluent (see recipe), 999 µl

Donkey anti-mouse IgG Alexa 594 (Life Technologies, A21203), 1 µl

Dilute 1 µl of donkey anti-mouse IgG Alexa 568 in 999 µl of M.O.M.™ Diluent to obtain a 2 µg/ml final dilution. Prepare a fresh dilution prior to use.

10 mM Tris/1 mM EDTA; pH 9.0

dH_2O, 1000 ml

EDTA (Ethylenediaminetetraacetic acid), 0.372 g

Tris (tris(hydroxymethyl)aminomethane), 1.21 g

Mix 1.21 g of Tris and 0.372 g of EDTA in 800 ml of dH_2O in a stirrer and dissolve. Adjust pH to 9.0 and bring volume to 1000 ml. Autoclave the solution. Can be stored up to 6 months at room temperature.

0.2% (v/v) Triton X-100 Solution

PBS, 50 ml

Triton™ X-100, 100 µl

Mix both solutions and stir. The solution is stable at room temperature for 6 months.

CAUTION: Triton is corrosive and may degrade the plastic overtime.

0.4% (v/v) Triton X-100 Solution

PBS, 50 ml

Triton™ X-100, 200 µl

Mix both solutions and stir. The solution is stable at room temperature for 6 months.

CAUTION: Triton is corrosive and may degrade the plastic overtime.

Vector® M.O.M.™ kit (Vector Laboratories, BMK-2202)

M.O.M.™ Diluent

M.O.M.™ Protein Concentrate, 600 µl

PBS, 7.5 ml

Dilute 600 µl of M.O.M.™ Protein Concentrate in 7.5 ml of PBS. Prepare always a fresh dilution prior to use.

Mouse Ig Blocking Solution

M.O.M.™ Mouse Ig Blocking Reagent, 90 µl

PBS, 2.5 ml

Dilute 90 µl of M.O.M.™ Mouse Ig Blocking Reagent in 2.5 ml of PBS. Always prepare a fresh dilution prior to use.

COMMENTARY

BACKGROUND INFORMATION

The methodology described here (Fig. 1) is of interest to the general cardiovascular research community when addressing the histo-pathological alterations after cardiac injury. This procedure enables representative histological sampling of the LV with well-preserved morphological features and is also compatible with complementary molecular analysis (*e.g.* immunofluorescence and immunohistochemistry, Basic

Protocol 1). As such, the protocol is optimized towards an ideal fixation with minimal antigenic epitope masking. Guidelines are also provided for antigen retrieval to restore the detrimental effects of formaldehyde (Support Protocol 1 and 2).

Herein protocol was also developed to assess histo-pathological alterations in the LV from 14 days post-MI onwards, when the collagenous scar is evident and can be useful for infarct size quantification with the software *MIQuant or alternative analysis tools* (Basic Protocol 2). Regardless, the sampling strategy provided in Basic Protocol 1, the neovascularization assessment provided in Support Protocol 1 and the detection of transplanted human cells in the murine myocardium in Support Protocol 2 are appropriate for any time point after injury as well as for the study of non-manipulated animals.

CRITICAL PARAMETERS

The important constraints considered during the execution of this set of protocols were specified in a stepwise mode during the experimental description. Nonetheless, the critical parameters to obtain reproducible results are further emphasized below.

Standardized heart collection for histological quantifications

The heartbeat is characterized by two stages: the systole (cardiomyocyte/myocardial wall contraction) and diastole (cardiomyocyte/myocardial wall relaxation). The systole and diastole impact the heart size and shape, and these size/shape differences interfere with accurate assessment of infarct size and morphometric measurements. In order to standardize the histological quantifications, we strongly advise the researcher to collect the hearts in diastole by inducing cardioplegia through intra-wall injection of KCl, (Kobayashi et al., 2004).

Impact of fixation in subsequent histological analysis

Tissue fixation prevents cellular degradation, subsequent to autolysis and bacterial invasion following death, and promotes stabilization of molecular components in their native location. Formaldehyde-based fixatives act by cross-linking proteins and are routinely used in histology since they provide excellent morphological preservation. However, fixation is a critical step and must be balanced to promote optimal results. Hence, if fixation is incomplete, tissue degradation occurs and compromises the downstream steps. On the other hand, excessive fixation is detrimental due to antigen masking, which may compromise immuno-detection of certain proteins. Fixation and histological processing (see Critical Parameters, Histological Processing) are two critical parameters that represent points of no return and therefore should be carefully performed according to the protocol.

The described fixation protocol (12 – 16 h at room temperature) attains balanced fixation of the adult mouse heart with well-maintained morphology and is suitable for subsequent *in situ* molecular analysis, such as immunofluorescence (Support Protocol 1 and 2) and fluorescence *in situ* hybridization (Bancroft, 2013; Carson, 1997; Freire et al., 2014a; Nascimento et al., 2014). Be aware that the duration of fixation should be constant between experiments to improve consistency. Instructions and advice for antigen retrieval prior to immunofluorescence are also provided in Support Protocol 1 and 2.

Impact of processing in subsequent histological analysis

Tissue processing consists of progressive tissue dehydration by immersion in a series of ethanol baths, clearing with an organic solvent (Clear-Rite^{TM} 3) and impregnation in paraffin wax to progressively replace the original water molecules (Bancroft, 2013;

Carson, 1997). Tissue processing is commonly performed in an automated tissue processor but can also be performed manually by immersing samples in the same sequence of solutions; always in a volume at least 10 times higher than the volume of the samples.

Tissue processing also contains critical steps that may irreversibly compromise sectioning and the microscopic detail of the tissue (Bancroft, 2013; Carson, 1997). In particular, excessive time in ethanol solutions, Clear-Rite^{TM} 3 and paraffin promote tissue hardening, which may influence the tissue properties and impair future analysis. When preparing for histological processing, double-check the selected program and whether the solutions are saturated or not.

Systematic sectioning for representative heart sampling

Representative heart sampling is a major determinant of accurate infarct size quantification and is a requisite for comparisons across studies and laboratories (Csonka et al., 2010; Nascimento et al., 2011; Takagawa et al., 2007). Herein, we propose a systematic transverse sectioning (3 µm thickness) of the LV, starting from the apex to the basal region. Basic Protocol 1 details the procedure to obtain sampling of 12 – 14 equidistant regions of the LV, from which 8 replicates (consecutive sections *per* region) slides are prepared (Fig. 3). To reach an equidistant interval between each sampled region, a defined amount of tissue has to be wasted (*i.e.* trimmed away). The thickness of trimming between each represented LV region depends on the number of replicate slides (Table 1). For infarct size quantification, only the LV is relevant; however, if sampling of the atrium is required, the user must continue the sectioning while maintaining the same strategy.

Be aware that because the heart tissue is trimmed away between regions (tissue that is lost), there is no more tissue left in the block after the sectioning procedure (Fig. 5H). Therefore, it is mandatory to be certain about the number of replicates required for the

analysis before beginning the sectioning. Additionally, consider collecting more replicates than the minimum required in case any analysis has to be repeated.

Modified Masson's Trichrome Staining

As already mentioned above, formaldehyde-based fixation crosslinks proteins. The 3-dimensional insoluble network that is formed is unique from each protein and depends on their physical features: proteins of erythrocytes will produce a dense network with small pores between amino acids; myocytes will form a more porous structure; and collagen fibers will form a less compact reticulation network. The differential density of the protein net established during fixation will influence the subsequent staining reactions.

Be aware that an incorrect fixation procedure may affect Masson's Trichrome, as discrimination between muscle and collagen deposition is highly dependent on the crosslink formed during fixation.

Infarct size quantification

MIQuant software is available as a freeware at the website "http://paginas.fe.up.pt/~quelhas/MIQuant/" (see Internet Resources), which contains all the instructions required for software installation.

Collagen deposition and cardiac remodeling (*e.g.* aneurysm formation) regionally and heterogeneously affect the ventricular wall, with the apex being considerably more affected than the basal LV region (Fig. 6). Hence, at least 7 histological sections of the LV were shown to be required for an accurate representation of the chamber (Takagawa et al., 2007). In line with this, MI size quantification tools as *MIQuant* must be used with caution and the user must certify the analysis of representative LV images for the correct infarct size estimation.

Be aware that inappropriate segmentation will result in an inaccurate calculation of infarct size. When using *MIQuant*, the user controls image segmentation parameters by displaying the original and segmented images side by side. Consult the color legend (Fig. 7A6) to verify the segmentation result. The user must adjust the threshold of "Normal tissue" and/or "LV lumen" segmentation until a correct segmentation appears on the screen (Fig. 7 3, 4-6).

In the case of extensive heart remodeling, particularly in the apex region, the midline is more problematic to predict with semi-automatic tools and should be adjusted manually. If *MIQuant* wrongly predicts the midline, the user must adjust the midline as detailed in *Step 25* of Basic Protocol 2 (Fig. 7I).

Molecular in situ analysis: identification of endothelial cells and discrimination of human cells in murine tissue

Following formaldehyde-based fixation, several methylene bridges crosslink with tissue proteins, masking antigenic sites. For this reason, antigen retrieval is commonly required prior to immunostaining of paraffin-embedded samples. Two different types of antigen retrieval are available: heat-mediated (heat-induced epitope retrieval or HIER) or enzymatically treated (proteolytic induced epitope retrieval or PIER). Here, we detail the procedure for the HIER type of antigen recovery. Basically, the crosslink sites are broken when incubated in an acidic or basic solution combined with high temperature (around 98°C). It is important to highlight that, since antigen retrieval conditions are stringent, there is an increased probability of tissue section detachment from the glass slide. Additionally, it is imperative to follow the exact protocol description, including the cooling down of the solutions to achieve the complete antigen retrieval (*Step 4d*, Support Protocol 1 and 2).

TROUBLESHOOTING

Table 2 lists the most common difficulties performing the described protocols along with possible causes and resolutions.

To obtain absolute measurements instead of relative values presented as percentages (i.e. wall thickness and indexes obtained with alternative image processing tools), a photograph of a micron ruler or object with known length should be acquired with the same magnification used in the heart sections image acquisition to determine the mm-to-pixel ratio of the image, according to the following equation:

$$mm/pixel = \frac{known\ distance\ in\ mm}{measured\ distance\ in\ pixels}$$

The distance in mm can be obtained by multiplying any result derived in pixels by the determined ratio. Moreover, throughout each experiment, all images should be acquired with the same magnification to avoid the introduction of scale conversion-related errors between samples. To obtain accurate pixel-to-micron conversions, a pixel aspect ratio of 1 (pixels width/pixel height) is required in image acquisition.

Table 2 Troubleshooting

BASIC PROTOCOL 1

Histological processing and paraffin embedding

Steps	**Problem**	**Possible reason**	**Resolution**
8 – 9	Heart tissue too hard after processing	Wrong sequence/program in the automated processing	Wrong processing cannot be solved!
		Saturated solutions (ethanol, Clear-Rite™ 3 or paraffin)	Apply the inverse sequence of processing, exchange all solutions of the system, and redo the overnight automated processing to ensure correct paraffin embedding.
		Excessive incubation time, especially	No solution!

		in 99.9% ethanol, Clear-Rite™ 3 and/or warmed paraffin	Try to proceed with samples in this condition.
		Paraffin temperature too high	No solution! Try to proceed with samples in the proper condition.

Sectioning

Steps	**Problem**	**Possible reason**	**Resolution**
16 and 19	Cutting surface friable during trimming	Paraffin block cutting surface too cold	Warm the cutting surface of the paraffin block to room temperature.
		Dirty paraffin	Melt the paraffin block and replace the wax with fresh melted paraffin by repeating *Steps 11 – 16*.
17	No ribbon formation	Lack of practice	Practice the sectioning more before restarting.
		Warmed cutting surface	Cool down the cutting surface.
		Debris on the blade edge	Clean with a xylene-moistened cloth.
		Knife angle too steep or too shallow	Adjust to reach an optimal angle, or consult the responsible for the apparatus.
	Different thickness in consecutive sections	Paraffin too soft	Re-embed the paraffin block with fresh melted paraffin by repeating *Steps 11 – 18*.
		Insufficient clearance angle between the microtome blade and the block	Slightly increase clearance angle, or consult the responsible for the apparatus.
	Sections too compressed, folded, or wrinkled	Paraffin block or blade loose	Tighten paraffin block or blade holders.
		Cutting surface not cold enough	Cool down the cutting surface.
		Blunt blade	Replace the used region of the blade or the whole knife.
		Paraffin too soft	Re-embed the paraffin block with fresh melted paraffin by

			repeating *Steps 11 – 18*.
	Tears in tissue or paraffin	Blunt blade or blade with grooves	Replace the used region of the blade or the whole knife.
		Dirty paraffin	Re-embed the paraffin block with fresh melted paraffin by repeating *Steps 11 – 18*.
18d	Sections expand and disintegrate into the warmed dH_2O	Inadequate fixation or histological processing	Inadequate fixation and/or processing are impossible to be solved!
			Complete fixation can be attained during processing in ethanol steps; however, this is not an optimal situation. Try to proceed with samples in this condition. For inadequate processing, melt the paraffin block and apply the inverse sequence of the processing solutions; exchange all solutions of the system and repeat the automated processing (*Step 9*) and the following procedure (*Steps 10 – 18*).
		Temperature of the water bath too high	Decrease the water bath temperature to 45°C.

BASIC PROTOCOL 2

Collagen staining – modified Masson's Trichrome staining

Steps	**Problem**	**Possible reason**	**Resolution**
Every time that a problem happens in one step of the Masson's Trichrome *staining, the ideal situation is to initiate the staining protocol in other tissue sections. If this is not possible, it is important to repeat all the steps of the* Masson's Trichrome *staining in the described sequence, since the order of the dyes is important to obtain the correct staining of the structures.*			

1 – 14	Loss of tissue sections	Insufficient drying of the slides after sectioning	Redo the Masson's Trichrome staining in well-dried slides (1 – 2 h at 60°C).
		Inadequate APES coating of the slides	Inadequate APES coating is impossible to be solved after the tissue section adhesion! To remedy the improper slides coating, the first step is to perform an extra period of drying 1 – 2 h at 60°C (*Step 22*, Basic Protocol 1). During the Masson's Trichrome staining protocol, incubations shall be not done by immersion, but by carefully dropping the dye on the slides (tissue faced upwards).
	Inappropriate nuclear staining	Lack of Celestine Blue, Gill's Hematoxylin or both	Repeat the staining, paying special attention to the nuclear staining dyes and their sequence.
		Old Celestine Blue or Gill's Hematoxylin solution	Prepare new Celestine Blue solution or Gill's Hematoxylin and initiate staining. Always store solutions in the dark at room temperature.
	Inappropriate cardiac muscle staining	Lack of Bouin mordant before the Biebrich Scarlet-Acid Fuchsin staining step	Initiate staining, paying special attention to the Bouin step.
	Inappropriate collagen deposition staining	Lack of Phosphomolybdic Acid/Phosphotungstic Acid treatment	Initiate staining, paying special attention to the Phosphomolybdic Acid/Phosphotungstic Acid treatment.
		Removal of Phosphomolybdic Acid/Phosphotungstic Acid treatment	Do not rinse slides between acid treatment and Aniline Blue staining.
		Old working solution of	Always prepare fresh working

		Phosphomolybdic Acid/Phosphotungstic Acid	solution of Phosphomolybdic Acid/Phosphotungstic Acid
		Excessive time in the ethanol steps faints Aniline Blue stain	Be quick on the dehydration step, or perform the alternative dehydration 2 h at 37°C (*Step 13*).
	Bubbles throughout the glass slide and tissue sections	Air bubbles in the mounting medium or during their transfer to the coverslip	Remove the coverslip by immersion in xylene, rinse in clean xylene and repeat *Steps 14 – 16*.
	Blurred image of heart sections and slide	Inadequate dehydration before slide mounting	Remove the coverslip by immersing in xylene. Rinse slides sequentially in clean xylene and quickly in 2 ethanol baths. Repeat the *Steps 13 – 16*.
	Background staining throughout the glass slide and the tissue sections	Presence of oxidative film on dye surface can stain non-specifically samples and glass slide	Filter oxidized solutions and redo the Masson's Trichrome staining in a different slide. To prevent this, always filter dye solution before use (particularly when stored for a long period).
		Dye precipitation occurs when dye solution dries on top of the slide (especially in coated slides)	Filter the oxidized solutions and redo the Masson's Trichrome staining in a different slide. To prevent this, do not allow the dye to dry during incubation periods.
	Difficult to focus	Slide mounted on the wrong side.	Remove the coverslip by immersing in xylene. Re-mount on the correct side by following the *Steps 14 – 16*.
		Inadequate dehydration	Remove the coverslip by immersing in xylene. Rinse slides sequentially in clean xylene and quickly in 2 ethanol baths. Repeat the *Steps 13 – 16*.

	Scratch marks in the sections	Rough slide handling during the staining	Handle the slides with care, mainly the tissue regions, throughout the protocol.

Myocardial infarct size calculation with MIQuant

Steps	**Problem**	**Possible reason**	**Resolution**
18 – 27	Segmented image different from the original image	Subjectivity	Be knowledgeable in cardiac anatomy/histology and accurate use of editing tools.
			Adjust threshold until segmentation result is well-matched with original image.
		Failed to remove the right ventricle	Remake the line for right ventricle removal (“Remove tissue” command), be sure that the line fully separates the two ventricles.
		Failed connection of scratched/torn tissue regions stained in same color	Redo “Connect tissue regions”. Be sure that connected tissues have the same color.
		Different color shades in the same structure	Select for segmentation of different shades for the same structure.
25	Midline is not well matched with the infarcted LV wall	Difficulty to automatically predict the midline of very irregular LV walls	Manually adjust the midline according to the instructions.

SUPPORT PROTOCOL 1 and 2

Steps	Problem	Possible reason	Resolution
1 – 14	Loss of tissue section	Insufficient drying of the slides after sectioning	Initiate immunostaining in well-dried slides.
		Inadequate APES coating of the slides	Inadequate APES coating is impossible to be solved after the tissue section adhesion! Use pre-pared APES coated sections
		Water bath temperature too high during antigen retrieval	Initiate immunostaining in new slides. Be sure that the water bath temperature is stable around 98 ºC.
	No staining	Too much time of fixation, of histological processing, or the paraffin temperature too high	Inadequate fixation and/or processing are impossible to be totally solved, especially for molecular *in situ* analysis! To improve epitope unmasking, increase antigen retrieval duration; or test other retrieval protocols. Be aware that the more stringent the conditions are the more tissue morphology is affected.
		Inadequate antigen retrieval (buffer solution did not reach 98°C)	Initiate immunostaining in new slides. Be sure that the water bath temperature is stable around 98°C.
		Lack of primary or secondary antibodies	Initiate immunostaining with new slides giving special attention to the concentration of the antibodies and incubation times.
		Slides placed on the wrong side (tissue sections missed contact with solutions)	
		Wrong dilution of the	

		antibodies (too dilute)	
	Weak staining	Too much fixation of histological processing, or the paraffin temperature was too high	Inadequate fixation and/or processing are impossible to be totally solved, especially for molecular *in situ* analysis! To improve epitope unmasking, increase antigen retrieval duration; or test other retrieval protocols. Be aware that the more stringent the conditions are the more tissue morphology is affected.
		Inadequate antigen retrieval (Buffer solution did not reach the 98°C)	Initiate immunostaining in new slides. Be sure that the water bath temperature is stable around 98°C.
		Lack of permeabilization step	Initiate immunostaining in new slides, giving special attention to the Triton X-100 dilution and incubation time.
		Wrong dilution of the antibodies (too dilute)	Initiate immunostaining in new slides giving special attention to the antibodies dilution and incubation.
		Incorrect mounting procedure/media	Remove the coverslip by immersion in PBS and re-mount the slide with correct mounting media by following the *Steps 13*.
		Too much time between staining procedure and microscopic visualization	Initiate immunostaining in new slides giving special attention to slide storage conditions after staining. Fluorochromes fade over time, even when kept at 4°C. Ideally, images shall be acquired soon

			after immunostaining. If this is not possible, store slides at -20°C.
	Staining not homogeneous	Inadequate fixation (small volume of fixative, heterogeneous fixation, or too little time)	Inadequate fixation and/or processing are impossible to be totally solved, especially for molecular *in situ* analysis!
		Antibodies or other solutions did not cover all the sample	Initiate immunostaining in new slides, giving special attention to the volume of antibodies and the correct spread of solutions.
	Background staining	Inadequate fixation (may cause antigen diffusion)	Inadequate fixation and/or processing are impossible to be totally solved, especially for molecular *in situ* analysis!
		Inadequate blocking before primary antibody (non-specific staining of secondary antibody)	Initiate immunostaining with new slides, giving special attention to the blocking step. Always run negative controls (a section with no primary antibody).
		Inadequate washing	Initiate immunostaining in new slides giving special attention to washing steps. For some antibodies, the use of weak detergents is helpful during the washing steps to decrease the background.
		Wrong dilution of the antibodies (too concentrated)	Initiate immunostaining with new slides giving special attention to the antibody dilution and incubation time.
		Samples dried out during antibody incubation	
		Pap contouring too close to the sample	Initiate immunostaining with new slides giving special attention to the hydrophobic contouring of the samples.

ANTICIPATED RESULTS

Following paraffin embedding and sectioning as outlined above, representative LV sampling of 12 to 14 equally distant transverse sections is expected (Fig. 3). An example of representative sampling of an infarcted LV (after Masson´s Trichrome stain) is demonstrated in Fig. 6. The expected results for infarct size quantification using the example provided on Fig 6 are presented in Fig. 10. For neovascularization assessment and for the detection of human cells in murine tissue, high-resolution microphotographs are acquired using an inverted fluorescence microscope (Fig. 8 and 9).

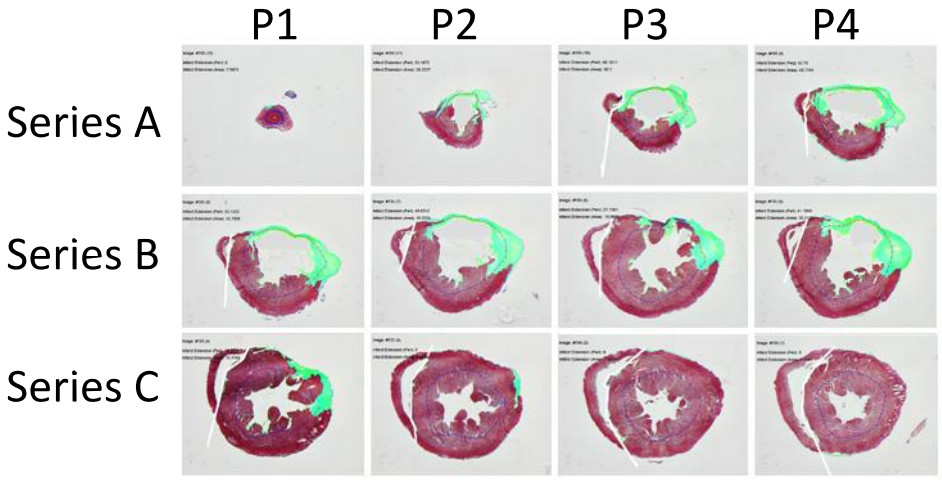

Figure 10. Expected results of MI quantification by area (highlighted in green) and midline-length (red and blue lines) methods using the *MIQuant* software. Each image retrieved by the software displays the MI size values on the top left corner and the result of segmentation (*i.e.* infarcted area (light green) and infarcted midline on top of the original image).

TIME CONSIDERATIONS

The execution of the methodologies fully detailed here requires prior training with animal handling and anesthesia experts (*Step 1* of Basic Protocol 1) as well as for sectioning (*Steps 12 – 22* of Basic Protocol 1). If experts are not available to generate the samples, then it is recommended that the techniques are practiced and perfected on non-critical samples prior to analysis of critical experiments.

Basic Protocol 1: 2.5 days

Euthanasia and sample collection can be performed in 10 min *per* heart (*Steps 1 – 6*) followed by 12 – 16 h of fixation (*Step 7*). Histological processing (*Steps 8 – 9*) takes 12 h and 30 min, and the paraffin embedding takes 5 min *per* heart (*Steps 10 – 11*). Basic Protocol 1 may be interrupted at this step (BREAK point). The duration of sectioning varies with the number of slides replicates (Table 1). The time required to obtain 8 replicates (*Steps 12 – 21*) is approximately 2 h *per* heart, followed by an overnight step at 37°C (that can be replaced by 1 – 2 h at 60°C) for adherencing sections to the slides (*Step 22*). This step is a BREAK point.

Basic Protocol 2: 2 days

Collagen staining with modified Masson's Trichrome Kit can be performed in approximately 3 h (*Steps 1 – 15*). Be careful as mounting medium takes around 16 h to be completely dried (*Step 15*). This step is a BREAK point. Photographs of the 12 – 14 sections *per* heart can be acquired in 15 min (*Step 16 – 17*). This step is a BREAK

point. MI size quantification with *MIQuant* software takes 10 min *per* heart (*Step 19 – 27*) and both morphometric analyses can be accomplished within 20 min *per* heart.

Support Protocol 1: approximately 6 h

CD31 staining protocol has the duration of 6 h and microphotographs can be acquired in 1 – 2 h *per* heart (*Steps 2 – 13*).

Support Protocol 2: approximately 10 h (or 1.5 days)

Anti-human nuclei staining procedure takes 10 h, microphotograph acquisition is time-consuming and highly dependent on the experimental aim (*Steps 2 – 13*).

CONFLICT OF INTEREST STATEMENT

The authors have no conflicting financial interests.

ACKNOWLEDGEMENT

The authors are indebted to the many colleagues who have through the years provided insightful help in several of the procedures herein described, among others we thank Rui Fernandes, Dr. Dirk J Duncker, Dr. M.J. Vaz-da-Silva, Dr. Isabel F. Carvalho, Dr. Paula Sampaio, Dr. Pedro Brites, Sofia Lamas (DVM), Isabel Duarte, all the animal caretakers at the IBMC animal facility and the Ipatimup Diagnósticos - Anatomia Patológica Service. The authors acknowledge P. Kennedy for manuscript revision. This

work was supported by Fundação para a Ciência e a Tecnologia [SFRH/BD/74218/2010] to M.V., QREN/ON.2 [NORTE-07-0124-FEDER-000005] to D.S.N., and Fundo Europeu de Desenvolvimento Regional, Programa Operacional Factores de Competitividade- COMPETE, Quadro de Referência Estratégico Nacional, Fundo Social Europeu [PEst-C/SAU/LA0002/2013, PTDC/SAU-ORG/118297/2010] and Programa Operacional Regional do Norte (ON.2 – O Novo Norte) [NORTE-07-0124-FEDER-000005 - *Project on Biomedical Engineering for Regenerative Therapies and Cancer*].

LITERATURE CITED

Please see references at *REFERENCES Chapter*.

INTERNET RESOURCES

http://paginas.fe.up.pt/~quelhas/MIQuant/

The webpage contains instructions and assess to MIQuant, including a detailed stepwise manual and associated publications.